Imprints of vector-like fermions on electroweak vacuum stability in extended Higgs frameworks

Kıvanç Yiğit Çıngıloğlu

A Thesis
In the Department
of
Physics

Presented in Partial Fulfillment of the Requirements
For the Degree of
Doctor of Philosophy (Physics) at
Concordia University
Montréal, Québec, Canada

March 2025

CONCORDIA UNIVERSITY
SCHOOL OF GRADUATE STUDIES

This is to certify that the thesis prepared

By: **Kıvanç Yiğit Çıngıloğlu**

Entitled: **Imprints of vector-like fermions on electroweak vacuum stability in extended Higgs frameworks**

and submitted in partial fulfillment of the requirements for the degree of

Doctor of Philosophy (Physics)

complies with the regulations of this University and meets the accepted standards with respect to originality and quality.

Signed by the Final Examining Committee:

_____ Chair
Ronald Stern

_____ External Examiner
Tom Steele

_____ External Program Examiner
Calvin S. Kalman

_____ Examiner
Manuel Toharia

_____ Examiner
Saurabh Maiti

_____ Thesis Supervisor
Mariana Frank

Approved by   _____
Saurabh Maiti
Graduate Program Director

_____ 2025   _____
Pascale Sicotte, Dean
Faculty of Arts and Science

Abstract

Imprints of vector-like fermions on electroweak vacuum stability in extended Higgs frameworks

Kıvanç Yiğit Çıngıloğlu, Ph.D.
Concordia University, 2025

The issue of electroweak vacuum stability in the Standard Model remains a significant theoretical challenge. This thesis investigates the role of vector-like fermions in stabilizing the electroweak vacuum. We focus on three scenarios: the Higgs-Scalar Model with Vector-Like Quarks, Two-Higgs Doublet Model with Vector-Like Quarks, and Vector-Like Leptons in the Standard Model, exploring how the introduction of these additional fermions can modify the stability of the vacuum. We examine all gauge-anomaly-free vector-like representations under the SM gauge symmetry, and we analyze each of these models, taking into account all experimental constraints and electroweak precision observables, and considering both direct and indirect constraints from collider and cosmological data. The work shows that, under certain conditions for the vector-like fermion masses and mixing parameters, the electroweak vacuum can be stabilized in all models studied, providing a viable mechanism for addressing the vacuum stability problem in the Standard Model.

To my father, Zekai Çıngıloğlu,
the titan who taught me to distinguish between mere appearances
and the underlying nature of negation.

"Koştururken ardından o uçmaktaki devin,
Ve daha başka tür aşklar, geniş sevdalar için
Açıldı nefesim, fikrim, canevim
Hayatta ben en çok babamı sevdim."

Acknowledgments

First and foremost, I must express my gratitude to my supervisor Mariana Frank, whom I have taken as not only a scientific but also an intellectual role model throughout my Ph.D. What she has contributed to my scientific competence and my life since the first moment I met her productive character is incomparably greater than the contents of this thesis. I have always associated the productive character and the existence of distinctive traits with the emergence of role models in one's life. In this context, the actual composition of a systematically portrayed scientific character of mine has been heavily influenced by her actions. The fact that she accurately analyzed my theoretical progress and guided me to a concept that I find close to myself in terms of productivity is the cornerstone of my current work. It would be absolutely appropriate to state that Mariana Frank has taken on one of the leading roles in removing the obstacles to my scientific productivity. As a result of all our work and all the deep conversations we shared, I hope that I have made her proud in this process in which she served as my scientific advisor. She has always been kind, insightful and full of constructive suggestion. Throughout the pandemic process and all the obstacles that followed, she never hesitated to have deep conversations with me about life and science, and she always made an intense effort to pave the way in those places where we thought the life was stuck. I am very delightful to have had the opportunity to work under your academic supervision and to get to know you. Thank you Dr. Frank for never withdrawing your support, you are one of the pillars of my life.

As I write the last lines of this thesis, I have lost my supreme hero, who has arguably had the greatest influence on every stage of my life and whom I define as the ultimate role model in defining myself. However, what I am going to write from now on is not an expression of grief or lament, nor that my father has left my life. On the contrary, these lines are a partial testimony to an expression of a titan, the Prometheus of my life, the true sun that gave me fire. In a book we both read, when a professor was asked about the reward for his efforts he responses: "If I have been able to pass on to at least one person the intellectual knowledge I have brought so far, I have fulfilled the most important productive task in this universe; if even one person has received it from me, the movement will continue and I will be eternal." You passed it to me, dad. You always did and I have always been aware of this. You were an outstanding intellectual who knew no boundaries, an infinity that never gave up mechanical negation, a scientist who absorbed analysis and synthesis very well, a flame that ignited aesthetics and human productivity in its brightest shades and the true embodiment of determination. You have scorched all the ages of my life and I am sailing with you through the fires of the cosmos and this great void of existence to all shores. We are going to eternity, father, and we are immortal. We are human, and we consider nothing that is human alien to us. You were a titan who fought again and again and again a relentless struggle to remove all obstacles to my and humanity's productive

force. It was you and my mother who ignited and fueled in me the whole philosophical idea of removing all obstacles to the productive forces. Which is the most fundamental pillar of my life today, tomorrow and until the end of the universe. I will always continue to critique and talk to you at every stage of my productivity and in every contradiction I find myself in. Your labor is the eternal soil in which I flourish, your love is my eternal sun that can never be outshined.

And my mother, the woman who taught me to always fight for something bigger than myself, who taught me that only in this way is life meaningful and worth living. She is still fighting and continues to be a role model for me with her immense love and determination. We move on with her now, but my father is with us and nothing of him is missing in us. We love you dad and we know... We carry within us the ultimate pride and joy of a human being, what your presence means. We know, father, and we continue to struggle for humanity...

Contribution of the Author

The original research contained in this thesis is presented in Chapters 4, 5, 6 and 7. The research in Chapter 4 was modified by the author to include VLF representations that have not been explored in the literature.

The research in Chapter 5 was conducted in collaboration with Mariana Frank and Ash Arsenault. The publication can be found in Ref. [1]. An earlier stage of this project was incomplete due to the absence of weak iso-triplet results and electroweak precision observables in all models. M.F. encouraged K.C. to work on VLQ+HSM. The author developed the theory and performed the computations. K.C. and M.F. discussed the results and contributed to the final manuscript.

The research in Chapter 6 was conducted in collaboration with Mariana Frank. The publication can be found in Ref. [2]. M.F. presented the idea and supervised the project. K.C. developed the theoretical framework and performed the analytic calculations throughout the work. All authors discussed the results and contributed to the final manuscript.

The research in Chapter 7 was conducted in collaboration with Mariana Frank. The publication can be found in Ref. [3]. M.F. presented the idea and supervised the project. K.C. developed the theoretical framework and performed the analytic calculations throughout the work. All authors discussed the results and contributed to the final manuscript.

Contents

List of Figures

List of Tables

Chapter 1

Introduction

The discovery of the Higgs boson at the Large Hadron Collider (LHC) in 2012 [4, 5], culminating a decades-long quest, provided a key piece to the Standard Model (SM) of particle physics. This discovery not only validated the electroweak symmetry breaking mechanism proposed in the 1960s by Higgs and others, but also set the stage for a deeper exploration of the fundamental forces and particles in nature. However, while the Higgs boson itself was an essential missing piece, its discovery serves as a marker for the many questions that remain unanswered in the SM, and signals the possible presence of new physics beyond it. In particular, understanding whether the Higgs particle matches the exact predictions of the SM, or if deviations exist, could offer insight into physics at energy scales far beyond the reach of current experiments. Despite its success, the Standard Model remains an effective theory that cannot provide a complete description of nature. Several open questions still linger, such as the nature of dark matter, the origin of the matter-antimatter asymmetry, and the elusive role of gravity in unification. Yet, rather than focusing on these well-known inconsistencies, the hunt for new physics is increasingly focused on the detailed properties of the Higgs boson and its interactions, as small deviations from SM predictions could reveal entirely new realms of physics.

One avenue of exploration involves the study of extended Higgs sectors. Models such as the Higgs Singlet Model (HSM), the Two-Higgs Doublet Model (THDM) and the Higgs Triplet Model (HTM) introduce additional scalar fields, allowing for richer dynamics in electroweak symmetry breaking. These extensions might naturally arise from more fundamental frameworks such as supersymmetry (SUSY) [6, 7], composite Higgs theories, or high-dimensional Higgs models (HEIDI) [8, 9], all of which aim to address not just the Higgs sector, but other fundamental issues such as hierarchy problems and quantum gravity. In SUSY, for example, the Higgs sector contains a richer array of particles, offering potential candidates for dark matter (such as the lightest supersymmetric particle, often a neutralino) while simultaneously addressing the fine-tuning problem in the SM. Similarly, axion models [10, 11] provide an intriguing solution to the strong CP problem, and in doing so, also offer potential candidates for dark matter. On a more speculative frontier, string theory [12–14] and extra dimensions [15, 16] promise a unified framework that could potentially explain all fundamental interactions, incorporating gravity alongside the other forces described in the SM. Another critical approach is to explore effective field theories (EFTs) [17, 18], where new physics is encoded in higher-dimensional operators that modify the SM at high energies. These modifications could manifest themselves in small

deviations from the SM predictions, allowing researchers to search for "fingerprints" of new physics even in the absence of direct discovery of new particles. This model-independent approach, especially in the context of the Higgs interactions, is a fertile ground for exploring Beyond the Standard Model (BSM) physics without making strong assumptions about the underlying theory.

One of the most distinctive features of particle physics is the concept of renormalization. This procedure is essential in quantum field theory (QFT) as it allows the removal of infinities that arise in loop calculations. In simple terms, renormalization involves redefining the parameters of the theory (such as masses and coupling constants) to absorb these infinities and obtain finite, physically meaningful results. While renormalization is a standard tool in most quantum field theories, its uniqueness in particle physics lies in the way it addresses the structure of fundamental forces. The SM is a renormalizable theory, which means that, despite its apparent infinities at higher orders in perturbation theory, the theory can be consistently defined and calculated at all orders. This is a significant property, distinguishing the SM from non-renormalizable theories, such as those that might describe quantum gravity. Moreover, the renormalization of gauge theories like QCD (quantum chromodynamics) and the electroweak interactions is particularly elegant, where symmetry principles dictate the structure of the theory and provide a pathway for resolving divergences. At higher orders, renormalization is more than just a computational tool; it also embodies a deeper conceptual principle about the nature of quantum fields and the structure of interactions at different scales. The sophisticated techniques required to compute corrections beyond leading order, such as next-to-leading Order (NLO) or even next-to-next-to-leading order (NNLO) calculations, have become a cornerstone of precision tests of the Standard Model and for making predictions for new physics scenarios.

To study new physics, physicists rely on advanced techniques from QFT, particularly in the context of high-energy collider experiments. The calculation of particle interactions often involves handling loop integrals, virtual particles, and divergences. One of the most challenging tasks in this domain is managing infrared (IR) and ultraviolet (UV) divergences that arise in loop diagrams. IR divergences appear when massless particles (like photons or gluons) are involved in low-energy processes. These can lead to an infinite contribution when integrating over momentum space. The Kinoshita-Lee-Nauenberg (KLN) theorem [19, 20] provides a way to handle such divergences by showing that when real and virtual corrections are combined, the infinities cancel out, yielding finite, observable results. This requires the development of sophisticated subtraction schemes, often called real-virtual subtraction or jet algorithms, to cancel the IR divergences in actual calculations. UV divergences, on the other hand, arise when particles interact at high energies. These divergences are removed through the process of renormalization, where one systematically redefines the parameters in the theory (masses, coupling constants, etc.) to absorb the infinities. Renormalization schemes such as $\overline{\text{MS}}$ (modified minimal subtraction) or on-shell renormalization provide the framework for handling these divergences, leading to finite, physical predictions.

Moreover, techniques like lattice QCD [21–23] are now extensively used for non-perturbative calculations, where the strong force governs the interactions between quarks and gluons. Lattice simulations provide a direct numerical approach to studying the strong interaction at low energies, allowing for precise calculations of hadronic quantities that are otherwise difficult to obtain analytically. Another important tool in the search for new physics is

Monte Carlo simulations, which are widely used to model particle collisions and detector responses. These simulations are crucial for understanding how BSM signals might emerge in high-energy collisions, such as those expected at future colliders or from rare decays. The accurate simulation of such events relies on both perturbative QCD and non-perturbative techniques, providing a robust framework for comparison with experimental results.

The study of new physics BSM often involves addressing long-standing issues that are not easily resolved by traditional perturbative methods alone. One such issue is the stability of the electroweak vacuum in the SM, which is sensitive to quantum corrections at high energy scales. While techniques like loop calculations, renormalization, and Monte Carlo simulations provide powerful tools for analyzing particle interactions, they are also critical in understanding the stability of the Higgs potential. The SM itself faces a potential instability at high energies due to large corrections to the Higgs self-coupling, which could lead to a destabilization of the electroweak vacuum. Here, the introduction of vector-like fermions (VLFs) offers a compelling solution. By mixing with the third-generation fermions through Yukawa interactions, VLFs modify the behavior of the Higgs potential, potentially stabilizing the vacuum. Their contribution can be studied using the same advanced techniques—loop integrals, renormalization group equations, and precision observables—that are used to handle divergences in high-energy physics. Thus, the inclusion of VLFs not only provides a framework for solving a theoretical challenge but also involves the application of sophisticated computational and theoretical methods to ensure consistency with experimental data and the stability of the electroweak vacuum.

This is the issue we tackle here, and which we explore more in the following chapters. This thesis is structured as follows:

- We give the theoretical basics in Chapter 2, where the SM is briefly discussed along with some important topics pertaining to the Higgs boson and some of the open problems in the current state of particle physics.

- Chapter 3 is mainly focused on the mechanism by which electroweak vacuum instability occurs in the SM due to the renormalization process in QFT. We also show how the gauge and fermionic sectors affect this outcome using a conventional method in QFT. We conclude the chapter by presenting an approximate lifetime for the metastable vacuum, assuming there is no additional mechanism that prevents it from decaying to a lower energy configuration.

- In Chapter 4, we extend the discussion to the main motivation of this thesis by exploring the effects of VLFs on renormalization group equations (RGEs). The modifications due to VLFs are twofold: they either manifest directly at the RGE level or alter the running of the SM couplings through portal effects. The RGE formalism we adopt here will also be useful for the research we conduct in Chapters 5, 6 and 7.

- Chapter 5 is devoted to the effects of vector-like quarks (VLQs) in the Higgs Singlet Model (SM model augmented by a Higgs singlet field). The driving goal here is to extract the parameter space that survives the vacuum stability condition by allowing VLQs to couple to the SM quarks through the Yukawa portal. We further apply electroweak precision observables to check for agreement with the RGE results.

- In Chapter 6, we extend the discussion of the effects of the VLQs in the Two-Higgs Doublet Model (THDM) (the SM augmented by a Higgs doublet field), up to next-to-leading order (NLO), where the vacuum stability condition becomes more complex due to the increased number of couplings and scalar particles. Fermion coupling to the Higgs doublets differs between type-I and type-II THDM models, which drastically affects the influence of VLQs on the running couplings and the parameter space. We compare the stability results for the two types of THDM when VLQs are present, although the oblique corrections from VLQs remain insensitive to the specific THDM type.

- Chapter 7 attempts to answer the radical question of whether the electroweak vacuum in the SM can be stabilized without an additional scalar. Although VLFs mitigate vacuum instability at the RGE level, their mass is largely constrained for uncolored flavors. Vector-like leptons (VLLs) can still be lighter than VLQs. Given that a sub-TeV-scale extension of the SM with leptons having non-chiral partners could create a scenario in which the vacuum remains stable up to the Planck scale, we further show that the allowed parameter space is extended by two-loop corrections. Furthermore, we check whether the mass regime of VLLs, as inferred from electroweak precision observables, is consistent with the surviving parameter space from the stability condition.

- Finally, in Chapter 8, we conclude the thesis by summarizing the main contributions examined in the previous chapters and providing an outlook for future research in these areas.

Chapter 2

The Standard Model

The Standard Model (SM) of particle physics is a renormalizable gauge field theory that provides a highly successful description of three of the four known fundamental forces in nature: the electromagnetic, weak, and strong forces. The SM does not include a quantum theory of gravity, which remains one of the key motivations for exploring physics beyond the SM.

The SM is built upon the gauge group structure $SU(3)_C \otimes SU(2)_L \otimes U(1)_Y$. This gauge symmetry describes the dynamics of the known particles and their interactions. The $SU(3)_C$ group governs quantum chromodynamics (QCD), which describes the strong interactions between quarks and gluons, while $SU(2)_L$ and $U(1)_Y$ are responsible for the electroweak unification of the weak and electromagnetic forces. The Glashow-Weinberg-Salam (GSW) model forms the theoretical foundation of this electroweak unification.

The particle content of the SM is categorized into two primary sectors: the fermionic sector, which constitutes matter, and the bosonic sector, which mediates forces. Fermions are spin-$\frac{1}{2}$ particles that obey Fermi-Dirac statistics and are classified into three families of quarks (which participate in all interactions) and leptons (which do not interact strongly). Each family contains two types of quarks (up-type and down-type) and two types of leptons (neutrinos and charged leptons). The first generation of fermions makes up the stable matter around us, while the heavier second and third generations are unstable and decay into lighter particles. Neutrinos, originally considered massless in the SM, are now known to have small masses [24], which points to physics beyond the SM.

Fermions in the SM interact based on their helicities (handedness). Left-handed fermions form isodoublets under the $SU(2)_L \otimes U(1)_Y$ gauge symmetry, while right-handed fermions are isosinglets. The strong interactions between quarks are mediated by eight massless gluons G_a^μ (a=1,..,8), corresponding to the generators[2] of non-Abelian SU(3)$_C$ algebra λ^a, while electroweak interactions are mediated by the $W^\pm$ and Z^0 bosons and the photon.

The bosonic sector of the SM consists of spin-1 gauge bosons that mediate the forces between fermions and obey Bose-Einstein statistics. The electroweak force carriers acquire mass through the Higgs mechanism, a process of spontaneous symmetry breaking. At high energies, the $SU(2)_L \otimes U(1)_Y$ symmetry is unbroken, and the gauge bosons are massless. However, at lower energies, this symmetry breaks down to $U(1)_{\text{EM}}$, giving mass of the weak bosons ($W^\pm$, Z^0) while leaving the photon massless. The mechanism predicts the existence of a scalar (spin-0) Higgs boson, which was experimentally confirmed in 2012 at CERN [4, 5, 25], filling in the last missing piece of the SM puzzle.

---

[2]The number of generators in any U(N) and SU(N) group are given respectively as N^2 and $N^2 - 1$.

The SM is a consistent and highly predictive quantum field theory. Its gauge structure ensures local gauge invariance, where the global phase transformations of the gauge groups are applied locally, requiring the introduction of vector fields (gauge bosons) to preserve invariance in spacetime. This leads to interaction terms in the SM Lagrangian that couple the fermions and gauge fields.

2.1 Framework of the Standard Model

2.1.1 Quantum Chromodynamics

Quantum Chromodynamics (QCD) is grounded in the gauge group $SU(3)_C$ of the Standard Model due to transformation of quarks according to the algebra, and the quarks are organized into color triplets each characterized by a distinct color charge (r, g, b). Moreover, local gauge invariance for the total Lagrangian of SU(N) theories dictate the presence of source terms due to interaction between field current and gauge field. This is achieved by introducing a gauge covariant derivative

$$D_\mu = \partial_\mu + ig_s G_a^\mu T^a, \qquad (T^a = \frac{\lambda^a}{2}), \tag{2.1}$$

which generates QCD Lagrangian

$$\mathcal{L}_{\text{QCD}} = \sum_q \bar{\psi}_q(i\slashed{D} - m_q)\psi_q - \frac{1}{4}G_{\mu\nu}^a G^{\mu\nu,a}. \tag{2.2}$$

The gluon field strength tensor is an artifact of the non-Abelian structure, allowing self-interactions for $SU(3)_C$ fields

$$G_{\mu\nu}^a = \frac{1}{g_s}[D_\mu, D_\nu] = \partial_\mu G_\nu^a - \partial_\nu G_\mu^a + g_s f^{abc} G_\mu^b G_\nu^c, \tag{2.3}$$

and g_s is the strong coupling constant. Non-Abelian gauge theories have gauge symmetries that can lead to redundancies in the physical degrees of freedom. Specifically, there are more gauge degrees of freedom than physical degrees of freedom for the gauge fields. Without gauge fixing, the path integral formulation would be ill-defined due to the presence of infinitely many configurations that are gauge equivalent. By fixing the gauge, these redundancies can be avoided and actual physical degrees of freedom become the relevant ones. This is done by gauge-fixing Lagrangian

$$\mathcal{L}_{\text{fix}} = -\frac{1}{2\xi}(\partial^\mu G_\mu^a)^2. \tag{2.4}$$

Gauge fixing introduces constraints that can lead to additional degrees of freedom in the theory. In non-Abelian gauge theories, these additional degrees of freedom can cause issues in the path integral formulation, as they may lead to contributions from unphysical states. To address this, new ghost fields (often denoted by c and $\bar{c}$) are introduced, which are necessary to maintain unitarity and the correct counting of degrees of freedom through path integrals. These ghost fields arise from the gauge-fixing procedure and are implemented in the Lagrangian through a term that ensures the cancellation of unphysical degrees of freedom

$$\mathcal{L}_{\text{ghost}} = -\bar{c}^a(-\partial^2 \delta^{ac} - g_s \partial^\mu f^{abc} G_\mu^a)c^c, \tag{2.5}$$

where f^{abc} is the structure constants of noncommutative algebra. Combining Eq. 2.2 - 2.5 completes the total Lagrangian for QCD. The time-ordering operation applied to gluon fields defines the two-point function, which describes the propagation of a gluon between spacetime points x and y

$$D_{\mu\nu}^{ab}(x-y) = \langle TG_\mu^a G_\nu^b \rangle_{xy} = \int \frac{d^d k}{(2\pi)^4} \frac{-i}{k^2 + i\epsilon} \left(g_{\mu\nu} - (1-\xi)\frac{k_\mu k_\nu}{k^2} \right) \delta^{ab} e^{-ik.(x-y)}, \quad (2.6)$$

where the time-ordering T ensures that

$$TG_\mu^a(x)G_\nu^b(y) = \begin{cases} G_\mu^a(x)G_\nu^b(y), & \text{if } x^0 > y^0, \\ G_\nu^b(y)G_\mu^a(x), & \text{if } x^0 < y^0. \end{cases} \quad (2.7)$$

This means that the propagator describes the probability amplitude for a gluon to propagate from x to y when $x^0 > y^0$, and from y to x when $y^0 > x^0$. Fourier transform of Eq. 2.6 to momentum space consequently leads to the gauge propagator of the theory[1]

$$D_{\mu\nu}^{ab} = \frac{-i}{k^2 + i\epsilon} \left(g_{\mu\nu} - (1-\xi)\frac{k_\mu k_\nu}{k^2} \right) \delta^{ab}. \quad (2.8)$$

2.1.2 Glashow-Salam-Weinberg (GSW) Model

The GSW model, which unifies the weak and electromagnetic forces, is built upon a non-Abelian gauge theory characterized by the combined gauge group $SU(2) \otimes U(1)_Y$. In this framework, the $W^\pm$ and Z bosons are observed to be massive. However, introducing a bare Proca mass term in the Lagrangian would violate local $U(1)$ gauge invariance. To address this, the Higgs–Kibble mechanism [26] is employed, which introduces a scalar field known as the Higgs field. This field possesses a non-vanishing vacuum expectation value, facilitating the spontaneous symmetry breaking of the gauge group. Crucially, this breaking is arranged so that the symmetry of the electromagnetic subgroup $U(1)_{\text{em}}$ remains intact, allowing the photon to remain massless while the other gauge bosons acquire mass. In the GSW model, left- and right-handed fermions transform differently under the $SU(2)$ group

$$\psi^i = \psi_L^i + \psi_R^i, \qquad \psi_L^i = P_-\psi_L^i, \qquad \psi_R^i = P_+\psi_R^i, \ (i = q, l) \quad (2.9)$$

where chirality operator $P_\pm = \frac{1 \pm \gamma_5}{2}$. This structure results in the weak interaction being maximally parity violating

$$\mathcal{L}_{\text{m}} = -m\bar{\psi}\psi = -m\bar{\psi}\left(P_- + P_+\right)\psi = -m(\bar{\psi}_R\psi_L + \bar{\psi}_L\psi_R). \quad (2.10)$$

In the context of a chiral gauge theory, it is important to note that mass terms for fermions are prohibited in the Lagrangian. Thus kinetic part of Lagrangian reads

$$\mathcal{L} = \bar{\psi}_L i\slashed{D}_L \psi_L + \bar{\psi}_R i\slashed{D}_R \psi_R \quad (2.11)$$

where the chirality preserving gauge covariant derivatives under the complete symmetry of the SM can be given as[2]

$$D_\mu^L = \partial_\mu - i\frac{g_1}{2}B_\mu - i\frac{g_2}{2}W_\mu^i.\tau^i - i\frac{g_s}{2}\lambda^a G_\mu^a, \qquad D_\mu^R = \partial_\mu - i\frac{g_1}{2}B_\mu - i\frac{g_s}{2}\lambda^a G_\mu^a. \quad (2.12)$$

---

[1]'t Hooft-Feynman gauge $\xi = 1$ reflects a balance between mathematical simplicity and physical clarity when transition between different gauges is present.

[2]The last terms in Eq. 2.12 are QCD contributions as mentioned earlier and the leptonic sector of the SM is completely insensitive to this rotation.

Furthermore, the gauge part of $SU(2)_L \otimes U(1)_Y$ in terms of the isotriplet[1] W_μ^a and the isosinglet B_μ

$$\mathcal{L}_{\text{gauge}} = -\frac{1}{4}W_{\mu\nu}^a W^{\mu\nu,a} - \frac{1}{4}B_{\mu\nu}^a B^{\mu\nu,a} \tag{2.13}$$

completes the Lagrangian of the GSW model. However, the theoretical mechanism giving rise to the observed masses in the SM is obviously not achieved by Dirac and Proca mass terms since they violate $SU(2)_L$ symmetry and local gauge invariance respectively.

The Higgs Field and Spontaneous Symmetry Breaking

The SM Higgs field is a complex scalar $SU(2)_L$ doublet $\in (2, \frac{1}{2})$

$$\Phi = \begin{pmatrix} \phi^\dagger \\ \phi^0 \end{pmatrix} = \frac{1}{\sqrt{2}} \begin{pmatrix} \phi_1 + i\phi_2 \\ \phi_3 + i\phi_4 \end{pmatrix}. \tag{2.14}$$

The potential of the scalar field Φ is dictated by Z_2 symmetry due to the global phase transformation. Consequently, only the even powers of field operators are allowed

$$\mathcal{L}_\Phi = \frac{1}{2}m^2\Phi^2 + \frac{1}{4!}\lambda\Phi^4 + \mathcal{O}(\Phi^6). \tag{2.15}$$

Moreover, $\mathcal{O}(\Phi^6)$ has renormalization issues[2] when $d \geq 4$. If $m^2 > 0$, and the Lagrangian describes an ordinary scalar field theory. However, for the case $m^2 < 0$, the extremum at $\phi = 0$ is a local maximum of the potential $V = -\mathcal{L}_{\text{int}} = \frac{1}{2}m^2\Phi^2 + \frac{1}{4!}\lambda\Phi^4$ instead of a minimum, and is unstable as shown in Fig. 2.1. Having a negative mass-squared implies that a momentum is spacelike.[3]

Replacing $m^2 \to -\mu^2$ so that μ^2 is still positive, the potential is now minimized when Φ has a constant non-zero value. There are two possible minima, $\phi_0 = \pm\sqrt{\frac{\mu^2}{\lambda}} = \pm v$. At either minimum, the Z_2 symmetry is spontaneously broken.

The choice of vacuum expectation value (VEV) $\doteq v = \pm\sqrt{\frac{\mu^2}{\lambda}}$ breaks the symmetry of the initial Lagrangian once the field perturbation around the VEV, $\phi(x) = \frac{1}{\sqrt{2}}(v + h + i\xi)$, is performed.

It is well known that electroweak unification results in three massive and one massless gauge bosons. That requirement is just an other motivation why the Higgs field is to be represented as a complex isospin doublet. By Goldstone theorem; for each broken generator of the original symmetry group, there will be massless scalar ξ, transferring its degree of freedom to the longitudinal state of the massless particle, therefore a mass term is revealed in the effective Lagrangian. In the unitary gauge, each component of the Higgs doublet obeys the transformation

$$\phi_i(x) \to e^{i\xi_i(x)/v}\phi_i(x). \tag{2.16}$$

---

[1]The non-Abelian nature of $SU(2)$ gauge covariant derivative generates a self interaction term for W_μ^a similar to that of Eq. 2.3, but scaled with the weak coupling g_2 and given in terms of the structure constants ϵ^{abc}.

[2]Additional details about the Higgs field can be found elsewhere [27].

[3]Spacelike momenta can be used to communicate faster than the speed of light, and therefore negative mass-squared particles are called tachyons.
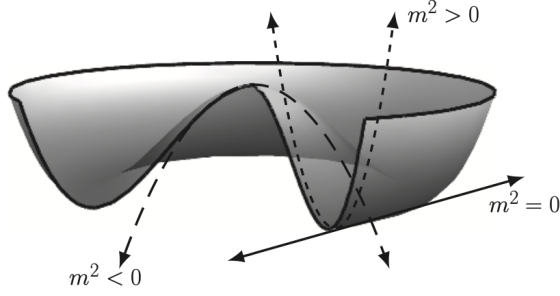
Figure 2.1: The Higgs potential. There are two tachyonic (negative mass-squared) modes (long-dashed line). Expanding around a minimum, there is one mode with positive mass-squared (small-dashed line), corresponding to excitations along the radial direction, and one massless mode (solid line), corresponding to excitations along the symmetry direction where the potential is flat.

Except ϕ_3, all components would gauged away.[1] The generators of $SU(2)_L$ acting on ϕ_0 give nonzero value, hence this symmetry remains broken, whereas Q acting on the vacuum state generates zero eigenvalue. So, the vacuum state is neutral and $U(1)_{em}$ remains unbroken.

To identify the mass terms of $SU(2)_L \otimes U(1)_Y$ gauge bosons, the gauge covariant derivative in Eq. 2.12 acts on the Higgs doublet in order to generate kinetic terms

$$\mathcal{D}_\mu \Phi = \frac{1}{2} \begin{pmatrix} 2\partial_\mu + ig_2 W_\mu^3 + ig_1 B_\mu & ig_2(W_\mu^1 - iW_\mu^2) \\ ig_2(W_\mu^1 + iW_\mu^2) & 2\partial_\mu - ig_2 W_\mu^3 + ig_1 B_\mu \end{pmatrix} \frac{1}{\sqrt{2}} \begin{pmatrix} 0 \\ v + h(x) \end{pmatrix}, \quad (2.17)$$

and carrying out a similar algebra for the hermitian conjugate $(\mathcal{D}_\mu \phi)^\dagger$ and calculating the contraction $(\mathcal{D}_\mu \Phi)(\mathcal{D}_\mu \Phi)^\dagger$ yields the effective Lagrangian[2]

$$\mathcal{L}_{eff} \supset \frac{1}{2}(\partial_\mu h)(\partial^\mu h) + \frac{1}{8}g_2^2 v^2 (W_\mu^{1^2} + W_\mu^{2^2}) + \frac{1}{8}(g_2 W_\mu^3 - g_1 B_\mu)(g_2 W^{\mu^3} - g_1 B_\mu)(v+h)^2. \quad (2.18)$$

Comparing the 2nd term to the Proca mass $m_W W_\mu W^\mu$, it is clearly seen that W_μ^1 and W_μ^2 have masses [3]

$$M_{W_{1,2}} = \frac{g_2 v}{2}. \quad (2.19)$$

Working on mass eigenstates is much illuminating. Rewriting W_μ^1 and W_μ^2 in terms of W_μ^+, W_μ^- and rewriting the last term of the Eq. 2.18 as a matrix

$$\mathcal{L}_{eff} \supset \frac{1}{4}g_2^2 v^2 (W_\mu^{+^2} + W_\mu^{-^2}) + \frac{v^2}{8} \begin{pmatrix} W_\mu^3 & B_\mu \end{pmatrix} \begin{pmatrix} g_2^2 & -g_2 g_1 \\ -g_2 g_1 & g_1^2 \end{pmatrix} \begin{pmatrix} W_\mu^3 \\ B_\mu \end{pmatrix}, \quad (2.20)$$

it is always possible to recover the hypercharge operator Y where B_μ is present. Thus, only if $Y_{\phi_0} \neq 0$, W^3 and B^μ mix. So the eigenvalues of the mass matrix become

$$\lambda_1 = 0, \qquad \lambda_2 = g_2^2 + g_1^2. \quad (2.21)$$

---

[1]The choice for index is immaterial, once one is chosen for a field excitation, others are gauged away all the same.

[2]The kinetic terms of gauge fields: $-\sum_i^3 \frac{1}{4} W_i^{\mu\nu} W_{\mu\nu}^i$ and $-\frac{1}{4} B^{\mu\nu} B_{\mu\nu}$ are omitted. The complete effective Lagrangian involves different kind of terms. But the essence of the Higgs mechanism is to compare the terms in $\mathcal{L}_{eff}$ to the mass terms of the initial theory; in that case, the Proca mass terms for each distinct vector boson.

[3]W_1, W_2 mix to form mass eigenstates W_μ^+, W_μ^-, whereas W_3 and B mix to form Z^μ and A^μ.

Having all the details brought to this point, the massless physical field is identified as photon A_μ, whereas the massive vector boson is called Z^0. In the diagonal basis, the mass eigenstates become

$$A_\mu = \frac{g_1 W_\mu^3 + g_2 B_\mu}{\sqrt{g_2^2 + g_1^2}}, \qquad Z_\mu = \frac{g_2 W_\mu^3 - g_1 B_\mu}{\sqrt{g_2^2 + g_1^2}}. \tag{2.22}$$

The SM includes a constant called the Weinberg angle, defined as $\frac{g_1}{g_2} = \tan\theta_W$, important for the mixing scale of the EW theory.

Finally, the photon remains massless since $U(1)_{\text{em}}$ is unbroken. And $SU(2)_L$ bosons acquire their mass as a result of the interaction with the Higgs field

$$m_A = M_\gamma = 0, \qquad M_Z = \frac{v}{2}\sqrt{g_2^2 + g_1^2}, \qquad M_{W^\pm} = \frac{g_2 v}{2}, \qquad \cos\theta_W = \frac{M_W}{M_Z}. \tag{2.23}$$

The mass of the Higgs field is obtained by comparison of the term in the effective Higgs potential to Klein-Gordon mass term, and is

$$m_h = 2\lambda v^2, \qquad \frac{g_2^2}{8M_W^2} = \frac{G_F}{\sqrt{2}} \longrightarrow v = \frac{1}{\sqrt{\sqrt{2}G_F}} \approx 246 \text{ GeV}. \tag{2.24}$$

Yukawa Couplings

Fermions acquire their masses in the same way as gauge bosons. As mentioned earlier, Dirac mass terms are not allowed since their chiral decomposition violates left-handed symmetry of the SM. To this end, a new kind of interaction with the Higgs field is required. Once evaluated in detail, a special interaction term between fermions and scalar sector is invariant under the SM gauge group $SU(2)_L \otimes U(1)_Y$

$$\mathcal{L}_{\text{Yuk}} = \bar{L}\Phi R + \bar{R}\Phi^\dagger L. \tag{2.25}$$

For instance, electron mass term corresponds to the following Yukawa interaction as

$$-y_e \left[\begin{pmatrix} \bar{\nu_{e_L}} & \bar{e_L} \end{pmatrix} \begin{pmatrix} \phi^\dagger \\ \phi^0 \end{pmatrix} e_R + \bar{e_R} \begin{pmatrix} \phi^{\dagger*} & \phi^{0*} \end{pmatrix} \begin{pmatrix} \nu_e \\ e_L \end{pmatrix} \right]. \tag{2.26}$$

Unfortunately, the conventional Higgs field is only useful for the lower components of $SU(2)_L$ doublets since the vacuum expectation value is chosen for the lower component of the Higgs field. After the symmetry is broken, effective electron Lagrangian becomes

$$\mathcal{L}_e = -\frac{y_e}{\sqrt{2}} v \bar{e}e - \frac{y_e}{\sqrt{2}} h\bar{e}e, \tag{2.27}$$

and the mass of electron is directly related to the Yukawa coupling y_e and to the vacuum expectation value similar to the case of the gauge bosons[1]

$$m_e = \frac{y_e}{\sqrt{2}} v. \tag{2.28}$$

---

[1]Since y_e is a free parameter, the mass of electron is not predicted in Higgs mechanism. The observation of a nonzero fermion mass implies that the electroweak gauge symmetry $SU(2)_L \otimes U(1)_Y$ is broken, but electroweak symmetry breaking is only a necessary, not a sufficient, condition for the generation of fermion mass. In the SM framework, new physics at an unknown scale must give rise to the Yukawa couplings.

For the upper components of doublets[1], an "alternative" Higgs doublet is promising as it obeys the symmetries of the SM.

$$\Phi^c = \begin{pmatrix} -\phi^{0*} \\ \phi^- \end{pmatrix} \longrightarrow \mathcal{L}_{\text{Yuk}}^{\text{upper}} = \bar{L}\Phi^c R + \bar{R}\Phi_c^\dagger L \qquad (2.29)$$

ends up with the masses of all the upper components fermions in the SM

$$y_f = \sqrt{2}\frac{m_f}{v}. \qquad (2.30)$$

Bare Dirac mass terms link the left-handed and right-handed fermions and thus violate the $SU(2)_L \otimes U(1)_Y$ gauge symmetry of the electroweak theory. If they persisted to arbitrarily high energies, such hard masses would destroy the renormalizability of the theory. That is why bare fermion masses were ruled out when electroweak theory was formulated.

Generalizing the Yukawa Lagrangian to include to all fermionic fields

$$\mathcal{L} = -\sum_{i,j} \left(Y_{ij}^d \bar{Q}_i^L \Phi d_j^R + Y_{ij}^u \bar{Q}_i^L \Phi^c u_j^R + Y_{ij}^l \bar{L}_i^L \Phi l_j^R \right), \qquad (2.31)$$

where the matrices $Y_{ij}^{u,d,l}$ are 3×3 structures within the framework of generation space of the SM. They need not be diagonal, as the fields associated with prime numbers represent eigenstates of the weak interaction, which do not necessarily align with the mass eigenstates. To express the Lagrangian using fields that correspond to mass eigenstates, the mass matrices are subjected to diagonalization via specific transformations, unique to each model, and given by

$$F_i^L = V_{ij}^{F,L} F_j^L, \qquad F_i^R = V_{ij}^{F,R} F_j^R. \qquad (2.32)$$

The mass eigenvalues after these specific transformations become

$$m_{F,i} = V_{ij}^{F,L} Y_{jk} V_{ki}^{F,L}. \qquad (2.33)$$

This results in the mixing of quark generations during interactions with W bosons. In contrast, the coupling between quarks and Z bosons involves fermions of the same type, maintaining a diagonal structure. Consequently, flavor-changing neutral currents (FCNC) do not occur at the tree level within the Standard Model. In the lepton sector, there is no analogous mixing matrix, provided we treat all generations of neutrinos as massless.

Finally, by comparing relative couplings of neutral current and charged current of the weak interactions; there has to be a parameter which scales to unity in the SM [28]

$$\rho = \frac{M_W^2}{M_Z^2 \cos\theta_W^2} = 1. \qquad (2.34)$$

Theoretically this parameter should remain fixed however, any shift from unity indicates physics beyond the SM. Finally, we note that the SM contains 25 free parameters:

- The parameters of the Higgs potential μ and λ;

- 12 Yukawa couplings related to the observed fermions masses (neutrinos are included due to the neutrino oscillations);

- 8 mixing angles from the PMNS and the CKM matrices [29];

- The fundamental gauge couplings (at tree level) g_1, g_2 and g_s.

---

[1]Yukawa terms are not supposed to be the source of neutrino masses. Nonetheless, none of the extensive theories have been approved as mass generation mechanism for neutrino masses because their masses have not been observed yet, though neutrino oscillations had proved they should have mass eigenstates.

2.2 The Shortcomings of the Standard Model and Open Problems

Despite its success, the SM has several known limitations. No theoretical mechanism explains the nature of the free parameters, hence the existence of these parameters in the SM framework remains a necessity for mathematical consistency and to fit experimental results, but their origins remain unexplained. Furthermore, although this will be discussed in more detail in the following chapters, the process of renormalization in quantum field theory has changed the interpretation of how fields interact differently depending on the measurement scale at which they are examined. Some of the major phenomena which have no valid explanation under the framework of the SM are

- **Dark Matter:** A hypothetical field called Dark Matter constitutes approximately 27% of the universe's mass-energy content [30] but remains undetected in terms of its fundamental particles due to its insensitiveness to $SU(3)_C \otimes SU(2)_L \otimes U(1)_Y$ gauge bosons. Yet it is assumed to interact with only massive fields via the Higgs channel. While candidates like weakly interacting massive particles (WIMPs) [31,32] and axion-like particles (ALPs) have been proposed [33,34], none are included in the Standard Model. The lack of observable interactions with standard particles challenges researchers to explore beyond the model, including theories such as supersymmetry (SUSY) or extra dimensions. The search for dark matter continues through various experimental efforts, including direct detection experiments and high-energy collider searches.

- **Baryon Asymmetry:** The universe is predominantly composed of matter, with the antimatter missing, a phenomenon that the Standard Model fails to account for due to insufficient CP violation [35]. Current models allow for CP-violating processes, but they do not produce enough asymmetry to explain the observed dominance of matter over antimatter. Proposed solutions include Grand Unified Theories (GUTs), which suggest the existence of heavy particles that could induce greater CP violation. Experimental searches for electric dipole moments and other processes aim to uncover new sources of CP violation, which may provide insights into this fundamental asymmetry.

- **Strong CP Problem:** The strong interaction appears to conserve CP symmetry with much higher precision than theoretical predictions suggest it should. This discrepancy is known as the strong CP problem [36,37]. Theoretical models predict a non-zero parameter, θ, in the QCD Lagrangian that would lead to significant CP violation, yet experimental measurements show it is consistent with zero. Proposed solutions include the introduction of new particles, such as axions, which could dynamically cancel the CP-violating effects.

- **Flavor-Changing Neutral Currents (FCNC):** FCNC occurs where a particle changes its flavor without altering its electric charge, typically mediated by neutral bosons like the Z boson. In the Standard Model, FCNCs are highly suppressed due to the Glashow-Iliopoulos-Maiani (GIM) mechanism, making their observation rare [38,39]. However, experimental results indicate that certain FCNC processes occur at rates higher than expected, challenging the predictions of the Standard Model. This anomaly suggests the possible existence of new physics, such as additional interactions

or particles that could enhance FCNC rates [40], prompting further investigation into flavor physics and the underlying symmetries that govern particle interactions.

- **Neutrino Masses:** In the Standard Model, neutrinos are treated as massless particles. However, experimental observations of neutrino oscillation—where neutrinos switch flavors—indicate they possess mass [41, 42]. This discrepancy suggests the need for extensions like the seesaw mechanism, which proposes the existence of heavy right-handed neutrinos that interact very weakly. The seesaw mechanism effectively explains the small masses of observed neutrinos, but it requires new physics beyond the Standard Model.

- **Rho Parameter:** The rho parameter in Eq. 2.34 is a measure of the strength of the weak interaction relative to the electromagnetic interaction [28]. In the context of the Standard Model, ρ is predicted to equal 1 at low energies due to the unification of the weak and electromagnetic forces. However, experimental measurements of ρ show deviations from unity, particularly in processes involving heavy vector bosons [43]. This discrepancy raises questions about the underlying symmetries of electroweak interactions and suggests potential new physics, possibly related to the dynamics of electroweak symmetry breaking or the existence of new particles that affect gauge boson interactions.

- **Fine-Tuning and Naturalness:** Certain parameters within the Standard Model, such as the Higgs mass and the cosmological constant, require careful tuning to match observed values rather than naturally occurring. This fine-tuning problem suggests an underlying principle or symmetry that could explain the observed values without the need for precise adjustments [44, 45]. On the other hand, the principle of naturalness posits that physical parameters should not require fine-tuning to be consistent with observations.

- **Quantum Gravity:** The quest for a theory of quantum gravity remains one of the most profound challenges in theoretical physics. While gravity is crucial to our understanding of the universe on large scales, it is not included in the Standard Model of particle physics. Quantum gravity seeks to unify gravity with these other forces, but doing so requires resolving several deep issues inherent in both quantum mechanics and general relativity. The central problem arises from the non-renormalizability of quantum gravity. In quantum field theory, forces are described by interactions mediated by particles, and these interactions are mathematically formulated through Feynman diagrams. Renormalization is the process of removing infinities that arise in loop diagrams (virtual particle exchanges) and making physical predictions finite and well-defined. The Standard Model is renormalizable, meaning that despite the infinities appearing in higher-order corrections, they can be systematically removed, allowing the theory to make precise, testable predictions. However, when we try to apply a similar quantum field theory approach to gravity, the situation changes dramatically. The gravitational interaction is mediated by the graviton, a hypothetical massless spin-2 particle, and the corresponding quantum field theory leads to severe problems. The loop corrections to graviton interactions result in infinite terms that cannot be removed by renormalization. This suggests that quantum gravity, as formulated through standard perturbative methods, is non-renormalizable — meaning the theory leads to uncontrollable infinities that cannot be tamed through the usual

techniques. This non-renormalizability implies that any perturbative approach to quantum gravity would break down at very high energies, such as near the Planck scale, where quantum gravitational effects are expected to become significant. The issue of non-renormalizability is one of the key reasons why a quantum theory of gravity has been so elusive. In fact, there is no consistent perturbative theory of quantum gravity that has been proven to yield finite results at all energy scales. This has motivated the search for alternative approaches [46–49] to quantum gravity that do not rely on conventional field-theoretic methods.

- **Gauge Hierarchy and Vacuum Stability:** Within the context of the naturalness, the hierarchy problem emerges prominently in particle physics, particularly concerning the Higgs boson mass. The mass of the Higgs field, approximately 125 GeV, is subject to significant quantum corrections from loop processes involving heavy particles. These corrections, which can diverge with high-energy scales, necessitate the introduction of a counterbalancing bare mass that must be finely adjusted to avoid yielding an effective mass far exceeding the observed value [50–52]. This situation implies an unnatural sensitivity of the Higgs mass to high-energy physics, leading to the hierarchy problem, where the question arises: why does the Higgs mass remain so much lighter than the scales associated with gravity or grand unification $\sim 10^{19}$ GeV? The apparent disparity suggests that a more profound mechanism must underlie the stability of the Higgs mass against these quantum corrections, pointing towards the potential need for new physics beyond the Standard Model.

  Concurrently, as one of the major aspect of this thesis, the vacuum instability issue presents an additional layer of complexity. The effective potential of the Higgs field, when analyzed at high energy, reveals that the potential can become unbounded from below as an inevitable outcome of renormalization, leading to a metastable vacuum state. If the Higgs mass were to receive large positive corrections, it could drive the system into a regime where the vacuum is destabilized, creating a scenario in which the universe transitions to a lower-energy state. This instability further underscores the unnaturalness associated with the Higgs mass, as it raises questions regarding the stability of the vacuum in the face of quantum fluctuations and high-energy physics. The intertwining of the hierarchy problem and vacuum instability thus highlights significant challenges within the Standard Model, emphasizing the necessity for a more comprehensive theoretical framework to address these profound issues.

Chapter 3

The Emergence of Vacuum Instability

In this section, only the essential part of renormalization scheme which causes to occurrence of vacuum stability problem will be discussed. Although there are several methods dedicated to underline numerous interpretations of renormalization aspects, we hereby stick with the most effective approach in order to describe the problem for which this thesis tries to offer possible remedies. To this end, we first describe the theoretical foundation of the problem in a comprehensive way, then highlight the motivation for new physics needed due to the SM falling short to insure vacuum stability.

3.1   The Unbounded Higgs Potential

The expression of the Higgs potential in the SM Lagrangian $\mathcal{L} = \mu^2 h^2 + \lambda h^4$ highlights a critical problem, as itself is sufficient to reveal mass terms in both bosonic and fermionic sectors. The late formalism of quantum field theory reveals that coupling strengths are scale dependent variables rather than constants of the observable spectrum. This aspect of QFT is known as renormalization flow. Propagator theory of QFT shows that each propagator (for fermions or bosons) brings divergent contributions in momentum space, which was initially thought as an analytical anomaly or unphysical consequence. Later, it had been revealed that infinities coming out from Feynman rules are simply our mathematical ignorance related to new physics that governs interactions at a different energy scale. Hence, the theoretical conditions set at the bare level are vulnerable to any imminent variation of the free parameters related to the SM and to the theories beyond the SM. To this end, the vacuum stability condition in the SM entails $V(\Phi)' > 0$, or equivalently, $\lambda > 0$ in Eq. 2.15.

The effective action $\Gamma[\Phi]$ is a functional that incorporates the effects of quantum corrections around a classical field configuration Φ. And it is defined as a functional integral over all field configurations

$$\Gamma[\Phi] = -\ln \int \mathcal{D}_\Phi e^{-S[\Phi]}, \tag{3.1}$$

where the $S[\Phi]$ is the classical action of the Higgs potential. Then fluctuations around a background field are considered as $\Phi(x) = \Phi_{\text{cl}}(x) + h(x)$ while Φ_{cl} and $h(x)$ represent classical background field and quantum fluctuation respectively. The effective action can

be expanded around the classical field configuration

$$\Gamma[\Phi_{\text{cl}}] = S[\Phi_{\text{cl}}] + \frac{1}{2} \int d^d x h \frac{\delta^2 S}{\delta \Phi^2} \Big|_{\Phi_{\text{cl}}} + \text{higher order terms.} \tag{3.2}$$

The effective potential $V_{\text{eff}}(\Phi)$ is the part of the effective action that depends on the field Φ but not on its derivatives. It can be extracted from the effective action by looking at the terms that are purely functions of the field

$$V_{\text{eff}}(\Phi) = \Gamma[\Phi]_{\text{no derivatives}}. \tag{3.3}$$

Or it can directly be calculated through path integral as

$$V_{\text{eff}}(\Phi) = -\frac{1}{TV} \ln \int \mathcal{D}_h e^{-S[\Phi_{\text{cl}}+h]}, \tag{3.4}$$

where T is the time extend and V is the three-dimensional volume of this region.

Using the functional method for renormalization scheme of the effective Higgs potential

$$\Gamma[\Phi] = \int [\mathcal{D}\phi]_\Lambda \exp\left(-\int d^d x \left[\frac{1}{2}(\partial_\mu \phi)^2 + \frac{1}{2}m^2\phi^2 + \frac{\lambda}{4!}\phi^4\right]\right), \tag{3.5}$$

where path integrals contain all possible field configurations up to cut-off momentum scale Λ

$$[\mathcal{D}\phi]_\Lambda = \prod_{|k|<\Lambda} d\phi(k),$$

and rescaling distance and momenta according to $k' = k/b$ and $x' = xb$, so that the variable k' is integrated over $|k'| < \Lambda$. Moreover, rewriting the effective action in Eq. 3.5 by simply shifting the field strength, the bare mass and the bare coupling respectively

$$\int d^d x \mathcal{L}_{\text{eff}} = d^d x \left[\frac{1}{2}(1 + \Delta Z)(\partial_\mu \phi)^2 + \frac{1}{2}(m^2 + \Delta m^2)\phi^2 + \frac{(\lambda + \Delta\lambda)}{4!}\phi^4 + \mathcal{O}(\phi^6)\right]. \tag{3.6}$$

Next, using the after effects of spontaneous symmetry breaking as $m^2 = \lambda v^2$ and $\phi = v + h$ in Eq. 3.6, and expanding the V_{eff} around the VEV

$$V_{\text{eff}}(h) = \frac{1}{2}(\lambda v^2 + \Delta m^2)(v^2 + 2vh + h^2) + \frac{\lambda + \Delta\lambda}{4!}(v^4 + 4v^3h + 6v^2h^2 + 4vh^3 + h^4), \tag{3.7}$$

where Δm^2 and $\Delta\lambda$ are quantum corrections, hence arise differently with respect to particle flavor that couples to the Higgs field h. Considering only the Higgs self-energy correction by using dimensional regularization yields

$$\Delta m^2 \sim \int \frac{d^4 k}{(2\pi)^4} \frac{1}{k^2 + m_H^2} \sim \frac{m_H^2}{64\Pi^2}(-\ln(m_H^2) + \frac{1}{\epsilon}), \tag{3.8}$$

where ϵ is a regularization parameter. Plugging the self-energy correction from one-loop back to the effective potential

$$V_{\text{eff}}^{1-loop}(h) = \frac{1}{64\pi^2}\left(h^2 \ln \frac{h^2}{\mu^2} - h^2 + \frac{(2\lambda v^2)^2}{\mu^2}\right). \tag{3.9}$$

Finally, we combine this with tree level expression

$$V_{\text{eff}}(h) = V_0(h) + V^{1-loop}(h) = \frac{\lambda}{4}(h^2 - v^2)^2 + \frac{3\lambda^2 v^4}{32\pi^2}(\ln\frac{2\lambda v^2}{\mu^2}) \tag{3.10}$$

in order to understand how the Higgs self-energy strength is scale dependent. The beta function describes how the coupling λ evolves with energy scale μ. It can be derived from the effective potential by looking at how the quartic coupling changes

$$\lambda(\mu) = \lambda + \frac{3\lambda^2}{16\pi^2}\ln\frac{\mu^2}{\mu_0^2} + \mathcal{O}(\lambda^3), \tag{3.11}$$

where $\mu_0 = 2\lambda v^2$. So, the beta function controlling the logarithmic scale dependence of the Higgs quartic coupling reads as

$$\beta_\lambda = \frac{d\lambda}{d\ln\mu} = \frac{1}{16\pi^2}(3\lambda^2) + \mathcal{O}(\lambda^3), \tag{3.12}$$

which is the 1-loop RGE for λ. This simplified result in pure scalar field theory shows that λ tends to increase as momentum increases over the entire spectrum. When combined with the negative contributions of fermions due to Fermi-Dirac statistics in the next step, the evolution of λ breaks the vacuum stability condition at a specific threshold, causing the Higgs potential to become unbounded from below. This unboundedness fundamentally means that there might be other minima, to which the so-called initial vacuum state can now transition. Consequently, this transition dictates that all massive states must decay since all massive fields acquire their masses through interactions with a particular value of the Higgs vacuum configuration.

As discussed above, the overall β-function that governs the dynamical nature of the Higgs quartic coupling receives corrections from all the fermions and gauge bosons of the Standard Model (SM). Hence, the loop corrections to the effective potential become significantly larger. Since the top quark is the heaviest of the SM fermions, it provides the largest correction compared to other flavors. Starting from the Yukawa Lagrangian

$$\mathcal{L}_{\text{t,Yuk}} = -y_t\bar{q}_L\Phi t_R + h.c., \tag{3.13}$$

adding to the effective potential from one-loop self-energy diagrams as

$$V_t(h) \sim \frac{1}{2}\int\frac{d^4k}{(2\pi)^4}\ln(k^2 + m_t^2) \quad\rightarrow\quad -\frac{3}{16\pi^2}m_t^4(\ln\frac{m_t^2}{\mu^2} + \gamma - \ln 4\pi - \frac{3}{2})$$

$$= -\frac{3y_t^4 v^4}{64\pi^2}\left(\ln\frac{y_t^2 v^2}{2\mu^2} + \gamma - \ln 4\pi - \frac{3}{2}\right). \tag{3.14}$$

Whereas the contributions of the gauge bosons to the effective potential are extracted from gauge covariant part of the kinetic Lagrangian

$$\mathcal{L}_{\text{gauge}} = (\text{contractions terms}) + |D_\mu\Phi|^2. \tag{3.15}$$

Additionally, there is also a contribution from Higgs field renormalization $h \rightarrow Z_h^{1/2}h_{\text{ren}}$ to Eq. 3.10 in the SM case. Combining all flavor corrections to the Higgs self-energy, we generate the one-loop effective potential

$$V_{\text{eff}}(h) = V_0(h) + V_\lambda(h) + V_{\text{top}}(h) + V_{\text{gauge}}(h), \tag{3.16}$$

17

$$16\pi^2 V_{\text{eff}}(h) = \frac{1}{4}\left(m^2 + \frac{\lambda}{2}h^2\right)^2\left(\ln\frac{m^2 + \frac{\lambda}{2}h^2}{\mu^2} + \gamma - \ln 4\pi - \frac{3}{2}\right)$$

$$+ \frac{3}{4}\left(m^2 + \frac{\lambda}{6}h^2\right)^2\left(\ln\frac{m^2 + \frac{\lambda}{6}h^2}{\mu^2} + \gamma - \ln 4\pi - \frac{3}{2}\right)$$

$$- \frac{3y_t^4 h^4}{4}\left(\ln\frac{y_t^2 h^2}{2\mu^2} + \gamma - \ln 4\pi - \frac{3}{2}\right)$$

$$+ \frac{3g_2^4 h^4}{32}\left(\ln\frac{g_2^2 h^2}{4\mu^2} + \gamma - \ln 4\pi - \frac{5}{6}\right)$$

$$+ \frac{3(g'^2 + g_2^2)^2 h^4}{64}\left(\ln\frac{(g'^2 + g_2^2)h^2}{4\mu^2} + \gamma - \ln 4\pi - \frac{5}{6}\right). \qquad (3.17)$$

The effective potential obeys the Callan–Symanzik(CS) equation [53]

$$\left(\mu\frac{\partial}{\partial\mu} + \sum_i \frac{\partial}{\partial\lambda_i} - \gamma\phi\frac{\partial}{\partial\phi}\right)V_{\text{eff}} = 0, \qquad (3.18)$$

where all the couplings in the effective potential are assumed $\lambda_i = \{\lambda, m^2, g', g_2, g_3, y_t\}$. A solution attempt starts from the leading order

$$-\mu\frac{\partial}{\partial\mu}V^{(1)} = \mathcal{D}^{(1)}V^{(\text{tree})}, \qquad \mathcal{D}^n = \sum_i \beta_i^{(n)}\frac{\partial}{\partial\lambda_i} - \gamma^{(n)}\phi\frac{\partial}{\partial\phi}. \qquad (3.19)$$

Using the effective Higgs potential in Eq. 3.17 in the expression above, we arrive at

$$16\pi^2\mathcal{D}V^{(\text{tree})} = \frac{1}{2}\left[4m^4 + 2m^2\lambda h^2 + \frac{1}{48}\left(16\lambda^2 - 144y_t^4 + 18g_2^4 + 9(g'^2 + g_2^2)^2\right)h^4\right]. \qquad (3.20)$$

Comparing the coefficients of quadratic and quartic terms of h to the right hand side of Eq. 3.19 respectively, the following results are obtained

$$16\pi^2(\beta_{m^2}^{(1)} - 2m^2\gamma^{(1)}) = 2m^2\lambda,$$

$$16\pi^2(\beta_\lambda^{(1)} - 4\lambda\gamma^{(1)}) = \frac{1}{4}(16\lambda^2 - 144y_t^4 + 9g'^4 + 18g'^2g_2^2 + 27g_2^4). \qquad (3.21)$$

Lastly, the anomalous dimension term reads

$$16\pi^2\gamma^{(1)} = \frac{1}{4}(12y_t^2 - 3g'^2 - 9g_2^2). \qquad (3.22)$$

Putting everything together, the β function of the Higgs quartic coupling adding to the total renormalization group equation(RGE) can be extracted as

$$\frac{d\lambda(\mu)}{d\ln\mu} = \frac{1}{16\pi^2}\left[4\lambda^2 + 12\lambda y_t^2 - 36y_t^4 - 9\lambda g'^2 - 3\lambda g_2^2 + \frac{9g_2^2}{4} + \frac{9g'^2 g_2^2}{2} + \frac{27}{4}g'^4\right]. \qquad (3.23)$$

For the convention we choose throughout this thesis, we use the $SU(5)$ normalization scheme which relates the hypercharge gauge coupling to g_1 as $g_1 = \sqrt{5/3}g'$. Additionally, it will be more instructive to recover color factor to Yukawa couplings in RGE level

$$\frac{d\lambda(\mu)}{d\ln\mu} = \frac{1}{16\pi^2}\left[12\lambda^2 + 2N_c\lambda y_t^2 - N_c y_t^4 - \frac{9\lambda g_1^2}{5} - 9\lambda g_2^2 + \frac{27g_1^4}{200} + \frac{9g_2^4}{8} + \frac{9g_1^2 g_2^2}{20}\right]. \qquad (3.24)$$

The model-independent general method for calculating the β-function coefficients of gauge couplings in both SUSY and non-SUSY model yields, at one-loop level [54]

$$\frac{dg}{d\mu} = -\frac{g^3}{(4\pi)^2}\left(\frac{11}{3}C_2(G) - \frac{4}{3}\kappa S_2(F) - \frac{1}{6}\eta S_2(S)\right). \tag{3.25}$$

In this context, C_2 denotes the quadratic Casimir invariants associated with the gauge multiplets (G) as

$$C_2(G) = \begin{cases} 0 & \text{for } U(1), \\ N & \text{for } SU(N), \end{cases} \tag{3.26}$$

whereas the Casimir invariants associated with the SM multiplets are given by the relation $C_2(G) = \frac{N^2-1}{2N}$ [55]

$$\begin{aligned}
C_R^3(i) &= \begin{cases} \frac{4}{3} & \text{for } \Phi_i = Q, \bar{u}, \bar{d}, \\ 0 & \text{for } \Phi_i = L, \bar{e}, H \end{cases} \\
C_R^2(i) &= \begin{cases} \frac{3}{4} & \text{for } \Phi_i = Q, L, H, \\ 0 & \text{for } \Phi_i = \bar{u}, \bar{d}, \bar{e} \end{cases} \\
C_R^1(i) &= \frac{3Y_i^2}{5} \quad \text{for each } \Phi_i \text{ with weak hypercharge } Y_i.
\end{aligned} \tag{3.27}$$

The terms $S_2(F)$ and $S_2(S)$ represent the Dynkin indices for the representations of fermions and scalars.

$$S_2(R) \equiv S(R) = \begin{cases} \frac{3}{5}Y_{\Phi_i}^2 & \text{for } U(1), \\ \frac{1}{2} & \text{for } SU(N). \end{cases} \tag{3.28}$$

The parameter κ takes the value 1 for Dirac fermions and $\frac{1}{2}$ for Weyl fermions, while η is equal to 1 for real scalar fields and 2 for complex scalar fields. Consequently, U(1) contributions from all the SM multiplets are simply related to hypercharge numbers

$$\begin{aligned}
b_1 &= 0 + \frac{4}{3}\cdot\frac{1}{2}\cdot\left(\sum_{\text{fermions}}\frac{3}{5}Y_{\text{fermions}}^2\right) + \frac{1}{6}\cdot 2\cdot\left(\sum_{\text{scalars}}\frac{3}{5}Y_{\text{scalars}}^2\right) \quad [\text{for } U(1), C_2(G)=0] \\
&= \frac{2}{3}\cdot\sum_{\text{fermions}}\frac{3}{5}Y_{\text{fermions}}^2 + \frac{1}{3}\cdot\sum_{\text{scalars}}\frac{3}{5}Y_{\text{scalars}}^2 \\
&= \frac{2}{5}\left[(3\cdot 2)\cdot\left(\frac{1}{6}\right)^2 + (3\cdot 1)\cdot\left(-\frac{2}{3}\right)^2 + (3\cdot 1)\cdot\left(\frac{1}{3}\right)^2 + 2\cdot\left(-\frac{1}{2}\right)^2 + 1\cdot 1^2\right]N_f \\
&+ \frac{1}{5}\left[2\cdot\left(-\frac{1}{2}\right)^2\right]N_H \quad = \frac{4}{3}N_f + \frac{1}{10}N_H.
\end{aligned} \tag{3.29}$$

And for SU(2) representation, there are three multiplets which non-trivially transform

$$\begin{aligned}
b_2 &= \frac{2}{3}\cdot\frac{1}{2}[(3\cdot 1)+(1\cdot 1)]N_f + \frac{1}{3}\cdot\frac{1}{2}(1\cdot 1)N_H - \frac{11}{3}\cdot 2 \\
&= \frac{4}{3}N_f + \frac{N_H}{6} - \frac{22}{3}.
\end{aligned} \tag{3.30}$$

Lastly, only the SM quark triplets contribute to SU(3) gauge corrections

$$b_3 = \frac{2}{3}\cdot\frac{1}{2}(2+1+1) - \frac{11}{3}\cdot 3 = \frac{4}{3}N_f - 11. \tag{3.31}$$

19

N_H is the number of scalar doublets and N_f is the number of fermion generations. From the expression Eq. 3.25, the gauge β-functions are derived with the coefficients given in Eq. 3.29 - 3.31

$$\frac{dg_i(\mu)}{d\ln\mu} = \frac{1}{16\pi^2}b_i g_i^3, \tag{3.32}$$

where

$$\begin{pmatrix} b_1 & b_2 & b_3 \end{pmatrix}_{SM} = \begin{pmatrix} U(1)_Y & SU(2)_L & SU(3)_C \end{pmatrix}_{SM} = \left(\frac{41}{10}, -\frac{19}{6}, -7 \right). \tag{3.33}$$

As the last piece of RGE analysis, in order to show complete behavior of the Higgs quartic coupling up to cut-off scale Λ, we simply quote[1] the RGE part of Yukawa couplings [56]. Since the 3rd generation quarks are the heaviest contribution to the RG flow, we ignore the other generations as they contribute insignificantly

$$\begin{aligned}
\frac{dy_t^2(\mu)}{d\ln\mu^2} &= \frac{y_t^2}{16\pi^2}\left[\frac{(2N_c+3)}{2}y_t^2 + \frac{y_b^2}{3} - \frac{17}{20}g_1^2 - \frac{9}{4}g_2^2 - 8g_3^2 \right], \\
\frac{dy_b^2(\mu)}{d\ln\mu^2} &= \frac{y_b^2}{16\pi^2}\left[\frac{(2N_c+3)}{2}y_b^2 + \frac{y_t^2}{3} - \frac{9}{4}g_1^2 - \frac{9}{4}g_2^2 - 8g_3^2 \right]
\end{aligned} \tag{3.34}$$

. The Yukawa RGEs are completely independent from the Higgs sector in one-loop level and $SU(3)$ corrections significantly decrease overall strength of the Yukawa couplings as the cut-off scale gets larger. Taking into account all the uncertainties in the measurements of m_h, m_t, m_b and α_s, the scale where the SM fails is $\mu \simeq 10^{10}$ GeV, as seen in Fig. 3.1.
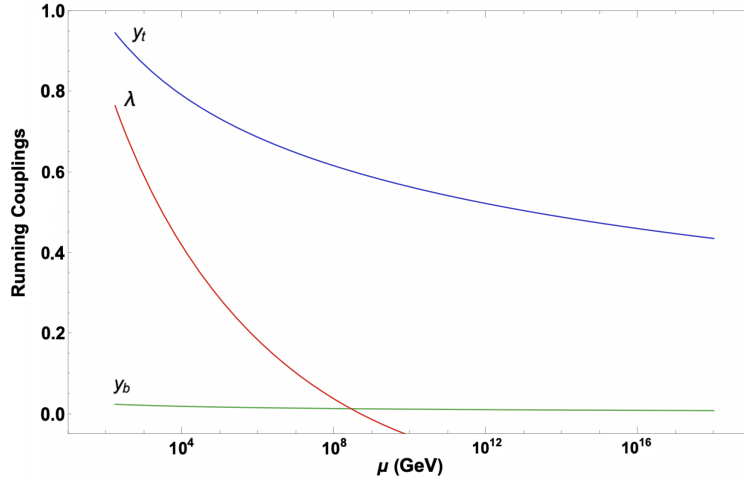
Figure 3.1: The RGE running of the top, bottom Yukawa and the SM Higgs quartic coupling. The initial conditions to set of coupled differential equations are set at $\mu_0 = m_t$.

3.2 Coleman-Weinberg Potential

An action $\Gamma(\phi, \psi, V^\mu, G^{\mu\nu})$ that reproduces all the physics of a full quantum theory when used at tree-level is called a 1PI (one-particle irreducible)[2] effective action. The 1PI effective

---

[1]The further sections of this work are dedicated to comprehensive analysis of RGE extension with new fields.

[2]A Feynman diagram is 1PI if all internal lines have some loop momentum going through them.

action can be computed by a matching procedure, which involves evaluating loops in the full theory and requiring that the effective action, when used at tree level, agrees order-by-order in perturbation theory with the full theory. This process effectively captures the effects of quantum corrections.

There is a direct connection between the "ordinary effective action" and the 1PI effective action. Starting with the ordinary effective action written around a background field ϕ_b with quantum fluctuations ϕ, integrating out ϕ leads to the 1PI effective action $\Gamma(\phi_b)$. If the background field ϕ_b is constant, the 1PI effective action can be expressed as

$$\Gamma(\phi_b) = -VTV_{\text{eff}}(\phi_b), \tag{3.35}$$

Quantum corrections are efficiently encoded in the effective potential as usual, which in this context, is also referred to as the Coleman–Weinberg potential [57].

As long as only 1PI graphs contribute to the effective action, one can shift the action to $S(\phi + \phi_b) - S'(\phi_b)\phi$, which eliminates all the tadpole terms from the Lagrangian. Then the effective action reads

$$e^{i\Gamma(\phi_b)} = e^{i\int d^4x\left(-\frac{1}{2}\phi_b\Box\phi_b - V(\phi_b)\right)}\int \mathcal{D}\phi \exp\left(i\int d^4x\left[-\frac{1}{2}\phi\Box\phi - \frac{1}{2}\phi^2 V''(\phi_b)\right]\right), \tag{3.36}$$

where only one-loop closed 1PI diagrams are included. This results is equivalently expressed as a Gaussian integral, which can be solved explicitly

$$i\Gamma[\phi_b] = \text{const.} \times e^{i\int d^4x\left(-\frac{1}{2}\phi_b\Box\phi_b - V(\phi_b)\right)}\frac{1}{\sqrt{\det\left(\Box + V''(\phi_b)\right)}}. \tag{3.37}$$

From the highest order in the exponent

$$\Gamma(\phi) = \int d^4x\left(-\frac{1}{2}\phi_b\Box\phi_b - V(\phi_b)\right) + \Delta\Gamma(\phi_b), \tag{3.38}$$

where

$$i\Delta\Gamma(\phi_b) = \ln\frac{1}{\sqrt{\det\left(\Box + V''(\phi_b)\right)}} + \text{const.} = -\frac{1}{2}\text{tr}\ln\left(\Box + V''(\phi_b)\right) + \text{const.} \tag{3.39}$$

This simplifies further as

$$\Delta\Gamma[\phi_b] = -\frac{1}{2}\int d^4x\langle x|\ln\left(1 + \frac{V''[\phi_b]}{\Box}\right)|x\rangle + \text{const.} \tag{3.40}$$

Next, assuming that ϕ_b is constant as mentioned earlier, $V''(\phi_b)$ becomes a function rather than a functional. By inserting a complete set of momentum states, we find

$$i\Delta\Gamma[\phi_b] = -\frac{1}{2}\int d^4x\int \frac{d^4k}{(2\pi)^4}\ln\left(1 - \frac{m_{\text{eff}}^2}{k^2}\right) + \text{const.}, \tag{3.41}$$

where m_{eff}^2 is the effective mass of the field. The spacetime integral is simply VT, which generates Eq. 3.35. On the other hand, the momentum integral is divergent. For scalar field theory, we follow Wick rotation $k^2 \to -k_E^2$ and impose a hard cutoff $k_E < \Lambda$ [58]. This yields

$$\Delta\Gamma(\phi_b) = -\frac{VT}{16\pi^2}\int_0^\Lambda dk_E k_E^3 \ln\left(1 + \frac{m_{\text{eff}}^2}{k_E^2}\right) + \text{const.}. \tag{3.42}$$

21

Evaluating this, we arrive at

$$\Delta\Gamma(\phi_b) = -\frac{VT}{128\pi^2}\left(2m_{\text{eff}}^2\Lambda^2 + 2m_{\text{eff}}^4\ln\frac{m_{\text{eff}}^2}{\Lambda^2} + \text{const.}\right). \tag{3.43}$$

Finally, using the connection Eq. 3.35, the 1PI effective potential becomes

$$V_{\text{eff}}(\phi_b) = V(\phi_b) + c_1 + c_2 m_{\text{eff}}^2(\phi_b) + \frac{m_{\text{eff}}^4}{64\pi^2}\ln\frac{m_{\text{eff}}^2(\phi_b)}{c_3}, \tag{3.44}$$

where c_i are divergent, regulator-dependent constants, but independent of ϕ_b.

In order to complete a general expression for one-loop CW potential, the statistics of the fields have to be taken into account according to the facts

- bosonic fields contribute positively,

- fermionic fields contribute negatively due to their Fermi-Dirac statistics,

- color factor for fermions: $N_c = 1$ for leptons and $N_c = 3$ for quarks,

- gauge bosons have polarization factor: $N_Z = 3$ and $N_{W^\pm} = 6$,

which are all counted in the final expression

$$V_{\text{eff}} = V_0(\phi) + \sum_i (-1)^{2s}\frac{n_i}{64\pi^2}m_{i,\text{eff}}^4(\phi)\left[\ln\left(\frac{m_{i,\text{eff}}^2}{\mu^2}\right) - c_i\right], \tag{3.45}$$

where s_i is the spin, n_i is the number of degrees of freedom, $m_{i,\text{eff}}$ is the field-dependent mass of the particle and c_i is a scheme-dependent constant[1].

Since it is a matter of interest throughout this work that RGEs will be constructed following the CW effective potential and the CS equation, we wish to regenerate the contributions from the top quark, the SM gauge bosons and the Higgs field in Eq. 3.17 by directly following Eq. 3.45.

The biggest contribution in the SM comes from the top quark as its Yukawa coupling is almost one. The relevant Lagrangian from the SM reads

$$\mathcal{L} = |D_\mu\Phi|^2 + m^2\Phi^2 + \lambda|\Phi|^4 + i\bar{Q}\slashed{\partial}Q + i\bar{t}_R\slashed{\partial}t_R + (y_t\bar{Q}\Phi^c t_R + \text{h.c.}). \tag{3.46}$$

After the spontaneous symmetry breaking, the effective masses become $m_{t,\text{eff}} = \frac{y_t h}{\sqrt{2}}$ and $m_{h,\text{eff}}^2 = -m^2 + 3\lambda h^2$ and also counting over 12 degrees of freedom for top quark (3 from colors and 4 components of Dirac spinor), CW effective potential becomes

$$V_{\text{eff}}(h) \supset -m^2 h^2 + \frac{\lambda h^4}{4} + \frac{(-m^2 + 3\lambda h^2)^2}{64\pi^2}\ln\left(\frac{-m^2 + 3\lambda h^2}{\mu^2}\right) - \frac{12}{64\pi^2}\left(\frac{y_t^2 h^2}{2}\right)^2\ln\left(\frac{\frac{y_t^2 h^2}{2}}{\mu^2}\right). \tag{3.47}$$

And the relevant EW Lagrangian

$$(D_\mu\Phi)^\dagger(D^\mu\Phi) = \frac{1}{2}(\partial_\mu h)^2 + \frac{v^2}{4}\left[g_2^2(W_\mu^+ W^{-\mu}) + \frac{(g_2^2 + g'^2)}{2}Z_\mu Z^\mu\right] + \cdots, \tag{3.48}$$

once again after spontaneous symmetry breaking, $m_{W,\text{eff}} = \frac{g_2^2 h^2}{4}$ and $m_{Z,\text{eff}}^2 = \frac{(g'^2 + g_2^2)h^2}{4}$. Additionally, counting over polarization states, $n_W = 6$ and $n_Z = 3$ in Eq. 3.45, we recover the last two lines in Eq. 3.17.

---

[1] $c_i = 3/2$ for fermions and scalars and $c_i = 5/6$ for gauge bosons in $\overline{MS}$-scheme

3.3 Zero-Temperature Vacuum Transition
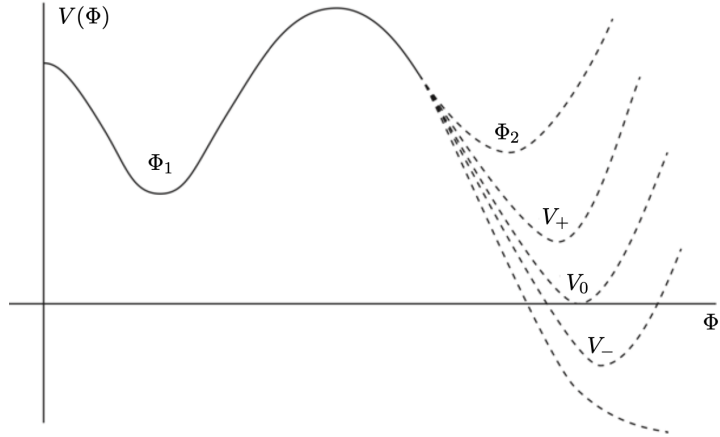
Figure 3.2: The configuration of the Higgs potential with respect to various field scale Φ due to the running quartic coupling λ.

The decay of the false vacuum is inherently a quantum tunnelling phenomenon. The vacuum decay rate cannot be calculated in the usual Minkowski spacetime because tunneling processes are not classical; instead, they require analyzing the system in Euclidean spacetime where the Euclidean time $\tau = it$ and Euclidean coordinates are given $\eta^\mu = (\tau, x^1, x^2, x^3)$. The Euclidean action for the Higgs field $h(x)$ is given as

$$S_E(h) = \int d^4\eta \left[\frac{1}{2}(\partial_\mu h)^2 + V_{\text{eff}}(h) \right].$$ (3.49)

The solutions of the SM RGE indicates[1] if $V_{\text{eff}}(h) < 0$ for $h \gg v$, then the false vacuum $h = v$ is separated from a deeper vacua by a significant potential barrier. As a result, transitions from the EW vacuum to the true vacuum can only proceed through quantum tunnelling. In such scenarios, it becomes crucial to estimate the tunnelling timescale and compare it to the age of the Universe T_0. If the vacuum tunnels to a deeper minimum as the field occupies large field values $h \gg v$ as seen in Fig. 3.2, the tunnelling probability is given by the bounce configuration [59], driven by the instanton that mediates tunnelling. The bounce is a non-trivial, finite-energy solution to the Euclidean field equations of motion derived from $S_E(h)$. Specifically, the bounce describes the configuration of the field $h(\eta)$ that starts at the false vacuum, bounces through the potential barrier, and asymptotically returns to the false vacuum [60, 61].

The equation of motion is derived from $\frac{\delta S}{\delta h} = 0$

$$\frac{d^2h}{d\eta^2} + \frac{3}{\eta}\frac{dh}{d\eta} = \frac{\partial V_{\text{eff}}}{\partial h},$$ (3.50)

subject to the boundary conditions $\frac{dh}{d\eta}\big|_{\eta=0} = 0$ and $h(\eta \to \infty) = v_{\text{false}}$. The bounce action S_B determines the tunnelling rate because it quantifies the suppression of the transition

---

[1]For $h \gg m_h$, λ_{eff} determines the dominant scale of $V_{\text{eff}}(h)$ where the running of m^2 is negligible [56].

probability due to the field configuration having to climb over the potential barrier in $V_{\text{eff}}(h)$. The transition probability is given by

$$\Gamma \sim \Lambda_B^4 e^{-S_B}, \tag{3.51}$$

where Λ_B is the instability scale of the potential. Assuming the Universe's spacetime volume is dominated by its age, the nucleation rate per unit spacetime volume is given as [62]

$$dP_{\text{tunnel}} = M^4 e^{-S_B} dV. \tag{3.52}$$

For tunnelling solutions (bounce solutions), the Euclidean action is assumed to be $O(4)$-symmetric because the bounce represents a spherical configuration in $d = 4$ space. This means that the field h depends only on the radial coordinate η, hence Eq. 3.49 becomes the bounce action

$$S_B = 2\pi^2 \int_0^\infty d\eta \eta^3 \left[\frac{1}{2} \left(\frac{dh_B}{d\eta} \right)^2 + V_{\text{eff}}(h_B) \right]. \tag{3.53}$$

This calculation is typically performed numerically because of the nonlinear nature of the bounce equation, we simply use approximation in Ref. [63] without taking cosmological effects into account ($\Lambda_B < M_{\text{Pl}}$)

$$S_B = \frac{8\pi^2}{|3\lambda(\Lambda_B)|}. \tag{3.54}$$

The scale at which the bounce makes the transition from large field values to v_{false} is set by $\beta_\lambda = 0$ in Eq. 3.24. At the transition scale $\lambda = 0.008$, the transition rate reads [64]

$$P_{\text{tunnel}} = T_0^4 \mu^4 \exp \left(\frac{-8\pi^2}{3\lambda(\Lambda_B)} \right) \approx 10^{-1094}. \tag{3.55}$$

The lifetime of the vacuum is astronomically long, far exceeding the current age of the Universe (10^{10} years), ensuring that the vacuum remains metastable on cosmological timescales. However, the actual lifetime of the present EW vacuum depends on the future cosmological history, depending on whether the matter or dark energy dominance takes over. If the Hilbert-Einstein action δS_G is involved then the tunnelling rate is weakened [65]. It is estimated with cosmological data that the metastable v_{false} has lifetime $\tau_{\text{EW}} > 10^{300}$ years due matter dominance in the universe and further reaches to a lifetime of 10^{800} years if cosmological constant dominates [56].

The metastability of the Higgs vacuum highlights an intriguing aspect of the SM: while the electroweak vacuum may have a lifetime vastly exceeding the current age of the Universe, this does not imply absolute stability and the negativity of λ at high energies, signaling an incomplete theory. The issue originates from the behavior of the Higgs quartic coupling under renormalization group evolution as shown in Fig. 3.1. As the energy scale increases, λ runs due to quantum corrections, which are influenced by the interplay between gauge bosons, fermions, and the Higgs self-interactions. To address vacuum instability, new physics scenarios are required to modify the running of λ and ensure its positivity up to the Planck scale $M_{\text{Pl}} = 10^{19}$ GeV.

3.4 Constraints on Scalar Extensions beyond the Standard Model

The ρ Parameter

Although scalar extensions of the Standard Model offer a straightforward way to satisfy vacuum stability conditions when new scalar fields mix with the Standard Model Higgs, potentially affecting the renormalization group running in a positive direction, any choice of quantum numbers assigned to the new scalar fields is theoretically and experimentally constrained. In terms of the electroweak symmetry group $SU(2)_L \otimes U(1)_Y$ with n number of scalar fields(with heavy masses $M_{\mathrm{NP}} \gg M_Z$) with charge conserving Higgs structure, the ρ parameter reads [66]

$$\rho = \frac{[T_i(T_i + 1) - T_{3i}^2]v_i^2}{\sum_1^n T_{3i}^2 v_i^2}, \tag{3.56}$$

where T_i is weak isospin. The global fit for ρ parameter [67]

$$\rho_0 = 1.00031 \pm 0.00019. \tag{3.57}$$

For the SM with $n = 1$ and $Y = 1$, Eq. 3.56 reduces to Eq. 2.34. While, singlet and doublet scalar extensions of the SM are not generally constrained in terms of new vacuum expectation values, the ρ parameter for triplet and for larger scalar multiplets are heavily dependent of vacuum ratios $\tan\beta = v_{\mathrm{new}}/v$ [66].

Model	ρ	β_{max}
Singlet	1	none
2HDM	1	none
Real Triplet	$\sec^2\beta$	0.030
Complex Triplet	$2(3 - \cos 2\beta)^{-1}$	0.014

Table 3.1: Tree level contribution to ρ parameter in models with additional scalars.

Apart from the quantum number assignment to Eq. 3.56, there are also corrections to M_W from electroweak precision measurements[1], though there might be numerous choices for new scalar field assignments with Gell-Mann–Nishijima relation $Q = T_3 + Y$ [68], allowed by ρ parameter.

Unitarity

While tree-level unitarity is a straightforward check, new scalar fields are generally similar across different models, such as the Higgs singlet (HSM), Higgs triplet (HTM) or two Higgs doublet models (2HDM) because the dominant contributions to the scattering amplitudes arise from the quartic interactions of these models. At tree level, the fundamental requirement is that the scattering amplitudes must not exceed the unitarity bound of[2]

$$\mathcal{A} < 8\pi. \tag{3.58}$$

---

[1] Z_2 symmetry allows to treat bosonic and fermionic corrections separately from electroweak precision observables, though a detailed analysis discussed in the next chapters.

[2] The tree level unitarity constraint in the SM Higgs structure equivalently means $|\lambda| < 8\pi$. Nonetheless, new scalar models have their unique unitarity relations.

However, including higher loops, the contributions from loop corrections can potentially enhance or suppress the amplitudes depending on the couplings involved. The effective couplings may not remain constant due to renormalization group running, which introduces scale dependence. Thus, while the fundamental unitarity condition persists, the specific bounds on couplings could vary based on the field content and their interactions.

Cosmological Inflation

If the scalar fields are light and have implications for inflation or dark energy, constraints from cosmological observations need to be investigated. For instance, if a scalar field contributes to inflation, its potential should satisfy the slow-roll conditions [69], which typically involve conditions on the first and second derivatives of the potential

$$\epsilon \equiv \frac{M_P^2}{2}\left(\frac{V'}{V}\right)^2, \qquad \eta \equiv \frac{M_P^2}{2}\frac{V''}{V}. \tag{3.59}$$

The conditions $\eta, \epsilon < 1$ are part of the slow-roll approximation, which ensures that the scalar field rolls slowly down its potential during inflation. This slow rolling is necessary for generating the desired flatness of the potential, hence maintains inflation for an extended period. Accordingly, slow roll conditions have to be checked for each direction in field space (ϕ_i) with respect to corrections in effective potential level.

Chapter 4

Contribution of Vector-like Fermions to RGE

4.1 Introduction

Chiral fermions coupled to the Higgs field are generally believed to destabilize the electroweak vacuum, a well-established idea in the Standard Model. However, this conclusion is not as absolute as it may seem, and in this chapter, we show that there are nuances to consider. Many extensions of the Standard Model introduce new fermions, and the central question we address here is how these additional fermions influence the stability of the Higgs vacuum, especially in light of the previous observation.

In this chapter, we derive a compact modification to the SM one-loop β-functions from vector-like fermions by following some of the analogous calculations in the SM. Such modifications to RG running of parameters allow to discuss the utility of stability portals by sticking with low-scale BSM mechanisms. The chirality of the fermions in the SM leads to distinct contributions to quantum corrections depending on whether a fermion is left-handed or right-handed. Vector-like fermions, on the other hand, transform in such a way that both the left- and right-handed components of the fermion field belong to the same representation of the gauge group. This symmetry between the two chiralities of the fermion significantly affects the structure of quantum corrections and the corresponding RGEs.

For a theory with vector-like fermions, the Coleman-Weinberg (CW) potential takes the form

$$V_{\text{CW}}^{\text{VLF}}(H) = -\frac{N_F}{64\pi^2} \sum_k n_{F_k} \left(M_{F_k}(\phi)^4 \left[\ln \frac{M_{F_k}(\phi)^2}{\mu^2} - \frac{3}{2} \right] \right). \tag{4.1}$$

Since the non-chiral structure of VLFs allow Dirac mass term M_D in Lagrangian, the field dependent VLF mass term in a decoupled nature from the SM fermions becomes

$$M_{F_k} = M_{D_k} + \frac{y_{F_k} v}{\sqrt{2}}, \tag{4.2}$$

where the statistical factors and fermion sectors are simply

$$N_F = (12, 4), \qquad F = (VLQ, VLL)$$
$$n_{F_1} \in (n_U, n_{L^0}), \qquad n_{F_2} \in (n_D, n_{L^-}). \tag{4.3}$$

We are particularly interested in how exactly the VLFs modify the running couplings at the RGE level. Since the one-loop analysis softly separates these modifications to the couplings, it is more comprehensive to work through the details by adopting the terminology of portals.

4.2 Gauge Portal

The new fermions modify the runnings of gauge couplings through kinetic term $\mathcal{L} \supset \bar{\psi} i \not{D} \psi$ [54]

$$\beta_{g_1} = \frac{g_1^3}{16\pi^2} \left[\sum_{F,\phi} \frac{2Y_F^2}{5} + \frac{Y_\phi^2}{5} \right]. \tag{4.4}$$

Both chiralities of VLFs contribute to the first term and introducing n_F as the fermion number in VLF multiplet, hence the corrections to hypercharge portal read

$$\delta b_1 = \frac{1}{5} G_2 G_3 n_F Y_F^2. \tag{4.5}$$

Similary, the weak gauge portal is simultaneously corrected with left- and right-handed components, hence removing the Higgs doublet correction in Eq. 3.30 and leaving only the VLF coefficient

$$\delta b_2 = \frac{4}{3} n_F G_2 S_2(G_2) \tag{4.6}$$

Finally, the SM quark is vector-like with respect to $SU(3)_C$, so the strong gauge portal is boosted in the same manner as the SM

$$\beta_{g_3} = \frac{g_3^3}{16\pi^2} \left(-\frac{11}{3} N_c + \frac{4}{3} n_F \right), \tag{4.7}$$

hence relevant contribution from a VLFs is only present for colored fields

$$\delta b_3 = \frac{4}{3} n_F G_3 S_3(G_3). \tag{4.8}$$

where G_i represent the dimensions of the representations under $SU(2)$ and $SU(3)$. For an energy scale larger than electroweak symmetry breaking $\mu > \mu_0 = v$, the running of gauge coupling at μ becomes

$$\alpha_i(\mu) = \frac{\alpha_i(\mu_0)}{1 + \alpha_i(\mu) b_i \ln\left(\frac{\mu}{\mu_0}\right)}, \tag{4.9}$$

Consequently, the gauge couplings run higher than the SM due to VLF corrections

$$\alpha_i(\mu) - \alpha_i^{SM}(\mu) = \delta b_i \ln\left(\frac{\mu}{\mu_0}\right) > 0. \tag{4.10}$$

This explains why the presence of vector-like fermions at energy scales larger than the EWSB scale helps stabilize the vacuum by shifting the running of the gauge couplings in a way that can prevent the electroweak vacuum from becoming unstable at high energies. Thus, the gauge portal mechanism at one-loop level, involving VLFs, plays a crucial role in improving the stability of the Standard Model vacuum.

4.3 Yukawa Portal

In order to construct β_{y_t}, we recall the formalism presented in Ref. [54]. The Goldstone bosons interacting with each Dirac fermion do not contribute to the β-function as they are not propagating dynamically (rather transferring degrees of freedom), and since we do not introduce a specific Yukawa interaction between Goldstone bosons and fermions, the self energy diagrams of fermions are insensitive to such fields. In terms of the remaining couplings and fields that correct the top Yukawa coupling, the renormalized fields and the wave function renormalization factors as a perturbation in y_t in leading order can be defined as

$$t_{L,R} = \sqrt{Z_{t_{L,R}}} t_{L,R}^{\text{ren}} \qquad y_t = Z_{y_t} y_{t_{\text{ren}}} \qquad h = \sqrt{Z_h} h_{\text{ren}}$$

$$\left[Z_{t_{L,R}} - 1 \right] = \Delta_{t_{L,R}} \frac{y_{t_{\text{ren}}}^2}{2} \qquad [Z_{y_t} - 1] = \Delta_{y_t} \frac{y_{t_{\text{ren}}}^2}{2} \qquad [Z_h - 1] = \Delta_h \frac{y_{t_{\text{ren}}}^2}{2}. \qquad (4.11)$$

The total Lagrangian in the top sector now reads

$$\begin{aligned}
\mathcal{L} \supset{} & \bar{t}_{\text{ren}} i\slashed{D} t_{\text{ren}} + \frac{1}{2}(D_\mu h)^2 - \left(\frac{y_{t_{\text{ren}}}}{2} h_{ren} \bar{t}_{\text{ren}} t_{\text{ren}} + h.c \right) + \frac{1}{2}(Z_h - 1)(D_\mu h)^2 \\
& + (Z_{t_{L,R}} - 1)\bar{t}_{L,R}^{\text{ren}} i\slashed{D} t_{L,R}^{\text{ren}} - \left(\frac{y_t^{ren}}{\sqrt{2}}(Z_{y_t}\sqrt{Z_h Z_{t_L} Z_{t_R}} - 1) h_{ren} \bar{t}_{\text{ren}} t_{\text{ren}} + h.c \right).
\end{aligned} \qquad (4.12)$$

For the last line, a new wave function renormalization factor can be defined as

$$(\mathbb{Z}_{y_t} - 1) = \left(Z_{y_t}\sqrt{Z_h Z_{t_L} Z_{t_R}} - 1 \right) = \left(\Delta_{y_t} + \frac{\Delta_h}{2} + \frac{\Delta_{t_L}}{2} + \frac{\Delta_{t_R}}{2} \right) \frac{y_{t_{\text{ren}}}^2}{2} = \delta_{y_t} \frac{y_{t_{\text{ren}}}^2}{2}. \qquad (4.13)$$

The overall one-loop correction to the top Yukawa is due to the Higgs two-point function (wave function renormalization of h_{ren}), the fermion two-point function (wave function renormalization of $t_{L,R}^{\text{ren}}$) and vertex correction respectively

$$-i\Sigma_h(p_h) = -i\frac{N_c y_{t_{\text{ren}}}^2}{16\pi^2} p_h^2 \left(\frac{1}{\epsilon} - \ln p_h - i\frac{\pi}{2} + \ln\sqrt{4\pi} - \frac{\gamma}{2} \right). \qquad (4.14)$$

The divergent term can be cancelled by the renormalization condition at $p_h = 0$,

$$i\Sigma_h(p_0) + i\Delta_h p_0^2 \frac{y_{t_{\text{ren}}}^2}{2} = 0, \qquad (4.15)$$

which gives

$$\Delta_h = -\frac{N_c}{8\pi^2} \left(\frac{1}{\epsilon} - \ln p_0 - i\frac{\pi}{2} + \ln\sqrt{4\pi} - \frac{\gamma}{2} \right). \qquad (4.16)$$

Thus the correction from the Higgs two-point function becomes

$$i\Sigma_h(p_h) + i\Delta_h \frac{y_{t_{\text{ren}}}^2}{2} p_h^2 = -i\frac{N_c y_{t_{\text{ren}}}^2}{16\pi^2} p_h^2 \ln\left(\frac{p_h}{p_0} \right). \qquad (4.17)$$

Next, the fermion two-point function yields

$$i\Sigma_{t_{L,R}}(p_t) = i\frac{y_{t_{\text{ren}}}^2}{32\pi^2} \slashed{p}_t \left(\frac{1}{\epsilon} - \ln\frac{p_t}{2} + \ln\sqrt{4\pi} - \frac{\gamma}{2} \right), \qquad (4.18)$$

similarly, the divergent term can be cancelled by using the condition

$$i\Sigma_t(p_0) + i\Delta_t p\!\!\!/_0 \frac{y_{t_{\mathrm{ren}}}^2}{2}, \tag{4.19}$$

hence it fixes

$$\Delta_{t_{L,R}} = -\frac{1}{16\pi^2}\left(\frac{1}{\epsilon} - \ln\frac{p_0}{2} + \ln\sqrt{4\pi} - \frac{\gamma}{2}\right). \tag{4.20}$$

Consequently, the fermion two-point function is renormalized as

$$i\Sigma_{t_{L,R}} + i\Delta_{t_{L,R}} p\!\!\!/_t \frac{y_{t_{\mathrm{ren}}}^2}{2} = -i\frac{y_{t_{\mathrm{ren}}}^2}{32\pi^2} p\!\!\!/_t \ln\left(\frac{p_t}{p_0}\right). \tag{4.21}$$

And the vertex contribution is proportional to

$$i\mathcal{V}(p_h) = i\frac{y_{t_{\mathrm{ren}}}^3}{16\sqrt{2}\pi^2}\left(\frac{1}{\epsilon} - \ln\frac{p_h}{2} + \ln\sqrt{4\pi} + \frac{1-\gamma}{2}\right). \tag{4.22}$$

Finally, the divergent term rising from vertex correction is to be absorbed by the condition

$$i\mathcal{V}(p_0) - i\Delta_{y_t}\frac{y_{t_{\mathrm{ren}}}^3}{2\sqrt{2}} = -\frac{iy_{t_{\mathrm{ren}}}^3}{16\sqrt{2}\pi^2}\ln\left(\frac{p_h}{p_0}\right), \tag{4.23}$$

which fixes

$$\Delta_{y_t} = \frac{3+2N_c}{16\pi^2}\left(\frac{1}{\epsilon} - \ln\frac{p_0}{2} + \ln\sqrt{4\pi} + \frac{1-\gamma}{2} - \frac{\ln 2}{3+2N_c}\right). \tag{4.24}$$

By combining all the corrections above, the top Yukawa is corrected at one-loop level as

$$y_t \supset y_{t_{\mathrm{ren}}} + \frac{y_{t_{\mathrm{ren}}}^3}{16\pi^2}\left(\frac{3+2N_c}{4}\right)\left(\frac{1}{\epsilon}\right). \tag{4.25}$$

For VLFs, both chiral states contribute to the top Yukawa corrections in each part, thus the top Yukawa β-function is proportional to

$$\beta_{y_t} \supset \frac{y_t^3}{16\pi^2}\left(\frac{3+2N_c}{2}\right). \tag{4.26}$$

Together with the well known result for $g_i^2 y_t$ contributions [56], y_t runs to smaller values than in the SM

$$\frac{y_t^2(\mu)_{\mathrm{NP}} - y_t^2(\mu)_{\mathrm{SM}}}{16\pi^2} \sim -\frac{y_t^2(\mu)}{16\pi^2}\left(\frac{17}{20}\delta b_1 g_1^2 + \frac{9}{4}\delta b_2 g_2^2 + 8\delta b_3 g_3^2\right)\ln^2\left(\frac{\mu}{\mu_0}\right) < 0. \tag{4.27}$$

This result shows that the effect of the top Yukawa on itself and on the Higgs quartic coupling becomes smaller as the energy scale increases, due to corrections to the gauge couplings by VLFs.

The manifestation of Yukawa portal is two-fold for VLFs. Either the SM fermions and VLFs directly couple in Lagrangian level $\mathcal{L} \supset -y_V\bar{\psi}_{\mathrm{SM}}H\psi_V$ or a VLF specific Yukawa connects left- and right-handed part of VLFs in decoupled nature $\mathcal{L} \supset -y_M\bar{\psi}_V H\psi_V$. Whereas the second option is only manifested at the RGE level due to the coupled nature of β-functions, the first one directly affects initial conditions according to mass splitting between the SM and VLF partners as well. For either of the these, the vertex contribution and the Higgs

two-point function are still given as in the first and the second term in Eq. 4.26 with the replacement: $y_t^3 \rightarrow y_{(M,V)}y_t^2$. The top Yukawa contribution in the Higgs two-point function is $2y_{(M,V)}\tilde{N}_c y_t^2$ where $\tilde{N}_c = 0, 1, 3$. For the second option with y_M, this term disappears as $\tilde{N}_c = 0$, disallowed by choice at Lagrangian level.

Despite the fact that g_2^2 and g_3^2 terms follow similar to the SM case, $y_{(M,V)}g_1^2$ is corrected by B_μ interaction with VLFs. Combining vertex correction, the Higgs two-point function and the fermion two-point function due to $U(1)_Y$ gauge field exchange and cancelling divergences from $y_M = Z_{y_M} y_{M_{\mathrm{ren}}}$

$$(Z_{Y_M} - 1) = -\frac{y_{M_{\mathrm{ren}}}}{16\pi^2}\left(\frac{9}{5}g_1^2(Y_H^2 + 2Y_{\mathrm{VLF}}^2)\right)\left(\frac{1}{\epsilon}\right). \tag{4.28}$$

Thus the hypercharge correction to β-function of VLFs reads

$$\beta_{y_M} \supset -\frac{y_M}{16\pi^2}\left(\frac{9g_1^2}{5}(Y_H^2 + 2Y_{\mathrm{VLF}}^2)\right). \tag{4.29}$$

Apart from the SM fermions and the Higgs contributions, VLF part of Yukawa RGE is given by

$$\frac{dy_M^2}{d\ln\mu^2} = \frac{y_M^2}{16\pi^2}\left((3 + 2G_2 G_3)y_M^2 - 6g_3^2 C_3(G_3) - 6g_2^2 C_2(G_2) + \frac{9}{20}g_1^2 Y_{\mathrm{VLF}}^2\right). \tag{4.30}$$

The loop contribution of VLFs to the Higgs quartic coupling is similar to that in the SM

$$\lambda \supset \lambda_{\mathrm{ren}} - \frac{2N_c y_{(M,V)}^4}{16\pi^2}\left(\frac{1}{\epsilon} + \text{finite terms}\right). \tag{4.31}$$

The fermion loop in any of the four legs of the quartic interaction is $\sqrt{\Sigma_h}$ and it gives

$$i\lambda_{\mathrm{eff}} \supset \frac{i\lambda}{p^2}4\Sigma_h, \tag{4.32}$$

and similar to the top Yukawa case in Eq. 4.17 we can write

$$\lambda(\mu) = \lambda(\mu_0) + \frac{4N_c\lambda y_{(M,V)}^2}{16\pi^2}\ln\left(\frac{\mu}{\mu_0}\right). \tag{4.33}$$

Hence we get the Yukawa contribution from VLFs to the beta function of the Higgs quartic coupling by combining these two results

$$\beta_\lambda^{VLF} = \frac{n_F}{16\pi^2}\left(4N_c y_{(M,V)}^2\lambda - 2N_c y_{(M,V)}^4\right). \tag{4.34}$$

The scale of the Yukawa portal alone is extremely effective on the Higgs quartic coupling, given that the balance between the quartic and quadratic Yukawa terms at the scalar RGE level is primarily determined by the initial conditions at low energy, μ_0. To this end, any possible mixing between the SM and new physics (NP) generally reduces the value of the initial conditions for the VLF Yukawa couplings, thereby opening up a region where $\lambda y_{M,V}^2 > y_{M,V}^4$ which improves the Higgs quartic running.

In the absence of a new scalar coupled to the SM Higgs field, rest of the direct effects

on the Higgs quartic coupling is due to the gauge portal. Since the Higgs is colorless, the shift from the SM due to the gauge portal is given as

$$
\begin{aligned}
\frac{\lambda_H^{NP}(\mu) - \lambda_H^{SM}(\mu)}{16\pi^2} \quad \approx \quad & \left[\frac{9}{40} g_1^2(\mu_0)[g_1^2(\mu_0) + g_2^2(\mu_0)]\delta b_1 \ln^2\left(\frac{\mu}{\mu_0}\right) \right. \\
+ \quad & \frac{3}{8} g_2^2(\mu_0)[g_1^2(\mu_0) + 3g_2^2(\mu_0)]\delta b_2 \ln^2\left(\frac{\mu}{\mu_0}\right) \\
+ \quad & \left. 16 y_t^2(\mu_0) g_3^4(\mu_0)\delta b_3 \ln^3\left(\frac{\mu}{\mu_0}\right) \right].
\end{aligned}
\tag{4.35}
$$

Since the right-hand side of Eq. 4.35 is always positive for scales beyond the EWSB, VLFs are natural candidates to stabilize the vacuum through the gauge and Yukawa portals, in addition to the widely used method involving the scalar portal. Consequently, in the following chapters, we will explore the impact of VLFs primarily on vacuum stability by introducing viable new physics representations within the hierarchy of the SM gauge symmetry.

Chapter 5

Vector-like Quarks in the Higgs Singlet Model

5.1   Introduction

Ever since the Higgs boson was discovered at the CERN Large Hadron Collider (LHC), confirming at last the last remaining puzzle of the Standard Model (SM) [4], the observed mass of the Higgs boson combined with the mass of the top quark, m_t, have caused concern because, as the theory stands, it violates stability of the electroweak vacuum [70]. In the SM there is a single Higgs h with effective potential characterized by two parameters only, the Higgs (mass)^2, κ^2 and its self coupling λ, $V = \kappa^2 h^2 + \lambda h^4$. The self-coupling λ can become negative at larger scales, so the potential becomes unbounded from below, and there is no resulting stability. Theoretical considerations indicate that if the validity of the SM is extended to M_{Planck}, a second, deeper minimum is located near the Planck scale such that the electroweak vacuum is metastable, i.e., the transition lifetime of the electroweak vacuum to the deeper minimum is finite with lifetime $\sim 10^{300}$ years [56].

If the electroweak vacuum is metastable then Higgs cannot play the role of inflaton [71]. Explanations involving a long lived-universe, where vacuum instability is not important, were proved to be faulty. Without vacuum stability, fluctuations in the Higgs field during inflation and in the hot early universe would have taken most of the universe into an anti-De Sitter phase, yielding a massive collapse, and the expansion of the universe would never have occurred [72]. The result of this is that either the SM must be incorrect or flawed in some way [73], or at the very least, that new physics beyond the SM which alters the Higgs potential so that it enhances its stability must exist at higher energies. Thus extra degrees of freedom are needed for the SM to explain the inflation of the Universe [71, 74, 75].

Minimal extensions of the SM which stabilize the Higgs vacuum are the most common theories which attempt to solve the Higgs mass problem. The correlation between the Higgs mass and vacuum stability is highly dependent on bosonic interactions. For instance, a model [76] with two Higgs doublets and large soft Higgs mass terms, satisfying the electroweak symmetry breaking conditions, has a stable vacuum and decay branching ratios that are very close to the SM ones, and this only one example.

The question remains if models with additional fermions, present in most beyond the SM

scenarios, can survive stability constraints, and if so, what are the restrictions imposed on their masses and mixing (if any) with the SM particles. To investigate how the hierarchy problem may be fixed, and what are the implications for vacuum stability, one could proceed by assuming a theory which supersedes the SM emerging at higher energies, such a supersymmetry. (Note however that minimal supersymmetry has its own difficulties with accommodating a Higgs boson of mass 125 GeV.) Or one could study the effect of adding particles to the SM, coupled in the simplest way, and investigate the conditions on their masses and couplings as emerging from vacuum stability conditions, as a simple and elegant way to obtain information about new particles and interactions without assuming complicated frameworks. The latter is the approach we wish to follow in this article, and we investigate inclusion of one additional generation of vector-like fermions, *i.e.*, fermions whose left-handed and right-handed components transform the same way under $SU(3)_c \times SU(2)_L \times U(1)_Y$. Unlike sequential fourth-generation quarks, which are ruled out by the one-loop induced Higgs production and decay mechanisms (the gluon fusion production and diphoton decay of the Higgs) [77], indirect bounds on vector-like quarks are much weaker. In particular, vector-like fermions can acquire a large Dirac mass without introducing a large Yukawa coupling to the Higgs.

Vector-like fermions appear in the context of many models of New Physics [78]. In warped or universal extra dimensional models, vector-like fermions appear as KK excitations of bulk fields [79], in Composite Higgs models, vector-like quarks emerge as excited resonances of bound states that form SM particles [80, 81], in Little Higgs Models, they are partners of the ordinary fermions within larger group representations and charged under the group [82], and in non-minimal supersymmetric extensions of the SM, they can increase the Higgs mass through loop corrections without adversely affecting electroweak precision [83]. Vector-like coloured particles are consistent with perturbative gauge coupling unification and are often invoked to explain discrepancies in the data, such as the $t\bar{t}H$ anomaly [84]. Vector-like particles have been considered before in the context of stabilizing the vacuum of the SM in [85, 86], in the context of baryogenesis [87], to account for the anomalous magnetic moment of the muon and discrepancies in the W boson mass [88], and to help explain the observed excess at 750 GeV [89, 90]. However, only particular representations have been considered [91], and a complete interplay of all possible vector-like quark representations and the SM does not exist at present. We redress this here, and analyze the restrictions on the masses and mixing angles for the all anomaly-free representations of vector-like quarks, as well as the associated boson field which is added to the SM for vacuum stabilization. In addition, we test the effects and restrictions induced by the vector-like fermions on the electroweak precision observables, $\mathbb{S}, \mathbb{T}$ and $\mathbb{U}$.

This chapter is organized as follows: In Sec. 5.2 we outline briefly the Higgs singlet model by giving the experimental and the theoretical constraints on the parameter space, then we will discuss the results of RGEs by showing how an additional scalar comes as a remedy to vacuum instability in the SM. In Sec. 5.4, we introduce all anomaly-free vector-like quark representations, their interaction Lagrangians, and derive their masses and mixing angles (assumed to be with the third generation quarks only). We then proceed to analyze the effects on vacuum stability of introducing singlet, doublet and triplet representations in Sec. 5.6, and give the expressions and analyze the effects of the additional fields on the electroweak precision observables in Sec. 5.7. We conclude in Sec. 5.8, and leave the relevant RGEs for the models studied to the Appendix (see appendix. A).

5.2 Higgs Singlet Model

In this section, we first consider the simplest remedy to the stability problem by extending the particle content of the SM by an extra real singlet scalar boson χ with its VEV u

$$\chi = (u + \chi_0),\tag{5.1}$$

which interacts solely with the SM Higgs, and we examine the constraints placed on its mass and its mixing angle with the SM Higgs boson on experimental and theoretical grounds. We leave Higgs vacuum stability condition, the main motivations of this work, to be analyzed in detail in the last discussion in this chapter. The addition of a boson provides a positive boost to the coupling parameter, counteracting the effect of the top quark and contributing towards repairing the Higgs vacuum stability [92].

We impose a Z_2 symmetry on the model, thereby eliminating the linear and cubic terms in χ and the most general renormalizable potential involving the SM Higgs doublet H and the singlet χ reads

$$V(\Phi, \chi) = -\kappa_H^2 \Phi^\dagger \Phi + \lambda_H (\Phi^\dagger \Phi)^2 - \frac{\kappa_S^2}{2}\chi^2 + \frac{\lambda_S}{4}\chi^4 + \frac{\lambda_{SH}}{2}(\Phi^\dagger \Phi)\chi^2.\tag{5.2}$$

After symmetry breaking, the minimization condition for the Higgs doublet reads

$$\frac{\partial V(\Phi, \chi)}{\partial \Phi^\dagger} = -2\kappa_H^2 \Phi + 4\lambda_H (\Phi^\dagger \Phi)\Phi + 2\lambda_{HS}\chi^2 \Phi = 0,\tag{5.3}$$

then substituting $\Phi = \frac{1}{\sqrt{2}}\begin{pmatrix} 0 \\ v + h \end{pmatrix}$, we get the first tadpole condition

$$-2\kappa_H^2 v + 2\lambda_H v^3 + \lambda_{HS}vu^2 = 0 \quad \longrightarrow \quad \kappa_H^2 = \lambda_H v^2 + \frac{\lambda_{SH}u^2}{2}.\tag{5.4}$$

Similarly, minimization with respect to χ and substituting $\chi = u + \chi_0$, gives the second tadpole condition

$$-\kappa_S^2 u + \lambda_S u^3 + \lambda_{HS}v^2 u = 0 \quad \longrightarrow \quad \kappa_S^2 = \lambda_S u^2 + \lambda_{SH}v^2.\tag{5.5}$$

Plugging these conditions back into the tree level potential $V(\Phi, \chi)$, the tadpole terms in h and χ_0 vanish (by definition of VEVs), and the potential now has only quadratic and higher-order terms in the fluctuations

$$V(h, \chi_0) = \frac{1}{2}m_h^2 h^2 + \frac{1}{2}m_\chi^2 \chi_0^2 + \frac{1}{2}(h\ \chi_0)\mathcal{M}_{H,S}\begin{pmatrix} h \\ \chi_0 \end{pmatrix},\tag{5.6}$$

where the mass matrix is given by

$$\mathcal{M}_{H,S} = \begin{pmatrix} 2\lambda_H v^2 & \lambda_{SH}vu \\ \lambda_{SH}vu & 2\lambda_S u^2 \end{pmatrix},\tag{5.7}$$

and the mass eigenvalues according to the mixing between the Higgs field and singlet scalar become

$$m_{H,S}^2 = \lambda_H v^2 + \lambda_S u^2 \mp \sqrt{(\lambda_S u^2 - \lambda_H v^2)^2 + \lambda_{SH}^2 u^2 v^2}.\tag{5.8}$$

Finally, the eigenvectors are simply given as

$$
\begin{pmatrix} H \\ S \end{pmatrix} = \begin{pmatrix} \cos\varphi & \sin\varphi \\ -\sin\varphi & \cos\varphi \end{pmatrix} \begin{pmatrix} \Phi \\ \chi \end{pmatrix}.
\tag{5.9}
$$

As in the SM, we require $\lambda_H > 0$ for a stable SM vacuum, and $\lambda_S > 0$ for the new particle. In addition we impose that the potential is positive for asymptotically large values of the fields,

$$
\lambda_H > 0, \qquad 0 < \lambda_S < 4\pi, \qquad |\lambda_{SH}| > -2\sqrt{\lambda_S \lambda_H}.
\tag{5.10}
$$

In addition we require that λ_{SH} is perturbative, thus bounded by $|\lambda_{SH}| > 4\pi$. The quartic couplings can be expressed in terms of the physical masses as

$$
\begin{aligned}
\lambda_H &= \frac{m_H^2 \cos^2\varphi + m_S^2 \sin^2\varphi}{2v^2}, \\
\lambda_S &= \frac{m_S^2 \cos^2\varphi + m_H^2 \sin^2\varphi}{2v^2}, \\
\lambda_{SH} &= \frac{m_S^2 - m_H^2}{2uv} \sin 2\varphi.
\end{aligned}
\tag{5.11}
$$

Here λ_H and λ_S are the quartic self-couplings of Φ and χ, and λ_{SH} the coupling describing their mixing with m_H, m_S (v, u) are the masses (VEVs) of the physical fields, respectively and φ their mixing angle.

The additional scalar is subjected to constraints from particle physics and cosmology [93, 94]. If the additional scalar is heavier than the Higgs boson at 125 GeV, in HSM the decay channel $S \to HH$ may exist, and act as an extra constraint for the mixing regime. The ρ parameter and its deviation from unity play an important role in measuring the effects of new physics on the masses of electroweak gauge bosons. Corrections to the mass of W-boson originate from the Higgs mediated loops, which enhance gauge boson self-energies, and these are dependent on the masses and the mixing between the scalar fields [95]. In the case where the heavier of the two scalars is the mostly-singlet S with $m_S \geq 125$ GeV, the mixing angle $\sin\varphi$ agrees with theoretical predictions up to 1σ. Although the region for ΔM_W[1] is less restricted compared to the other case (where m_H=125 GeV), this scenario is disfavoured by collider bounds and Higgs data. If the lighter scalar corresponds to the SM Higgs boson with m_H=125 GeV, larger heavy singlet scalar masses impose smaller mixing angles between the two scalars in order to fit ΔM_W to 1σ level. The minimum scale for the mass of heavier scalar in this work is at least 500 GeV, which in return, corresponds to $\sin\varphi$=0.37 due only to the constraint on ΔM_W.

The bounds on HSM are also constrained by electroweak precision observables (EWPO). The singlet scalar contributes to the gauge boson self-energy diagrams at loop level, generating a shift in the oblique parameters S, T, U [97]. Checking the results from EWPO fit [98] by taking into account only the deviation of the oblique parameters with respect to the SM [96], Fig. 5.1 shows that, for values of m_S below 1 TeV, the restrictions from the bounds from Higgs signal strength are stronger than those from EWPO. For the case considered in this work, where $m_S \leq 2$ TeV, the parameter space corresponding to agreement between oblique parameters and the EWPO fit imposes an upper bound for $\sin\varphi < 0.4$

---

[1]Please note that in this work we assumed $M_W = 80.377 \pm 0.012$ GeV [96] and did not take into account the new CDF measurement, awaiting further conformation. Our results are thus more conservative.

around m_S=500 GeV. The effects arising from electroweak precision in HSM, at 1σ level [95] are consistent with our later considerations of S, T, U parameters in Sec. 5.7 which indicate that, for mass of the singlet Higgs at 1 TeV, the mixing angle must be $\sin\varphi < 0.2$ from the requirement of consistency of new physics with allowed deviations from the SM. These results are consistent with those in Fig. 5.7.
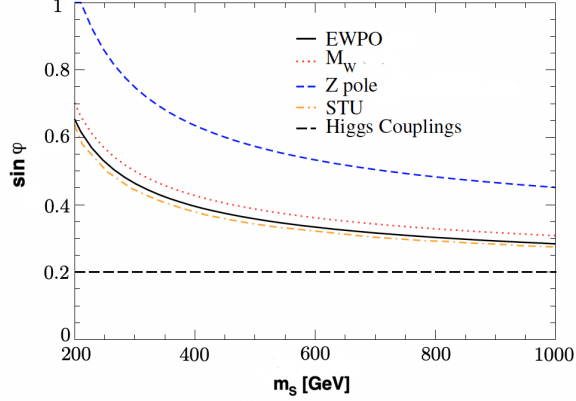
Figure 5.1: Allowed parameter space for the singlet scalar mass m_S and the maximum value of the mixing angle $\sin\varphi$ in HSM with respect to various constraints in HSM.

An additional theoretical bound comes from tree-level perturbative unitary. Two body scattering of scalars at tree level and loop effects to $SS \to SS$ and $HH \to HH$ partial decay widths were derived for HSM in [99–102]

$$a_0(HH \to HH)|_{s \gg m_H^2} = -\frac{3}{16}(\lambda_H \cos^4\varphi + \lambda_{HS} \sin^2\varphi \cos^2\varphi + \lambda_S \sin^4\varphi),$$

$$a_0(SS \to SS)|_{s \gg m_S^2} = -\frac{3}{16}(\lambda_S \cos^4\varphi + \lambda_{HS} \sin^2\varphi \cos^2\varphi + \lambda_H \sin^4\varphi). \quad (5.12)$$

Near the decoupling region $\sin\varphi \sim 0$, the condition $|a_0| < 1/2$ entails $\lambda_H, \lambda_S \leq \frac{8\pi}{3}$, or equivalently

$$m_S^2 \sin^2\varphi + m_H^2 \cos^2\varphi \leq \frac{8\pi\sqrt{2}}{3G_F}. \quad (5.13)$$

Near the decoupling region $\sin\varphi \sim 0$, unitarity alone puts a lower bound for $m_S \geq 700$ GeV and increases to 1 TeV from one-loop correction level, whereas otherwise m_S can be as large as 7 TeV. Additionally, $HS \to HS$ requires only $\lambda_{HS} \leq 8\pi$. But in general, perturbative unitarity generates a more flexible parameter space compared to other constraints.

The Higgs singlet also affects signal rates due to loop effects on the Higgs decay widths through the channels $H \to gg, \gamma\gamma$ at leading order. Previous analyses used various benchmark to test behaviours for different $\tan\beta$, defined as the ratio of the VEVs $\tan\beta = \frac{u}{v}$, and m_S scales [103]. The mixing between scalars ranges in the interval $\sin\varphi = (0.31-0.20)$, corresponding to $m_S = (200-800 \text{ GeV})$. The parameter space generated from the additional Higgs production channel $S \to HH$ is in agreement with $H \to VV$ (di-boson) decays for

37

$\sin \varphi \le 0.22$ in the mass range $m_S = (260 - 770 \text{ GeV})$, corresponding to the minimum of $BR(S \to HH) = 0.17$. The mixing is further constrained with increasing mass values of the Higgs singlet, $\sin \varphi \le 0.16$, for $m_S \le 1$ TeV [104].

Apart from the SM Higgs quartic coupling λ_H, the couplings λ_S and λ_{HS} from Eq. 5.2 are inversely proportional to $\tan \beta$, which yields $\lambda_i > 1$ at $\tan \beta \sim 1$, $m_S \ge 900$ GeV. So, λ_S and λ_{HS} reach the non-perturbativity region for small $\tan \beta$ values. Taking relatively larger VEV scales, the couplings are perturbative for $\tan \beta = 5, 10$, which correspond to the singlet VEV scales, $u = 1, 2$ TeV throughout our work. Fig. 5.2 shows the electroweak corrections to the production $gg \to H$ while Fig. 5.3 shows the decay $H \to \gamma\gamma$, indicating that the electroweak correction δ_{EW} becomes more consistent with the SM limit (blue line) as $\tan \beta$ becomes larger. For $\tan \beta = 10$, $u \sim 2$ TeV, δ_{EW} further tends to the SM scale, however, variations in $\sin \varphi$ become $\tan \beta$ suppressed.

Fig. 5.2 yields a strong constraint on the scalar mixing, because for electroweak deviations δ_{EW} to converge towards the SM limit, $\sin \varphi \le |0.2|$ at TeV scale. Electroweak constraints are more relaxed from diphoton decay Fig. 5.3. Deviations from the SM are not too severe on $\sin \varphi$ when $m_S \ge 800$ GeV. Clearly, as $\tan \beta$ becomes larger (and so does the singlet VEV u), the constraints obtained from $H \to$ diboson channels are satisfied for $m_S = \mathcal{O}(\text{TeV})$ scale. On the other hand, the region with small $\tan \beta$ in HSM is restricted from perturbativity and relatively larger δ_{EW} inconsistencies.
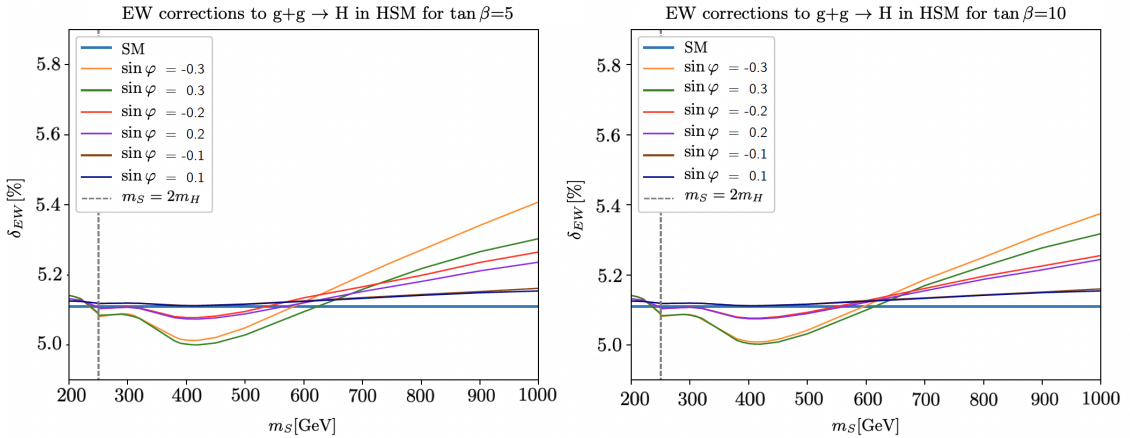
Figure 5.2: Electroweak corrections δ_{EW} to leading order of cross section of SM Higgs production via gluon fusion in HSM for different VEV ratios, $\tan \beta = \frac{u}{v} = 5, 10$, as a function of the additional singlet mass.

The production and decay channels of the singlet scalar are shown in Fig. 5.4 and Fig. 5.5, respectively. The processes $gg \to S$ and $S \to \gamma\gamma$ have no useful experimental bounds for extracting various constraints on HSM. However the corrections δ_{EW} are more dependent on the sign of $\sin \varphi$ than on $\tan \beta$. Similarly, smaller β values restrict the perturbativity of λ_S and λ_{HS} for $m_S \ge 900$ GeV.

Cosmological constraints on models with additional scalars are interested particularly in cases where the additional singlet is a dark matter candidate. Among the Higgs related dark matter (DM) portal studies, only the scalar portal is renormalizable. However, when it comes to scalar portals, the coupling between different scalars can take values in a relatively large interval. In HSM, λ_{HS} sets various constraints on the freezing temperature T_f at which
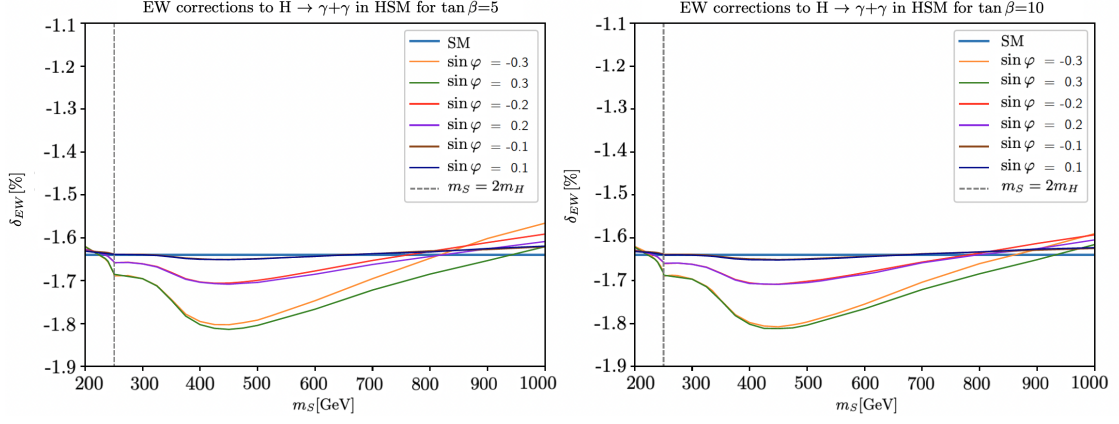
Figure 5.3: Electroweak corrections δ_{EW} to the partial decay width of the diphoton decay $H \to \gamma\gamma$ in HSM for different VEV ratios, $\tan\beta = \frac{u}{v} = 5, 10$, as a function of the additional singlet mass.
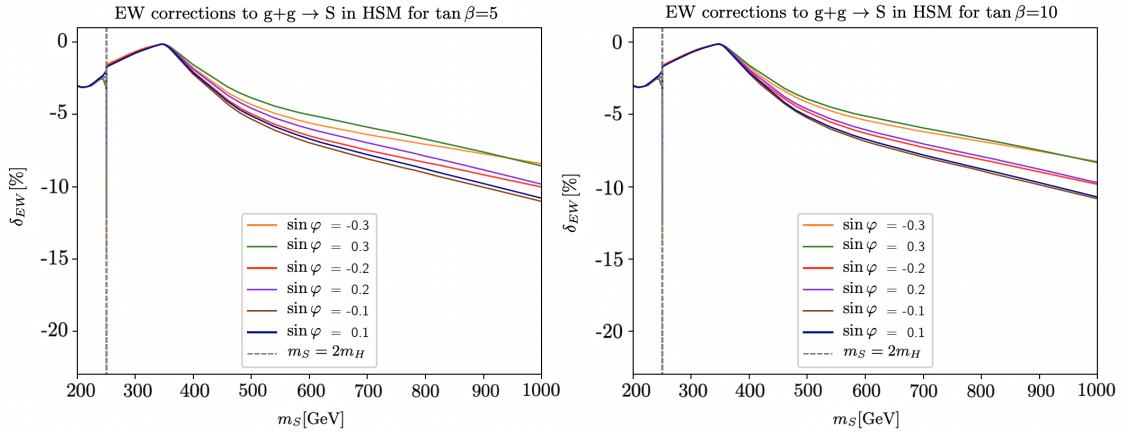
Figure 5.4: Electroweak corrections δ_{EW} to leading order of cross section of the singlet Higgs production via gluon fusion in HSM for different VEV ratios, $\tan\beta = \frac{u}{v} = 5, 10$, as a function of the singlet mass.
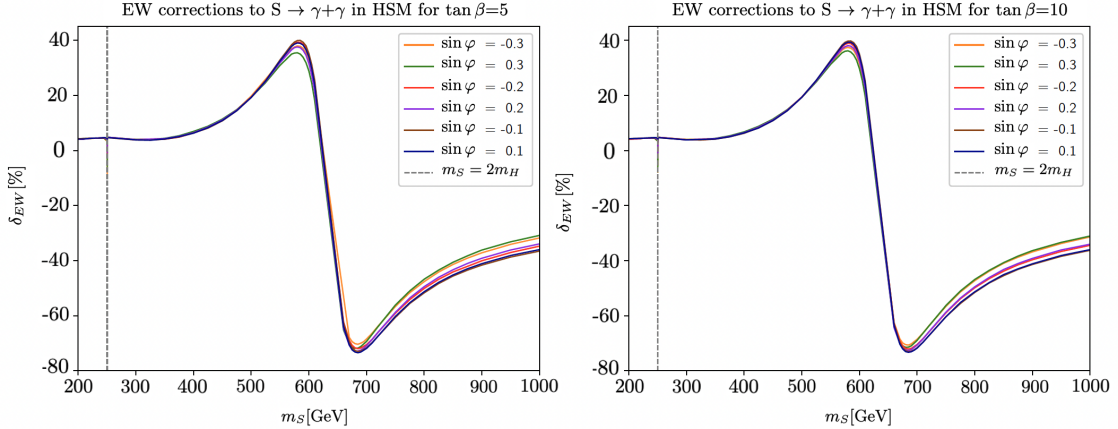
Figure 5.5: Electroweak corrections δ_{EW} to leading order of the partial decay width of the diphoton decay $S \to \gamma\gamma$ (bottom panel) in HSM for different VEV ratios, $\tan\beta = \frac{u}{v} = 5$, 10, as a function of the singlet mass.

DM decouples from cosmic heat reservoir [105]. Although additional DM candidates such as singlet fermions can be added to any theory in order to decrease extremely divergent characteristic of λ_{HS} in RGE level, mixing constraints are still in agreement with other constraints; m_S <1 TeV (without extra fermionic DM), and $200 < m_S < 300$ GeV (with extra fermionic DM) as the Universe cools down $T < T_f$ [106]. Furthermore, if the singlet VEV $u < 400$ GeV, $\tan\beta$ <2 in order to allow perturbativity of λ_{HS}; this is however outside the parameter region we considered. Electroweak vacuum stability is affected by the renormalization group equations for the coupling of λ_H to λ_{HS} in Eq. 5.23, hence the connection between coupling evolutions gives limited freedom to control the dependence of λ_{HS} on m_S. The combined cosmological constraints were explored within the GAMBIT framework [107], and they concluded that for $1 < m_S < 4$ TeV the singlet scalar portal only can account for the relic abundance. A more recent work [108] treats the electroweak stability problem by analyzing the HSM potential and transition probability of VEVs through radiation dominated era by an transcendental function of temperature. In accordance with the results of this work [108], m_S might have to extend to TeV scale to have a stable vacuum, though the exact lower value of m_S depends on the scale of λ_{HS}.

5.3   Coleman-Weinberg Potential

For any QFT, the CS equation describes how the effective action changes with energy scale. It expresses the dependence of the effective action on the renormalization scale, and in particular, it gives the equations that describe the running of the coupling constants. Similar to the SM case in Sec. 3.1, a possible derivation of RGEs is related to CW potential [109]. To this end, the field dependent masses in H and S directions have to be revealed after spontaneous symmetry breaking in terms of the bare couplings of the model and field statistics are to be counted in the CW potential. The field-dependent masses after symmetry breaking are generally computed by taking the second derivative of the effective potential with respect to the field at the vacuum $M_i^2(\phi_i) = \frac{\partial^2 V_{\text{eff}}(\phi_i)}{\partial \phi_i^2}|_{\phi_i=\phi_{i_0}}$. For the scalar sector, it

was already shown in Eq. 5.7

$$
\begin{pmatrix} \partial_h^2 V_{\text{eff}} & \partial_h \partial_\chi V_{\text{eff}} \\ \partial_h \partial_\chi V_{\text{eff}} & \partial_\chi^2 V_{\text{eff}} \end{pmatrix}_{v,u} = P \mathcal{M}(M_H^2, M_S^2)_{\text{Diag}} P^{-1},
\tag{5.14}
$$

where P is a bi-unitarity matrix that orthogonally diagonalizes the mass matrix in Eq. 5.7. The field dependent masses of the gauge bosons are same as the SM case since the kinetic portal is not changed with the additional scalar. Furthermore, the SM Yukawa terms are still given with respect to the Higgs VEV. Hence, one-loop corrections to the CW potential in H direction becomes

$$
\begin{aligned}
V^{(1)}(H)|_v &= \frac{1}{64\pi^2} F_H^2 \left(\ln \frac{F_H}{\mu^2} - \frac{3}{2} \right) + \frac{3}{64\pi^2} F_G^2 \left(\ln \frac{F_G}{\mu^2} - \frac{3}{2} \right) \\
&+ \frac{3}{32\pi^2} F_W^2 \left(\ln \frac{F_W}{\mu^2} - \frac{5}{6} \right) + \frac{3}{64\pi^2} F_Z^2 \left(\ln \frac{F_Z}{\mu^2} - \frac{5}{6} \right) \\
&+ \frac{1}{64\pi^2} F_Q^2 \left(\ln \frac{F_Q}{\mu^2} - \frac{3}{2} \right) - \frac{3}{16\pi^2} F_T^2 \left(\ln \frac{F_T}{\mu^2} - \frac{3}{2} \right),
\end{aligned}
\tag{5.15}
$$

where

$$
\begin{aligned}
F_H &= -\kappa_H^2 + 2\lambda_H v^2, & F_G &= -\kappa_H^2 + \lambda_H v^2, & F_T &= \frac{y_t^2 v^2}{2}, \\
F_W &= \frac{g^2 v^2}{4}, & F_Z &= \frac{(g^2 + g'^2) v^2}{4}, & F_Q &= -\kappa_S^2 + \lambda_{HS} v^2,
\end{aligned}
\tag{5.16}
$$

and also in S direction

$$
\begin{aligned}
V^{(1)}(S)|_u &= \frac{1}{64\pi^2} P_S^2 \left(\ln \frac{P_S}{\mu^2} - \frac{3}{2} \right) + \frac{3}{64\pi^2} P_G^2 \left(\ln \frac{P_G}{\mu^2} - \frac{3}{2} \right) \\
&+ \frac{1}{64\pi^2} P_Q^2 \left(\ln \frac{P_Q}{\mu^2} - \frac{3}{2} \right),
\end{aligned}
\tag{5.17}
$$

where

$$
P_S = -\kappa_S^2 + 3\lambda_S u^2, \qquad P_G = -\kappa_H^2 + \lambda_{HS} u^2, \qquad P_Q = -\kappa_H^2 + \lambda_{HS} u^2.
\tag{5.18}
$$

All that remains is to find the beta functions for the scalar potential parameters. These are determined by requiring scale independence of the effective potential $V_{\text{eff}}(H, S) = V(H, S)^{(0)} + V(H, S)^{(1)}$ as

$$
\mu \frac{dV_{\text{eff}}(H, S)}{d\mu} = \mu \frac{dV(H, S)^{(0)}}{d\mu} + \mu \frac{dV(H, S)^{(1)}}{d\mu} = 0.
\tag{5.19}
$$

Differentiating the effective potential with respect to coupling constants is not a major issue. However, the derivative of the effective potential with respect to the renormalization scale μ will yield terms that depend on the scale μ including the explicit dependence of the couplings on μ from the loop integrals and counterterms. And anomalous dimension term γ_ϕ describes how the field itself scales with the renormalization scale μ. The anomalous dimension is computed from the field's contribution to the one-loop effective potential

$$
\gamma_\phi = \frac{1}{2} \frac{d \ln Z_\phi}{d \ln \mu},
\tag{5.20}
$$

41

where Z_ϕ is the field's wavefunction renormalization factor. Actually, $\gamma = \mathcal{O}(\lambda^3)$ as there are no propagator corrections to scalar two-point function at 1-loop. So the anomalous dimension for background scalar fields have to be included at 2-loop level as $\gamma^{(1,2)} = 0 + \mathcal{O}(\lambda^3)$[1]. Rewriting the bare HSM Lagrangian in terms of renormalized field and couplings

$$H = \sqrt{Z_H} H_R \mu^{-\epsilon/2} \qquad S = \sqrt{Z_S} S_R \mu^{-\epsilon/2} \qquad \psi = \sqrt{Z_\psi} \psi_R \mu^{-\epsilon/2},$$

$$\kappa_H^2 = \frac{Z_{\kappa_H}}{Z_H} \kappa_{H_R}^2 \qquad \kappa_S^2 = \frac{Z_{\kappa_S}}{Z_S} \kappa_{S_R}^2 \qquad y_t = \frac{Z_{y_t}}{\sqrt{Z_H}} \mu^{\epsilon/2} y_{t_R},$$

$$\lambda_H = \frac{Z_{\lambda_H}}{Z_H^2} \lambda_{H_R} \mu^\epsilon \qquad \lambda_S = \frac{Z_{\lambda_S}}{Z_S^2} \lambda_{S_R} \mu^\epsilon \qquad \lambda_{HS} = \frac{Z_{\lambda_{HS}}}{Z_H Z_S} \lambda_{HS_R} \mu^\epsilon. \qquad (5.21)$$

Once the divergent terms in the effective action are absorbed into counterterms through scaling factors $Z_i = 1 + \delta_i$, anomalous dimension in every field configuration can be computed and plugged into CS equation. Then matching of the counter terms can be used to identify β-functions [110].

$$\delta Z_{\lambda_H} = \frac{1}{\epsilon} \frac{1}{16\pi^2} \left(12\lambda_H + \frac{1}{4} \frac{\lambda_{HS}}{\lambda_H} - \frac{N_c y_t^4}{\lambda_H} + 2N_c y_t^2 \right),$$

$$\delta Z_{\lambda_S} = \frac{1}{\epsilon} \frac{1}{16\pi^2} \left(9\lambda_S + \frac{\lambda_{HS}}{\lambda_S} \right),$$

$$\delta Z_{\lambda_{HS}} = \frac{1}{\epsilon} \frac{1}{16\pi^2} \left(2\lambda_{HS} + 3\lambda_S + 3\lambda_H + N_c y_t^2 \right),$$

$$\delta Z_{y_t} = \frac{1}{\epsilon} \frac{1}{16\pi^2} \left(\frac{3 + 2N_c}{2} y t^2 \right), \qquad (5.22)$$

where the terms $\mathcal{O}(g_i^2, g_i^4)$ are not shown.

Finally, taking all the constraints discussed above into account for the vacuum stability analysis in HSM and requiring perturbativity up to Planck scales, we apply the Yukawa and Higgs sector RGEs by adding well known gauge effects on the HSM couplings

$$\frac{dy_t^2}{d\ln\mu^2} = \frac{y_t^2}{16\pi^2} \left(\frac{9y_t^2}{2} - \frac{17g_1^2}{20} - \frac{9g_2^2}{4} - 8g_3^2 \right),$$

$$\frac{d\lambda_H}{d\ln\mu^2} = \frac{1}{16\pi^2} \left[\lambda_H \left(12\lambda_H + 6y_t^2 - \frac{9g_1^2}{10} - \frac{9g_2^2}{2} \right) \right.$$

$$\left. + \left(\frac{\lambda_{SH}^2}{4} - 3y_t^4 + \frac{27g_1^4}{400} + \frac{9g_2^4}{16} + \frac{9g_1^2 g_2^2}{40} \right) \right],$$

$$\frac{d\lambda_S}{d\ln\mu^2} = \frac{1}{16\pi^2} \left(9\lambda_S^2 + \lambda_{SH}^2 \right),$$

$$\frac{d\lambda_{SH}}{d\ln\mu^2} = \frac{\lambda_{SH}}{16\pi^2} \left(2\lambda_{SH} + 6\lambda_H + 3\lambda_S + 3y_t^2 - \frac{9g_1^2}{20} - \frac{9g_2^2}{4} \right). \qquad (5.23)$$

Eqs. 5.11 describe the coupling parameters at relatively small energy scales, and therefore serve as initial conditions in addition to the gauge couplings

$$g_1^2(\mu_0) = 4\pi\alpha, \qquad g_2^2(\mu_0) = 4\pi\alpha \left(\frac{1}{\sin\theta_W} + 1 \right), \qquad g_3^2(\mu_0) = 4\pi\alpha_s. \qquad (5.24)$$

---

[1] The non-zero terms contributing to the Higgs field's anomalous dimension at 1-loop can be found in Ref. [56]

Here α, α_s are the weak and strong coupling constants. Additionally we ignore the contributions of all Yukawa couplings except for that of the top quark, and also we include electroweak radiative correction terms for increased accuracy. To this end, we replace the top Yukawa coupling and Higgs self-coupling boundary conditions with [111]

$$
\begin{aligned}
y_t &= \frac{\sqrt{2}m_t}{v}\left[1 + \Delta_t(\mu_0)\right], \\
\lambda_H &= \frac{m_H^2 \cos^2\varphi + m_S^2 \sin^2\varphi}{2v^2}\left[1 + \delta_H(\mu_0)\right],
\end{aligned}
\tag{5.25}
$$

where

$$
\Delta_t(\mu_0) = \Delta_W(\mu_0) + \Delta_{QED}(\mu_0) + \Delta_{QCD}(\mu_0),
\tag{5.26}
$$

with

$$
\begin{aligned}
\Delta_W(\mu_0) &= \frac{G_F m_t^2}{16\sqrt{2}\pi^2}\left(-9\ln\frac{m_t^2}{\mu_0^2} - 4\pi\frac{m_H}{m_t} + 11\right), \\
\Delta_{QED}(\mu_0) &= \frac{\alpha}{9\pi}\left(3\ln\frac{m_t^2}{\mu_0^2} - 4\right), \\
\Delta_{QCD}(\mu_0) &= \frac{\alpha_s}{9\pi}\left(3\ln\frac{m_t^2}{\mu_0^2} - 4\right),
\end{aligned}
\tag{5.27}
$$

and we include the RGEs for the gauge couplings as in the SM, Eq. 3.32. The radiative decay constant for the Higgs is [112]

$$
\delta_\lambda(\mu) = \frac{G_F M_Z^2}{8\sqrt{2}\pi^2}\left[\xi f_1(\xi,\mu) + f_0(\xi,\mu) + \xi^{-1}f_{-1}(\xi,\mu)\right],
\tag{5.28}
$$

with $\xi = m_H^2/M_Z^2$, $G_F = 1.16635 \times 10^{-5}$ GeV^{-2} and

$$
\begin{aligned}
f_1(\xi,\mu) &= 6\ln\frac{\mu^2}{m_H^2} + \frac{3}{2}\ln\xi - \frac{1}{2}Z\left(\frac{1}{\xi}\right) - Z\left(\frac{c^2}{\xi}\right) - \ln c^2 + \frac{9}{2}\left(\frac{25}{9} - \sqrt{\frac{1}{3}}\pi\right) \\
f_0(\xi,\mu) &= 6\ln\frac{\mu^2}{M_Z^2}\left[1 + 2c^2 - 2\frac{m_t^2}{M_Z^2}\right] + \frac{3c^2\xi}{\xi - c^2} + 2Z\left(\frac{1}{\xi}\right) + 4c^2 Z\left(\frac{c^2}{\xi}\right) + \frac{3c^2 \ln c^2}{s^2} \\
&\quad + 12c^2\ln c^2 - \frac{15}{2}(1 + 2c^2) - 3\frac{m_t^2}{M_Z^2}\left[2Z\left(\frac{m_t^2}{\xi M_Z^2}\right) + 4\ln\frac{m_t^2}{M_Z^2} - 5\right], \\
f_{-1}(\xi,\mu) &= 6\ln\frac{\mu^2}{M_Z^2}\left[1 + 2c^4 - 24\frac{m_t^2}{M_Z^2}\right] - 6Z\left(\frac{1}{\xi}\right) - 12c^4 Z\left(\frac{c^2}{\xi}\right) - 12c^4 \ln c^2 \\
&\quad + 8(1 + 2c^4) + \left[Z\left(\frac{m_t^2}{\xi M_Z^2}\right) + \ln\frac{m_t^2}{M_Z^2} - 2\right]
\end{aligned}
\tag{5.29}
$$

with

$$
Z(z) = \begin{cases} 2A\tan^{-1}(1/A), & z > 1/4 \\ A\ln[(1+A)/(1-A)], & z < 1/4, \end{cases}
\tag{5.30}
$$

$$
A = |1 - 4z|^1/2
\tag{5.31}
$$

where c, s are abbreviations for $\cos\theta_W$, $\sin\theta_W$. Fig. 5.6 illustrates the running of the
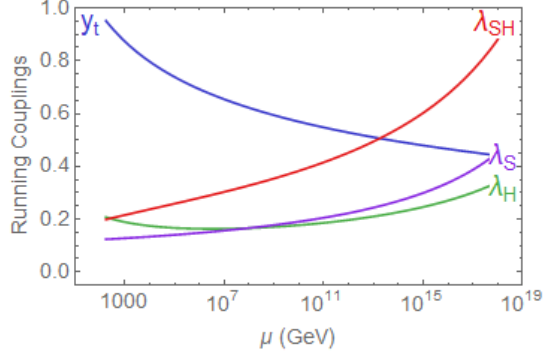
Figure 5.6: The RGE running of the top Yukawa coupling and scalar couplings for the scalar boson model with $m_S = 1$ TeV, $\sin\varphi = 0.1$, $u = 2$ TeV, and the initial conditions are set at $\mu_0 = m_t$.

coupling parameters for a typical set of parameter values. Notice that in this model, the scalar couplings increase with increasing energy scales, compensating for the SM Higgs coupling, which becomes negative at around 10^{10} GeV in Fig. 3.1. Therefore, the addition of an extra scalar boson to the SM secures the conditions in Eq. 5.10 for absolute vacuum stability.

Of course, we may investigate the mass and mixing angle of this singlet scalar with the Higgs boson by eliminating all parameter values that do not satisfy Higgs vacuum stability. For this we perform a scan over a broad parameter space and disallow all parameter values which do not satisfy the vacuum stability conditions outlined in Eq. 5.10. The resulting allowed parameter space is illustrated in Fig. 5.7. While the blue points represent restrictions from vacuum stability bounds only, the shaded red region represents the region excluded by constraints from Higgs production and couplings (as discussed below), which are dominant and are the only parameters limiting the parameter space, especially for lighter singlet masses, $m_S \leq 700$ GeV.

(a) $u = 1$ TeV. (b) $u = 2$ TeV. (c) $u = 4$ TeV.
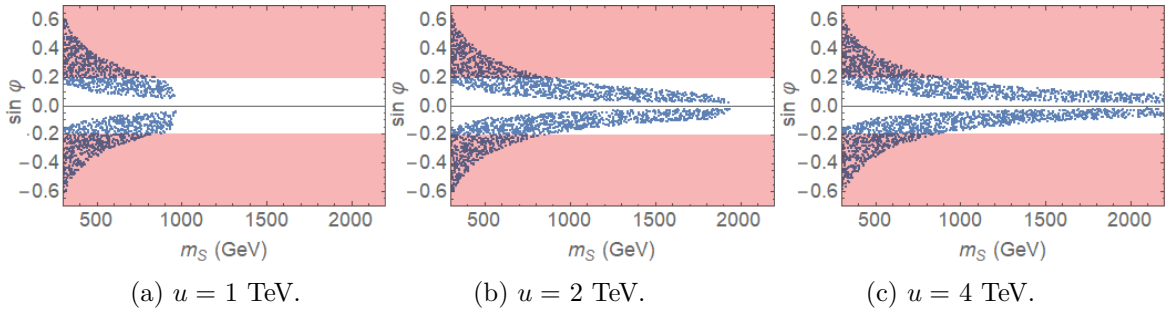
Figure 5.7: The allowed parameter space for the mass m_S and mixing angle φ with the SM Higgs for the additional scalar boson model, for different vacuum expectation values: $u = 1$ TeV (left panel); $u = 2$ TeV (middle panel); and $u = 4$ TeV (right panel). The shaded region represents the region excluded by constraints from the Higgs data.

Note that, while the mass region allowed for the additional boson for $u = 1$ TeV is

quite restricted, for larger VEVs it is quite large, and increasing with the new boson VEV. However, in all cases, the mixing with the SM Higgs boson is required to be non-zero ($\varphi \neq 0$), consistent with the observation of Higgs potential instability in the absence of the additional boson.

Overall, our explored parameter space of SM with the additional scalar is consistent with Higgs data, electroweak constraints, and cosmological constraints. We showed that regions with singlet masses and VEVs around the TeV scale are much preferred. We now proceed to analyze the effects of introducing vector-like quarks to the model and show that there, as we add more fermions, stability emerges be the most stringent constraint.

5.4 Theoretical Framework

Using the stable potential in the previous section, we investigate the effect of introducing vector-like fermions into this SM + additional scalar model. Unlike SM-like (chiral) fermions which act as doublets under $SU(2)_L$ if left-handed and as singlets if right-handed, and spoil the agreement of loop-induced production and decays of the SM Higgs, vector-like fermions have the same interactions regardless of chirality. They appear in many new physics models, such as models with extra dimensions, and many explanations put forward of deviations from SM physics include vector-like fermions. Thus it is important that, when considering the addition of a vector-like fermions to the SM, the presence of a new scalar boson is essential to ensure the stability of the Higgs potential, otherwise, as the fermions decrease the effective self coupling, the singular divergence of the Higgs quartic coupling would worsen compared to the one in the SM. As before we require the Higgs sector potential to be positive at asymptotically large values of the fields, up to Planck scale. The question we need to address is: what are the constraints on the masses of the vector-like fermions, and mixing angles with ordinary fermions, such as to maintain vacuum stability.

The new states interact with the Higgs bosons through Yukawa interactions. The allowed anomaly-free multiplet states for the vector-like quarks, together with their nomenclature, are listed in Table 5.1 [78, 91, 113]. The first two representations are U-like and D-like singlets, the next three are doublets (one SM-like, two non-SM like), and the last two are triplets. The various representations are distinguished by their $SU(2)_L$ and hypercharge numbers. In these representations, the Yukawa and the relevant interaction terms between

Table 5.1: *Representations of Vector-Like Quarks, with quantum numbers under $SU(2)_L \times U(1)_Y$.*

Name	$\mathcal{U}_1$	$\mathcal{D}_1$	$\mathcal{D}_2$	$\mathcal{D}_X$	$\mathcal{D}_Y$	$\mathcal{T}_X$	$\mathcal{T}_Y$
Type	Singlet	Singlet	Doublet	Doublet	Doublet	Triplet	Triplet
	T	B	$\begin{pmatrix} T \\ B \end{pmatrix}$	$\begin{pmatrix} X \\ T \end{pmatrix}$	$\begin{pmatrix} B \\ Y \end{pmatrix}$	$\begin{pmatrix} X \\ T \\ B \end{pmatrix}$	$\begin{pmatrix} T \\ B \\ Y \end{pmatrix}$
$SU(2)_L$	1	1	2	2	2	3	3
Y	2/3	−1/3	1/6	7/6	−5/6	2/3	−1/3

the vector-like quarks and SM quarks are, in the mixed (H, S) basis

$$
\begin{aligned}
\mathcal{L}_{SM+S} &= -y_u \bar{q}_L H^c u_R - y_d \bar{q}_L H d_R \\
\mathcal{L}_{\mathcal{U}_1,\mathcal{D}_1} &= -y_T \bar{q}_L H^c U_{1_R} - y_B \bar{q}_L H D_{1_R} - y_M (\bar{U}_{1_L} S U_{1_R} + \bar{D}_{1_L} S D_{1_R}) \\
&\quad - M_U \bar{U}_L U_R - M_D \bar{D}_L D_R, \\
\mathcal{L}_{\mathcal{D}_2} &= -y_T \bar{D}_{2_L} H^c u_R - y_B \bar{D}_{2_L} H d_R - y_M (\bar{D}_{2_L} S^c D_{2_R} + y_B \bar{D}_{2_L} S D_{2_R}) \\
&\quad - M_D \bar{D}_{2_L} D_{2_R}, \\
\mathcal{L}_{\mathcal{D}_X,\mathcal{D}_Y} &= -y_T \bar{D}_{X_L} H u_R - y_B \bar{D}_{Y_L} H^c d_R - y_M (\bar{D}_{X_L} S D_{X_R} + y_B \bar{D}_{Y_L} S^c D_{Y_R}) \\
&\quad - M_X \bar{D}_{X_L} D_{X_R} - M_Y \bar{D}_{Y_L} D_{Y_R}, \\
\mathcal{L}_{\mathcal{T}_X,\mathcal{T}_Y} &= -y_T \bar{q}_L \tau^a H^c \mathcal{T}_{X_R}^a - y_B \bar{q}_L \tau^a H \mathcal{T}_{Y_R}^a - y_M (\bar{\mathcal{T}}_{X_L} \tau^a S^c \mathcal{T}_{X_R}^a + y_B \bar{\mathcal{T}}_{Y_L} \tau^a S \mathcal{T}_{Y_R}^a) \\
&\quad - M_X \bar{\mathcal{T}}_{X_L} \mathcal{T}_{X_R} - M_Y \bar{\mathcal{T}}_{Y_L} \mathcal{T}_{Y_R}, \quad\quad\quad\quad\quad\quad\quad\quad (5.32)
\end{aligned}
$$

where $H^c = i\sigma^2 H^\star$, $S^c = i\sigma^2 S$, y_u, y_d, y_T and y_B and the Yukawa couplings of the SM-like Higgs field H, and y_M is the Yukawa coupling of the S field to vector-like quarks. After spontaneous symmetry breaking, the Yukawa interactions generate mixing between the SM quarks and the vector-like quarks at tree level. The singlet vector-like quark and the triplet vector-like quark exhibit similar mixing patterns, while the doublet vector-like quarks have a different mixing pattern. To avoid conflicts with low energy experimental data (flavor changing neutral interactions), we limit the vector-like quarks mixing with the third generation of SM quarks only. This is reasonable also because of the large mass gap between vector-like fermions and the first two generations of quarks. The mixing patterns will be described below.

The gauge eigenstate fields resulting from the mixing can be written in general as,

$$\mathcal{T}_{L,R} = \begin{pmatrix} t \\ T \end{pmatrix}_{L,R} \qquad \mathcal{B}_{L,R} = \begin{pmatrix} b \\ B \end{pmatrix}_{L,R}. \tag{5.33}$$

The mass eigenstate fields are denoted as (t_1, t_2) and (b_1, b_2) and they are found through bi-unitary transformations,

$$\mathbf{T}_{L,R} = \begin{pmatrix} t_1 \\ t_2 \end{pmatrix}_{L,R} = V^t_{L,R} \begin{pmatrix} t \\ T \end{pmatrix}_{L,R}$$

$$\mathbf{B}_{L,R} = \begin{pmatrix} b_1 \\ b_2 \end{pmatrix}_{L,R} = V^b_{L,R} \begin{pmatrix} b \\ B \end{pmatrix}_{L,R}, \tag{5.34}$$

where

$$V^t_{L,R} = \begin{pmatrix} \cos\theta & -\sin\theta \\ \sin\theta & \cos\theta \end{pmatrix}_{L,R}, \qquad V^b_{L,R} = \begin{pmatrix} \cos\beta & -\sin\beta \\ \sin\beta & \cos\beta \end{pmatrix}_{L,R}. \tag{5.35}$$

In the following we abbreviate $\cos\theta^t_L \equiv c^t_L,...$ Through these rotations we obtain the diagonal mass matrices

$$M^t_{diag} = V^t_L M^t (V^t_R)^\dagger = \begin{pmatrix} m_{t_1} & 0 \\ 0 & m_{t_2} \end{pmatrix} \quad, \quad M^b_{diag} = V^b_L M^b (V^b_R)^\dagger = \begin{pmatrix} m_{b_1} & 0 \\ 0 & m_{b_2} \end{pmatrix}, \tag{5.36}$$

where M^t, M^b represent the 2×2 mass mixing matrix between the t, T and b, B states, before diagonalization. The eigenvectors now become, for instance for the top sector

$$m^2_{t_1,t_2} = \frac{1}{4}\left[(y_t^2 + y_T^2)v^2 + y_M^2 u^2\right]\left[1 \pm \sqrt{1 - \left(\frac{2y_t y_M vu}{(y_t^2 + y_T^2)v^2 + y_M^2 u^2}\right)^2}\right] \tag{5.37}$$

with eigenvectors

$$\begin{pmatrix} t_1 \\ t_2 \end{pmatrix}_{L,R} = \begin{pmatrix} \cos\theta_{L,R} & \sin\theta_{L,R} \\ -\sin\theta_{L,R} & \cos\theta_{L,R} \end{pmatrix}\begin{pmatrix} t \\ T \end{pmatrix}_{L,R}. \tag{5.38}$$

where the mixing angles are

$$\tan\theta_L = \frac{2y_T y_M vu}{y_M^2 u^2 - (y_t^2 + y_T^2)v^2}$$

$$\tan\theta_R = \frac{2y_t y_T v^2}{y_M^2 u^2 - (y_t^2 + y_T^2)v^2}, \tag{5.39}$$

and similarly for the b-quark sector, with the replacement $t \to b$ and $\theta \to \beta$. Note that, because of their charge assignments, the X and Y fields do not mix with the other fermions and are therefore also mass eigenstates.

Relationships between mixing angles and mass eigenstates depend on the representation [113, 114].

$$
\begin{aligned}
\text{For doublets}: \quad (XT): \quad & m_X^2 = m_T^2 (\cos\theta_R)^2 + m_t^2 (\sin\theta_R)^2 \\
(TB): \quad & m_T^2 (\cos\theta_R)^2 + m_t^2 (\sin\theta_R)^2 = m_B^2 (\cos\beta_R)^2 + m_b^2 (\sin\beta_R)^2 \\
(BY): \quad & m_Y^2 = m_B^2 (\cos\beta_R)^2 + m_b^2 (\sin\beta_R)^2
\end{aligned}
$$

$$
\begin{aligned}
\text{For triplets}: \quad (XTB): \quad & m_X^2 = m_T^2 (\cos\theta_L)^2 + m_t^2 (\sin\theta_L)^2 \\
& = m_B^2 (\cos\beta_L)^2 + m_b^2 (\sin\beta_L)^2 \,, \\
& \text{where } \sin(2\beta_L) = \sqrt{2}\,\frac{m_T^2 - m_t^2}{(m_B^2 - m_b^2)}\,\sin(2\theta_L) \,. \\
(TBY): \quad & m_Y^2 = m_B^2 (\cos\beta_L)^2 + m_b^2 (\sin\beta_L)^2 \\
& = m_T^2 (\cos\theta_L)^2 + m_t^2 (\sin\theta_L)^2 \,, \\
& \text{where } \sin(2\beta_L) = \frac{m_T^2 - m_t^2}{\sqrt{2}(m_B^2 - m_b^2)}\,\sin(2\theta_L) \,, \quad\quad (5.40)
\end{aligned}
$$

and where

$$
\begin{aligned}
m_T \tan\theta_R &= m_t \tan\theta_L && \text{for singlets, triplets} \\
m_T \tan\theta_L &= m_t \tan\theta_R && \text{for doublets} \\
m_B \tan\beta_R &= m_b \tan\beta_L && \text{for singlets, triplets} \\
m_B \tan\beta_L &= m_b \tan\beta_R && \text{for doublets} \,. \quad\quad (5.41)
\end{aligned}
$$

For doublet models, while the Higgs mixing is the same as in the previous section, the mixing between the top quark t and the new vector-like singlet T, characterized by the mixing θ_L, results in the shift in the Yukawa couplings as follows

$$
\begin{aligned}
y_t(\mu_0) &= \frac{\sqrt{2}m_t}{v}\frac{1}{\sqrt{\cos^2\theta_L + x_t^2 \sin^2\theta_L}}\,, \\
y_T(\mu_0) &= \frac{\sqrt{2}m_T}{v}\frac{\sin\theta_L \cos\theta_L (1 - x_t^2)}{\sqrt{\cos^2\theta_L + x_t^2 \sin^2\theta_L}}\,, \\
y_B(\mu_0) &= \frac{\sqrt{2}m_B}{v}\frac{\sin\theta_L \cos\theta_L (1 - x_b^2)}{\sqrt{\cos^2\theta_L + x_t^2 \sin^2\theta_L}}\,, \\
y_M(\mu_0) &= \frac{m_T + m_B}{\sqrt{2}u}\sqrt{\cos^2\theta_L + x_t^2 \sin^2\theta_L}\,, \quad\quad (5.42)
\end{aligned}
$$

with $x_b = m_b/m_B$, and as before $x_t = m_t/m_T$. We use these expressions as initial conditions to the RGE equations (see appendix. A). We review the mass bounds on vector-like quarks, then proceed with our numerical analysis in Sec. 5.6.

5.5 Experimental bounds on vector-like quark masses

Searches for vector-like quarks have been performed at the LHC and various limits exist [115], all obtained assuming specific decay mechanisms. The Run 2 results from the LHC have improved previous limits from Run 1 by about 500 GeV [116]. All measurements assume top and down-type vector-like quarks to decay into one of the final states involving Z, W or Higgs bosons with 100% branching ratios. So far, lower limits around 800 GeV have been obtained. The most recent search at ATLAS obtains, with 95% C.L., lower limits on the T mass of 870 GeV (890 GeV) for the singlet model, 1.05 TeV (1.06 TeV) for the doublet model, and 1.16 TeV (1.17 TeV) for the pure Zt decay mode quark [117]. The current experimental lower bound on the mass of the down-type vector-like quark which mixes only with the third generation quark is around 730 GeV from Run 2 of the LHC and around 900 GeV from Run 1. The current lower bound for a vector-like quark which mixes with the light quarks is around 760 GeV from Run 1. In our analyses, we set a lower limit on all masses of 800 GeV, to allow for the consideration of the largest parameter space.

We proceed with analyzing the representations in turn, showing the effects of the additional fermions on the RGEs, and the mass and mixing angles constraints on the fermions and additional boson for each. All the relevant RGE for the Yukawa couplings, couplings between the bosons, and gauge coupling constants are given in the Appendix A.

5.6 RGE Analysis of Vector-like Quarks in Higgs Singlet Model

The evolution of the RGE's under different vector-like fermion representations are illustrated in Fig. 5.8 for singlet model $\mathcal{U}_1$ for different values of the VEVs of the new scalar field ($u = 1, 2, 4$ TeV) along with ($u = 2, 4$ TeV) for singlet model $\mathcal{D}_1$ in Fig.5.9. In the case of $u = 1$ TeV, we have taken the mass of the scalar boson to be 0.8 TeV, because for $m_S = 1$ TeV, the Higgs sector couplings diverge, leading to singularities, whereas in the case of $u = 2$ TeV and $u = 4$ TeV, we chose $m_S = 1$ TeV because the smaller mass of 0.8 TeV is not large enough to ensure a positive Higgs quartic coupling. In the case of other representations only $u = 2$ TeV case is set for running couplings as shown in Fig. 5.10 for doublet VLQs and Fig. 5.11 for triplet VLQs. We compared our results to the findings of Ref. [85], where the parametric solutions to the RGEs and the running couplings for singlet VLQs are in good agreement, while the RGE solutions for the larger representations provide novel contributions to the literature. As required, all of the Higgs sector couplings remain positive up to Planck scale. As expected, the fermion Yukawa couplings tend to decrease with increasing energy, while the scalar bosonic couplings tend to increase. As we discussed previously, the addition of extra scalar bosons to the Standard Model helps maintain a positive Higgs self-coupling at larger energy scales, while the addition of extra fermions only aids in lowering it further. A common trend with respect to the models is that the Yukawa couplings are generally negatively affected by added loops at higher energy scales, while the Higgs sector couplings are generally affected positively (they tend to increase with increasing energy).

The obvious exception here is the SM Higgs coupling, which strays dangerously close to zero at high energy scales, and even becomes negative for the additional singlet vector-like fermion case. The models that augment the scalar boson by vector-like representations vary significantly among each other in predictions for the various couplings with the scalar VEV

(a) $u = 1$ TeV
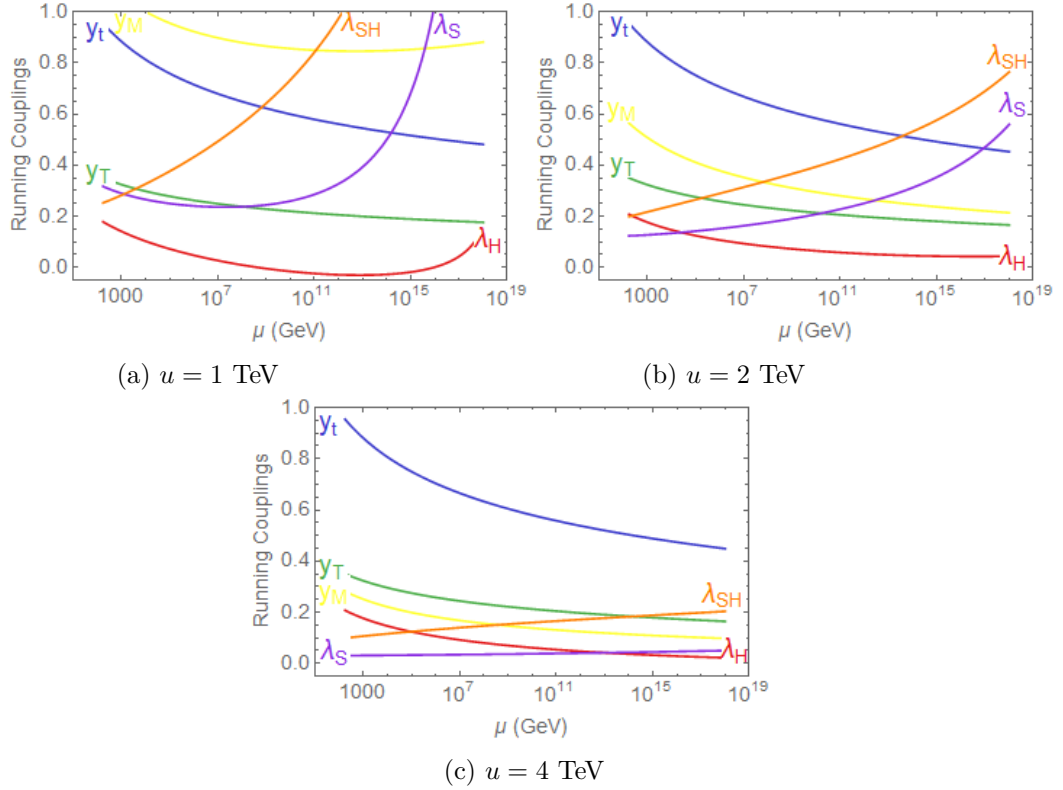
(b) $u = 2$ TeV

(c) $u = 4$ TeV

Figure 5.8: The RGE running of the Yukawa and scalar couplings in singlet vector-like quark model $\mathcal{U}_1$. We set $m_S = 0.8$ TeV, $u = 1$ TeV, (top left panel), $m_S = 1$ TeV, $u = 2$ TeV (top right panel), $m_S = 1$ TeV, $u = 4$ TeV (bottom panel) and $\sin\varphi = 0.1$ for scalar sector. For fermionic sector: $m_T = 0.9$ TeV, $\sin\theta_L = 0.08$ and $\mu_0 = m_t$.
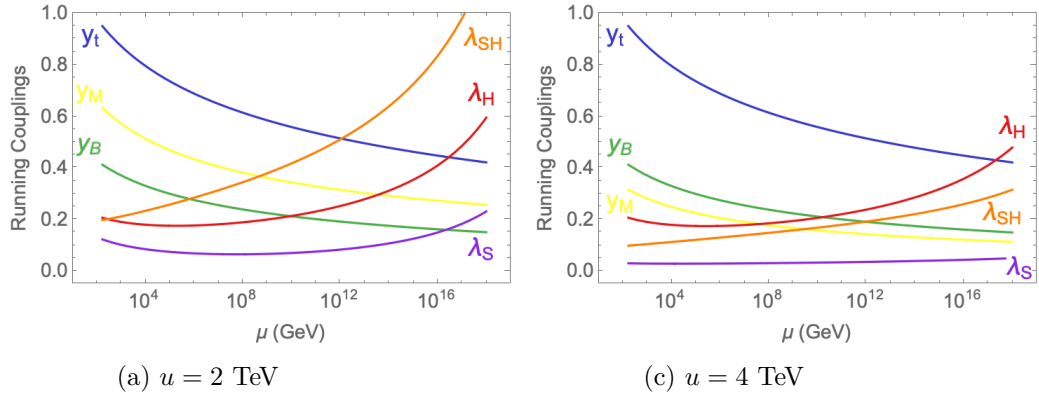
(a) $u = 2$ TeV

(c) $u = 4$ TeV

Figure 5.9: The RGE running of the Yukawa and scalar couplings in singlet vector-like quark model $\mathcal{D}_1$. We set $m_S = 1$ TeV, $u = 2$ TeV (left panel), $m_S = 1$ TeV, $u = 4$ TeV (right panel) and $\sin\varphi = 0.1$ for scalar sector. For fermionic sector: $m_B = 1$ TeV, $\sin\theta_L = 0.08$ and $\mu_0 = m_t$.

(a) $\mathcal{D}_2$ (b) $\mathcal{D}_X$

(c) $\mathcal{D}_Y$
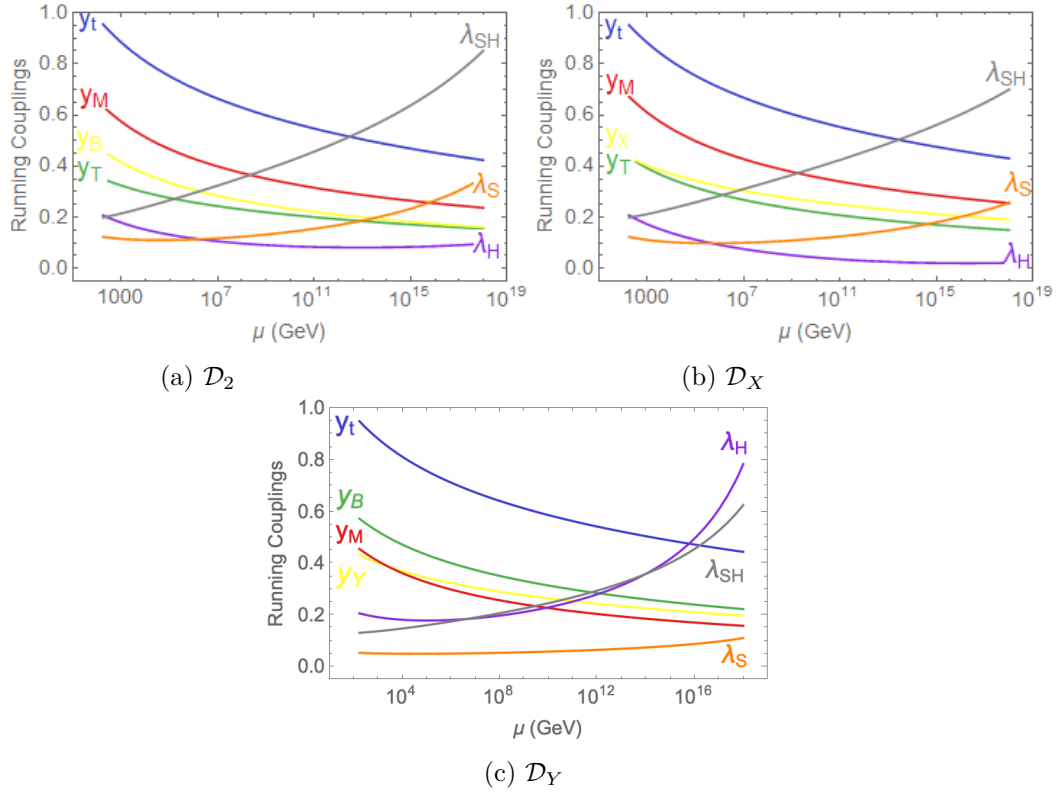
Figure 5.10: The RGE running of the Yukawa and scalar couplings in doublet vector-like quark models $\mathcal{D}_2$ (top left panel), $\mathcal{D}_X$ (top right panel), $\mathcal{D}_Y$ (bottom panel). We set $m_S = 1$ TeV, $u = 2$ TeV, $\sin\varphi = 0.1$ for scalar sector and $m_T = 0.9$ TeV, $m_B = 1$ TeV, $m_X = 1$ TeV, $m_Y = 1$ TeV, $\sin\theta_L = 0.08$ and $\mu_0 = m_t$ for all doublet VLQ models.

(a) $\mathcal{T}_X$ (b) $\mathcal{T}_Y$
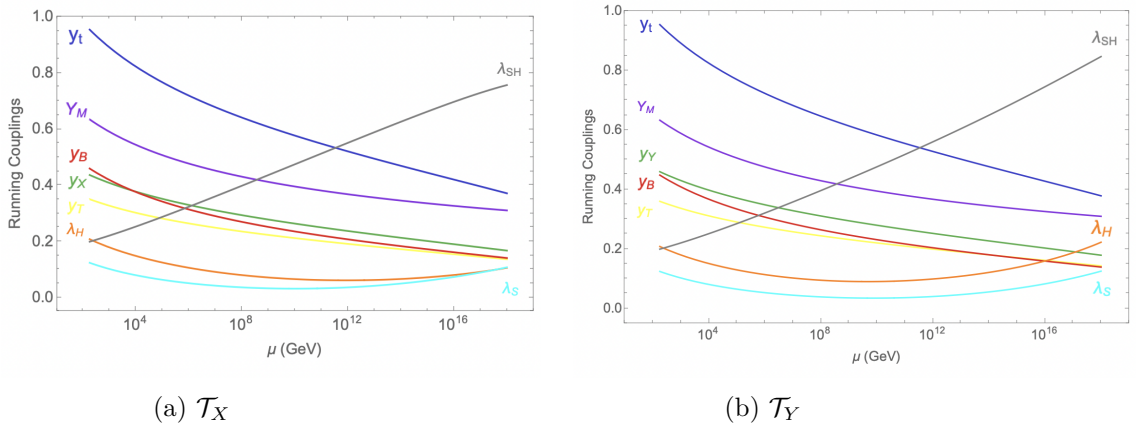
Figure 5.11: The RGE running of the Yukawa and scalar couplings in triplet vector-like quark models $\mathcal{T}_X$ (left panel), $\mathcal{T}_Y$ (right panel). We set $m_S = 1$ TeV, $u = 2$ TeV, $\sin\varphi = 0.1$ for scalar sector and $m_T = 0.9$ TeV, $m_B = 1$ TeV, $m_X = 1$ TeV, $m_Y = 1$ TeV, $\sin\theta_L = 0.08$ and $\mu_0 = m_t$ for both triplet VLQ models.

u. Note in particular that for the the first case, for the singlet vector-like case, where $u = 1$, the Higgs couplings increase, and λ_H becomes negative at $\mu \sim 10^{11}$ in Fig. 5.8, rendering the theory unstable, while if the additional scalar VEV is increased to $u = 2$, or 4 TeV, the problem is ameliorated. The same problem recurs for the doublet and triplet models (not shown), but the theory is safe[1] for $u = 2$ and 4 TeV. Differences in the running RGE's are more pronounced for λ_S, the new boson self-coupling, and negligible for the others. Note in particular, the difference between the values in Fig. 5.8 and 5.6. For the doublet and triplet vector-like fermions, the RGE evolutions are similar, and the Higgs self-coupling remains positive at all energies. The additional scalar quartic coupling does not lie close to the origin as its interactions with fermions are small. There are some variations among models in the new scalar coupling, and the one describing the mixing with the SM Higgs. We have put less emphasis on the vacuum stability bound for the additional scalar, since its mass and VEV are unknown, and thus limiting concrete information from a detailed study of its vacuum stability bound.

Imposing the same conditions on the positivity of the potential as in Eq. 5.10, we study the allowed masses and mixing angles corresponding to each vector-like fermion representation. In Figs. 5.12 and 5.13 we perform a scan over random values of the relevant vector-like quarks between 300 and 2200 GeV, and for the mixing angles $\sin\beta_L$ (in the bottom sector) and $\sin\theta_L$ (in the top sector) between -1 and 1. The allowed values of the scalar mass m_S are plotted against the mixing angle in the scalar sector, $\sin\varphi$ for different values of the expectation values u (1, 2 and 4 TeV), providing an illustration of the possible quantitative properties of the scalar boson in this model. The results are given for all models. In Fig. 5.12 we plot the scans for singlet vector-like T (top row), singlet vector-like B (second row), (T, B) doublet (third row), (X, T) doublet (fourth row), (B, Y) doublet (bottom row). And in Fig. 5.13 we consider the (X, T, B) triplet (top row), and (T, B, Y) triplet (bottom row), providing an illustration of the possible quantitative properties of the scalar boson in these models. We remark from Figs. 5.12 and 5.13 that just as in the SM extension containing only an extra scalar boson, considered in the previous section, mass mixing between the two scalar bosons is always required, and this mixing is significant, $\sin\varphi \geq 0.2$. Also, consistent with previous discussions, increasing the VEV u enlarges the parameter space, which is now quite restricted for $u = 1$ TeV. As expected, the addition of vector-like fermions worsens the stability of the potential, but larger VEVs (mass scales) survive. The mixing in the singlet $\mathcal{U}_1$ model is the most effective counter-term addition, in fact pretty much ruling out the scenario where $u = 1$ TeV (unless the additional scalar is light, 600-1000 GeV), while the other representations provide much milder bounds for the same VEV.

We now investigate the restrictions on the vector-like fermion masses and mixing from requiring the stability of the Higgs potential. We concentrate first on the vector-like T, which has the same charge as the top quark, and which, through mixing can affect changes in the Higgs potential, both in the fermion and in the scalar sector. In order to investigate this, we perform the same scan over random values of m_S and M_U between 300 and 2200 GeV, and for the mixing angles $\sin\varphi$ and $\sin\theta_L$ between -1 and 1, and show the results in Fig. 5.14. The first row shows the results for the singlet T vector-like quark, the second row shows the results for the doublet vector-like (T, B), the third for the (X, T) doublet, the fourth for the (X, T, B) triplet and the last for the (T, B, Y) triplet. Unlike the case of

---

[1] In fact even $u = 1$ TeV generates an allowed parameter space that survives from vacuum stability constraints as to be shown in the next section. Nevertheless, it should be noted that for smaller u values, parameters leading to vacuum instability are more likely to be encountered.
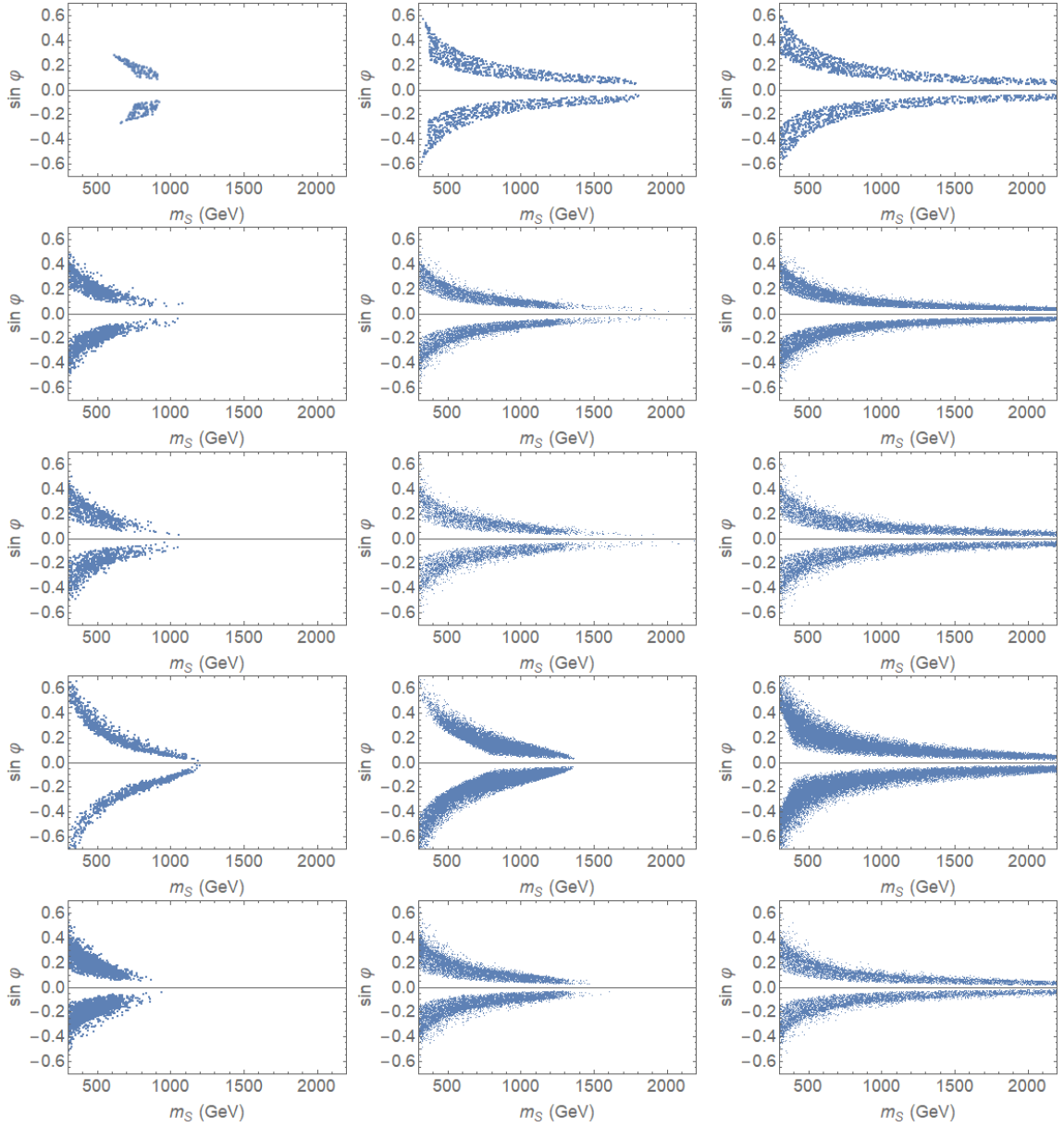
Figure 5.12: The allowed parameter space for the scalar boson mass and mixing angle with the SM Higgs. In the (top panel) scalar + vector-like T; (second panel) scalar + vector-like B; (third panel) in the scalar + vector-like (T, B) model; (fourth panel) scalar + vector-like (X, T) fermion model; and (bottom panel) scalar + vector-like (B, Y) fermion model, for different vacuum expectation values of the additional scalar: $u = 1$ TeV (left panel); $u = 2$ TeV (middle panel); and $u = 4$ TeV (right panel).

53
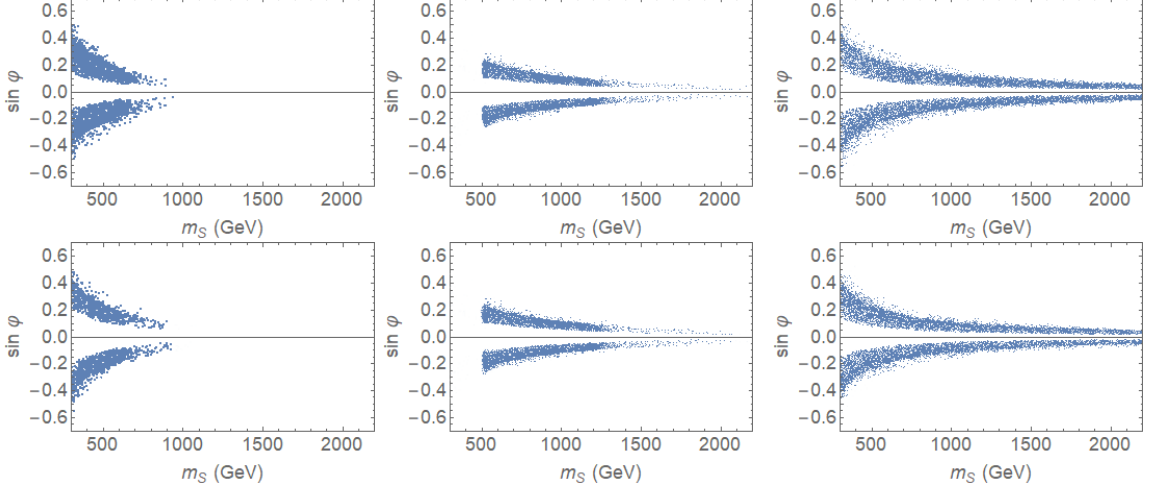
Figure 5.13: (Continued) The allowed parameter space for the scalar boson mass and mixing angle with the SM Higgs. In the (top panel) the scalar + triplet (X, T, B) model , and for (bottom panel) the scalar + (T, B, Y) triplet model, for different vacuum expectation values of the additional scalar: $u = 1$ TeV (left panel); $u = 2$ TeV (middle panel); and $u = 4$ TeV (right panel).

scalar mixing, here the mixing between the top quark and the vector-like one is required to be small, in general, for most cases, in the region $\sin \theta_L \in (-0.2, 0.2)$ (with some exceptions, where it can be larger, discussed below), and it can be zero. The allowed masses of the T quark are restricted for the scalar VEV $u = 1$ TeV, and increase with increasing VEVs, so that in the singlet T and doublet (X, T) models cases, practically no T masses are allowed for $u = 1$ TeV, while masses up to 1400 GeV are allowed for $u = 4$ TeV. For the SM like doublet (T, B), for $u = 1$ TeV, $m_T \leq 800$ GeV, for $u = 2$ TeV, $m_T \leq 1600$ GeV, while for $u = 4$ TeV, m_T spans the whole axis. Note that here, like in the scalar sector, there are marked differences between the scenarios. For the doublet (X, T), any mixing between the T and t quark is allowed. We expect this case to be somewhat similar to the singlet, however, the Yukawa coupling of the X quark lowers the Higgs coupling further, the parameter space continues to be severely constrained, and the mass is allowed in a narrow region near $m_T = 1$ TeV for all values of the additional singlet. Here, as an exception to small mixing, the constraints on the mixing with the top are lifted. The case with triplets (X, T, B), affected by both the X and B vector-like quarks, exhibits a behaviour independent of the singlet VEV. Masses again are favoured to be near $m_T = 1$ TeV (we rule out light masses, ~ 500 from direct searches) and the mixing is allowed to be small or large. The strong enhancements are for the cases where the t and T mix. The mixing is expected to be stronger than between B and b quarks, due to the differences between mass of the top and of the bottom (making the denominator in Eq. 6.36 smaller). It is interesting to note here the effect of the X vector-like quark, which, while not mixing with SM quarks, is nevertheless important for the mass of the T vector-like quark (seen clearly if we compare the singlet T model with the doublet (X, T), and the doublet (T, B) model with the triplet (X, T, B)).

The scans in Fig. 5.15 illustrate the allowed masses and mixing angles of the B vector-like quark with the bottom quark for the SM augmented by the additional scalar. We show, in the top panel, the vector-like singlet B model, in the second panel, the vector-like (T, B)

54
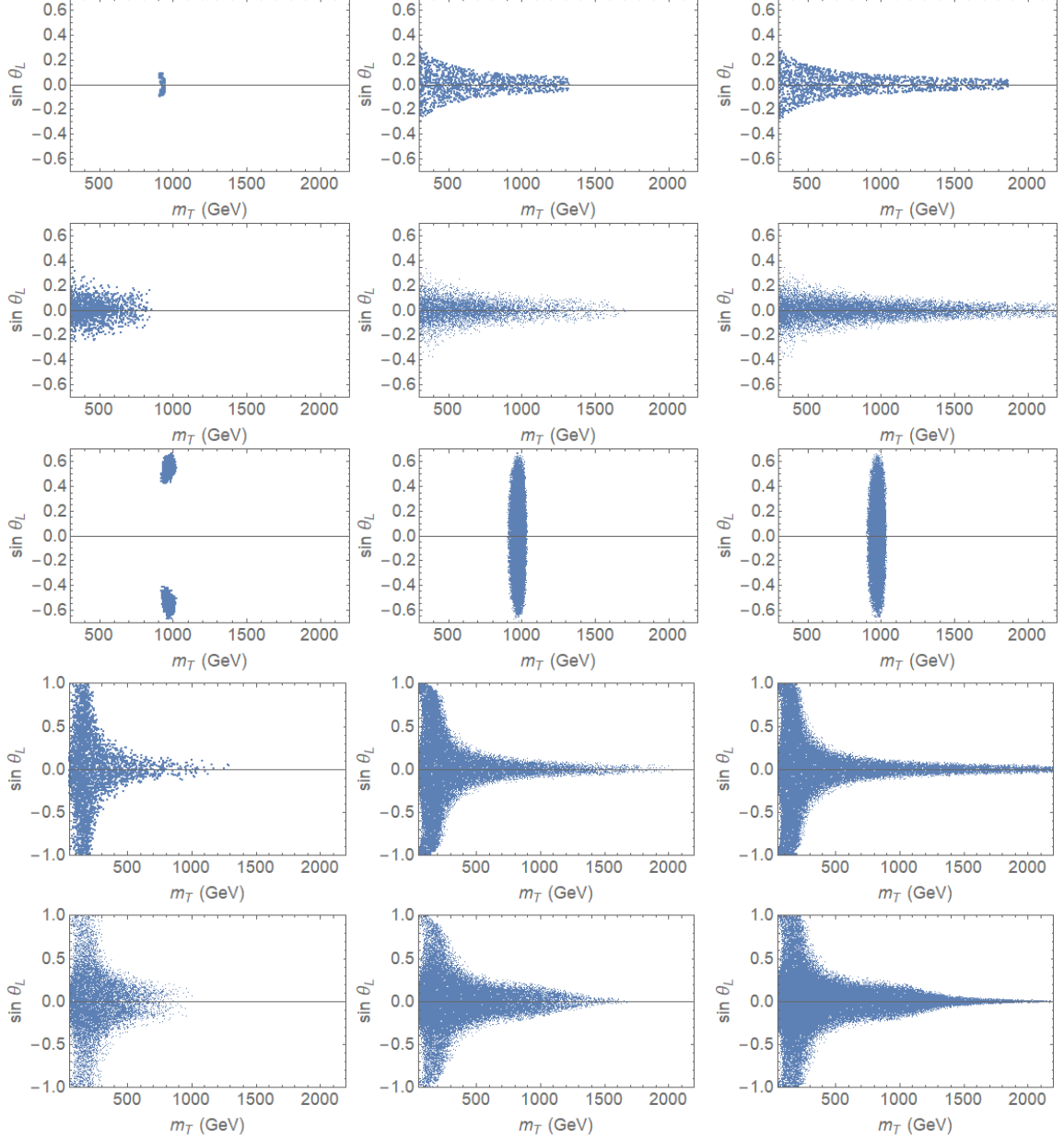
Figure 5.14: The allowed parameter space for the T fermion mass and mixing angle with the top quark for: (top panel) in the scalar + singlet vector-like T model; (second panel) in scalar + vector-like (T, B) model; (third panel) for the T fermion mass and mixing angle in the scalar + (X, T) fermion doublet model, (fourth panel) for the scalar + (X, T, B) triplet, and (bottom panel) for the triplet (T, B, Y) model, for different vacuum expectation values, $u = 1$ TeV (left panel); $u = 2$ TeV (middle panel); and $u = 4$ TeV (right panel).

model, in the third panel, the vector-like (B, Y) model, in the fourth panel, in the vector-like (X, T, B) triplet, and in the bottom panel, the (T, B, Y) triplet. We again perform the same scan over the m_B and m_S masses and mixing angles $\sin \beta_L$ constrained by vacuum stability requirement, and plot the resulting m_B against the mixing the b-sector $\sin \beta_L$. The effect of the B quark is markedly different from that of the T quark due to weaker constraints on

its angle (the denominator in $\tan \beta_L$ is larger than $\tan \theta_L$). For the B singlet model, the mixing and mass range are restricted, especially for $u = 1$ TeV, while for the (T, B) model the mass restrictions are lifted, but the mixing limits still remain. For the (B, Y) doublet and for the (T, B, Y) triplet model, the situation is very similar to that of the T mass and mixing in these models: the mixing is restricted everywhere except around 1000 GeV, and this result is independent on the scalar VEV. Finally, we investigate constraints on the vector-like fermions with non-SM like hypercharge, X, with charge 5/3, and Y, with charge -4/3. As the additional vector-like quarks X and Y do not mix with SM particle, a plot of mass against the mixing angle does not make sense, Instead, in Fig. 5.16, the allowed values of the scanned fermion mass m_X is plotted against m_T, and m_Y is correlated with m_B. Note that in the (X, T) quark doublet, the X and T masses are strongly correlated (as seen from the third row of Fig. 5.14) and the expected m_X is required to be close to 1000 GeV regardless of m_T values. We see that, similarly, in the (B, Y) doublet model, m_Y must have an allowed mass of approximately 1000 GeV, regardless of m_B, or the VEV u, unless both m_X and m_Y would be much lighter (100-200 GeV) in agreement with our earlier results. This seems to severely constrain models with vector-like quarks with exotic hypercharges.

For completeness, all the relevant RGE for the Yukawa couplings, couplings between the bosons and coupling constants are included in the Appendix A.
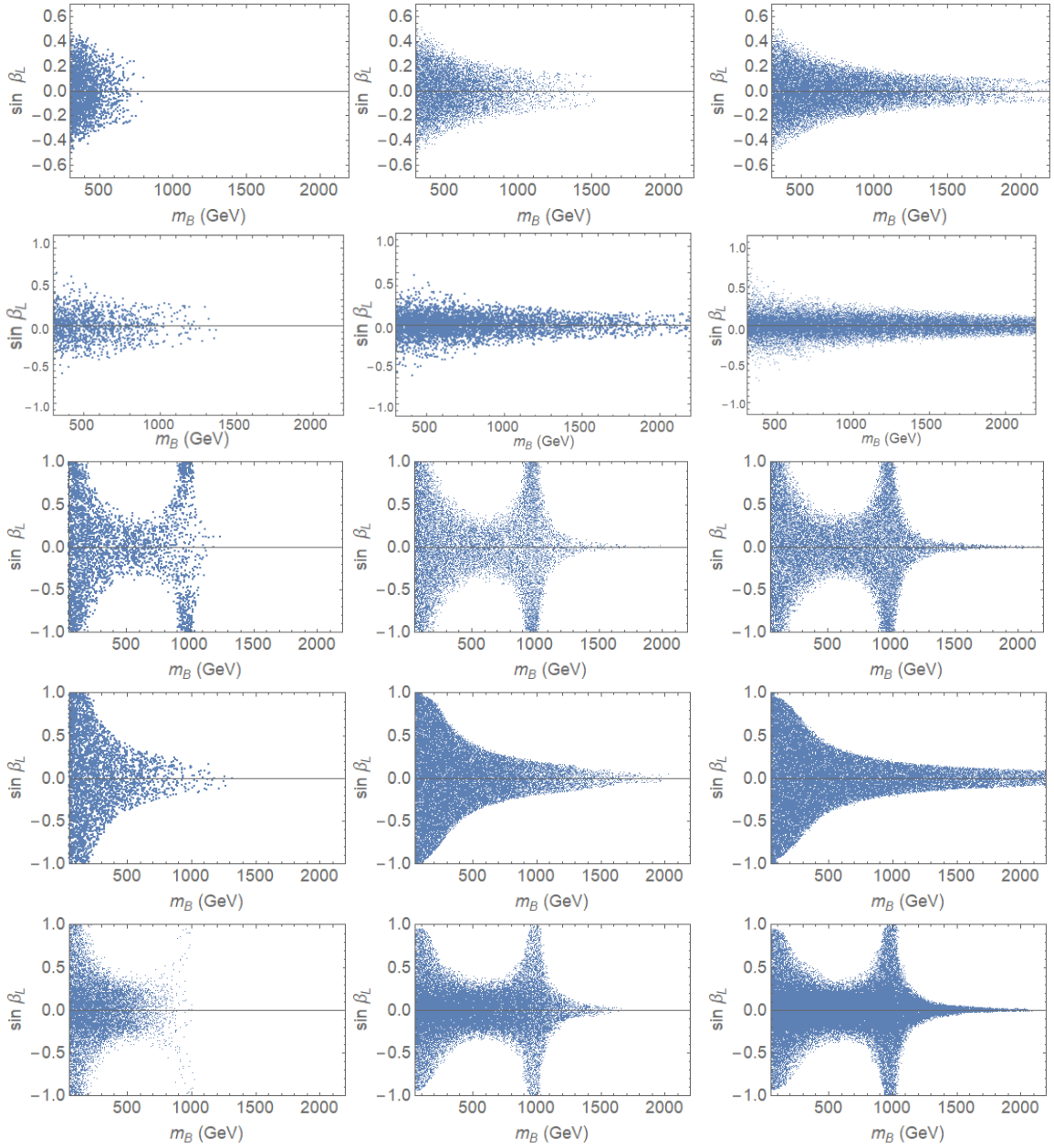
Figure 5.15: The allowed parameter space for the B fermion mass and mixing angle in: (top panel) the vector-like singlet B model, (second panel) the vector-like (T, B) model, (third panel) the vector-like (B, Y) model, (fourth panel) the vector-like (X, T, B) triplet, and (bottom panel) the (T, B, Y) triplet, for different vacuum expectation values of the additional scalar: $u = 1$ TeV (left panel); $u = 2$ TeV (middle panel); and $u = 4$ TeV (right panel).
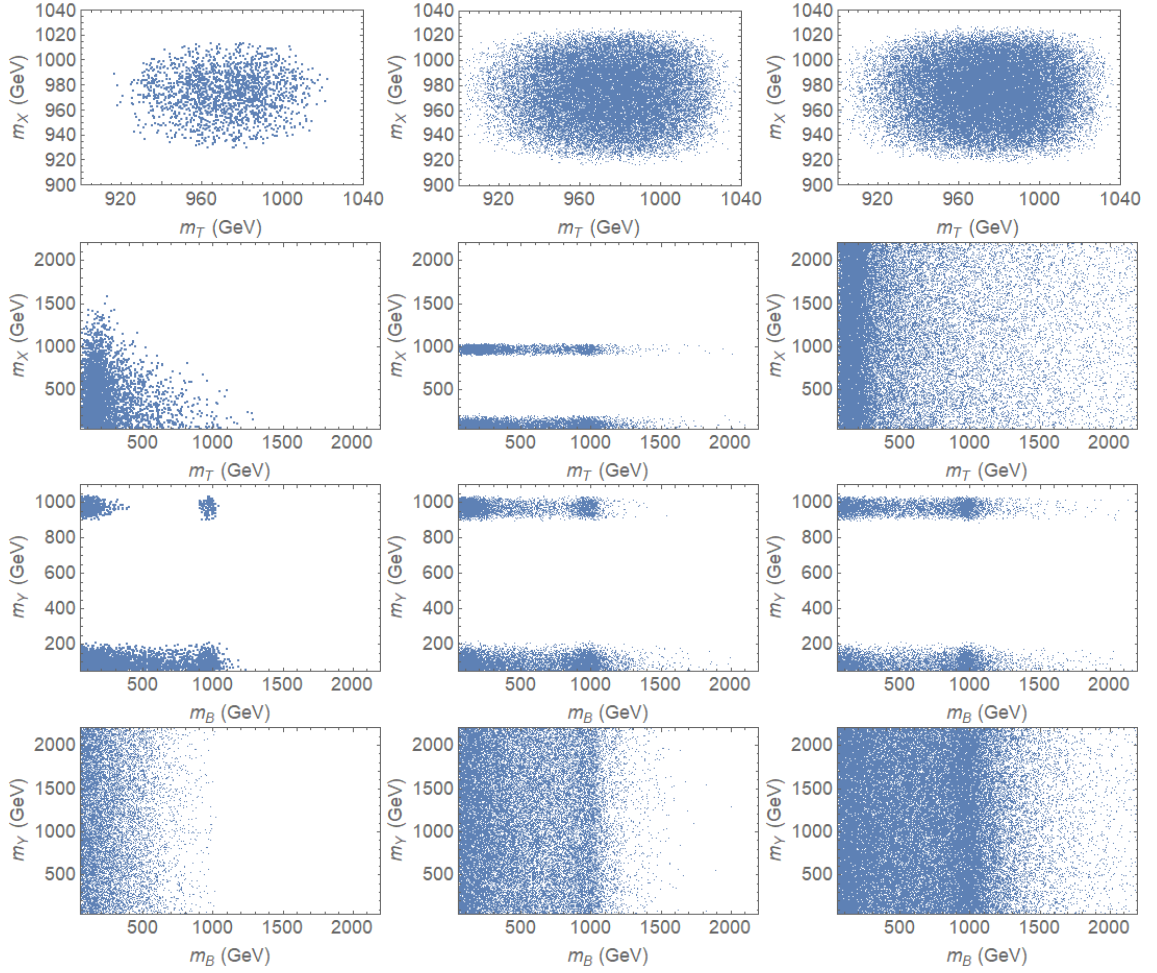
Figure 5.16: The correlated parameter space for the X and T quark masses in the (X, T) quark doublet model (top panel) and in the (X, T, B) triplet model (second panel), and for the Y and B quark masses for the (B, Y) doublet model (third panel), and for the (T, B, Y) triplet model (bottom panel) for different vacuum expectation values.

5.7 Electroweak Precision Measurements

Constraints on possible new physics also emerge from precision electroweak measurements. The extra singlet scalar and vector-like states induce modifications to the vacuum polarizations of electroweak gauge bosons at loop level as shown in Fig. 5.17, which are parameterized by the oblique parameters $\mathbb{S}, \mathbb{T}$, and $\mathbb{U}$.
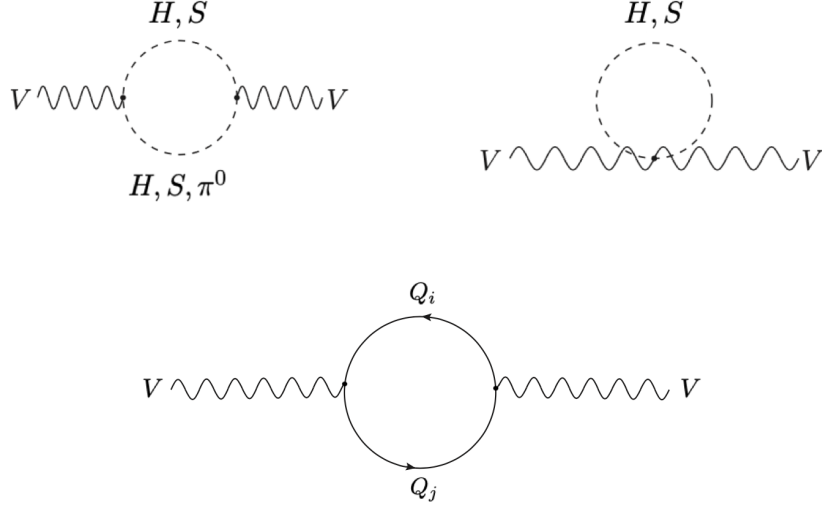
Figure 5.17: Scalar boson and VLQ contributions to vacuum polarization amplitude of the SM gauge bosons Π_{VV}.

For a large class of new physics models, corrections to precision electroweak observables are universal, in the sense that they are revealed only in self-energies of electroweak gauge bosons. There are solid constraints from these oblique corrections, pushing the scale of new physics around 1 TeV. The oblique parameters can be calculated perturbatively for any model from the gauge boson propagators, and are defined as [97]

$$
\begin{aligned}
\mathbb{S} &= 16\pi\Re\left[\bar{\Pi}_\gamma^{3Q}(m_Z^2) - \bar{\Pi}_Z^{33}(0)\right], \\
\mathbb{T} &= \frac{4\sqrt{2}G_F}{\alpha_e}\Re\left[\bar{\Pi}^{3Q}(0) - \bar{\Pi}^{11}(0)\right], \\
\mathbb{U} &= 16\pi\Re\left[\bar{\Pi}_Z^{33}(0) - \bar{\Pi}_W^{11}(0)\right].
\end{aligned}
\tag{5.43}
$$

The current experimental values are obtained by fixing $\Delta\mathbb{U} = 0$ are $\Delta\mathbb{T} = 0.08 \pm 0.07$, $\Delta\mathbb{S} = 0.05 \pm 0.09$. The overall calculation of $\mathbb{S}, \mathbb{T}$ and $\mathbb{U}$ parameters via loop contributions can be separated into contributions from scalars and from fermions since VLQs is odd under Z_2 symmetry.

5.7.1 HSM contributions to the $\mathbb{S}$ and $\mathbb{T}$ parameters

Rewriting Eq. 6.42 explicitly in terms of the scalar loop contributions to the gauge boson two point functions [118].

$$
\begin{aligned}
\mathbb{S}_{SH} &= \frac{16\pi}{m_Z^2}\Re\left[\frac{c_W^2}{eg_z}\left(\Pi_{z\gamma}(m_Z^2)-\Pi_{z\gamma}(0)\right)+\frac{s_W^2 c_W^2}{e^2}\left(\Pi_{\gamma\gamma}(m_Z^2)-\Pi_{\gamma\gamma}(0)\right)\right. \\
&\quad + \left.\frac{1}{g_z^2}\left(\Pi_{ZZ}(m_Z^2)-\Pi_{ZZ}(0)\right)\right], \\
\mathbb{T}_{SH} &= \frac{1}{\alpha_e}\Re\left[-\frac{\Pi_{WW}(0)}{m_W^2}+\frac{\Pi_{ZZ}(0)}{m_Z^2}+\frac{2s_W}{c_W}\frac{\Pi_{\gamma Z}(0)}{m_Z^2}+\frac{s_W^2}{c_W^2}\frac{\Pi_{\gamma\gamma}(0)}{m_Z^2}\right], \\
\mathbb{U}_{SH} &= 16\pi\Re\left[\frac{1}{g_z^2 m_Z^2}\left(\Pi_{ZZ}(m_Z^2)-\Pi_{ZZ}(0)\right)+\frac{2s_W^2}{eg_z m_Z^2}\left(\Pi_{z\gamma}(m_Z^2)-\Pi_{Z\gamma}(0)\right)\right. \\
&\quad + \left.\frac{s_W^4}{e^2 m_Z^2}\left(\Pi_{\gamma\gamma}(m_Z^2)-\Pi_{\gamma\gamma}(0)\right)+\frac{1}{g^2 m_W^2}\left(\Pi_{WW}(m_W^2)-\Pi_{WW}(0)\right)\right]. \quad (5.44)
\end{aligned}
$$

The explicit expressions for the $\Delta\mathbb{S}$ and $\Delta\mathbb{T}$ parameters for the SHM, including the extra singlet scalar representation, but without the vector-like quarks, are

$$
\Delta\mathbb{T}=\mathbb{T}_{SH}-\mathbb{T}_{SM}=-\frac{3s_\phi^2}{16\pi c_W^2}\left([t_S]-[t_H]\right), \quad (5.45)
$$

where

$$
[t_S]=\left[\frac{m_S^4\ln(m_S^2)s_W^2-(m_S^2-m_W^2)m_Z^2\ln(m_Z^2)-m_W^2\ln(m_W^2)c_w^2(m_S^2-m_Z^2)}{s_W^2(m_S^2-m_Z^2)(m_S^2-m_W^2)}\right], \quad (5.46)
$$

and similarly for $[t_H]$ function, with the replacement $m_S\to m_H$.

$$
\Delta\mathbb{S}=\mathbb{S}_{SH}-\mathbb{S}_{SM}=\frac{s_\phi^2}{12\pi}\left(2\ln(\frac{m_S}{m_H})+[s_S]-[s_H]\right), \quad (5.47)
$$

where

$$
[s_S]=\frac{m_Z^4(9m_S^2+m_Z^2)}{(m_S^2-m_Z^2)^3}\ln(\frac{m_S^2}{m_Z^2})-\frac{m_Z^2(4m_S^2+6m_Z^2)}{(m_S^2-m_Z^2)^2} \quad (5.48)
$$

and similarly for $[s_H]$ function, with the replacement $m_S\to m_H$.

Although pure scalar contributions to $\Delta\mathbb{S}$ and $\Delta\mathbb{T}$ relatively fit better with the experimental bounds as the scalar mixing angle is increased (Fig. 5.18), we are particularly interested in numerical values at $\sin\varphi\sim0.1$ and $m_S\sim 2$ TeV since the constraints coming from vacuum stability are more restricted. Moreover, in Fig. 5.18, it is seen that the whole scalar parameter space $m_S,~\sin\varphi$ is allowed, considering only the constraints from oblique parameters.

(a) $\sin \varphi = 0.1$

(b) $\sin \varphi = 0.2$

(c) $\sin \varphi = 0.4$
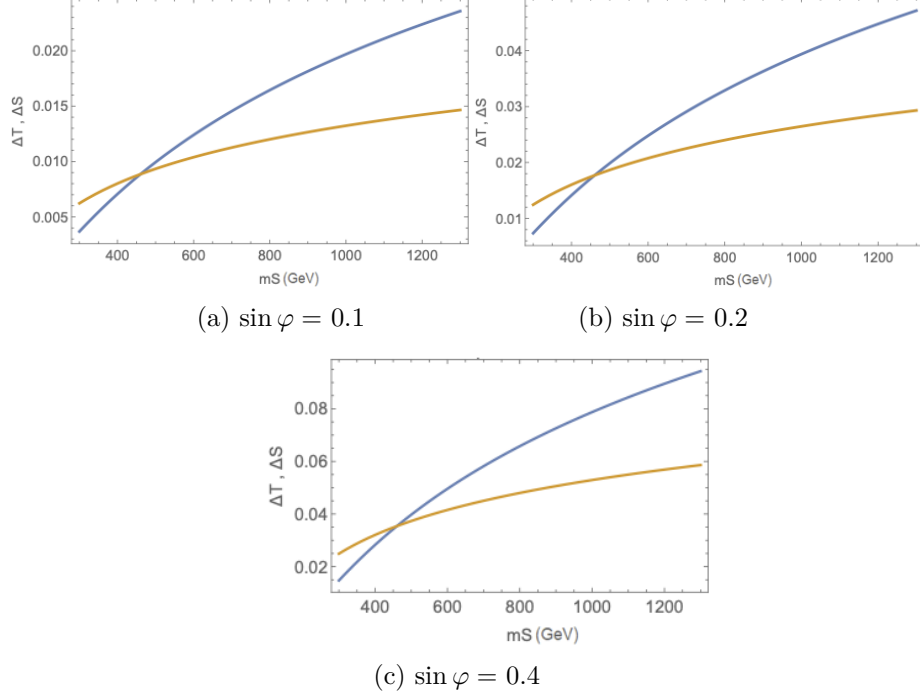
Figure 5.18: The contribution to the $\mathbb{T}$ (orange) and $\mathbb{S}$ (blue) parameters in the SM augmented by a singlet scalar, as a function of the singlet scalar mass. We take $u = 1$ TeV for our consideration to remain in the vicinity of vacuum stability constraints.

5.7.2 VLQ contributions to the $\mathbb{S}$ and $\mathbb{T}$ parameters

The oblique correction parameter $\mathbb{T}$ for vector-like quarks is given as [119]

$$
\begin{aligned}
\mathbb{T} \;=\; & \frac{N_c}{16\pi s_W^2 c_W^2} \Bigg[\sum_{\alpha,i} [(|V_{\alpha i}^L|^2 + |V_{\alpha i}^R|^2)\theta_+(y_\alpha, y_i) + 2Re(V_{\alpha i}^L V_{\alpha i}^{R*})\theta_-(y_\alpha, y_i)] \\
& - \sum_{\alpha,\beta} [(|U_{\alpha\beta}^L|^2 + |U_{\alpha\beta}^R|^2)\theta_+(y_\alpha, y_\beta) + 2Re(U_{\alpha\beta}^L U_{\alpha\beta}^{R*})\theta_-(y_\alpha, y_\beta)] \\
& - \sum_{i,j} [(|D_{ij}^L|^2 + |D_{ij}^R|^2)\theta_+(y_i, y_j) + 2Re(D_{ij}^L D_{ij}^{R*})\theta_-(y_i, y_j)] \Bigg] ,
\end{aligned}
\tag{5.49}
$$

where the fermion ratio functions $\theta_\pm$ are given as

$$
\begin{aligned}
\theta_+ \;&=\; y_1 + y_2 - \frac{2y_1 y_2}{y_1 - y_2} \ln \frac{y_1}{y_2}, \\
\theta_- \;&=\; 2\sqrt{y_1 y_2} \left(\frac{y_1 + y_2}{y_1 - y_2} \ln \frac{y_1}{y_2} - 2 \right),
\end{aligned}
\tag{5.50}
$$

where $y_i = (\frac{m_i}{m_Z})^2$, and for the $\mathbb{S}$ parameter,

$$
\begin{aligned}
\mathbb{S} &= \frac{N_c}{2\pi} \Bigg[\sum_{\alpha,i} [(|V_{\alpha i}^L|^2 + |V_{\alpha i}^R|^2)\psi_+(y_\alpha, y_i) + 2Re(V_{\alpha i}^L V_{\alpha i}^{R*})\psi_-(y_\alpha, y_i)] \\
&\quad - \sum_{\alpha,\beta} [(|U_{\alpha\beta}^L|^2 + |U_{\alpha\beta}^R|^2)\chi_+(y_\alpha, y_\beta) + 2Re(U_{\alpha\beta}^L U_{\alpha\beta}^{R*})\chi_-(y_\alpha, y_\beta)] \\
&\quad - \sum_{i,j} [(|D_{ij}^L|^2 + |D_{ij}^R|^2)\chi_+(y_i, y_j) + 2Re(D_{ij}^L D_{ij}^{R*})\chi_-(y_i, y_j)] \Bigg].
\end{aligned}
\tag{5.51}
$$

$V_{\alpha i}^{L,R}, U_{\alpha\beta}^{L,R}$ and $D_{ij}^{L,R}$ can be found in [113], and the functions $\psi_\pm$, $\chi_\pm$ are given respectively by

$$
\begin{aligned}
\psi_+ &= \frac{22y_\alpha + 14y_i}{9} - \frac{1}{9}\ln\frac{y_\alpha}{y_i} + \frac{1 + 11y_\alpha}{18}f(y_\alpha, y_\alpha) + \frac{7y_i - 1}{18}f(y_i, y_i), \\
\psi_- &= -\sqrt{y_\alpha y_i}\left(4 + \frac{f(y_\alpha, y_\alpha) + f(y_i, y_i)}{2}\right),
\end{aligned}
\tag{5.52}
$$

$$
\begin{aligned}
\chi_+ &= \frac{y_1 + y_2}{2} - \frac{(y_1 - y_2)^2}{3} + \left[\frac{(y_1 - y_2)^3}{6} - \frac{1}{2}\frac{y_1^2 + y_2^2}{y_1 - y_2}\right]\ln\frac{y_1}{y_2} + \frac{y_1 - 1}{6}f(y_1, y_1), \\
&\quad + \frac{y_2 - 1}{6}f(y_2, (y_2)) + \left[\frac{1}{3} - \frac{y_1 + y_2}{6} - \frac{(y_1 - y_2)^2}{6}\right]f(y_1, y_2) \\
\chi_- &= -\sqrt{y_1 y_2}\left[2 + (y_1 - y_2 - \frac{y_1 + y_2}{y_1 - y_2})\ln\frac{y_1}{y_2} + \frac{f(y_1, y_1) + f(y_2, y_2)}{2} - f(y_1, y_2)\right].
\end{aligned}
\tag{5.53}
$$

Except $\mathcal{U}_1$ and $\mathcal{D}_1$ cases, the contributions to $\mathbb{T}$ and $\mathbb{S}$ parameters from VLQ can be given by leading order approximation.

Singlet $\mathcal{U}_1$ (T), $Y = 2/3$

$$
\begin{aligned}
\Delta\mathbb{T} &= \frac{m_t^2 N_c(s_L^t)^2}{16\pi c_W^2 s_W^2 m_Z^2}\left[x_T^2(s_L^t)^2 - (c_L^t)^2 - 1 + 4(c_L^t)^2\frac{m_T^2}{m_T^2 - m_t^2}\ln(x_T)\right], \\
\Delta\mathbb{S} &= \frac{N_c(s_L^t)^2}{18\pi}\left(\frac{(c_L^t)^2}{(x_T - 1)^3}\left[2\ln(x_T)(3 - 9x_T^2 - 9x_T^4 + 3x_T^6) + 5 - 27x_T^2 - 27x_T^4 - 5x_T^6\right].\right. \\
&\quad - 2\ln(x_T))
\end{aligned}
\tag{5.54}
$$

Singlet $\mathcal{D}_1$ (B), $Y = -1/3$

$$
\begin{aligned}
\Delta\mathbb{T} &= \frac{m_t^2 N_c x_B}{16\pi c_W^2 s_W^2 m_Z^2(x_B - 1)}\left[(s_L^b)^4(x_B - 1) - 2(s_L^b)^2\ln(x_B)\right], \\
\Delta\mathbb{S} &= \frac{N_c(s_L^b)^2}{18\pi}\left[2\ln(\frac{m_b}{m_B})(3(s_L^b)^2 - 4) - 5(c_L^b)^2\right].
\end{aligned}
\tag{5.55}
$$

Doublet $\mathcal{D}_2$ (T, B), $Y = 1/6$

$$\Delta\mathbb{T} \simeq \frac{m_t^2 N_c (s_R^t)^2}{8\pi c_W^2 s_W^2 m_Z^2} \left[2\ln(x_T) - 2\right],$$

$$\Delta\mathbb{S} \simeq \frac{N_c}{18\pi} \left[(s_R^b)^2 \left(2\ln(x_T) - 2\ln(x_b) - 2\right) + (s_R^t)^2 \left(4\ln(x_T) - 7\right)\right]. \qquad (5.56)$$

Doublet $\mathcal{D}_X$ (X, T), $Y = 7/6$

$$\Delta\mathbb{T} \simeq \frac{m_t^2 N_c (s_R^t)^2}{8\pi c_W^2 s_W^2 m_Z^2 (x_T - 1)} \left[\ln\left((c_R^t)^2 + \frac{(s_R^t)^2}{x_T}\right) - \ln(x_T)[x_T + \mathcal{O}(x_T^{-4})]\right],$$

$$\Delta\mathbb{S} \simeq \frac{N_c (s_R^t)^2}{18\pi} \left[3 + \ln(x_T) + \mathcal{O}\left(\frac{(s_R^t)^4}{x_B}\right)\right]. \qquad (5.57)$$

Doublet $\mathcal{D}_Y$ (B, Y), $Y = -5/6$

$$\Delta\mathbb{T} \simeq \frac{m_t^2 N_c x_B}{128\pi c_W^2 s_W^2 m_Z^2} \left[-16 c_R^b \left(-3 + c_R^{2b} \cot_R^b \ln(c_R^b)\right) + s_R^b \left(-13 - 20 c_R^{2b} + 4 c_R^{2b}\right)\right],$$

$$\Delta S \simeq \frac{N_c}{144\pi} \left[-3\ln(x_B) + 20\ln(c_R^b) + \ln(x_b) + 19 + c_R^{4b}\left(5 + 3\ln(x_b)\right)\right.$$
$$\left. - \ 4 c_R^{2b}\left(6 + \ln(x_b)\right)\right]. \qquad (5.58)$$

Triplet $\mathcal{T}_X$ (X, T, B), $Y = 2/3$

$$\Delta\mathbb{T} \simeq \frac{m_t^2 N_c (s_L^t)^2}{16\pi c_W^2 s_W^2 m_Z^2} \left[6\ln(x_T) - 10 + \mathcal{O}((s_L^t)^4, (c_L^t)^4, x_T^{-4})\right],$$

$$\Delta S \simeq -\frac{N_c (s_L^t)^2}{18\pi} \left[9 - 6\ln(x_T) + 4\ln(x_b) + \mathcal{O}((c_L^t)^4, (c_L^t)^2 (s_L^t)^2)\right]. \qquad (5.59)$$

Triplet $\mathcal{T}_Y$ (T, B, Y), $Y = -1/3$

$$\Delta\mathbb{T} \simeq -\frac{m_t^2 N_c (s_L^t)^2}{16\pi c_W^2 s_W^2 m_Z^2} \left[2\ln(x_T) - 6 + \mathcal{O}((s_L^t)^4, (c_L^t)^2 (s_L^t)^2, x_T^{-3})\right],$$

$$\Delta\mathbb{S} \simeq \frac{N_c (s_L^t)^2}{18\pi} \left[2\ln(x_T) + 4 + \mathcal{O}((c_L^t)^4, (s_L^t)^4, (c_L^t)^2 (s_L^t)^2)\right]. \qquad (5.60)$$

where $x_i = \frac{m_F}{m_t}$ for all representations. We now scan over the oblique parameters from different VLQ masses with respect to the expression given in Eq. 5.54 - 5.60.

The $\mathbb{S}$-parameter agrees with the experimental bounds for small mixing angles, and does not bring tighter constraints on the masses of vector-like quarks. However, the $\mathbb{T}$-parameter becomes negative for small mixing angles for the $\mathcal{D}_1$ and $\mathcal{D}_X$ representations. This feature in return might exclude some regions of the parameter space once combined with the contributions from the SM + additional scalar, and imposes further conditions on the mass of singlet scalar. Apart from the vacuum stability constraints that connects the two sectors, this unique feature of electroweak precision accounts for the destructive interference

(a) $\mathcal{U}_1$ (T) (b) $\mathcal{D}_1$ (B)
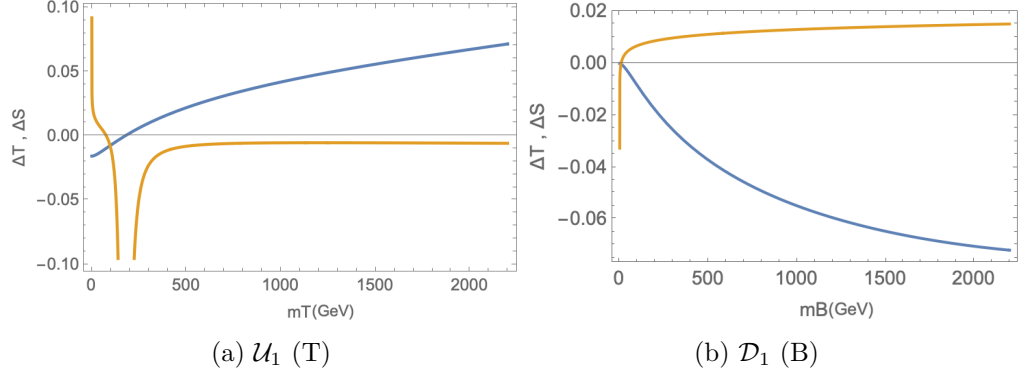
Figure 5.19: The contributions to the $\mathbb{T}$ (blue) and $\mathbb{S}$ (orange) parameters in the singlet representations, as functions of the vector-like quark mass.

(a) $\mathcal{D}_2$ (T,B) (b) $\mathcal{D}_X$ (X,T)

(c) $\mathcal{D}_Y$ (B,Y)
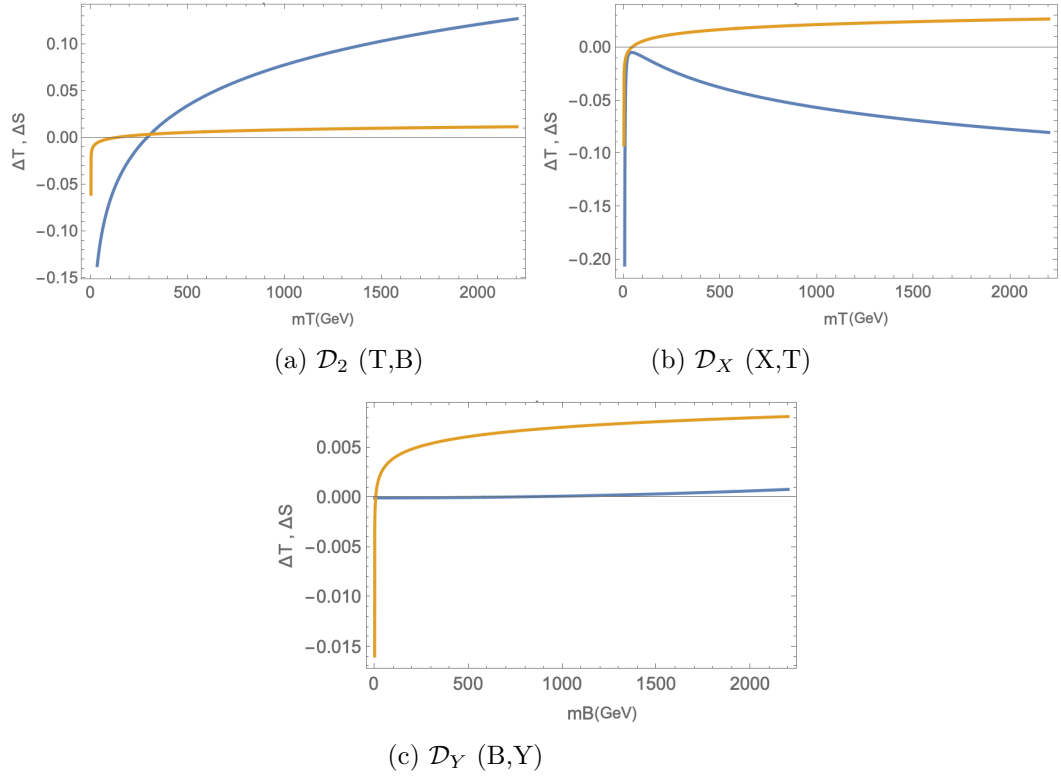
Figure 5.20: The contributions to the $\mathbb{T}$ (blue) and $\mathbb{S}$ (orange) parameters in the doublet representations as functions of the vector-like quark mass.

between parameter spaces of scalars and vector-like fermions. Similar studies have been carried out in the literature [120] to impose more restricted constraints on parameter spaces of additional scalars. Checking the Eq. 5.55 for $\Delta\mathbb{T}$, the logarithmic term suppress the linear term in the small mixing domain of $\mathcal{D}_1$. Similarly, for $\mathcal{D}_X$, the first term in Eq. 5.57 is inversely proportional to vector-like quark mass, which is rapidly suppressed by the second term, growing with opposite sign with respect to mass of vector-like quark. Numerical values for $\Delta\mathbb{T}$ and $\Delta\mathbb{S}$ at $m_{VLQ} \sim 1$ TeV agree with the experimental limits in small mixing

(a) $\mathcal{T}_X$ (X,T,B) (b) $\mathcal{T}_Y$ (T,B,Y)
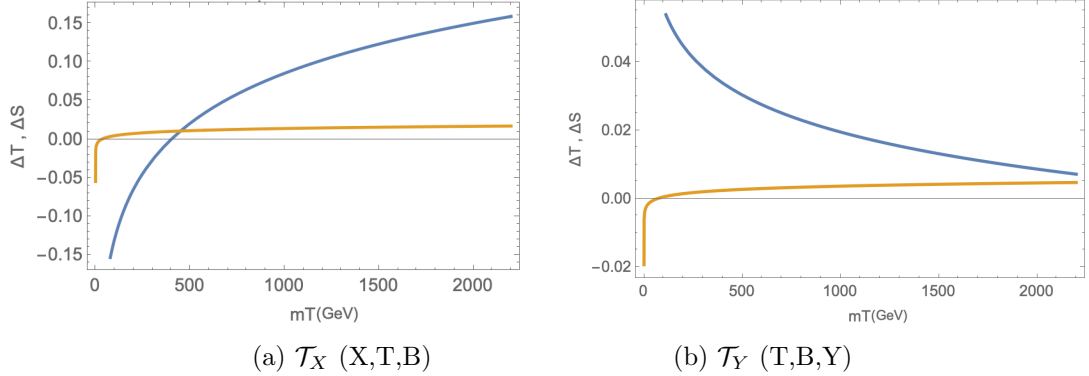
Figure 5.21: The contributions to the $\mathbb{T}$ (blue) and $\mathbb{S}$ (orange) parameters in the triplet representations, as functions of the vector-like quark mass.

throughout all representations. However, it is shown from the mutual regions satisfying $\mathbb{S}, \mathbb{T}$-parameters and vacuum stability parameter spaces that, in general, vector-like quark masses and mixings are inversely proportional to each other. Moreover, in the mixing interval $\sin\theta_{L,R} > 0.3$, although not shown here, $\Delta\mathbb{T}$ and $\Delta\mathbb{S}$ dangerously stray away from the experimental bounds, yielding more restrictions on m_S, as seen in Fig. 5.18. Therefore, negative contributions to $\Delta\mathbb{T}$ and $\Delta\mathbb{S}$ are very likely to be compensated with relatively heavier scalars in various models.

5.8   Conclusions

In this work, we presented a detailed analysis of the stability conditions on the Higgs potential under the presence of extra vector-like fermions. Since these have the same couplings for left and right components, they do not affect the loop-induced decays of the SM Higgs boson, and indeed, can have arbitrary bare masses in the Lagrangian. We asked the question of whether they can have an effect on the Higgs sector, in particular, we concentrated on one of the outstanding problems in the SM, vacuum stability of the Higgs potential. While vector-like fermions appear in many beyond the SM models, here we have taken a model-independent approach. We allowed mixing of the vector-like fermions with the third generation chiral fermions only, and we considered all possible anomaly free possibilities for the vector-like representations, with the additional fermions allowed to be in singlet, doublet, or triplet representations.

As all other fermions, their effect on the RGE's of the Higgs self-coupling constant is to lower it further, worsening the vacuum stability. An additional boson is introduced to alleviate this problem (representing an additional Higgs boson which would naturally appear in most New Physics models). Its presence is essential, and by itself it remedies the stability problem. The allowed additional scalar mass varies with its assigned VEV, but for all scenarios the mixing with the SM Higgs is required to be non-zero. We analyze constraints on the parameter space coming from theory, experiment and cosmology, and accordingly, we require the singlet mass to be preferably in the $\mathcal{O}(\text{TeV})$ scale. Thus this work focuses on TeV scale with small mixing because once vector-like quarks are introduced, stability becomes the most restrictive theoretical constraint. Even in bare HSM (without vector-like quarks), stability is one of the most stringent ones. In addition, the singlet scalar

VEV must be in the TeV scale as well, as smaller VEVs spoil perturbativity and severely restrict the parameter space.

Additional fermionic representations survive for scalar VEVs $u = 1, 2$ or 4 TeV, and the agreement improves with increasing the scalar VEVs, indicating that higher scale physics is more likely to improve the vacuum stability problem. For most models, $u = 1$ TeV is highly restricted, and likely ruled out, especially for top-like vector fermions, or in doublet models where this fermion is the only one mixing with the SM top. The situation worsens for the (X, T) doublet model, where for all values of the VEV u, the mass m_T hovers around 1000 GeV and is independent of the mixing. For triplet representations, the parameter spaces for $T - t$ mixing have similar characteristics in imposing a small vector-like quark mass limit, regardless of the value for the singlet VEV. Compared to the doublet (T, B) representation, large mixing angles are permitted, for a relatively wide allowed mass spectrum. Comparatively, the model (X, T, B) is more sensitive to large vector-like quark masses, and shrinks the mixing angles to a small range as m_T becomes large, whereas the model (T, B, Y) allows for more parameter space for masses and mixing angles space for various singlet VEVs. The differences in parameter spaces can be attributed to the fact that although the vector-like quark X does not mix with the SM particles, its Yukawa term appears in the RGE for y_T, which is unique to the (X, T, B) model.

Vacuum stability is improved if the bottom-like fermion is also present, and allowed to mix with the b quark. The mixing angles are in general small (an exception are extreme cases where the mass is extremely restricted and the mixing completely free). However the difference between models with top-like or bottom-like quarks offer a way to distinguish between them, complimentary to collider searches.

Compared to T vector-like quarks, constraints on the B-like fermion masses and mixing angles are much more relaxed. For the (T, B) doublet model, the restrictions affect mostly m_T and are relaxed for m_B (the mixing with the b quark is required to be small). While the mixing can be larger for the (B, Y) and (T, B, Y) models, and for $m_B = 1000$ GeV, the mixing with the bottom quark is unrestricted. (On the other hand, the models (T,B,Y) and (B,Y) have almost identical parameter spaces for B mixings regardless of the singlet VEV. The mixings are constrained everywhere except $m_B = 1000$ GeV. Although it's possible, the model (T, B, Y) is relatively less sufficient to impose mass values for m_B around 1000 GeV for $u = 1$ TeV. And finally, B mixings become less relaxed as the mass of vector-like quark gets larger for the models (T, B) and (X, T, B).) The vector-like quarks carrying non-SM hypercharge do not mix with quarks, and seem to be required to have masses of around 1000 GeV, irrespective of the model, other vector-like fermion masses, or scalar VEV.

Compared to vacuum stability restrictions, electroweak precision constraints are more relaxed. Although the $\mathbb{S}$-parameter does not introduce strong restrictions on parameter space, the $\mathbb{T}$-parameter evolves in negative direction in different models. Combined with scalar contributions to $\mathbb{S}$ and $\mathbb{T}$-parameters, deviations from the experimental precision data might impose further restrictions on additional scalars and mixings with Higgs.

In conclusion, models where T-quark is unaccompanied by a B-quark yield very restrictive constraints for the masses m_T and mixing angles $\sin \theta_L$. As well, additional vector-like fermions with hypercharge 5/3 or -4/3 are shown to restricted the additional fermions to masses close to 1 TeV, for the sampled range of the parameter space, which, in association with their exotic charges, renders them predictable, making it easy to confirm or rule out the existence of these fermions. Our considerations which constrain the masses and mixings of vector-like fermions are complimented by analyses on the parameters of models with vector-like quarks from electroweak fits to the parameters in these models.

Chapter 6

Vector-like Quarks in the Two Higgs Doublet Model

6.1 Introduction

The discovery of the Higgs boson [4, 5] marked a significant milestone in particle physics, validating the existence of the missing piece of the Standard Model (SM). Yet the data collected supporting the Higgs discovery seem to indicate that principles of stability, renormalizability, and naturalness, which motivated the introduction the Higgs boson in the first place, appear in conflict with the properties of the Higgs field itself. The idea of naturalness seems to be in conflict with the surprising degree of fine-tuning of both parameters in the Higgs field potential [56, 70]. Related to this is the issue of the stability of the electroweak vacuum which arises from the behaviour of the Higgs potential under renormalization group equations. To address this issue, it became imperative to explore extensions of the SM that could resolve this instability while remaining consistent with experimental observations. These explorations involve extending the particle content by additional states, and/or extending the symmetry group (which in turn, result in the presence of new particles).

Such additional particles can be fermions or bosons. While the former are limited, the later appear to have a wider range of applicability. The issue with additional fermions is the following. In the SM, gauge invariance does not allow for the introduction of bare mass terms for quarks and leptons, since these terms are not gauge invariant. So quark and lepton masses only arise from Yukawa interactions, after spontaneous gauge symmetry breaking. Additional fermionic families (quark or lepton) are ruled out by the Higgs data, since both the digluon production cross section (and decay), and diphoton decay channel, agree with the SM predictions and thus are inconsistent with the existence of additional fermions in the loops. The reason is the following. For the gluon fusion, the lowest order process proceeds through a loop involving quarks. The loop function which depends on ratio of the quark mass over the Higgs mass, both squared. The loop function is negligible for light quarks, where this ratio is < 1, leaving only the top contribution to be significant. However if there are additional generations of *chiral* fermions, their contributions will also add to that of the top quark and enhance the cross section, rendering it inconsistent with the experimental value [121, 122]. Thus surprisingly, heavy chiral quark contributions do not decouple [123, 124].

However, if the fermionic components have vector-like structure, rather than SM-chiral-like, their left- and right-handed components have the same couplings, allowing for bare mass terms which are gauge invariant. The addition of these particles is one of the simplest extensions of the SM. Because of their vector-like nature, they do not contribute to gauge anomalies and are less restricted than their chiral counterparts by current experimental data. They may populate the desert between the SM and the scale of grand-unification, without worsening the hierarchy problem. Vector-like quarks (VLQs), allowed to mix that couple with the third generation quarks (top and bottom partners), appear in composite Higgs models with a partially-composite top quark [125–128]. They are naturally present in theories with extra dimensions [79, 129–133] and in Little Higgs Models [134–136]. Finally, VLQs can be introduced in non-minimal supersymmetric models to increase corrections to the Higgs mass without significantly affecting electroweak precision observables [137–139], and they appear also in GUT-inspired, supersymmetric models [140].

Additionally, VLQ may explain some of the mismatch between the SM predictions and observed data. For instance the CKM matrix, which encodes couplings for each of the three generation quarks is, by construction, unitarity. However, the recent dataset collected after 2018 [141] disfavours the CKM unitarity of the first row for three generations of quarks to 99.998% C.L., a problem confirmed by the determination of V_{ud} from superallowed beta decays [142]. While improved lattice evaluations of decay constants and form factors for kaons and pions, and corrections to the nuclear beta decay have shrunk the discrepancy to 3σ, referred to as the Cabibbo Angle Anomaly [143, 144], introducing VLQs seems the most promising avenue, because of they are able to yield right-handed charged quark currents, which can modify the CKM matrix results [145]. An additional VLQ family could also explain quark and lepton mass hierarchies [146].

In the context of the SM, vector-like quarks (VLQ) contribute to the stability of the vacuum, due to their strong coupling. It is well-known that in the SM, the stability of the vacuum is threatened by the strong coupling of the top to the Higgs boson [147]. The simplest cure is to add a scalar singlet field, which mixes with the SM Higgs boson and compensates for the top quark contribution [92]. Vector-like quarks, due to their distinct representation under the electroweak group, offer a promising avenue for mitigating the vacuum stability problem. The question remains, how would the vacuum stability be affected by the addition of VLQs to the particle content.

In a previous work [1], we analyzed the effects of all possible representations of vector-like quarks and their implications for maintaining vacuum stability within the SM augmented by an additional scalar. We have shown that, even with the addition of VLQs, the presence of the additional scalar was still a necessity. We extend this analysis here to the study of the effect of introducing vector-like quarks into the a simple extension of the SM, the Two-Higgs Doublet Model (2HDM). Thus we effectively replace the singlet scalar by scalars in a doublet representation. Our study involves analyzing all anomaly-free representations of vector-like quarks and their implications for maintaining vacuum stability within this model. As several versions of the model exist, we shall concentrate here on Type-I (where the fermions couple to only one Higgs doublet and the other is inert) and Type-II (where up quarks and neutrinos couple to one Higgs doublet, while down quarks and charged leptons couple to the other). The latter is of particular interest as it is consistent with the interaction structure required in supersymmetry.

The Two-Higgs doublet models, seen as one of the simplest extensions of the SM, have received a great deal of attention in the literature, see for example [148–166] and references therein. There are several motivations for extending the SM to 2HDMs. The best known is, as alluded to before, supersymmetry. In supersymmetric theories, the scalars belonging to multiplets of different chiralities cannot couple together in the Lagrangian, and thus a single Higgs doublet cannot give mass to both up- and down-type quarks. In addition, cancellation of anomalies also requires the presence of an additional doublet. Another motivation for 2HDMs comes from axion models [167]. It was noted [168] that a possible CP-violating term in the QCD Lagrangian can be rotated away if the Lagrangian contains a global $U(1)$ symmetry, but this is possible only if there are two Higgs doublets. And yet another motivation for 2HDMs comes from the fact that the SM is unable to generate a sufficiently large baryon asymmetry of the Universe, while 2HDMs can, due to additional sources of CP violation [169].

In this paper, we investigate the effects of vector-like quarks in the context of extending of SM to the 2HDM framework. By incorporating vector-like quarks into 2HDM, we analyze whether we can overcome the negativity of quartic Higgs boson self couplings by finding a viable parameter space consistent with various theoretical and experimental constraints in Type-I and Type-II 2HDM scenarios. Furthermore, we delve into the consequences of these extensions on precision electroweak observables. We focus on two separate components: first the oblique parameters originating from purely the 2HDM and second, on the impact of vector-like quark contributions on these observables. These analyses shed light on the potential alterations to electroweak measurements that arise from the inclusion of vector-like quarks in multi-Higgs scenarios. Through numerical simulations, we demonstrate the significant role that vector-like quarks play in stabilizing the electroweak vacuum while maintaining agreement with precision electroweak measurements. Our aim is to provide insights into the potential avenues for extending the SM to address some of its shortcomings and set the theoretical framework for future explorations and for experimental validations.

Our work is organized as follows. In Section 6.2 we review the 2HDM. In the following Section 6.3 we review vector-like quarks, in singlet, doublet or triplet representations, setting the general Lagrangian responsible for their interaction, as well as reviewing experimental searches and theoretical considerations responsible for restricting their masses. Section 6.5 is dedicated to our exploration of the parameter space of the 2HDM with VLQs which satisfies vacuum stability bounds. Section 6.6 explores the constraints imposed by electroweak precision observables on the surviving parameter space, looking separately at the restrictions coming from the 2HDM alone, in 6.6.1, and from the VLQs, in 6.6.2. We summarize our findings and conclude in Section 6.7. Finally, in the Appendices B.1-B.2 we gather all RGE formulas for the VLQ representations used in this work.

6.2   The Two Higgs Doublet Model

In what follows, we present brief summary of the Two Higgs Doublet Model (2HDM). Extensive reviews of the 2HDMs of Type-I and Type-II are in *e.g.* [148, 149]. The most general scalar potential contains 14 parameters and can have CP-conserving, CP-violating, and charge violating minima. We make several simplifying assumptions: that CP is conserved in the Higgs sector, allowing one to distinguish between scalars and pseudoscalars,

that CP is not spontaneously broken, and that discrete symmetries eliminate from the potential all quartic terms odd in either of the doublets.

The 2HDM scalar potential for the two doublet fields with hypercharge $Y = 1$, which is invariant under the gauge symmetry of the SM, $SU(3)_C \otimes SU(2)_L \otimes U(1)_Y$ and satisfy a discrete Z_2 symmetry is given by [148]

$$
\begin{aligned}
V(\Phi_1, \Phi_2) &= m_{11}^2 \Phi_1^\dagger \Phi_1 + m_{22}^2 \Phi_2^\dagger \Phi_2 - m_{12}(\Phi_1^\dagger \Phi_2 + \Phi_2^\dagger \Phi_1) + \frac{\lambda_1}{2}(\Phi_1^\dagger \Phi_1)^2 + \frac{\lambda_2}{2}(\Phi_2^\dagger \Phi_2)^2 \\
&+ \lambda_3(\Phi_1^\dagger \Phi_1)(\Phi_2^\dagger \Phi_2) + \lambda_4(\Phi_1^\dagger \Phi_2)(\Phi_2^\dagger \Phi_1) + \frac{\lambda_5}{2}\left[(\Phi_1^\dagger \Phi_2)^2 + (\Phi_2^\dagger \Phi_1)^2\right],
\end{aligned}
\tag{6.1}
$$

where the complex doublets are perturbed around their minimums v_i as

$$
\Phi_i = \begin{pmatrix} w_i^+ \\ \frac{v_i + \rho_i + i\eta_i}{\sqrt{2}} \end{pmatrix}, \qquad (i = 1, 2)
\tag{6.2}
$$

with $\sqrt{v_1^2 + v_2^2} = v = 246$ GeV, and the m_{12}^2 term softly breaks the Z_2 symmetry. The reason for introducing Z_2 symmetry is to avoid tree-level flavour-changing neutral currents. Minimizing the 2HDM potential Eq. 6.1 breaks electroweak symmetry and allows the scalar potential be fully described in terms of seven independent parameters. Unlike the Standard Model, where spontaneous symmetry breaking leaves only a single free Higgs field, the 2HDM features five fields, corresponding to five distinct Higgs particles. For the doublets Φ_i to have their minima precisely at $\langle \Phi_i \rangle$, the two conditions for the minima must be satisfied

$$
\frac{\partial V(\Phi_1, \Phi_2)}{\partial \Phi_1^\dagger} = 0, \qquad \frac{\partial V(\Phi_1, \Phi_2)}{\partial \Phi_2^\dagger} = 0.
\tag{6.3}
$$

Such requirement equivalently generates the tadpole relations for the 2HDM, which must vanish in the lowest level

$$
\begin{aligned}
T_1 &= m_{11}^2 v_1 - m_{12}^2 v_2 + \frac{\lambda_1 v_1^3}{2} + \frac{\lambda_{345} v_1 v_2^2}{2} = 0, \\
T_2 &= m_{22}^2 v_2 - m_{12}^2 v_1 + \frac{\lambda_2 v_2^3}{2} + \frac{\lambda_{345} v_1^2 v_2}{2} = 0.
\end{aligned}
\tag{6.4}
$$

The tadpole conditions enable the removal of two parameters m_{11}^2, m_{22}^2 from the 2HDM potential, allowing them to be expressed in terms of the remaining parameters. In addition to the terms that are linear in the fields, substituting the doublet expansions from Eq. 6.2 into the 2HDM potential introduces bilinear terms involving the fields $w_i^\pm, \rho_i, \eta_i$. These bilinear terms affect the propagators of the eight fields, leading to the generation of mass terms as

$$
V(w_i^\pm, \rho_i, \eta_i) = \frac{1}{2}\begin{pmatrix} w_1^+ & w_2^+ \end{pmatrix} M_w^2 \begin{pmatrix} w_1^- \\ w_2^- \end{pmatrix} + \frac{1}{2}\begin{pmatrix} \rho_1 & \rho_2 \end{pmatrix} M_\rho^2 \begin{pmatrix} \rho_1 \\ \rho_2 \end{pmatrix} + \frac{1}{2}\begin{pmatrix} \eta_1 & \eta_2 \end{pmatrix} M_\eta^2 \begin{pmatrix} \eta_1 \\ \eta_2 \end{pmatrix}, \tag{6.5}
$$

where the mass matrices are expressed as

$$
\begin{aligned}
M_w^2 &= \left(\frac{m_{12}^2}{v_1 v_2} - \frac{\lambda_4 + \lambda_5}{2}\right)\begin{pmatrix} v_2^2 & -v_1 v_2 \\ -v_1 v_2 & v_1^2 \end{pmatrix} + \begin{pmatrix} \frac{T_1}{v_1} & 0 \\ 0 & \frac{T_2}{v_2} \end{pmatrix}, \\
M_\rho^2 &= \begin{pmatrix} m_{12}^2 \frac{v_2}{v_1} + \lambda_1 v_1^2 & -m_{12}^2 + \lambda_{345} v_1 v_2 \\ -m_{12}^2 + \lambda_{345} v_1 v_2 & m_{12}^2 \frac{v_1}{v_2} + \lambda_2 v_2^2 \end{pmatrix} + \begin{pmatrix} \frac{T_1}{v_1} & 0 \\ 0 & \frac{T_2}{v_2} \end{pmatrix}, \\
M_\eta^2 &= \left(\frac{m_{12}^2}{v_1 v_2} - \lambda_5\right)\begin{pmatrix} v_2^2 & -v_1 v_2 \\ -v_1 v_2 & v_1^2 \end{pmatrix} + \begin{pmatrix} \frac{T_1}{v_1} & 0 \\ 0 & \frac{T_2}{v_2} \end{pmatrix}.
\end{aligned}
\tag{6.6}
$$

Diagonalization of mass matrices are necessary to have physical particles in the 2HDM with bi-unitary transformation

$$V_\alpha = \begin{pmatrix} c_\alpha & -s_\alpha \\ -s_\alpha & c_\alpha \end{pmatrix}, \qquad V_\beta = \begin{pmatrix} c_\beta & -s_\beta \\ -s_\beta & c_\beta \end{pmatrix}. \tag{6.7}$$

The diagonal mass matrices of the 2HDM is found by applying a set of orthogonal transformation[1]

$$D_w^2 = V_\beta^\dagger M_w^2 V_\beta, \qquad D_\rho^2 = V_\alpha^\dagger M_\rho^2 V_\alpha, \qquad D_\eta^2 = V_\eta^\dagger M_\eta^2 V_\alpha, \tag{6.8}$$

where

$$D_w^2 = \begin{pmatrix} M_{G^\pm}^2 & 0 \\ 0 & M_{H^\pm}^2 \end{pmatrix}, \qquad D_\rho^2 = \begin{pmatrix} M_H^2 & 0 \\ 0 & M_h^2 \end{pmatrix}, \qquad D_\eta^2 = \begin{pmatrix} M_G^2 & 0 \\ 0 & M_A^2 \end{pmatrix}. \tag{6.9}$$

The mass eigenvalues of the physical particles read

$$
\begin{aligned}
M_{H^\pm}^2 &= v^2 \left(\frac{m_{12}^2}{v_1 v_2} - \frac{\lambda_4 + \lambda_5}{2} \right), \\
M_H^2 &= \frac{1}{2} \left(M_{\rho_{11}}^2 + M_{\rho_{22}}^2 + \sqrt{(M_{\rho_{11}}^2 - M_{\rho_{22}}^2)^2 + 4(M_{\rho_{12}}^2)^2} \right), \\
M_h^2 &= \frac{1}{2} \left(M_{\rho_{11}}^2 + M_{\rho_{22}}^2 - \sqrt{(M_{\rho_{11}}^2 - M_{\rho_{22}}^2)^2 + 4(M_{\rho_{12}}^2)^2} \right), \\
M_A^2 &= v^2 \left(\frac{m_{12}^2}{v_1 v_2} - \lambda_5 \right), \\
M_G^2 &= M_{G^\pm}^2 = 0.
\end{aligned}
\tag{6.10}
$$

For clarity, it is important to point out that the diagonalization process links the two angles, α and β to the 2HDM parameters via the following tree-level relation

$$t_{2\alpha} = \frac{s_{2\beta} \left(\frac{m_{12}^2}{s_\beta c_\beta} - \lambda_{345} v^2 \right)}{c_\beta^2 \left(\frac{m_{12}^2}{s_\beta c_\beta} - \lambda_1 v^2 \right) - s_\beta^2 \left(\frac{m_{12}^2}{s_\beta c_\beta} - \lambda_2 v^2 \right)} \tag{6.11}$$

along with $\tan \beta = v_2/v_1$, α is the mixing angle between the two CP-even scalars and $\lambda_{345} = \lambda_3 + \lambda_4 + \lambda_5$. The scalar couplings at μ_0 can be expressed in terms of the physical masses of the two CP-even scalars, h, H, CP-odd Higgs A and two charged Higgs bosons $H^\pm$ as

$$
\begin{aligned}
\lambda_1 &= \frac{M_H^2 \cos^2 \alpha + M_h^2 \sin^2 \alpha}{v^2 \cos^2 \beta}, \\
\lambda_2 &= \frac{M_h^2 \cos^2 \alpha + M_H^2 \sin^2 \alpha}{v^2 \sin^2 \beta}, \\
\lambda_3 &= \frac{\sin 2\alpha}{v^2 \sin 2\beta} (M_H^2 - M_h^2) + \frac{2M_{H^\pm}^2}{v^2}, \\
\lambda_4 &= \frac{M_A^2 - 2M_{H^\pm}^2}{v^2}, \\
\lambda_5 &= -\frac{M_A^2}{v^2}.
\end{aligned}
\tag{6.12}
$$

---

[1]Here s_α, c_α and t_β denotes sine, cosine and tangent of the given parameters.

In contrast to the SM vacuum which conserves CP symmetry but breaks $SU(2)_L \otimes U(1)_Y$ symmetry, there are four possible vacuum states in 2HDM. Charge-breaking vacuum occurs when the charged component of either of scalars acquires a non-zero VEV. $U(1)$ symmetry is spontaneously broken, and the photon gets a non-zero mass

$$\langle \Phi_1 \rangle_{CB} = \frac{1}{\sqrt{2}} \begin{pmatrix} 0 \\ c_1 \end{pmatrix}, \qquad \langle \Phi_2 \rangle_{CB} = \frac{1}{\sqrt{2}} \begin{pmatrix} c_2 \\ c_3 \end{pmatrix}, \tag{6.13}$$

CP-breaking vacuum occurs when there is a relative phase difference between the vacuum expectation values (VEVs) of the neutral components of the scalar doublets

$$\langle \Phi_1 \rangle_{CP} = \frac{1}{\sqrt{2}} \begin{pmatrix} 0 \\ v_1 \end{pmatrix}, \qquad \langle \Phi_2 \rangle_{CP} = \frac{1}{\sqrt{2}} \begin{pmatrix} 0 \\ v_1 e^{i\eta} \end{pmatrix}. \tag{6.14}$$

The inert vacuum state happens when either one of the scalar fields acquire a non-zero VEV.

$$\langle \Phi_1 \rangle_{IN} = \frac{1}{\sqrt{2}} \begin{pmatrix} 0 \\ v \end{pmatrix}, \qquad \langle \Phi_2 \rangle_{IN} = \frac{1}{\sqrt{2}} \begin{pmatrix} 0 \\ 0 \end{pmatrix}, \tag{6.15}$$

while mixed (normal) vacuum occurs when both of the neutral components of the scalar doublets have non-zero and positive VEVs

$$\langle \Phi_1 \rangle_N = \frac{1}{\sqrt{2}} \begin{pmatrix} 0 \\ v_1 \end{pmatrix}, \qquad \langle \Phi_2 \rangle_N = \frac{1}{\sqrt{2}} \begin{pmatrix} 0 \\ v_2 \end{pmatrix} \tag{6.16}$$

If all different vacua could have existed simultaneously in 2HDM potential, then one can undoubtedly think that the probability of transition between these states is non-zero. It was shown in Ref. [170] that if 2HDM potential has a CP conserving vacuum, then the different vacua (CP and CB) become saddle points[1], with energy larger than that of the CP preserving vacuum, insuring that normal vacua stays global. If two different pair of normal vacua can coexist, for a choice of $\tan \beta$ value, more than one pair of v_1, v_2 $(\hat{v}_1, \hat{v}_2)$, might survive away from the origin [171]. The relative depth of the potentials is given by[2].

$$\Delta V = \frac{1}{2} \left[\left(\frac{M_{H^\pm}^2}{v_1^2 + v_2^2} \right) - \left(\frac{M_{H^\pm}^2}{\hat{v}_1^2 + \hat{v}_2^2} \right) \right] (v_1 \hat{v}_2 - v_2 \hat{v}_1)^2. \tag{6.17}$$

However, a new pair of deeper minima $(\hat{v}_1, \hat{v}_2)$ in a special form of the 2HDM potential conflicts with SM phenomenology (the Higgs boson data) for a large region of the parameter space while a small parameter space still survives, preserving the mass spectrum of the SM and yet developing a non-zero transition rate between different normal vacua pairs. Nevertheless, the coexistence of two pair neutral vacua $\sqrt{v_1^2 + v_2^2} < \sqrt{\hat{v}_1^2 + \hat{v}_2^2}$ results in a particle spectrum which might yield decays conflicting with the SM predictions, even without RG flow, given the age of universe exceeds the tunnelling time. A sufficient condition that the normal vacua $v^2 = v_1^2 + v_2^2$ remains a global minimum is [162]

$$m_{12}^2 \left(m_{11}^2 - \sqrt{\frac{\lambda_1}{\lambda_2}} m_{22}^2 \right) \left(\tan \beta - \left[\frac{\lambda_1}{\lambda_2} \right]^{1/4} \right) > 0. \tag{6.18}$$

---

[1]This is not necessarily so for the CP breaking case, though normal vacua remains deeper.

[2]A similar relation in terms of inert and inert-like minimum cases is given elsewhere [172]

Additionally, one loop effects rise in the effective 2HDM potential, hence the relative depth of potential under the presence of the coexistence of inert [172] and of CB vacua [173] cases involve further corrections. Consequently the parameter space extracted from the relative depth of potential is extended. In fact, such effect is an alternative way for renormalized couplings to manifest themselves according to RGEs, since the complete form of the effective potential runs over all gauge boson, fermion and scalar fields contributions. In return, renormalized couplings and masses according to a cut-off scale modify the relative depth between two effective potential under the coexistence of vacua. The procedure follows according to the general structure of β-functions under the SM symmetry group, whereas gauge and scalar couplings extend the parameter space in a similar way. The Yukawa couplings do not affect the inert-like minimum since the fermions remain massless. The non-coexistence of CB and normal vacua is assured by the relative depth between different vacua nature $V_{CB} - V_{EW} > 0$, hence the normal vacuum remains global minimum at tree level. However, there exists a finite allowed region [173] from one loop corrections to V_{EW}^{eff} that might develop a larger effective potential than the one of V_{CB}^{eff}. Since the effective potential is RG scale independent, this phenomena is not related to the energy scale for which the loop corrections are performed. Thus at one-loop level, different from at tree level, the effective scalar potential that measures transition rates between EW and CB vacua is extremely dependent on particle content given. Nonetheless, the study of the surviving rates is meaningful in the case where $V_{EW} - V_{CB} > 0$ and concludes remarkably that the tree level relation for EW vacuum stability may not hold for a unique choice of parameters.

Furthermore, tree level vacuum stability is insured if the following necessary and sufficient conditions are satisfied for the potential parameters in softly broken Z_2 symmetry [174]

$$
\begin{aligned}
&\lambda_1(\mu) > 0, \qquad \lambda_2(\mu) > 0, \\
&\lambda_3(\mu) + \sqrt{\lambda_1(\mu)\lambda_2(\mu)} > 0, \\
&\lambda_3(\mu) + \lambda_4(\mu) - |\lambda_5(\mu)| > -\sqrt{\lambda_1(\mu)\lambda_2(\mu)}\,.
\end{aligned}
\tag{6.19}
$$

While these conditions may not necessarily hold true at the one-loop level, within the range where perturbative methods apply, the minor adjustments in the one-loop corrections to the effective potential should not substantially alter the potential's asymptotic trends. Typically, this is managed by scrutinizing the RG evolution of scalar couplings in the potential and ensuring that the criteria outlined in Eq. 6.19 remain applicable across all scales. Throughout our work in Section 6.5, the conditions Eq. 6.19 and Eq. 6.20 on all the quartic couplings are satisfied up to the Planck scale. In principle, assuming the most general 2HDM potential (*e.g.* Z_2 is not preserved, $\lambda_6, \lambda_7 \neq 0$), it was shown [152, 175, 176] that necessary and sufficient conditions for boundedness from below (BFB) can be numerically solved for limited cases. Inclusion of λ_6 and λ_7 extends the parameter space that satisfies BFB conditions. Without loss of generality, the BFB conditions for the most general 2HDM potential reduce to Eq. 6.19. To this end, by adopting Z_2 conserving case only, our scanning of complete RGEs in Section 6.5 obeys Eq. 6.19 at all energy scale up to $\mu = M_{Pl}$. Additional conditions on the parameters of the 2HDM potential at the tree

level emerge when ensuring the theory maintains unitarity [177, 178]

$$
\begin{aligned}
|\lambda_3 - \lambda_4| &< 8\pi \\
|\lambda_3 + 2\lambda_4 \pm 3\lambda_5| &< 8\pi \\
\left| \frac{1}{2} \left(\lambda_1 + \lambda_2 \sqrt{(\lambda_1 - \lambda_2)^2 + 4\lambda_4^2} \right) \right| &< 8\pi \\
\left| \frac{1}{2} \left(\lambda_1 + \lambda_2 \sqrt{(\lambda_1 - \lambda_2)^2 + 4\lambda_5^2} \right) \right| &< 8\pi
\end{aligned} \tag{6.20}
$$

At the end of Section 6.4, the tree level expressions[1], Eqs. 6.20, will be further modified to one-loop corrections for perturbative unitarity conditions in order to be examined throughout complete 2HDM+VLQ RGE scan. We consider the case where $M_h < M_H$ (with h the SM-like Higgs boson), the light Higgs masses scenario and normal vacuum in this study. Based on how Z_2 symmetry is imposed on the 2HDM Lagrangian, four types of Yukawa interactions arise. Here we consider only two versions of the model:

- Type-I: All fermions couple to the Φ_2 doublet, and the discrete symmetry is described as $\Phi_2 \to -\Phi_2$.

- Type-II: All charged leptons and down type quarks couple to Φ_1 and all up type quarks couple to Φ_2.

Adopting a similar method as the HSM, the effective potential of the 2HDM can be used to construct one-loop RGEs once the tree level expression is corrected by CW potential

$$
V^1(\Phi_i) = \frac{1}{64\pi^2} \sum_i \left(M_i^2(\Phi) \right)^2 \left[\ln \left(\frac{M_i^2(\Phi_i)}{\mu^2} \right) - \frac{3}{2} \right], \tag{6.21}
$$

where the field-dependent masses are set by second order variation of the tree level potential

$$
M_{ij} = \frac{1}{2} \frac{\partial^2 V^{(0)}}{\partial \phi_i \partial \phi_j}. \tag{6.22}
$$

Since the degrees of freedom that the vector fields have exceeds the degrees of freedom of the physical gauge fields, the 2HDM gives rise to gauge-freedom. However, choosing Landau gauge $\chi = 0$ set that the additional gauge-dependent pieces do not contribute to field-dependent scalar masses. For Z_2-symmetric case we adopt, the scalar part is already given in Eq. 6.10. For the gauge bosons, the field-dependent masses are derived from the kinetic part of the Lagrangian $\supset (D_\mu \Phi_i)^\dagger (D^\mu \Phi_i)$ in terms of the expectation values of both doublets

$$
\begin{aligned}
\mathcal{L}(\Phi_1, \Phi_2) &= \frac{1}{4} g_1^2 B_\mu B^\mu \left(\langle \Phi_1 \rangle^2 + \langle \Phi_2 \rangle^2 \right) + g_2^2 W_\mu^a W^{\mu, a} \left(\langle \Phi_1 \rangle^2 + \langle \Phi_2 \rangle^2 \right) \\
&+ \frac{1}{2} g_1 g_2 B_\mu W^{\mu, a} \left(\langle \Phi_1 \rangle^\dagger \sigma^a \langle \Phi_1 \rangle + \langle \Phi_2 \rangle^\dagger \sigma^a \langle \Phi_2 \rangle \right),
\end{aligned} \tag{6.23}
$$

where σ^a are the standard Pauli matrices. It is much easier to compute field-dependent masses by introducing a general gauge vector

$$
V_\mu = \begin{pmatrix} W_\mu^1 \\ W_\mu^2 \\ W_\mu^3 \\ B_\mu \end{pmatrix}. \tag{6.24}
$$

---

[1]The analytic expressions for the most general 2HDM potential appear elsewhere [176].

Thus the squared mass eigenvalues for the gauge bosons become

$$\frac{\partial^2 \mathcal{L}}{\partial V_\mu^i \partial V_\mu^j} = M_{G_{ij}}^2(\phi_i) = \frac{g_2^2}{4} \begin{pmatrix} p+q & 0 & 0 & 2r\frac{g_1}{g_2} \\ 0 & p+q & 0 & 2s\frac{g_1}{g_2} \\ 0 & 0 & p+q & (q-p)\frac{g_1}{g_2} \\ 2r\frac{g_1}{g_2} & 2s\frac{g_1}{g_2} & (q-p)\frac{g_1}{g_2} & (p+q)\frac{g_1^2}{g_2^2} \end{pmatrix}, \qquad (6.25)$$

where

$$\begin{aligned} p &= \phi_3^2 + \phi_7^2 + \phi_4^2 + \phi_8^2, \\ q &= \phi_1^2 + \phi_2^2 + \phi_5^2 + \phi_6^2, \\ r &= \phi_2\phi_4 + \phi_6\phi_8 + \phi_1\phi_3 + \phi_5\phi_7, \\ s &= \phi_1\phi_4 + \phi_5\phi_8 - \phi_2\phi_3 - \phi_6\phi_7. \end{aligned} \qquad (6.26)$$

Diagonalization of Eq. 6.25 generate the mass eigenvalues for the gauge bosons[1]

$$\begin{aligned} M_Z^2 &= \frac{g_2^2}{8}\left(1 + \frac{g_1^2}{g_2^2}\right)\left(p + q + \sqrt{(p+q)^2 + 16s_W^2 c_W^2(s^2 - pq + r^2)}\right), \\ M_{W^\pm}^2 &= \frac{g_2^2}{4}(p+q), \\ M_\gamma^2 &= \frac{g_2^2}{8}\left(1 + \frac{g_1^2}{g_2^2}\right)\left(p + q - \sqrt{(p+q)^2 + 16s_W^2 c_W^2(s^2 - pq + r^2)}\right). \end{aligned} \qquad (6.27)$$

The field-dependent squared mass of the top quark is determined by Φ_2 through the Yukawa part

$$\mathcal{L}_{\text{Yuk}}^t = -y_t \bar{q}_L \Phi_2^c t_R + h.c. \qquad (6.28)$$

since lower component of weak isospin doublets always couple to Φ_2 as

$$m_t^2 = \frac{y_t^2}{2}(\phi_5^2 + \phi_6^2 + \phi_7^2 + \phi_8^2) \overset{\langle\phi_7\rangle = v_2}{\longrightarrow} m_t^2 = \frac{y_t^2 v_2^2}{2}. \qquad (6.29)$$

Carrying out similar but tedious analysis with the effective potential and CS equation gives the complete RGEs for the 2HDM[2].

Although the conditions Eq. 6.18 - 6.19 are necessary, they are not sufficient to guarantee absolute stability of the electroweak vacuum at next-to leading order (NLO). In fact, the renormalization group equations (RGE) running of quartic couplings $\lambda_{1,2}$ in Type-I and Type-II are severely affected by negative corrections of top and bottom Yukawa couplings

$$\begin{aligned} \frac{d\lambda_2^I}{d\ln\mu^2} &= \frac{1}{16\pi^2}\left[12\lambda_2^2 + 4\lambda_3^2 + 4\lambda_3\lambda_4 + 2\lambda_4^2 + 2\lambda_5^2 - 3\lambda_1(-4y_t^2 + g_1^2 + 3g_2^2)\right. \\ &\quad \left. - 12y_t^4 - 12y_b^4 + \cdots\right], \\ \frac{d\lambda_1^{II}}{d\ln\mu^2} &= \frac{1}{16\pi^2}\left[12\lambda_1^2 + 4\lambda_3^2 + 4\lambda_3\lambda_4 + 2\lambda_4^2 + 2\lambda_5^2 - 3\lambda_1(g_1^2 + 3g_2^2)\right], \\ \frac{d\lambda_2^{II}}{d\ln\mu^2} &= \frac{1}{16\pi^2}\left[12\lambda_2^2 + 4\lambda_3^2 + 4\lambda_3\lambda_4 + 2\lambda_4^2 + 2\lambda_5^2 - 3\lambda_2(-4y_t^2 + g_1^2 + 3g_2^2)\right], (6.30) \end{aligned}$$

---

[1]This is only valid for mixed(normal) vacua, otherwise none of eigenvalues can be set to zero.
[2]For brevity we discard the details of a complete derivation.

where gauge portal terms are not shown here due to their positive contributions. In Fig. 6.1, we present the running couplings of the quartic couplings λ_1 and λ_2 in 2HDM Type-II by considering a toy-model, without showing RG evolution of $\lambda_{3,4,5}$. The first two conditions in Eq. 6.19 are not satisfied at one loop level by simply imposing the existence of a mixing between scalars. We adopt this toy-model to show that, unlike the common misconception rising from the absence of an additional scalar in the SM, the model including an additional scalar also relies on the other free parameters of 2HDM[1]. According to the initial value of λ_2 in Eq. 6.12, $M_H = 450$ GeV is insufficient to preserve the positivity of λ_2 around $\mu \sim 10^5$ GeV. Increasing the mass to $M_H = 600$ GeV and $M_H = 700$ GeV lifted the initial value and ameliorated the positivity of quartic coupling up to M_{Pl}. Introducing additional freedom in the scalar sector proved to be the best scenario for a remedy for the vacuum stability as well as enlarging allowed parameter space consistent with the SM phenomenology so far, because the SM can be recovered in the decoupling of BSM scalar extension (mixing angle $\alpha = 0$).
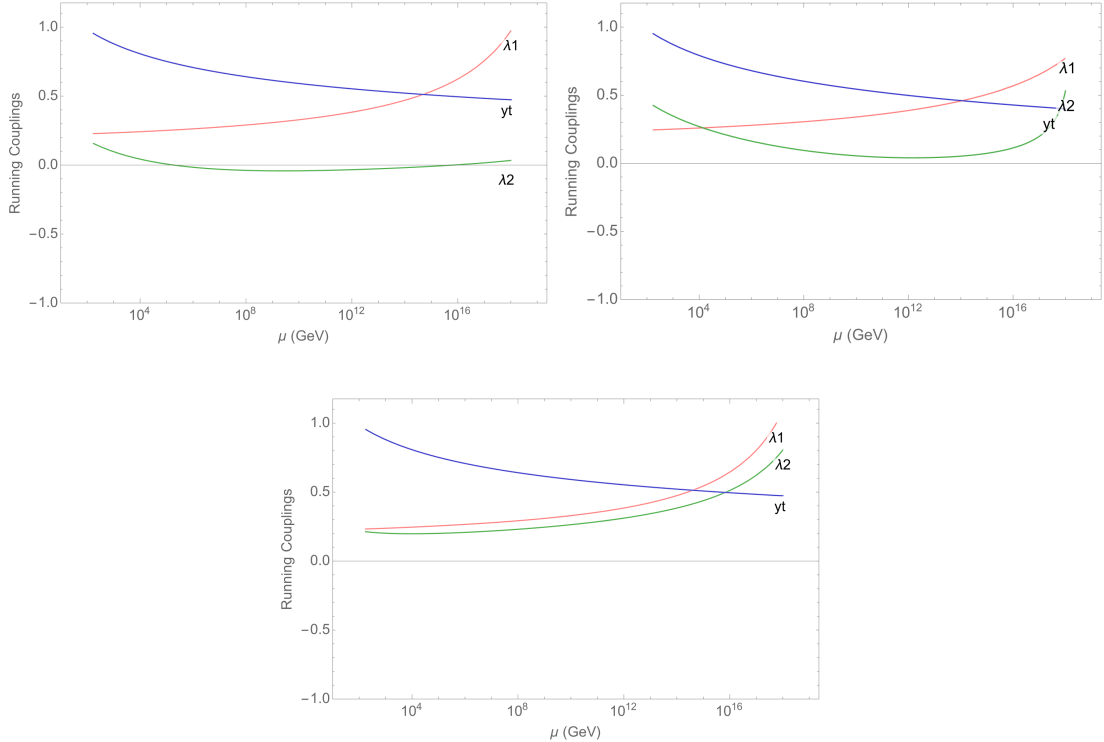
Figure 6.1: The RGE running of the top Yukawa and scalar couplings λ_1 and λ_2 in 2HDM fixed at $\tan\beta = 6$ for (a) $M_H = 450$ GeV, (b) $M_H = 600$ GeV, (c) $M_H = 700$ GeV

While the initial conditions to RGEs require utmost attention, radiative corrections to the Yukawa and the quartic couplings are only justified for the top quark and for the Higgs quartic terms that experience fermionic effects depending on type-I and type-II. To this end, the corrections in Eq. 5.28 are taken into consideration from the $h \to \gamma\gamma$ amplitude. Since the signals from the photon decay of the Higgs have also corrections from the loop level

---

[1]Similar analyses for the Higgs singlet model (HSM) and 2HDM have been performed in Ref. [92, 179].

diagrams, we only take the account the SM gauge bosons and the top quark appearing in one loop level. Furthermore, the deviation patterns in the Yukawa couplings due to mixing effects at the tree level remain consistent with the Standard Model predictions even when considering the inclusion of radiative corrections. Moreover, the scale factor corrections in one loop level due to extra scalars remain under 5% due to stability and perturbativity constraints in 2HDM. This emerges according to the following relation

$$\hat{\Gamma}_{hff}^{2HDM} \sim \hat{\Gamma}_{hff}^{SM} + \frac{1}{16\pi^2} \frac{m_f M_\Phi^2}{v^3} (1 - M^2/M_\Phi^2)^2 \sim \hat{\Gamma}_{hff}^{SM} + \frac{1}{16\pi^2} \frac{m_f v \lambda_i^2}{M_\Phi^2}. \tag{6.31}$$

Specifically for the top quark radiative correction, if the soft breaking scale of the $\mathcal{Z}_2$ symmetry is around the masses of extra scalars $H^\pm$, H and A, then the corrections remain under 1% for $\tan\beta > 3$. In fact, the peak value is around 6% for $\tan\beta = 1$ and this scale becomes even smaller and negligible for $\tan\beta > 3$ [180]. This is also shown to be correct for all the SM fermions studied therein. Hence, we can safely assume that for $\tan\beta$ and the mass range of extra scalars we choose for this work, the following electroweak radiative corrections to the initial condition on the top quark for increased accuracy hold [111].

6.3 2HDM+VLQ: Model Framework

Using 2HDM potential in Section 6.2, we investigate the effect of introducing vector-like quarks on the stability of electroweak vacuum. Unlike SM-like (chiral) fermions whose left-handed and right-handed components transform differently under $SU(3)_C \otimes SU(2)_L \otimes U(1)_Y$, vector-like fermions have the same interactions regardless of chirality. However when we consider incorporating them into the SM framework, it becomes necessary to introduce a new scalar boson into the Lagrangian. The additional scalar boson plays a crucial role in maintaining the stability of the 2HDM potential up to Planck scale. The rationale behind this requirement stems from the fact that the inclusion of extra fermions leads to a decrease in the effective self-coupling of the Higgs boson. Consequently, this extension could potentially exacerbate the negative evolution of the Higgs quartic coupling when compared to the scenario within the SM without additional particles. The presence of the new scalar boson serves as a remedy to this situation.

The question remains how would VLQs affect models with different scalar representations, such as 2HDMs. Throughout our work, we uphold the condition that the potential of 2HDM must remain positive up to the Planck scale. Previous works analyzed several collider signatures that would be expected in Type-II 2HDM with vector-like quark (singlets and doublets) [181–185]. The main motivation for our study, is to establish the limitations that constrain the masses of vector-like quarks and the mixing angles with the SM quarks. Establishing these constraints is essential in preserving the stability of the electroweak vacuum. While VLQ are also allowed to appear in loop level of the radiative Higgs decay and their contributions, because of their vector-like character, they do not affect the branching ratio. The oblique corrections to the mass of W-boson rely on various VLQ representations as well, and thus making Eq. 5.28 model-dependent. Because of this, only the corrections from W-boson and the top quark are considered to slightly increase the relevant initial conditions on the quartic couplings without contradicting to experimental data. Furthermore, if effects from $m_{VLQ} \sim \mathcal{O}$ TeV are taken into account in Eq. 6.31, effects due to VLQ break perturbativity of the top Yukawa coupling as setting its initial value too

large. Moreover, as to be seen in Fig. 6.2-6.4, the initial value of the top Yukawa coupling according to radiative corrections we assume herein, ensures the observed top quark mass throughout all representations of VLQ+2HDM-I,II. Since all the initial conditions are set at $\mu_0 = m_t$, any VLQ effect contradicts with the experimental data. One might argue that the mixing relations between the SM quarks and VLQ could further correct the initial condition on the top Yukawa, however Eq. 6.38 and Eq. 6.39 are only allowed to reduce $y_t(\mu_0)$ if the mixing angle (denoted below by $\sin\theta_{L,R}^t$) becomes larger than the constraints[1] in Section 6.4.

The new VLQs states interact with the Higgs bosons through Yukawa interactions. The allowed anomaly-free multiplet states for the vector-like quarks, together with their nomenclature, are listed in Table 6.1 [78, 91, 113, 186]. The first two representations are U-like and D-like singlets [140, 187, 188], the next three are doublets (one SM-like, two non-SM like), and the last two are triplets. Note that the latter allow for quarks with exotic charges, $Q_X = 5/3$ and $Q_Y = -4/3$. The various representations are distinguished by their $SU(2)_L$ and hypercharge numbers.

Table 6.1: *Quantum number assignments of VLQ models under $SU(2)_L \times U(1)_Y$ symmetry.*

Model	$\mathcal{U}_1$	$\mathcal{D}_1$	$\mathcal{D}_2$	$\mathcal{D}_X$	$\mathcal{D}_Y$	$\mathcal{T}_X$	$\mathcal{T}_Y$
Type	Singlet	Singlet	Doublet	Doublet	Doublet	Triplet	Triplet
Representation	T	B	$\begin{pmatrix} T \\ B \end{pmatrix}$	$\begin{pmatrix} X \\ T \end{pmatrix}$	$\begin{pmatrix} B \\ Y \end{pmatrix}$	$\begin{pmatrix} X \\ T \\ B \end{pmatrix}$	$\begin{pmatrix} T \\ B \\ Y \end{pmatrix}$
SU(2)$_\mathbf{L}$	1	1	2	2	2	3	3
Y	$\frac{2}{3}$	$-\frac{1}{3}$	$\frac{1}{6}$	$\frac{7}{6}$	$-\frac{5}{6}$	$\frac{2}{3}$	$-\frac{1}{3}$

The Yukawa and other relevant interaction terms between the vector-like quarks and SM quarks are, in the bare (Φ_1, Φ_2) basis for Type-I:

$$
\begin{aligned}
\mathcal{L}_{SM}^I &= -y_u \bar{q}_L \Phi_2^c u_R - y_d \bar{q}_L \Phi_2 d_R, \\
\mathcal{L}_{\mathcal{U}_1,\mathcal{D}_1}^I &= -y_T \bar{q}_L \Phi_2^c U_{1_R} - y_B \bar{q}_L \Phi_2 D_{1_R} - y_M(\bar{U}_{1_L}\Phi_2 U_{1_R} + \bar{D}_{1_L}\Phi_2 D_{1_R}) \\
&\quad - M_U \bar{U}_L U_R - M_D \bar{D}_L D_R, \\
\mathcal{L}_{\mathcal{D}_2}^I &= -y_T \bar{D}_{2_L} \Phi_2^c u_R - y_B \bar{D}_{2_L} \Phi_2 d_R - y_M(\bar{D}_{2_L}\Phi_2^c D_{2_R} + y_B \bar{D}_{2_L}\Phi_2 D_{2_R}) \\
&\quad - M_D \bar{D}_{2_L} D_{2_R}, \\
\mathcal{L}_{\mathcal{D}_X,\mathcal{D}_Y}^I &= -y_T \bar{D}_{X_L} \Phi_2 u_R - y_B \bar{D}_{Y_L} \Phi_2^c d_R - y_M(\bar{D}_{X_L}\Phi_2 D_{X_R} + y_B \bar{D}_{Y_L}\Phi_2^c D_{Y_R}) \\
&\quad - M_X \bar{D}_{X_L}^I D_{X_R} - M_Y \bar{D}_{Y_L} D_{Y_R}, \\
\mathcal{L}_{\mathcal{T}_X,\mathcal{T}_Y}^I &= -y_T \bar{q}_L \tau^a \Phi_2^c \mathcal{T}_{X_R}^a - y_B \bar{q}_L \tau^a \Phi_2 \mathcal{T}_{Y_R}^a - y_M(\bar{\mathcal{T}}_{X_L} \tau^a \Phi_2^c \mathcal{T}_{X_R}^a + y_B \bar{\mathcal{T}}_{Y_L}\tau^a \Phi_2 \mathcal{T}_{Y_R}^a) \\
&\quad - M_X \bar{\mathcal{T}}_{X_L} \mathcal{T}_{X_R} - M_Y \bar{\mathcal{T}}_{Y_L} \mathcal{T}_{Y_R}
\end{aligned}
$$

$$(6.32)$$

---

[1]Nonetheless, for the mixing scale between the SM quarks and VLQ set here, the radiative corrections for $y_t(\mu_0)$ can always be neglected without significantly effecting the parameter space generated by the complete RGE analysis.

and for Type-II:

$$
\begin{aligned}
\mathcal{L}_{SM}^{II} &= -y_u \bar{q}_L \Phi_2^c u_R - y_d \bar{q}_L \Phi_1 d_R, \\
\mathcal{L}_{\mathcal{U}_1,\mathcal{D}_1}^{II} &= -y_T \bar{q}_L \Phi_2^c U_{1_R} - y_B \bar{q}_L \Phi_1 D_{1_R} - y_M(\bar{U}_{1_L}\Phi_2 U_{1_R} + \bar{D}_{1_L}\Phi_1 D_{1_R}) \\
&\quad - M_U \bar{U}_L U_R - M_D \bar{D}_L D_R, \\
\mathcal{L}_{\mathcal{D}_2}^{II} &= -y_T \bar{D}_{2_L}\Phi_2^c u_R - y_B \bar{D}_{2_L}\Phi_1 d_R - y_M(\bar{D}_{2_L}\Phi_2^c D_{2_R} + y_B \bar{D}_{2_L}\Phi_1 D_{2_R}) \\
&\quad - M_D \bar{D}_{2_L} D_{2_R}, \\
\mathcal{L}_{\mathcal{D}_X,\mathcal{D}_Y}^{II} &= -y_T \bar{D}_{X_L}\Phi_2 u_R - y_B \bar{D}_{Y_L}\Phi_1^c d_R - y_M(\bar{D}_{X_L}\Phi_2 D_{X_R} + y_B \bar{D}_{Y_L}\Phi_1^c D_{Y_R}) \\
&\quad - M_X \bar{D}_{X_L} D_{X_R} - M_Y \bar{D}_{Y_L} D_{Y_R}, \\
\mathcal{L}_{\mathcal{T}_X,\mathcal{T}_Y}^{II} &= -y_T \bar{q}_L \tau^a \Phi_2^c \mathcal{T}_{X_R}^a - y_B \bar{q}_L \tau^a \Phi_1 \mathcal{T}_{Y_R}^a - y_M(\bar{\mathcal{T}}_{X_L}\tau^a \Phi_2^c \mathcal{T}_{X_R}^a + y_B \bar{\mathcal{T}}_{Y_L}\tau^a \Phi_1 \mathcal{T}_{Y_R}^a) \\
&\quad - M_X \bar{\mathcal{T}}_{X_L}\mathcal{T}_{X_R} - M_Y \bar{\mathcal{T}}_{Y_L}\mathcal{T}_{Y_R},
\end{aligned}
\tag{6.33}
$$

where $\Phi_i^c = i\sigma^2\Phi_i^\star$, (i=1,2), y_u, y_d, y_T, and y_B are the Yukawa couplings of the scalar fields $\Phi_{1,2}$ to vector-like and to SM quarks, while y_M is the Yukawa coupling of the scalar fields to only vector-like quarks. The connection between gauge eigenstates and mass eigenstate is similar to Eq. 5.33 with bi-unitary transformation. However, the mass matrices that generate the mixing are unique to Lagrangian in Eq. 6.32 - 6.33, and follow after spontaneous symmetry breaking for the top and bottom sector as

$$
\begin{aligned}
-\mathcal{L}_{Yuk}^t &= \begin{pmatrix} t_L & T_L \end{pmatrix} \begin{pmatrix} y_t \frac{v}{\sqrt{2}} & y_T \frac{v}{\sqrt{2}} \\ y_T \frac{v}{\sqrt{2}} & y_M \frac{v}{\sqrt{2}} + M_T \end{pmatrix} \begin{pmatrix} t_R \\ T_R \end{pmatrix}, \\
-\mathcal{L}_{Yuk}^b &= \begin{pmatrix} b_L & B_L \end{pmatrix} \begin{pmatrix} y_b \frac{v}{\sqrt{2}} & y_B \frac{v}{\sqrt{2}} \\ y_B \frac{v}{\sqrt{2}} & y_M \frac{v}{\sqrt{2}} + M_B \end{pmatrix} \begin{pmatrix} b_R \\ B_R \end{pmatrix}.
\end{aligned}
\tag{6.34}
$$

The mass eigenvalues for top partners in Type-I, II+VLQ model are

$$
m_{t_1,t_2}^2 = \frac{1}{4}\left[(y_t^2 + y_T^2 + y_M^2)v^2\right]\left[1 \pm \sqrt{1 - \left(\frac{2y_t y_M}{(y_t^2 + y_T^2 + y_M^2)}\right)^2}\right].
\tag{6.35}
$$

Diagonalization of the mass matrices Eq. 6.34 is useful for expressing the mixing angles for top and bottom sector in terms of the free parameters of the model

$$
\begin{aligned}
\tan(2\theta_L^t) &= \frac{2y_T y_M}{y_M^2 - y_t^2 - y_T^2}, \\
\tan(2\theta_R^t) &= \frac{2y_t y_T}{y_M^2 + y_t^2 - y_T^2}.
\end{aligned}
\tag{6.36}
$$

Charge assignments of the non-SM-like quarks do not allow the X and Y fields to mix with the other fermions. Therefore, these vector-like quarks are also mass eigenstates. Bottom sector mixing angle can be obtained with the replacement $t \to b$ and $\theta^t \to \theta^b$. And solving Eq. 6.36 for the Yukawa couplings we end up with the relations between mass eigenvalues and mixing angles:

$$
\frac{y_T}{y_t} = s_L^t c_L^t \frac{m_t^2 \frac{\tan\theta_L^{t2}}{\tan\theta_R^{t2}} - m_T^2 \frac{\tan\theta_R^{t2}}{\tan\theta_L^{t2}}}{m_T m_t}.
\tag{6.37}
$$

The mixing relations between mass eigenstates in Eq. 5.41 are modified in 2HDM depending on how fermions couple to the CP-even scalars as $m_T = M_{\text{Dirac}} + y_T v \sin\beta/\sqrt{2}$, $m_B = M_{\text{Dirac}} + y_B v \cos\beta/\sqrt{2}$, $m_t = y_t v \sin\beta/\sqrt{2}$, $m_b = y_b v \cos\beta/\sqrt{2}$ for type-II models (for type-I, replace $v \cos\beta$ and $v \sin\beta$ by v) , while $m_X = M_X$ and $m_Y = M_Y$.

Initial conditions for all Yukawa couplings are modified with mixing relations. For Type-I+VLQ, all fermions acquire mass by interacting with VEV of Φ_2

$$
\begin{aligned}
y_t^I(\mu_0) &= \frac{\sqrt{2} m_t}{v} \frac{1}{\sqrt{\cos^2\theta_L + x_t^2 \sin^2\theta_L}}\,, \\
y_T^I(\mu_0) &= \frac{\sqrt{2} m_T}{v} \frac{\sin\theta_L \cos\theta_L (1 - x_t^2)}{\sqrt{\cos^2\theta_L + x_t^2 \sin^2\theta_L}}\,, \\
y_B^I(\mu_0) &= \frac{\sqrt{2} m_B}{v} \frac{\sin\theta_L \cos\theta_L (1 - x_b^2)}{\sqrt{\cos^2\theta_L + x_b^2 \sin^2\theta_L}}\,, \\
y_M^I(\mu_0) &= \sum_{i=X,T,B,Y} \frac{C_R m_i}{v} \sqrt{\cos^2\theta_L + x_t^2 \sin^2\theta_L}\,,
\end{aligned}
$$
(6.38)

whereas in Type-II+VLQ, $\tan\beta$, which is the ratio of VEVs, modifies the initial conditions to read

$$
\begin{aligned}
y_t^{II}(\mu_0) &= \frac{\sqrt{2} m_t}{v \sin\beta} \frac{1}{\sqrt{\cos^2\theta_L + x_t^2 \sin^2\theta_L}}\,, \\
y_T^{II}(\mu_0) &= \frac{\sqrt{2} m_T}{v \sin\beta} \frac{\sin\theta_L \cos\theta_L (1 - x_t^2)}{\sqrt{\cos^2\theta_L + x_t^2 \sin^2\theta_L}}\,, \\
y_B^{II}(\mu_0) &= \frac{\sqrt{2} m_B}{v \cos\beta} \frac{\sin\theta_L \cos\theta_L (1 - x_b^2)}{\sqrt{\cos^2\theta_L + x_b^2 \sin^2\theta_L}}\,, \\
y_M^{II}(\mu_0) &= \sum_{i=X,T,B,Y} \frac{C_R m_i}{v} \sqrt{\cos^2\theta_L + x_t^2 \sin^2\theta_L}\,,
\end{aligned}
$$
(6.39)

where $C_R = (\sqrt{2}, \frac{1}{\sqrt{2}}, \frac{\sqrt{2}}{3})$ is the representation dependent weight factor with $x_b = m_b/m_B$, and as before $x_t = m_t/m_T$. Since X and Y fields do not mix with other fermions of the model, their low-energy Yukawa couplings are not altered by mixing relations. However, y_X and y_Y have indirect effects on the coupled RGEs, as seen from Eq. B.1-B.2 for Type-I and Type-II analyzed in this work. Furthermore, the initial conditions on the VLQ Yukawa couplings in Type-II have different β dependences in Eq. 6.39 based on which field is an up- or down-type member of the multiplets.

6.4 Experimental and Theoretical Constraints on VLQ+2HDM

Bounds on masses of VLQs were established by the direct searches at the LHC by ATLAS [189–192] and by CMS [115,193,194,194–197] collaborations, obtained from specific

mechanisms such as single production [198] and pair production [117,199] at $s = \sqrt{13}$ TeV. The constraints are sensitively dependent on the assumed decay channels of the light VLQs, which are allowed by kinematics to decay into a SM quark. If VLQs decay only to the third generation quarks, then following channels could be observed:[1] $T(B) \rightarrow W^+(W^-)t(b)$, $T(B) \rightarrow Zt(b)$, $T(B) \rightarrow Ht(b)$, hence the bounds become relatively stronger due to the final states. The constraints $m_T > 1.27$ TeV, $m_B > 1.2$ TeV are obtained for singlets, whereas doublets require slightly higher mass limits $m_T > 1.46$ TeV, $m_B > 1.32$ TeV through pair production. Nonetheless, the lower limits on the VLQ masses in the range of $[800, 1400]$ GeV and $\sin\theta < 0.18$ from Run 2 [200] are still compatible with the data [201]. It should be noted that these limits are decreased if the first and the second generation SM quarks are also included. However, since the Yukawa couplings play an essential role due their direct relations to masses, these models are commonly unfavored. As our work concerns 2HDMs, we consider a lowest limit on m_T of 800 GeV, to allow for the consideration of the largest parameter space for the electroweak vacuum stability and electroweak observables (EWPOs).

Corrections to the mass of W-boson are calculated using the oblique parameters. To this end, precision experiments carried out at the Tevatron [202] that signal any type of shift in ΔM_W are used to describe effects from new physics (NP). Since both the scalar and the fermion sector contribute to EWPO, the combined corrections significantly rely on scalar extensions in addition to vector-like fermions. Singlet (HSM) [85,95] and triplet (HTM) scalar models [120,203] have already been studied. However, for 2HDM+VLQ, we are only interested in constraints coming from the $\chi^2(S,T)$[VLQ+2HDM] analysis in order to generate a viable space for the electroweak vacuum stability requirements.

There are alternative ways for corrections to Higgs self-energies which would manifest themselves, especially when the new particles carry SM-like colour and electroweak quantum numbers. In these scenarios, for every diagrammatic contribution to the self-energies, one could replace one of the Higgs bosons by its vacuum expectation value and attach two SM gauge bosons to the loop. From there, one can obtain a corresponding diagrammatic contribution to the Higgs decays to SM gauge bosons. A rough estimation of possible deviations from precision electroweak measurements, which pushed new physics to $\Lambda_{NP} \sim$ 1 TeV, is based on the estimate of the size of Higgs oblique corrections roughly given by $\mathcal{O}(v^2/\Lambda^2) \sim 5\%$. If VLQs enter the loop diagrams, new fermions or charged bosons contribute to the loop-induced diphoton decay and/or gluon fusion channels of the Higgs bosons. Effects of VLQs on Higgs couplings have been explored in studies for singlet [85,204], doublet [205] and triplet models [206]. The T- singlet VLQ model established an upper bound $\sin\theta_L < 0.4$ from the combined $H \rightarrow gg$ and $H \rightarrow \gamma\gamma$ cross section and branching ratio, respectively, while in the doublet (TB) representation an upper limit $\sin\theta_L < 0.115$ was obtained only from contribution to gluon fusion cross section $\mu_{\gamma\gamma} \leq 1.03$, while the triplet (XTB) model contribution is $\mu_{\gamma\gamma} \leq 1.18$ around $m_{VLQ} \simeq 1$ TeV. Consequently, all these studies have shown VLQ corrections which match the earlier correction scale from NP models.

By far the most significant constraint here comes from B-physics, namely from $b \rightarrow s\gamma$,

---

[1]For VLQs that carry non-SM-like hypercharges, the following CC and NC channels are also allowed and searched for accordingly: $X \rightarrow tW^+$, $Y \rightarrow bW^-$, $T(B) \rightarrow X(Y)W^-(W^+)$. See also [113].

since $\tan\beta$ alone varies in a significantly large interval for the 2HDM models without VLQs. Studies in literature which extend 2HDM with singlet [207] and doublet [208] VLQs provide solid constraints to working around $\tan\beta \leq 12$, $M_{H^\pm} = [80, 1000]$ GeV for 2HDM-I and $M_{H^\pm} = [580, 1000]$ GeV for 2HDM-II along with $m_{VLQ} > 1$ TeV and small mixings, $\sin\theta_L < 0.2$, between VLQ and the SM quarks. We further explain the difference between mass regimes regarding the charged scalars of Type-I and of Type-II as RG evolutions are analyzed in the next section.

In what follows, we will scan the parameter space for $\tan\beta \in [6, 12]$. The reason for such a restriction is as follows.

- LHC data mostly constraints $\tan\beta - \cos(\beta - \alpha)$ plane in 2HDM-II models. This is known from [155] within the exceptional region beyond the alignment limit (Fig. 2 in the reference). The LHC data alone in 2HDM does not exclude $\tan\beta < 6$. However, the addition of VLQ to 2HDM slightly extends the space, [207]. Hence, taking both the exceptional and the ordinary regions into account, $\tan\beta > 5$ is favoured for 2HDM in the alignment region and if VLQ mixing < 0.2. Although smaller values for $\tan\beta$ are still possible too.

- The biggest motivation to assuming $\tan\beta > 5$ throughout our study is unique to us. This is because in the regime we choose for VLQ masses, if $\tan\beta$ becomes slightly smaller, meaning that v_2 becomes smaller with respect to v_1, the initial conditions on up-like quarks Yukawa couplings (VLQ or SM) become larger (Eq. 6.39) and these break the perturbativity of Yukawa couplings as well as violate the stability conditions due to excess weight of Yukawa couplings on the evolutions of all λ's. As a consequence, if $\tan\beta << 6$, then VLQ masses need to be < 0.8 TeV to satisfy perturbative unitarity and stability conditions. This mass scale is ruled out by the experimental data.

Unitarity requires the S-matrix for scalar scattering to be unitary at high energy [178]. At tree tree level, this translates into imposing upper limits as $M_{\Phi^0} < \sqrt{\frac{4\pi}{\sqrt{2}G_F}} = 870$ GeV for scalar-scalar scattering and $M_{\Phi^0} < \sqrt{\frac{8\pi}{3\sqrt{2}G_F}} = 712$ GeV for gauge boson-scalar scattering in 2HDM. At NLO, unitarity condition of the S-matrix yields terms proportional to $\mathcal{O}(\lambda_i\lambda_j/16\pi^2)$, hence one-loop corrections to the tree level unitarity conditions are modified by β-functions of scalar couplings. The combined perturbativity and unitarity conditions for the quartic couplings are bounded under RG evolutions [209]

$$|\lambda_i(\mu)| \lesssim 4, \tag{6.40}$$

and hence this will be required up to M_{Pl} in the next section. The perturbativity of the Yukawa couplings y_i is one of the weakest constraints at tree level, extending the upper bound of the mixing angle as $\sin\theta_L^t = [0.77, 0.31]$ for $m_T = [0.8, 2]$ TeV [113]. Lastly, for VLQ mixing, we choose the recent unitarity constraints [145] at $\mathcal{O}(\text{TeV})$ scale.

6.5 RGE Analysis of Vector-like Quarks with Two Higgs Doublet Model

The effect of fermions on the stability of the electroweak vacuum without extending scalar sector beyond the SM Higgs field is to drive the Higgs self-coupling negative at larger scales, so the potential becomes unbounded from below, and there is no resulting stability. Theoretical considerations indicate that if the validity of the SM is extended to M_{Pl}, a second, deeper minimum is located near the Planck scale such that the electroweak vacuum is metastable [56, 70]. The additional scalar bosons maintain positivity of the Higgs self coupling while the renormalization flow tends to decrease it further at higher energy scales [147]. Moreover, a common feature of both observed and exotic fermions is that Yukawa couplings generally further lower scalar couplings since Yukawa couplings are negatively affected by NLO contributions. However, this is not always the case, and it depends on how the structure of gauge interactions have been affected by new fields. Through the possibility of various interaction portals, vector-like fermions open new ways to remedy stabilizing the electroweak vacuum.

A straightforward approach would be to extend the gauge sector of the SM as the gauge beta-functions have positive effects on quartic coupling RGEs [210]. However, additional gauge symmetries might also come short of being able to express the current SM interactions as they have relatively small contributions compared to other remedies. Nonetheless, these corrections, $\Delta\beta_1 = \frac{8}{3}n_F G_2 G_3 y_f^2$ and $\Delta\beta_{2,3} = \frac{8}{3}n_F d_{2,3} S_2(G_{2,3})$[1], are multiplicative with respect to new fermion families and these contributions are already manifest at the RGE level, as we shall see in Section B.1. Yukawa and scalar portals have shown promising results, providing non-critical surfaces of electroweak vacuum stability [86]. As shown in Section 6.3, Yukawa portals lead to mixing between vector-like quarks and the SM quarks. Due to mixing constraints, for an energy scale less than the mass of m_{VLQ}, decoupling occurs and VLQs contribute to RGE running as if they were massless. Furthermore, in the presence of VLQs, beyond-SM gauge couplings have larger values compared to the SM ones, thus reducing the corrections to Yukawa couplings running at energy scale $\mu \geq m_{VLQ}$. This could be shown, for instance, for the top quark, where the beta function

$$\beta_t \supset y_t[C_f y_f - C_1 g_1 - C_2 g_2 - C_3 g_3] \tag{6.41}$$

which in turn shows that $y_t(\mu) < y_t^{SM}(\mu)$. Moreover, gauge and Yukawa couplings have opposite sign contributions in scalar RGEs Eq. B.1 - B.2 when fermions are allowed to interact with the scalars of the model. This characteristic can be seen from all scalar RGEs except the one governs λ_1^I, which is not allowed to interact with fermions through Yukawa couplings due to Z_2 symmetry. Thus, from RGE structure, the gauge and Yukawa couplings could lead to upward shifts in the Higgs quartic couplings though the condition $\lambda_{1,2} > \lambda_{1,2}^{SM}$ in the presence of VLQ. We note that, in this context, vector-like quarks have been studied with only the SM Higgs field [211] and within the additional Higgs singlet model [1].

In Fig. 6.2 - 6.4 we present the RGE evolution for all vector-like quark representations given in Eqs. 6.32 - 6.33, combined with 2HDM couplings respectively, for Type-I and Type-II, in the case where the lightest CP-even scalar is taken to be the observed 125 GeV Higgs boson.

---

[1]Here $S_2(G_i)$ are Dynkin indices for the groups G_2 and G_3.

Among various bare 2HDM constraints, the limits on $M_{H^\pm}$ and M_A are extremely sensitive to the VEV ratios $\tan\beta$ and to experimental data from B-physics [212], which affects how quarks are coupled in Type-I and Type-II models. Electroweak corrections to the W-boson, for a fixed value of $\tan\beta = 5$ in Type-I model, yield a degenerate mass spectrum for all scalars in the model, found to be $M = [100, 1000]$ GeV, if these EW corrections remain $\Delta_{EW}^W < 5\%$ as indicated from Higgs oblique corrections [99]. We have also compared our parameter space from the oblique parameters in 2HDM, Fig. 6.5 indicating that larger values of $\tan\beta$ reduce the upper bound of $M_{H^\pm}$ and M_A, in good agreement with the results in Ref. [99]. The allowed parameter space from the oblique corrections yields a solid interval for the stability and perturbativity analyses throughout this work, as we choose some of the fixed parameters from the scalar sector to run the RG evolutions. However, bounds on $M_{H^\pm}$ as a function of $\tan\beta$ from B-physics constraints are different in Type-I and Type-II models [213]. Lower bounds on $M_{H^\pm}$ are inversely proportional to $\tan\beta$ value in Type-I model, yielding a relatively lower minimum than the LEP result $M_{H^\pm} > 80$ GeV [214]. On the other hand, the lower bound on $M_{H^\pm}$ in Type-II model behaves almost $\tan\beta$ independent as $\tan\beta > 2$ and scales about the minimum $M_{H^\pm} = 580$ GeV. Apart from this distinguishing feature, both types are constrained to generate lower bounds on $M_{H^\pm}$ as $\tan\beta$ increases. The Type-II model in the heavy Higgs scenario is affected by the lower bound on $M_{H^\pm}$, while the mass difference between in 2HDM scalars is required to be small $M_{H^\pm} - M_A \lesssim 160$ GeV in order for the RG evolutions to survive about $\Lambda_{cut} \sim M_{Pl}$ [215]. As we run RG evolutions from 2HDM+VLQ up to $\mu = M_{Pl}$, Type-I and Type-II models can be better compared in the light Higgs scenario while setting fixed values to RGEs. The relative difference between masses $M_H - M_{H^\pm}$ and $M_{H^\pm} - M_A$ is important, though theoretical constraints do not strictly forbid large splittings between these parameters. However, bounds from EWPO [155] and from B-physics [154, 216] strongly correlate these mass differences if 2HDM+VLQ RGEs are to survive without having a Landau pole up to the Planck scale. We have investigated that large splitting between $M_H, M_{H^\pm}$ and M_A could not satisfy RG evolutions for 2HDM-II+VLQ, due to the non-perturbativity of scalar couplings and the vacuum instability in sub-Planckian region. The parameter space of 2HDM that survives from RGEs running will be discussed in detail below.

We note that the overall effect of RGE on running couplings up to a cut-off scale Λ_{cut} is sensitively dependent on initial conditions given for a fixed set of parameters. Scalar couplings tend to generate a Landau pole and break perturbativity if they start from relatively large initial values due to their evolution (increase with energy scales). On the other hand, new in this work, when combined with $m_{VLQ} \gtrsim \mathcal{O}(\text{TeV})$, scalar RG evolutions also result in vacuum instability in case the initial values are too small and the mass limits of VLQ are too large. Although RGEs of the fermion sector are coupled due to the Yukawa couplings in the model, scalar RGEs are coupled due to any free parameters in 2HDM+VLQ. The parameter space of scalar masses which survive up to Planck scale according to the initial conditions given in Eq. 6.12 and to bare 2HDM RGEs scanning, spans over a wide range for $\tan\beta = [1, 50]$ [216]. Nonetheless, the spectrum for $\tan\beta$ activated from 2HDM RGEs alone faces experimental constraints related to VLQ contributions to LHC Higgs data from di-boson channels [207] and constraints from B-physics results [208]. The presence of VLQs at $\mathcal{O}$ (TeV), carrying the SM-like quantum numbers, further constrain $\tan\beta = [1, 15]$ and $M_{H^\pm} > 600$ GeV in 2HDM-II+VLQ. Before delving into RGEs results, we also discuss the analytical nature of initial conditions depending on the mass difference $M_{H^\pm} - M_A$ and on $\tan\beta$. The quartic coupling $\lambda_1(\mu_0)$ rapidly grows for larger M_H and $\tan\beta$ values, therefore it can generate a Landau pole faster than the rest of couplings in the sub-Planckian

scale, particularly in Type-I model without presence of any Yukawa term to drive it lower. In contrast, $\lambda_2(\mu_0)$, $\lambda_3(\mu_0)$ become heavily suppressed for larger $\tan\beta$ and smaller M_H values, hence vacuum instability can occur due to the evolution of λ_2, more dominantly so in Type-I model. The initial condition on λ_4 is by far the most sensitive to the constraints on the mass difference between the pseudoscalar and the charged scalar. Being $\tan\beta$ independent, and due to a large separation between M_A and $M_{H^\pm}$, the quartic coupling λ_4 can easily reach a Landau pole in either direction[1], hence this initial condition alone develops an approximate limit for the separation $|M_{H^\pm} - M_A|$. As shown in [154], by inverting Eq. 6.12 and relating the separation between scalar masses to numerical values of $\lambda_4 + \lambda_5$ that survive up to M_{Pl}, the mass difference is bound to ~ 160 GeV. However, this scale is based on scanning over all values of $\tan\beta = [1, 50]$. Consequently, we have cross checked that such separation is allowed by RG analyses, considering smaller VEV ratios $\tan\beta = [6, 12]$ [216]. Taking into account that VLQs become unfrozen at $\Lambda \sim \mathcal{O}$ (TeV), the strategy we follow to search the parameter space can be summarized as

- We scan RGE over a large number of parameters from 2HDM+VLQ by imposing theoretical and experimental bounds discussed above from both sector.

- We extract the parameter space that survives from running RGEs requiring stability, perturbativity and unitarity conditions up to the Planck scale.

- The initial conditions for all of the couplings that appear in the combined model are set at the energy scale $\mu_0 = m_t$.

- We calculate the corrections to the oblique parameters $\mathbb{S}$ and $\mathbb{T}$ from 2HDM and VLQs, then check if the allowed parameter space for $\tan\beta$ range is consistent with the RG analyses.

The scanning ranges in the VLQ and 2HDM are given in Table 6.2. Note that the parameter space of VLQ+2HDM that satisfies the vacuum stability constraint extends to $m_{VLQ} < \mathcal{O}(\text{TeV})$ and to larger mixing angle $\sin\theta_{L,R}^{t,b}$ (not shown). However, the recent experimental constraints [198, 199, 201, 217] and constraints from EWPO, Fig. 6.7-6.8, discard large mixings and the light m_{VLQ} domain. The mixing angle $\alpha \neq 0$ (means the neutral scalars are not decoupled), because otherwise the perturbativity and the stability conditions are not satisfied at initial condition μ_0 as seen from Eq. 6.12 with respect to the range of M_H and $\tan\beta$ we scanned, especially for the minimum bound on $M_{H^\pm}$ in Type-II.

---

[1] We observed that for larger VLQs multiplets, λ_4 tends to diverge from a positive direction if $|M_{H^\pm} - M_A| \gg 150$ GeV, due to a relatively large number of Yukawa terms, though λ_4 always starts from a negative direction.

Model	Parameter	Range
VLQ	m_T	$[0.8, 2]$ TeV
	m_B	$[0.85, 2]$ TeV
	m_X	$[0.9, 2]$ TeV
	m_Y	$[0.9, 2]$ TeV
	$\sin\theta_{L,R}$	$[0.05, 0.2]$
2HDM-I	$M_{H^\pm}$	$[80, 900]$ GeV
	M_A	$[300, 1000]$ GeV
	M_H	$[400, 1100]$ GeV
	t_β	$[6, 12]$
	$\sin\alpha$	$[0.05, 0.15]$
2HDM-II	$M_{H^\pm}$	$[600, 900]$ GeV
	M_A	$[300, 1000]$ GeV
	M_H	$[400, 1100]$ GeV
	t_β	$[6, 12]$
	$\sin\alpha$	$[0.05, 0.2]$

Table 6.2: Scanning range of parameter space of 2HDM-I,II combined with VLQ models.

6.5.1 Singlet VLQs: $\mathcal{U}_1$ and $\mathcal{D}_1$

Type-I 2HDM+VLQ singlets yield the most stringent mass limits for VLQs required to satisfy the stability bounds, as expected from form of the Yukawa terms appear in both scalar and fermion RGEs. We present RG running of the couplings for singlet VLQ+2HDM-I,II in Fig. 6.2. The relative difference regarding the initial condition of top Yukawa coupling between $\mathcal{U}_1$ and $\mathcal{D}_1$ occurs due to absence of top mixing in $\mathcal{D}_1$ model. For mixing angles $\sin\theta_{L,R} > 0.15$, the mass scale region $m_T > \mathcal{O}(\text{TeV})$ leads to negative top Yukawa coupling in sub-Planckian region. The RGEs of singlet VLQ in Type-I are similar, therefore the difference between initial values of λ_2 stems from the mass difference between the top and the bottom VLQ sector. Although all the initial conditions are set at the top quark mass, the overall shift of VLQ Yukawa couplings between Type-I and Type-II is always due to how strong extra fermions couple to scalars, depending on $\tan\beta$. As discussed previously, a small separation between mass values of scalars in Type-II models together with a larger value of the minimum bound on $M_{H^\pm}$ ameliorate the stability result compared to Type-I models, and hence larger λ_2 values in Type-II models are allowed by extending the bounds on scalar parameter space. In contrast to the proximity of λ_2 values to instability region, λ_1 evolves safer away from non-perturbativity region in Type-II models, as expected from the splitting of Yukawa couplings in top and bottom sectors. In Table 6.3, we list the allowed mass ranges due to RG analyses of the combined model that survive from stability, perturbativity and unitarity up to $\mu = M_{Pl}$.

$\mathcal{U}_1$ (T) - Type I

$\mathcal{U}_1$ (T) - Type II

$\mathcal{D}_1$ (B) - Type I

$\mathcal{D}_1$ (B) - Type II
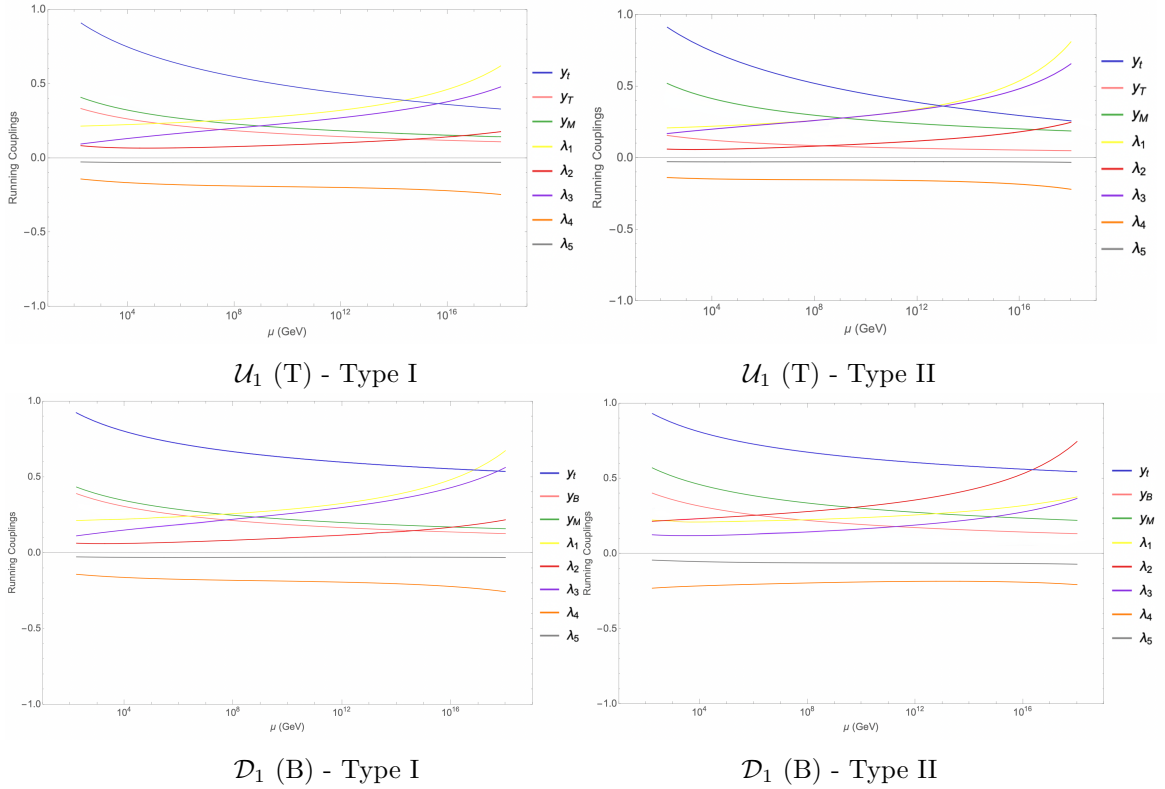
Figure 6.2: The RGE running of the Yukawa and scalar couplings for models with vector-like quarks. We plot results for Type-I on the left column and for Type-II on the right column. Top panel: singlet vector-like representation, $\mathcal{U}_1$. Bottom panel: singlet vector-like representation, $\mathcal{D}_1$. For singlet models, we have set $m_T = 0.8$ TeV, $m_B = 0.85$ TeV, $M_H = 800$ GeV, $M_{H^\pm} = 750$ GeV, $M_A = 650$ GeV $\mu_0 = m_t$, $\tan\beta = 10$, and mixing angles $\sin\alpha = 0.1$ and $\sin\theta_L = 0.08$.

Model	m_{VLQ} (GeV)	$M_{H^\pm}$ (GeV)	M_H (GeV)	M_A (GeV)
$\mathcal{U}_1$ + Type-I	$m_T \in [800, 920]$	$[80, 830]$	$[700, 810]$	$[510, 770]$
$\mathcal{U}_1$ + Type-II	$m_T \in [820, 930]$	$[600, 840]$	$[720, 860]$	$[715, 600]$
$\mathcal{D}_1$ + Type-I	$m_B \in [850, 970]$	$[80, 840]$	$[725, 870]$	$[500, 800]$
$\mathcal{D}_1$ + Type-II	$m_B \in [870, 980]$	$[600, 840]$	$[740, 870]$	$[770, 860]$

Table 6.3: Allowed parameter space for 2HDM + singlet VLQs that survives the constraints from unitarity, perturbativity, and vacuum stability.

A few comments regarding the behaviour of the couplings for all VLQ representations are in order.

(i) The upper mass bounds on the scalars of 2HDM can be extended further if $\tan\beta$ is increased according to the RG scanning. Otherwise, larger $\tan\beta$ leads to λ_i suppressions by flattening all scalar RG flows and might lead to instabilities by causing Yukawa divergences for $\tan\beta > 12$ beyond the range scanned. This characteristic can always be read from the denominator term through initial conditions in Eq. 6.12. Ref. [218] discusses the details of "squeezing" regions of stability for VLQ in various models.

(ii) The high energy enhancement of λ_2 in Type-II models occurs due to the presence of the Yukawa terms y_M^2 and $y_f^2 y_M^2$ appearing in the $\lambda_{3,4,5}$, contribution to running coupling constants as y_M approaches to M_{Pl}, this being the largest correction among all VLQ Yukawa couplings.

(iii) Due to the splitting of Yukawa terms between Φ_1 and Φ_2, Type-II+VLQ models are safer for vacuum stability as λ_2^I stays closer to zero as compared to λ_2^{II}, though this distinction alone is not enough for the stability requirements.

6.5.2 Doublet VLQs: $\mathcal{D}_X$, $\mathcal{D}_2$ and $\mathcal{D}_Y$

As seen in Fig. 6.3, where we plot the variation of the scalar and Yukawa coupling constants as functions of the energy scale, the evolution of λ_1 in Type-I+$\mathcal{D}_2$ is safer compared to $\mathcal{D}_X$ and $\mathcal{D}_Y$ models. In fact, faster coupling increases for these models are seen from the upper bound of scalar masses, which exceeds the bounds extracted from $\mathcal{D}_2$. Furthermore, the allowed space for the heavier CP-even scalar M_H in $\mathcal{D}_Y$ is quite restricted compared to other Type-I+ doublet VLQ models, hence λ_2 increases very fast, consistent with its initial condition as well. Due to fact that B and Y VLQs are relatively heavier than T and X VLQs, the evolution of λ_1 stays closer to zero in $\mathcal{D}_Y$+Type-II model as this coupling is connected to the down-sector VLQ. Among all the doublet models, $\mathcal{D}_X^{II}$ yields the most sensitive parameter space for the mass of heavier CP-even scalar M_H, resulting in a very narrow range for the combined RG scanning. Furthermore, as seen from the absence of bottom and top sector mixings in $\mathcal{D}_X$ and $\mathcal{D}_Y$ respectively, and also the fact that these VLQ are pure eigenstates, the evolution of y_X and y_Y is enhanced compared to y_T and y_B in $\mathcal{D}_2$. Therefore, the quartic Yukawa cross terms proportional to $y_M^2 y_{X,Y}^2$ lead to positive evolution for λ_4, within the perturbative range for VLQ models with non-SM-like quantum numbers. Actually, this reciprocal RG connection between λ_4 and λ_5 determines how stringent the scalar parameter space is constrained. This will be further shown in the analysis of the parameter space for triplet VLQ+2HDM. The complete allowed mass range for doublet models that survives from unitarity, perturbativity and stability up to $\mu = M_{Pl}$ is given in Table 6.4.
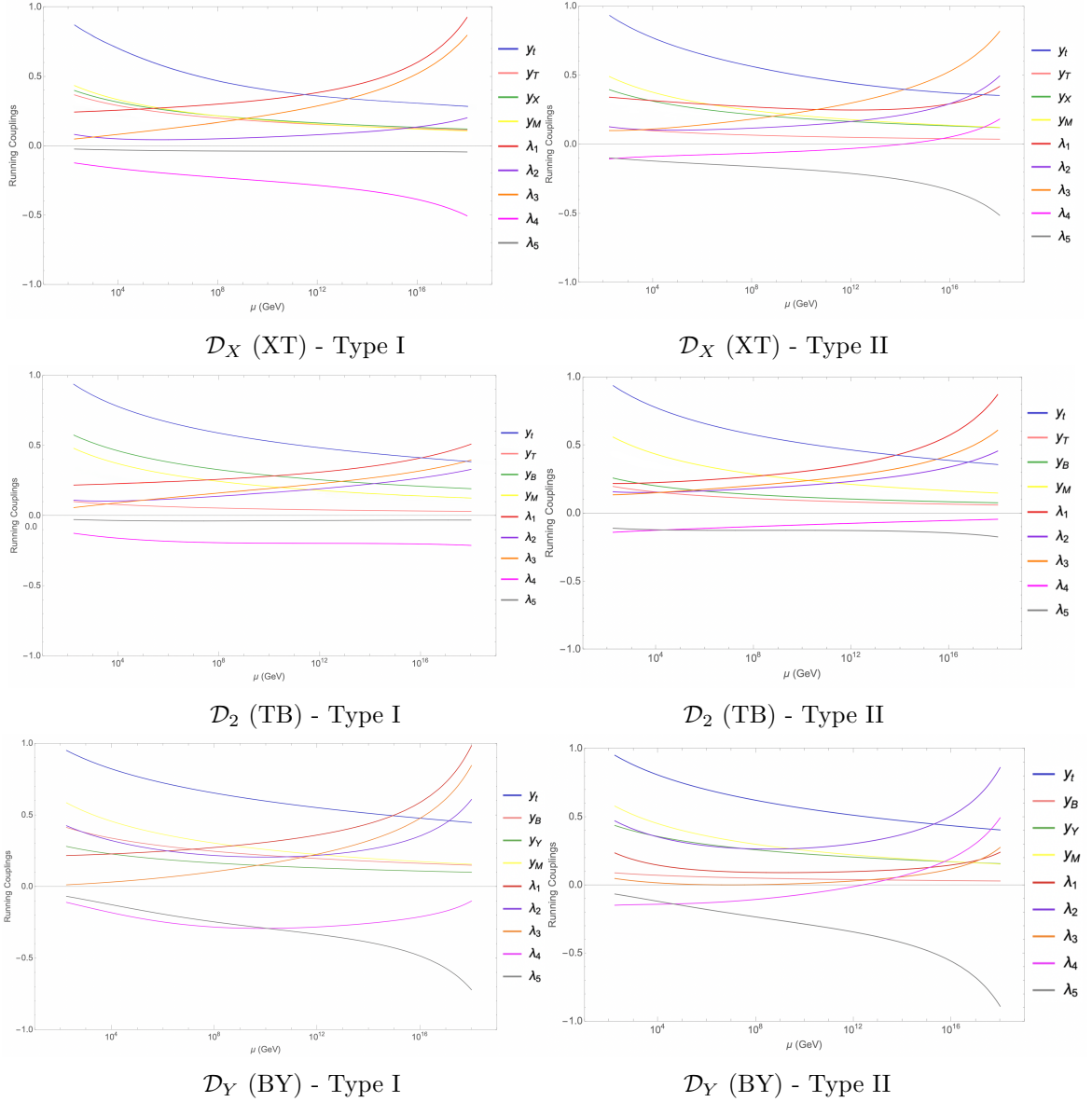
Figure 6.3: The RGE running of the Yukawa and scalar couplings for models with vector-like fermions. As before, we plot results for Type-I on the left column and for Type -II on the right column. Top panel: doublet vector-like representation, $\mathcal{D}_X$. Middle panel: doublet vector-like representation, $\mathcal{D}_2$. Bottom panel: doublet vector-like representation, $\mathcal{D}_Y$. For doublet models, we have set $m_T = 0.85$ TeV, $m_B = 1$ TeV, $m_X = 1$ TeV, $m_Y = 1$ TeV, $M_H = 800$ GeV, $M_{H^\pm} = 750$ GeV, $M_A = 650$ GeV, $\mu_0 = m_t$, $\tan\beta = 10$, and mixing angles $\sin\alpha = 0.1$ and $\sin\theta_L = 0.08$.

Model	m_{VLQ} (GeV)	$M_{H^\pm}$ (GeV)	M_H (GeV)	M_A (GeV)
$\mathcal{D}_X$ + Type-I	$m_X \in [800, 1040]$ $m_T \in [850, 970]$	$[80, 840]$	$[690, 870]$	$[520, 860]$
$\mathcal{D}_X$ + Type-II	$m_X \in [880, 1050]$ $m_T \in [870, 1000]$	$[600, 865]$	$[820, 890]$	$[760, 880]$
$\mathcal{D}_2$ + Type-I	$m_T \in [800, 930]$ $m_B \in [860, 970]$	$[80, 810]$	$[670, 830]$	$[490, 870]$
$\mathcal{D}_2$ + Type-II	$m_T \in [840, 1010]$ $m_B \in [900, 1040]$	$[600, 840]$	$[810, 980]$	$[640, 860]$
$\mathcal{D}_Y$ + Type-I	$m_B \in [900, 970]$ $m_Y \in [900, 990]$	$[80, 840]$	$[750, 890]$	$[610, 875]$
$\mathcal{D}_Y$ + Type-II	$m_B \in [925, 1010]$ $m_Y \in [950, 1050]$	$[600, 870]$	$[750, 930]$	$[670, 890]$

Table 6.4: Allowed parameter space for 2HDM + doublet VLQs that survives the constraints from unitarity, perturbativity, and vacuum stability.

6.5.3 Triplet VLQs: $\mathcal{T}_X$ and $\mathcal{T}_Y$

Finally, for triplets, plotted in Fig. 6.4, our RGE scanning indicates that mass of CP-even scalar exceeds 1 TeV, whereas $M_{H^\pm}$ approaches an upper limit < 1 TeV, which is in good agreement with the mass limits extracted from the deviation of the oblique parameters according to CDF W-mass anomaly [219]. For triplet VLQs, a unique feature of the Yukawa couplings is that due to the dependence on y_M, their evolution becomes less suppressed as the energy scale grows. In fact, y_M which is Yukawa representation of Dirac mass terms for VLQs surpasses the top Yukawa coupling at a scale around 10^{13} GeV. The parameter space for triplet VLQ+2HDM extends the upper bounds compared to other representations, because the opposite convolution of λ_4 and λ_5 always occurs for triplet VLQs due to the abundance of coupled terms. We also note that the stability condition on the electroweak vacuum is at its most critical state around 10^6 GeV regardless of the 2HDM type for triplet VLQs. This critical proximity to the instability case occurs at almost the same energy level regardless of all the parameters that satisfy the combined stability, perturbativity and unitarity conditions. Finally, the allowed parameter space for triplet VLQs+2HDM-I,II that survives the constraints from stability, perturbativity and unitarity up to $\mu = M_{Pl}$ is given in Table 6.5.

$\mathcal{T}_X$ (XTB) - Type I $\qquad\qquad$ $\mathcal{T}_X$ (XTB) - Type II

$\mathcal{T}_Y$ (TBY) - Type I $\qquad\qquad$ $\mathcal{T}_Y$ (TBY) - Type II
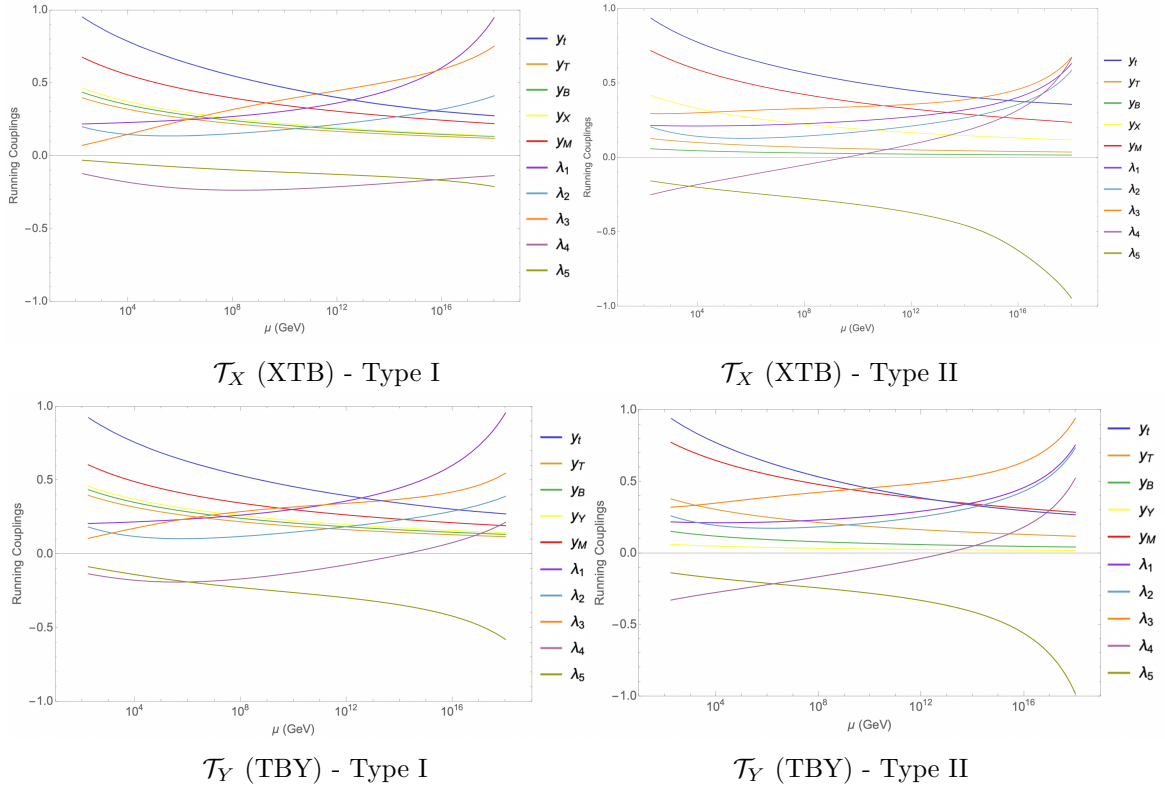
Figure 6.4: The RGE running of the Yukawa and scalar couplings for models with vector-like fermions. As before, we plot results for Type-I on the left column and for Type-II on the right column. Top panel: triplet vector-like representation, $\mathcal{T}_X$. Bottom panel: triplet vector-like representation, $\mathcal{T}_Y$. For triplet models, we have set $m_T = 0.9$ TeV, $m_B = 1$ TeV, $m_X = 1$ TeV, $m_Y = 1$ TeV, $M_H = 850$ GeV, $M_{H^\pm} = 800$ GeV, $M_A = 650$ GeV, $\mu_0 = m_t$, $\tan\beta = 10$, and mixing angles $\sin\alpha = 0.1$ and $\sin\theta_L = 0.08$.

Model	m_{VLQ} (GeV)	$M_{H^\pm}$ (GeV)	M_H (GeV)	M_A (GeV)
$\mathcal{T}_X$ + Type-I	$m_X \in [900, 1070]$ $m_T \in [870, 990]$ $m_B \in [900, 1040]$	$[80, 890]$	$[780, 1030]$	$[560, 930]$
$\mathcal{T}_X$ + Type-II	$m_X \in [950, 1100]$ $m_T \in [890, 1000]$ $m_B \in [925, 1040]$	$[600, 885]$	$[790, 910]$	$[700, 890]$
$\mathcal{T}_Y$ + Type-I	$m_T \in [840, 950]$ $m_B \in [890, 970]$ $m_Y \in [880, 1020]$	$[80, 900]$	$[740, 1050]$	$[525, 940]$
$\mathcal{T}_Y$ + Type-II	$m_T \in [860, 975]$ $m_B \in [910, 1035]$ $m_Y \in [950, 1100]$	$[600, 890]$	$[820, 1020]$	$[580, 910]$

Table 6.5: Allowed parameter space for 2HDM + triplet VLQs that survives the constraints from unitarity, perturbativity, and vacuum stability.

For completeness, explicit expressions for all the relevant RGE for the Yukawa couplings, the couplings between the bosons and coupling constants, are included in the Appendix B.

6.6 Electroweak Precision Constraints

Signals from new physics are also constrained through electroweak precision observables, which are highly correlated to large logarithms of extra masses when the scale of new model is significantly larger than electroweak scale [54, 220, 221]. The modifications to electroweak gauge boson loops at loop level are calculated through the oblique parameters, $\mathbb{S}, \mathbb{T}$, and $\mathbb{U}$, defined as [97]

$$
\begin{aligned}
\mathbb{S} &= 16\pi\Re\left[\bar{\Pi}_\gamma^{3Q}(M_Z^2) - \bar{\Pi}_Z^{33}(0)\right], \\
\mathbb{T} &= \frac{4\sqrt{2}G_F}{\alpha_e}\Re\left[\bar{\Pi}^{3Q}(0) - \bar{\Pi}^{11}(0)\right], \\
\mathbb{U} &= 16\pi\Re\left[\bar{\Pi}_Z^{33}(0) - \bar{\Pi}_W^{11}(0)\right].
\end{aligned}
\tag{6.42}
$$

The $\mathbb{S}$, $\mathbb{T}$ parameters in new physics models, such as VLQ scenarios and 2HDMs, are different from those in the SM due to extra scalars and fermions appearing in gauge boson self energies at the loop level. Additionally, the mixing between the SM fields and the new particles modifies the Higgs and electroweak couplings as well. Consequently, electroweak precision observables are universal. The current experimental values [222] are obtained by fixing the differences between the new physics and the SM contributions by setting $\Delta\mathbb{U} = 0$, yielding $\Delta\mathbb{T} = 0.09 \pm 0.07$, $\Delta\mathbb{S} = 0.05 \pm 0.08$ (and $\rho_{S,T} = 0.92 \pm 0.11$). For the work carried here, we can split the oblique parameters calculation of $\mathbb{S}, \mathbb{T}$ and $\mathbb{U}$ parameters via loop contributions into two independent contributions, one due to bosons and the other to fermions circulating in self-energy diagrams. We extracted gauge boson self energies using `LoopTools` and `FormCalc` [223], and implemented analytical expressions of Passarino-Veltman (PV) functions in `FeynCalc` [224] to obtain oblique parameters.

6.6.1 Contributions to the $\mathbb{S}$ and $\mathbb{T}$-parameters from 2HDM

Further expanding Eq. 6.42 explicitly in terms of the scalar loop contributions to the gauge boson two point functions

$$
\begin{aligned}
\mathbb{S}_{2HDM} &= 16\pi\Re\left[\frac{\Pi_{2HDM}^{Z\gamma}(M_Z^2)}{s_W c_W g_Z^2} + \frac{\Pi_{2HDM}^{\gamma\gamma}(M_Z^2)}{c_W^2 g_Z^2} - \frac{\Pi_{2HDM}^{ZZ}(M_Z^2) - \Pi_{2HDM}^{ZZ}(0)}{g_Z^2}\right. \\
&\quad \left. - \frac{2s_W\Pi_{2HDM}^{Z\gamma}(0)}{c_W g_Z^2}\right], \\
\mathbb{T}_{2HDM} &= \frac{4\sqrt{2}G_F}{\alpha_e}\Re\left[\frac{\Pi_{2HDM}^{ZZ}(0)}{g_Z^2} + \frac{2s_W\Pi_{2HDM}^{Z\gamma}(0)}{c_W g_Z^2} - \frac{\Pi_{2HDM}^{WW}(0)}{c_W^2 g_Z^2}\right].
\end{aligned}
\tag{6.43}
$$

The coupling factors are $g_Z = g/c_W$ and the photon two-point function in the 2HDM is

$$
\begin{aligned}
\Pi_{2HDM}^{\gamma\gamma}(p^2) &= e^2 B_5(p^2, M_{H^\pm}^2, M_{H^\pm}^2) - e^2 p^2[5B_0(p^2, M_W^2, M_W^2) \\
&\quad + 12B_3(p^2, M_W^2, M_W^2) + \frac{2}{3}].
\end{aligned}
\tag{6.44}
$$

The photon-Z mixing is given by

$$\Pi_{2HDM}^{Z\gamma}(p^2) = -eg_Z p^2 \left(\frac{11}{2}B_0(p^2, M_W^2, M_W^2) + 10B_3(p^2, M_W^2, M_W^2) + \frac{2}{3}\right)$$
$$+ \frac{eg_Z}{2}B_5(p^2, M_{H^\pm}^2, M_{H^\pm}^2)$$
$$- \frac{s_W}{c_W}\left[e^2 B_5(p^2, M_{H^\pm}^2, M_{H^\pm}^2) - e^2 p^2[5B_0(p^2, M_W^2, M_W^2)\right.$$
$$+ \left. 12B_3(p^2, M_W^2, M_W^2) + \frac{2}{3}]\right]. \tag{6.45}$$

The Z-boson two-point function in the 2HDM is

$$\Pi_{2HDM}^{ZZ}(p^2) = g_Z^2\left[\frac{s_{\beta-\alpha}^2}{4}B_5(p^2, M_H^2, M_A^2) + \frac{c_{\beta-\alpha}^2}{4}B_5(p^2, M_h^2, M_A^2)\right.$$
$$+ \frac{1}{4}B_5(p^2, M_{H^\pm}^2, M_{H^\pm}^2) - \frac{2p^2}{3} + 2M_W^2 B_0(p^2, M_W^2, M_W^2)$$
$$+ s_{\beta-\alpha}^2[M_Z^2 B_0(p^2, M_h^2, M_Z^2) + \frac{1}{4}B_5(p^2, M_h^2, M_Z^2)]$$
$$+ c_{\beta-\alpha}^2[M_Z^2 B_0(p^2, M_H^2, M_Z^2) + \frac{1}{4}B_5(p^2, M_H^2, M_Z^2)]$$
$$\left. - \frac{23p^2}{4}B_0(p^2, M_W^2, M_W^2) - 9p^2 B_3(p^2, M_W^2, M_W^2)\right]$$
$$+ \frac{s_W^2}{c_W^2}\left(e^2 p^2[5B_0(p^2, M_W^2, M_W^2) + 12B_3(p^2, M_W^2, M_W^2) + \frac{2}{3}]\right.$$
$$- \left. e^2 B_5(p^2, M_{H^\pm}^2, M_{H^\pm}^2)\right)$$
$$+ \frac{2s_W}{c_W}\left[eg_Z p^2\left(\frac{11}{2}B_0(p^2, M_W^2, M_W^2) + 10B_3(p^2, M_W^2, M_W^2) + \frac{2}{3}\right)\right.$$
$$- \frac{eg_Z}{2}B_5(p^2, M_{H^\pm}^2, M_{H^\pm}^2) - \frac{s_W}{c_W}e^2 B_5(p^2, M_{H^\pm}^2, M_{H^\pm}^2)$$
$$+ \left.\frac{s_W}{c_W}\left(e^2 p^2[5B_0(p^2, M_W^2, M_W^2) + 12B_3(p^2, M_W^2, M_W^2) + \frac{2}{3}]\right)\right]. \tag{6.46}$$

The W-boson two-point function in the 2HDM follows as

$$\Pi_{2HDM}^{WW}(p^2) = g^2\left[\frac{1}{4}B_5(p^2, M_A^2, M_{H^\pm}^2) + \frac{s_{\beta-\alpha}^2}{4}B_5(p^2, M_H^2, M_{H^\pm}^2) - \frac{2p^2}{3}\right.$$
$$+ s_{\beta-\alpha}^2[M_W^2 B_0(p^2, M_h^2, M_W^2) + \frac{1}{4}B_5(p^2, M_h^2, M_W^2)]$$
$$+ \frac{c_{\beta-\alpha}^2}{4}B_5(p^2, M_h^2, M_{H^\pm}^2) - 8p^2 c_W^2 B_0(p^2, M_Z^2, M_W^2)$$
$$+ c_{\beta-\alpha}^2[M_W^2 B_0(p^2, M_H^2, M_W^2) + \frac{1}{4}B_5(p^2, M_H^2, M_W^2)]$$
$$+ (\frac{1}{4} + 2c_W^2)B_5(p^2, M_Z^2, M_W^2) + M_W^2(1 - 4s_W^2)B_0(p^2, M_Z^2, M_W^2)$$
$$+ M_Z^2 B_0(p^2, M_Z^2, M_W^2) + 2s_W^2 B_5(p^2, 0, M_W^2)$$
$$+ \left. 2M_W^2 B_0(p^2, 0, M_W^2) - 4p^2 B_0(p^2, 0, M_W^2)\right]. \tag{6.47}$$

The Passarino - Veltman functions and relevant identities are given in Appendix D. Subtracting the SM contributions from $\mathbb{S}$ and $\mathbb{T}$ parameters of the 2HDM yields the new physics contributions to oblique parameters:

$$
\begin{aligned}
\Delta\mathbb{T}_{2HDM} =\ & \frac{1}{4\pi M_Z^2 c_W^2 s_W^2}\Big[B_{00}(0, M_A^2, M_{H^\pm}^2) + B_{00}(0, M_Z^2, M_W^2) - B_{00}(0, M_W^2, M_h^2) \\
& - B_{00}(0, M_W^2, M_Z^2) + (4s_W^4 - 1)B_{00}(0, M_{H^\pm}^2, M_{H^\pm}^2) \\
& - 2M_{H^\pm}^2 s_W^4[1 + B_0(0, M_{H^\pm}^2, M_{H^\pm}^2] \\
& + s_{\beta-\alpha}^2[B_{00}(0, M_H^2, M_{H^\pm}^2) + B_{00}(0, M_h^2, M_W^2) - B_{00}(0, M_H^2, M_A^2)] \\
& + c_{\beta-\alpha}^2[M_W^2 B_0(0, M_h^2, M_W^2) + B_{00}(0, M_h^2, M_Z^2) - M_Z^2 B_0(0, M_h^2, M_Z^2) \\
& + B_{00}(0, M_h^2, M_{H^\pm}^2) - B_{00}(0, M_h^2, M_A^2) + B_{00}(0, M_H^2, M_W^2) \\
& - M_W^2 B_0(0, M_H^2, M_W^2) + M_Z^2 B_0(0, M_H^2, M_Z^2) - B_{00}(0, M_H^2, M_Z^2)]\Big], \quad (6.48)
\end{aligned}
$$

$$
\begin{aligned}
\Delta\mathbb{S}_{2HDM} =\ & \frac{1}{\pi M_Z^2}\Big[2s_W^2 c_W^2 A_0(M_{H^\pm}^2) - B_{00}(M_Z^2, M_{H^\pm}^2, M_{H^\pm}^2) \\
& + (c_W^2 - s_W^2)^2 B_{00}(0, M_{H^\pm}^2, M_{H^\pm}^2) \\
& + s_{\beta-\alpha}^2[B_{00}(M_Z^2, M_H^2, M_A^2) - B_{00}(0, M_H^2, M_A^2)] \\
& + c_{\beta-\alpha}^2[B_{00}(M_Z^2, M_H^2, M_A^2) + B_{00}(0, M_h^2, M_Z^2) + B_{00}(M_Z^2, M_h^2, M_Z^2) \\
& - B_{00}(M_Z^2, M_H^2, M_Z^2) - B_{00}(0, M_H^2, M_A^2) - B_{00}(0, M_H^2, M_Z^2) \\
& + M_Z^2 B_0(M_Z^2, M_h^2, M_Z^2) + M_Z^2 B_0(0, M_H^2, M_Z^2) \\
& - M_Z^2 B_0(0, M_h^2, M_Z^2) - M_Z^2 B_0(M_Z^2, M_H^2, M_Z^2)]\Big]. \quad (6.49)
\end{aligned}
$$

In Fig. 6.5 (left panel), the correlation between M_A and $M_{H^\pm}$ due to EWPO does not constrain the masses in a stringent way, though when $M_A > 550$ GeV, the correlation becomes significantly important. The red region has already been discarded by direct searches at LEP [214]. Considering the imposing theoretical bounds only, the findings from EWPO are consistent with the unitary bounds in $M_A - M_{H^\pm}$ plane [178]. Note that, $\tan\beta$ dependence of the oblique parameters alone is more relaxed, allowing a wide mass spectrum. This is due to fact that the mixing between CP-even scalars can be shifted away from the $\sin\alpha = 0$ (decoupling) limit, hence the variation in $\tan\beta$ compensates for the Higgs data requirement of the near-alignment limit, $\cos(\beta - \alpha) \approx 0$. Consequently, imposing the alignment limit on the mass spectrum of scalars is by choice (to fit the Higgs data) rather than requirement of the theory when RG running $\mu < 1$ TeV. This consequence is highlighted particularly for Type-I with various $\tan\beta$ values [215]. On the other hand, as seen from Fig. 6.5 (right panel), the limit is stronger in the $M_H - \sin\alpha$ plane for fixed value of $\tan\beta$ in both types of 2HDMs. It is seen that for $\tan\beta = 6$, EWPO constrain the masses in a way that the decoupling limit of CP-even scalars occurs in a natural way at a scale $\sim \mathcal{O}$ (TeV). Although the $\sin\alpha = 0$ (decoupling) limit is not forbidden by EWPO, we combined it with the minimum stability requirement on $\sin\alpha$ near the decoupling limit. Moreover, the constraints on M_H obtained from EWPO and from the vacuum stability match with the constraint for signal rates of $H \to WW^\star \to e\nu\mu\nu$ [225, 226]. Furthermore, we excluded the $\sin\alpha = 0$ region because a nonzero mixing between CP-even scalars ($\sin\alpha \neq 0$) is required to preserve the vacuum stability up to the Planck scale. As keeping $\cos(\beta - \alpha)$ closer to zero is motivated by the alignment limit from the Higgs data [155], we impose this
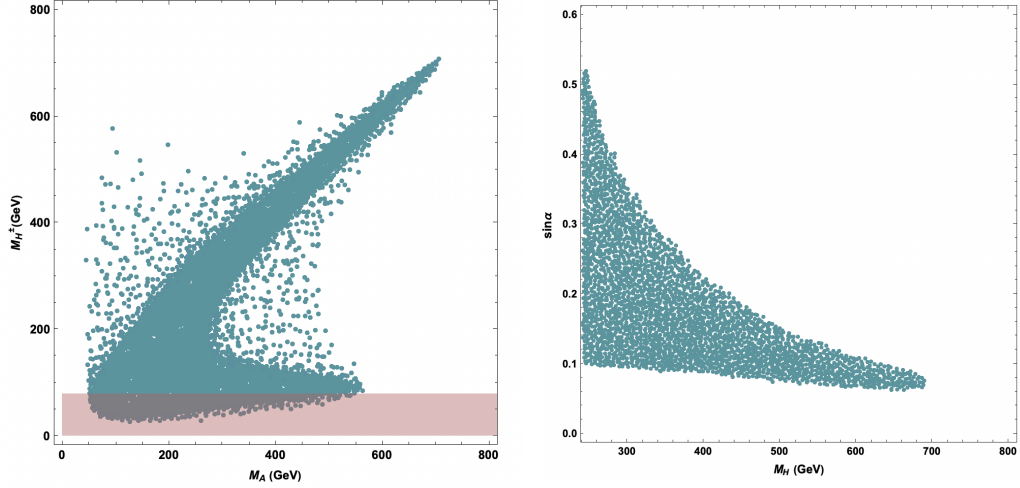
Figure 6.5: The allowed mass regions from EWPO for the pseudoscalar boson mass M_A and charged Higgs mass $M_{H^\pm}$ (left panel). The allowed parameter space from EWPO for scalar mass M_H and scalar mixing angle with the SM Higgs $\sin \alpha$ (right panel) in 2HDM. The $\sin \alpha = 0$ limit of CP-even scalars mixing is allowed by EWPO but excluded due to the vacuum stability constraint. We have set $\tan \beta = 6$.
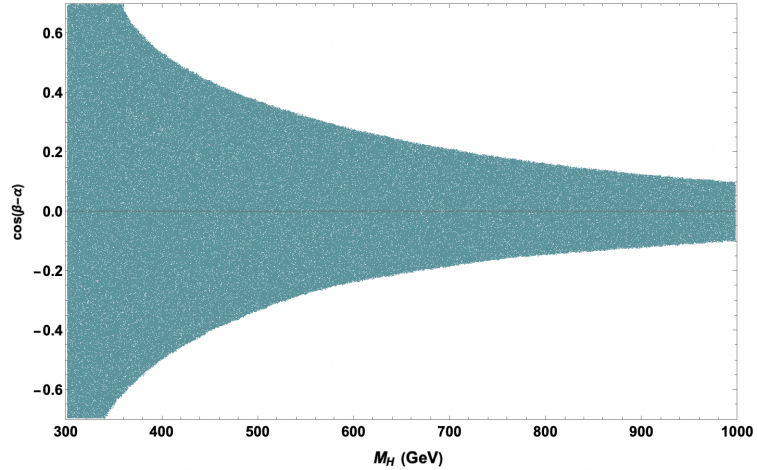
Figure 6.6: The allowed mass regions extracted from EWPO for M_H versus $\cos(\beta - \alpha)$ mixing between CP-even scalars in 2HDM.

along with the requirement that the couplings evolved with the RGEs remain away from the vacuum instability. Hence, using the mass spectrum allowed from EWPO constraints fit with the stability analysis. It is important that the theoretical constraints align with each other as the limits rising from vacuum stability become stronger at the scale $[10^3, 10^{10}]$ GeV [218], thus restricting $M_{H^\pm} > 580$ GeV with smaller mass differences between extra scalars, as the cut-off scale increases in Type-II. However, the mass limits in Type-I are weaker. Favoured also by collider bounds [154], there exists a parameter space for which

the mass separation between scalars remains small for 2HDM, while validated up to the Planck scale. Our results from the oblique parameters do not conflict with the parameter space obtained from RGE in Section 6.5, however the effects of VLQs on RGE slightly shift the upper limits compared to the findings of EWPO.

In Fig. 6.6, we have considered the energy scale $\mu = [800 - 1000]$ GeV in self energy diagrams, and scan over values up to 1 TeV with respect to the oblique parameters. The upper limit of M_H is chosen to be in a good agreement with the limits from vacuum stability on scalars+VLQs at $\tan\beta = [6, 12]$. The current experimental data constraining h to having SM-like Higgs behaviour restrict values of $\cos(\beta - \alpha)$ much closer to the decoupling limit. Consequently, the electroweak vacuum stability requirements and EWPO impose naturally occurring near decoupling limit when $M_A, M_H > 600$ GeV. We should also note that, Type-I and Type-II dependent effects are highly manifestable through Higgs channels, for which the signal strengths $\kappa_{hbb}, \kappa_{hcc}$ also favour regions slightly beyond the decoupling limit, particularly for $\tan\beta \sim [2, 12]$ [155]. The contribution to $\mathbb{T}_{2HDM}$ is twofold, depending on the mass parameter space of scalars and on $\sin(\beta - \alpha)$ whereas a negative contribution to $\mathbb{T}_{2HDM}$ can always be generated by varying $M_{H^\pm}$. For general scale of $\sin(\beta - \alpha)$, M_h and M_H splitting has to be small for pushing $\mathbb{T}_{2HDM}$ to be large and negative values. Hence, negative corrections to $\mathbb{T}$ in 2HDM can render overall positive corrections rising from various fermion representations and further enhancing limitations on additional scalars and mixing among Higgs bosons.

6.6.2 VLQ contributions to the $\mathbb{S}$ and $\mathbb{T}$ parameters

The contributions of VLQs to $\mathbb{S}$ and $\mathbb{T}$ parameters are different for each representation (singlets, doublets or triplets) in the current framework. Since the electroweak Lagrangian is constructed with gauge eigenstate fields, any mixing of fermions with extra anomaly-free fields alters the structure of the bare electroweak Lagrangian, as seen from Eq. 7.10. As we have already seen in Section 6.3, the mixing regime is model dependent. Ref. [88] highlighted the emergence of disagreement of the oblique parameters for triplets in [119], where the external momenta of gauge bosons are omitted in self-energy diagrams Π_{VV}. This leads to a discrepancy in the $\mathbb{S}$ parameter, which becomes positive in triplet representations in the large logarithm of $m_T \sim \mathcal{O}(\text{TeV})$, as in Ref. [114]. Following the corrections carried in Ref. [88], we obtained better approximations to $\Delta\mathbb{S}_{\mathcal{T}_X,\mathcal{T}_Y}$ and $\Delta\mathbb{T}_{\mathcal{T}_X,\mathcal{T}_Y}$. Consequently, in to our calculations $\Delta\mathbb{S} < 0$ and $\Delta\mathbb{T} > 0$, and we found agreement with the results in [227]. As we mentioned in Section 6.6.1, the self energies of gauge bosons are extracted so that UV divergences are properly cancelled. Here we present the contributions of VLQs to the oblique parameters in terms of PV functions.

The couplings to W-boson and Z-boson are been modified by the VLQs through their mixing with SM quarks

$$
\begin{aligned}
\mathcal{L}_W &= \frac{g}{\sqrt{2}}\bar{Q}_i\gamma^\mu(C^L_{Q_iQ_j}P_L + C^R_{Q_iQ_j}P_R)Q_jW^+_\mu + h.c.\,, \\
\mathcal{L}_Z &= \frac{g}{2c_W}\bar{Q}_i\gamma^\mu(N^L_{Q_iQ_j}P_L + N^R_{Q_iQ_j}P_R - 2\delta_{ij}\mathbb{Q}s^2_W)Q_jZ^\mu\,, \quad (6.50)
\end{aligned}
$$

where $Q_{i,j}$ are any type of quarks in our convention of electroweak Lagrangian. The condition $|\mathbb{Q}_i - \mathbb{Q}_j| = 1$ holds for all form of $W - Q_i - Q_j$ interactions.

Further compression of the modified electroweak couplings take the following forms:

$$\begin{aligned}
\mathcal{L}_W &\supset \gamma^\mu(\Omega^L_{WQ_iQ_j}\mathbb{L} + \Omega^R_{WQ_iQ_j}\mathbb{R})W^+_\mu\,, \\
\mathcal{L}_Z &\supset \gamma^\mu(\Omega^L_{ZQ_iQ_j}\mathbb{L} + \Omega^R_{ZQ_iQ_j}\mathbb{R})Z_\mu\,.
\end{aligned} \tag{6.51}$$

For the cases $i = j$ of $Z - Q_i - Q_j$ interactions, the last term of Eq. 7.10 is absorbed in $\Omega^{L,R}_{ZQ_iQ_j}$ throughout all VLQ representations.

$$\begin{aligned}
\mathbb{T}_{VLQ} &= \frac{1}{\alpha_e}\Re\left[\frac{2s_W}{c_W M_Z^2}\sum_i \mathcal{F}_{Z\gamma}(\Omega^L_{ZQ_iQ_i}, \Omega^R_{ZQ_iQ_i}, \mathbb{Q}_i, m_i^2, p^2 = 0)\right. \\
&+ \frac{-2}{M_Z^2}\sum_{i\neq j}\delta(\mathbb{Q}_i - \mathbb{Q}_j)\mathcal{F}_{ZZ}(\Omega^L_{ZQ_iQ_j}, \Omega^R_{ZQ_iQ_j}, m_i^2, m_j^2, p^2 = 0) \\
&+ \frac{1}{M_Z^2}\sum_i \mathcal{F}_{ZZ}(\Omega^L_{ZQ_iQ_i}, \Omega^R_{ZQ_iQ_i}, m_i^2, m_i^2, p^2 = 0) \\
&+ \left.\frac{1}{M_W^2}\sum_{i\neq j}\delta(\mathbb{Q}_i - \mathbb{Q}_j)\mathcal{F}_{WW}(\Omega^L_{WQ_iQ_j}, \Omega^R_{WQ_iQ_j}, m_i^2, m_j^2, p^2 = 0)\right], \quad (6.52)
\end{aligned}$$

$$\begin{aligned}
\mathbb{S}_{VLQ} &= \frac{4s_W^2 c_W^2}{\alpha_e}\Re\left[\left(\frac{c_W^2 - s_W^2}{s_W c_W M_Z^2}\right)\left(\sum_i \mathcal{F}_{Z\gamma}(\Omega^L_{ZQ_iQ_i}, \Omega^R_{ZQ_iQ_i}, \mathbb{Q}_i, m_i^2, M_Z^2)\right.\right. \\
&+ \left.\sum_i \mathcal{F}_{Z\gamma}(\Omega^L_{ZQ_iQ_i}, \Omega^R_{ZQ_iQ_i}, \mathbb{Q}_i, m_i^2, 0)\right) - \frac{1}{M_Z^2}\sum_i \mathcal{F}_{\gamma\gamma}(\mathbb{Q}_i, \mathbb{Q}_i, m_i^2, m_i^2, M_Z^2) \\
&+ \frac{2}{M_Z^2}\sum_{i\neq j}\delta(\mathbb{Q}_i - \mathbb{Q}_j)\mathcal{F}_{ZZ}(\Omega^L_{ZQ_iQ_j}, \Omega^R_{ZQ_iQ_j}, m_i^2, m_j^2, M_Z^2) \\
&- \frac{2}{M_Z^2}\sum_{i\neq j}\delta(\mathbb{Q}_i - \mathbb{Q}_j)\mathcal{F}_{ZZ}(\Omega^L_{ZQ_iQ_j}, \Omega^R_{ZQ_iQ_j}, m_i^2, m_j^2, 0) \\
&+ \frac{1}{M_Z^2}\sum_i \mathcal{F}_{ZZ}(\Omega^L_{ZQ_iQ_i}, \Omega^R_{ZQ_iQ_i}, m_i^2, m_i^2, M_Z^2) \\
&- \left.\frac{1}{M_Z^2}\sum_i \mathcal{F}_{ZZ}(\Omega^L_{ZQ_iQ_i}, \Omega^R_{ZQ_iQ_i}, m_i^2, m_i^2, 0)\right], \quad (6.53)
\end{aligned}$$

where the fermion functions $\mathcal{F}_{VV,Z\gamma}$ contributing to the gauge boson two-point functions are calculated as

$$\begin{aligned}
\mathcal{F}_{Z\gamma}(\Omega_1, \Omega_2, \mathbb{Q}, m^2, p^2) &= \frac{N_c}{8\pi^2}[\mathbb{Q}(\Omega_1 + \Omega_2)\left(2B_{00}(p^2, m^2, m^2) - A_0(m^2)\right. \\
&- \left.p^2 B_1(p^2, m^2, m^2)\right)], \\
\mathcal{F}_{VV}(\Omega_1, \Omega_2, m_1^2, m_2^2, p^2) &= \frac{N_c}{8\pi^2}\left[\left((\Omega_1^2 + \Omega_2^2)m_1^2 - 2\Omega_1\Omega_2 m_1 m_2\right)B_0(p^2, m_1^2, m_2^2)\right. \\
&+ (\Omega_1^2 + \Omega_2^2)\left(p^2 B_1(p^2, m_1^2, m_2^2) + A_0(m_2^2)\right. \\
&- \left.\left.2B_{00}(p^2, m_1^2, m_2^2)\right)\right]. \quad (6.54)
\end{aligned}$$

Complete expressions of the oblique parameters for doublets and triplets are lengthy. Thus, we give the full contributions to $\mathbb{S}$ and $\mathbb{T}$ parameters from singlet VLQ representations $\mathcal{U}_1$ and $\mathcal{D}_1$. The deviations $\Delta\mathbb{T}, \Delta\mathbb{S}$ of the oblique parameters from their SM values are

$$
\begin{aligned}
\Delta\mathbb{T}_{\mathcal{U}_1} = {} & \frac{N_c m_t^4 (s_L^t)^2}{16\pi s_W^2 M_W^2 (m_T^2 - m_t^2)} \left[\frac{m_T^2 - m_t^2}{m_t^2} (s_L^t)^2 \left(\frac{m_T^2 + m_t^2}{m_t^2} \right) \right. \\
& \left. + 2 \left(1 - \frac{A_0(m_T^2)}{m_T^2} \right) - 4\frac{m_T^2}{m_t^2}(c_L^t)^2 \Big(B_0(0; m_T^2, m_t^2) - B_0(0; m_t^2, m_t^2) \Big) \right], \quad (6.55)
\end{aligned}
$$

$$
\begin{aligned}
\Delta\mathbb{S}_{\mathcal{U}_1} = {} & \frac{N_c}{12\pi M_Z^2} \left[(s_L^t)^2 A_0(m_t^2) \left[6m_T^2(c_L^t)^2 - 6m_t^2(c_L^t)^2 - M_Z^2 \left(9(s_L^t)^2 - 10 \right) \right] \right. \\
& - 32 A_0(m_T^2) M_Z^2 s_W^2 c_W^2 - 18 m_t^2 (s_L^t)^2 (c_L^t)^2 B_0(0, m_t^2, m_T^2) \\
& + 6(s_L^t)^2 (c_L^t)^2 B_0(M_Z^2, m_t^2, m_T^2) \left(M_Z^2(m_t^2 + m_T^2) - 2M_Z^4 + (m_T^2 - m_t^2)^2 \right) \\
& + (s_L^t)^2 A_0(m_T^2) \left(M_Z^2 \left(9(s_L^t)^2 - 10 \right) - 6m_T^2(c_L^t)^2 + 6m_t^2(c_L^t)^2 \right) \\
& + m_T^2 \left((s_L^t)^2 + 32 s_W^2 c_W^2 \right) - (s_L^t)^2 m_t^2 - 3m_t^2(s_L^t)^2 B_0(0, m_t^2, m_t^2) \left(3(s_L^t)^2 - 10 \right) \\
& + m_T^2 B_0(0, m_T^2, m_T^2) \left(32 s_W^2 c_W^2 - 12(s_L^t)^2 \right) \\
& + 2(s_L^t)^2 B_0(M_Z^2, m_T^2, m_T^2) \left[m_T^2 \left((s_L^t)^2 + 8 \right) - M_Z^2 \left(3(s_L^t)^2 - 4 \right) \right] \\
& \left. + 2(s_L^t)^2 B_0(M_Z^2, m_t^2, m_t^2) \left[m_t^2 \left(3(s_L^t)^2 - 16 \right) - M_Z^2 \left(3(s_L^t)^2 - 4 \right) \right] \right], \quad (6.56)
\end{aligned}
$$

$$
\begin{aligned}
\Delta\mathbb{T}_{\mathcal{D}_1} =\ & \frac{N_c}{8\pi c_W^2 s_W^2 M_Z^2}\Bigg[\left((s_L^b)^2(c_L^b)^2\left[B_{00}(0,m_b^2,m_B^2)-\frac{A_0(m_B^2)}{2}\right]\right. \\
& -\frac{m_b^2(s_L^b)^2(c_L^b)^2}{2}B_0(0,m_b^2,m_B^2)\Bigg) \\
& +\ \left(\frac{1}{16}(1-\frac{4s_W^2}{3})^2+\frac{4s_W^4}{9})\left[A_0(m_t^2)-2B_{00}(0,m_t^2,m_t^2)\right]\right) \\
& +\ \left(\frac{m_t^2}{4}(1-\frac{4s_W^2}{3})^2+\frac{m_t^2}{9}(4s_W^4-18)+\frac{2m_t^2 s_W^2}{3}(1-\frac{4s_W^2}{3})\right)B_0(0,m_t^2,m_t^2) \\
& +\ \left[\left(\frac{1}{4}(\frac{2s_W^2}{3}-(c_L^b)^2)\right)^2+\frac{s_W^4}{9}\right]\left[A_0(m_b^2)-2B_{00}(0,m_b^2,m_b^2)\right] \\
& +\ \left[\frac{m_b^2}{4}\left(\frac{2s_W^2}{3}-(c_L^b)^2\right)^2+\frac{m_b^2 s_W^4}{9}-\frac{m_b^2 s_W^2}{3}\left(\frac{2s_W^2}{3}-(c_L^b)^2\right)\right]B_0(0,m_b^2,m_b^2) \\
& +\ \left(\frac{1}{4}\left[\frac{2s_W^2}{3}-(s_L^b)^2\right]^2+\frac{s_W^4}{9}\right)\left[A_0(m_B^2)-2B_{00}(0,m_B^2,m_B^2)\right] \\
& +\ \left(\frac{m_B^2}{4}\left[\frac{2s_W^2}{3}-(s_L^b)^2\right]^2+\frac{m_B^2 s_W^4}{9}-\frac{m_B^2 s_W^2}{3}\left[\frac{2s_W^2}{3}-(s_L^b)^2\right]\right)B_0(0,m_B^2,m_B^2) \\
& +\ \frac{2s_W^2}{3}\left(\frac{8s_W^2}{3}-(s_L^t)^2\right)\left[A_0(m_t^2)-2B_{00}(0,m_t^2,m_t^2)\right] \\
& +\ \frac{s_W^2}{3}\left(\frac{4s_W^2}{3}-(c_L^b)^2\right)\left[A_0(m_b^2)-2B_{00}(0,m_b^2,m_b^2)\right] \\
& +\ \frac{s_W^2}{3}\left(\frac{4s_W^2}{3}-(s_L^b)^2\right)\left[A_0(m_B^2)-2B_{00}(0,m_B^2,m_B^2)\right] \\
& +\ \frac{(c_L^b)^2}{2}\left[A_0(m_b^2)-2B_{00}(0,m_t^2,m_b^2)\right]+\frac{m_t^2(c_L^b)^2}{2}B_0(0,m_t^2,m_b^2) \\
& +\ \frac{(s_L^b)^2}{2}\left[A_0(m_B^2)-2B_{00}(0,m_t^2,m_b^2)\right]+\frac{m_t^2(s_L^b)^2}{2}B_0(0,m_t^2,m_B^2)\Bigg]. \qquad (6.57)
\end{aligned}
$$

$$\Delta\mathbb{S}_{\mathcal{D}_1} = \frac{N_c}{12\pi M_Z^2}\Bigg[\frac{2}{3}\ln\left(\frac{m_t^2}{m_b^2}\right) - 2 + (s_L^b)^2(c_L^b)^2\Big(6B_{00}(m_Z^2, m_b^2, m_B^2) - 6B_{00}(0, m_b^2, m_B^2)$$

$$+ \quad 3m_Z^2 B_1(M_Z^2, m_b^2, m_B^2)\Big) + m_b^2(s_L^b)^2(c_L^b)^2(B_0(M_Z^2, m_b^2, m_B^2) - B_0(0, m_b^2, m_B^2))$$

$$- \quad \frac{1}{c_W^2 s_W^2}\Bigg(\frac{16}{3}\big[A_0(m_t^2) - 2B_{00}(M_Z^2, m_t^2, m_t^2) + M_Z^2 B_1(M_Z^2, m_t^2, m_t^2)\big]$$

$$+ \quad \frac{4}{3}\big[A_0(m_b^2) - 2B_{00}(M_Z^2, m_b^2, m_b^2) + M_Z^2 B_1(M_Z^2, m_b^2, m_b^2)\big]$$

$$+ \quad \frac{4}{3}\big[A_0(m_B^2) - 2B_{00}(M_Z^2, m_B^2, m_B^2) + M_Z^2 B_1(M_Z^2, m_B^2, m_B^2)\big]\Bigg)$$

$$+ \quad \left(\frac{3}{2}\left(1 - \frac{4s_W^2}{3}\right)^2 + \frac{8s_W^4}{3}\right)\big[M_Z^2 B_1(M_Z^2, m_t^2, m_t^2) + 2B_{00}(0, m_t^2, m_t^2)$$

$$- \quad 2B_{00}(M_Z^2, m_t^2, m_t^2)\big] + \left(\frac{3m_t^2}{2}\left(1 - \frac{4s_W^2}{3}\right)^2 + \frac{8m_t^2 s_W^4}{3}\right.$$

$$+ \quad 4m_t^2 s_W^2\left(1 - \frac{4s_W^2}{3}\right)\bigg)\big[B_0(M_Z^2, m_t^2, m_t^2) - B_0(0, m_t^2, m_t^2)\big]$$

$$+ \quad \left(\frac{3}{2}\left(\frac{2s_W^2}{3} - (c_L^b)^2\right)^2 + \frac{2s_W^4}{3}\right)\big[M_Z^2 B_1(M_Z^2, m_b^2, m_b^2) + 2B_{00}(0, m_b^2, m_b^2)$$

$$- \quad 2B_{00}(M_Z^2, m_b^2, m_b^2)\big] + \left(\frac{3m_b^2}{2}\left(\frac{2s_W^2}{3} - (c_L^b)^2\right)^2 + \frac{2m_b^2 s_W^4}{3}\right.$$

$$- \quad 2m_b^2 s_W^2\left(\frac{2s_W^2}{3} - (c_L^b)^2\right)\bigg)\big[B_0(M_Z^2, m_b^2, m_b^2) - B_0(0, m_b^2, m_b^2)\big]$$

$$+ \quad \left(\frac{3}{2}\left(\frac{2s_W^2}{3} - (s_L^b)^2\right)^2 + \frac{2s_W^4}{3}\right)\big[M_Z^2 B_1(M_Z^2, m_B^2, m_B^2) + 2B_{00}(0, m_B^2, m_B^2)$$

$$- \quad 2B_{00}(M_Z^2, m_B^2, m_B^2)\big] + \left(\frac{3m_B^2}{2}\left(\frac{2s_W^2}{3} - (s_L^b)^2\right)^2 + \frac{2m_B^2 s_W^4}{3}\right.$$

$$- \quad 2m_B^2 s_W^2\left(\frac{2s_W^2}{3} - (s_L^b)^2\right)\bigg)\big[B_0(M_Z^2, m_B^2, m_B^2) - B_0(0, m_B^2, m_B^2)\big]$$

$$+ \quad (c_W^2 - s_W^2)\bigg[\left(\frac{16s_W^2}{3} - 2\right)\big[M_Z^2 B_1(M_Z^2, m_t^2, m_t^2) - 2B_{00}(M_Z^2, m_t^2, m_t^2)$$

$$- \quad 2B_{00}(0, m_t^2, m_t^2)\big] + \left(\frac{4s_W^2}{3} - (c_L^b)^2\right)\big[M_Z^2 B_1(M_Z^2, m_b^2, m_b^2) - 2B_{00}(M_Z^2, m_b^2, m_b^2)$$

$$- \quad 2B_{00}(0, m_b^2, m_b^2)\big] + \left(\frac{4s_W^2}{3} - (s_L^b)^2\right)\big[M_Z^2 B_1(M_Z^2, m_B^2, m_B^2) - 2B_{00}(M_Z^2, m_B^2, m_B^2)$$

$$- \quad 2B_{00}(0, m_B^2, m_B^2)\big]\bigg]\Bigg]. \tag{6.58}$$

Contributions to $\mathbb{S}$ and $\mathbb{T}$ parameters from doublet and triplet VLQ representations follow from Eq. 6.52-6.53 by a straightforward calculation with the relevant electroweak couplings as in the Appendix E. In Fig. 6.7-6.8, we plot the parameter space restricting the

(a) $\mathcal{U}_1$ (T)

(b) $\mathcal{D}_1$ (B)

(c) $\mathcal{D}_X$ (XT)

(d) $\mathcal{D}_2$ (TB)

(e) $\mathcal{D}_Y$ (BY)
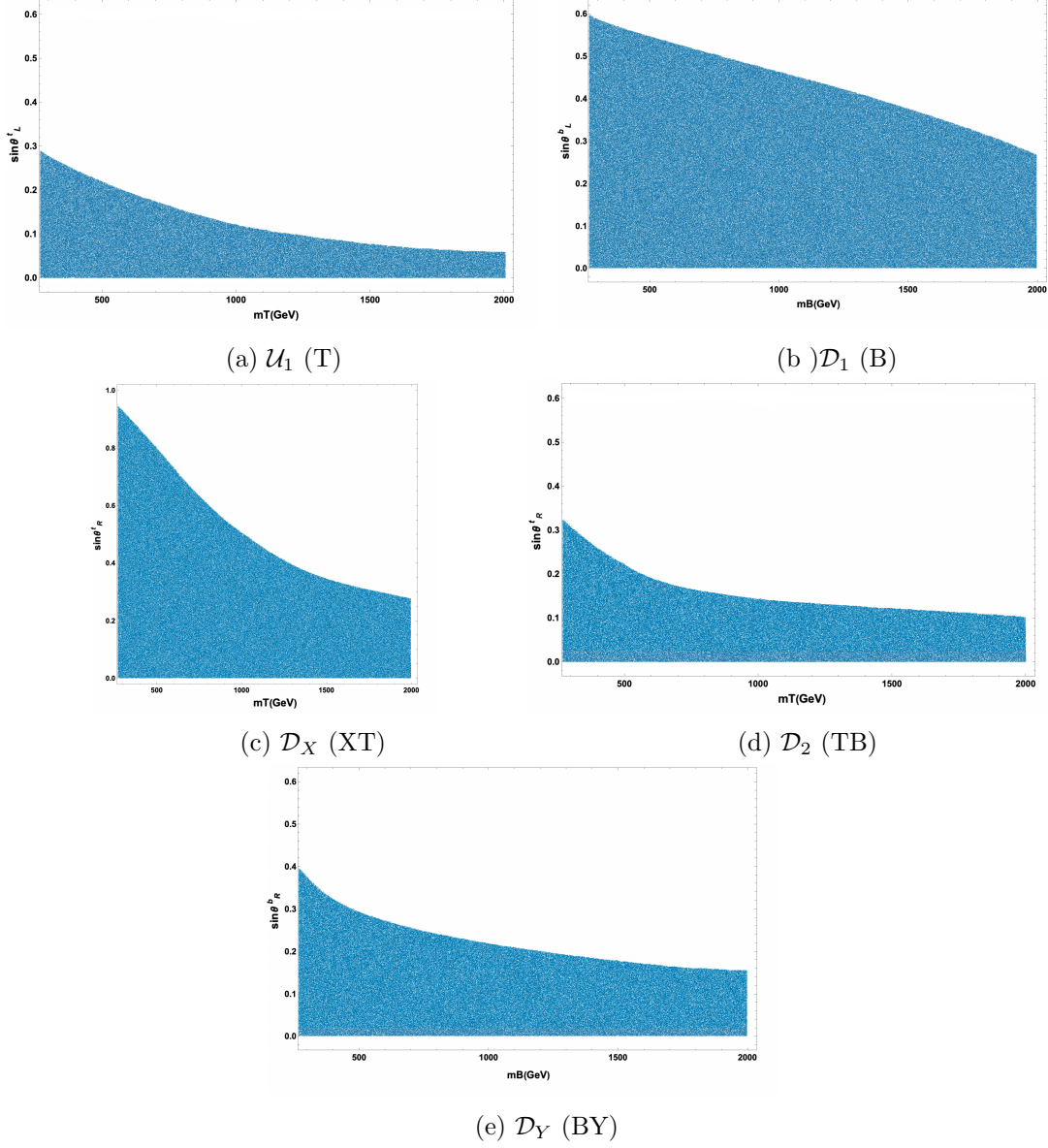
Figure 6.7: The allowed parameter space from EWPO: fermion masses versus mixing angle with the SM quark for singlet $\mathcal{U}_1$ model (top left panel), $\mathcal{D}_1$ model (top right panel), doublet $\mathcal{D}_X$ (middle left panel), doublet $\mathcal{D}_2$ (middle right panel), and doublet $\mathcal{D}_Y$ model (bottom panel). Loop functions are calculated at energy scale $\mu = m_t$.

mixing between $t - T$ and $b - B$ versus the corresponding VLQ masses satisfying EWPO, in accordance with the expressions given before. The largest deviations arise from the $\mathbb{T}$ parameter due to large logarithm of $(m_T/m_t)^2$, yielding a wide range for the mass-mixing spectrum compared to the $\mathbb{S}$ parameter for all multiplets. In analogy with the case of $\sin \alpha = 0$ behaviour in the scalar sector, decoupling between the VLQs and the SM quarks

(a) $\mathcal{T}_X$ (XTB)

(b) $\mathcal{T}_Y$ (TBY)
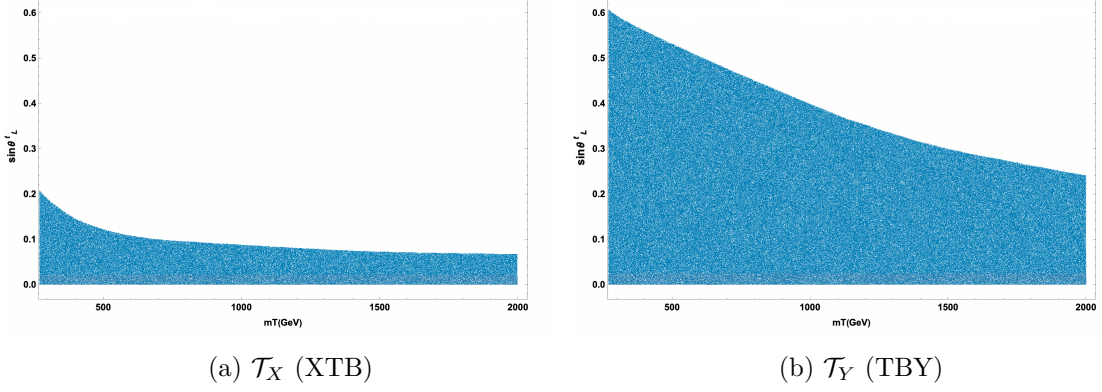
Figure 6.8: The allowed parameter space from EWPO: fermion masses versus mixing angle with the SM quark for triplet $\mathcal{T}_X$ model (left panel), $\mathcal{T}_Y$ model (right panel). Loop functions are calculated at energy scale $\mu = m_t$.

becomes much prominent as $m_{VLQ} \rightarrow \mathcal{O}(\text{TeV})$ scale. The behaviour of the decoupling zone due to larger values of m_{VLQ} can be seen from Eq. 6.55, $\frac{\Delta}{m_{VLQ}} \sim s_L^{t^2}$. This consequence can always be viewed as a rule-of-thumb to explain why EWPO constraints are already satisfied in decoupling limit. However, regardless of m_{VLQ}, there are no model parameter contributions to $\mathbb{S}$ and $\mathbb{T}$ parameters in zero mixing ($\sin \alpha = 0$) domain.

The mixing angle in the singlet $\mathcal{D}_1$ model, Fig. 6.7 (b), is much more relaxed compared to that in the $\mathcal{U}_1$ model due to the fact that up and down type mixings are exclusively dependent on mass splitting between VLQ and the SM quark as seen from Eq. 6.36. In fact, this holds true for all models if the parameter space allows for $b-B$ mixing. The allowed space for $t-T$ mixing in $\mathcal{U}_1$ model matches input values we used to assure the stability in Type-I and Type-II models, whereas scenario $\mathcal{D}_1$ lifts the upper bound of $b-B$ mixing to a scale which cannot stabilize the electroweak vacuum around $m_B \geq 1$ TeV. Hence, the stability requirements is much severe than the oblique parameters requirements for singlets. The values of $\Delta \mathbb{T}_{VLQ}$ in $\mathcal{U}_1$ are always positive and accordingly have more potential to compensate the negative effect of $\Delta \mathbb{T}_{2HDM}$, whereas $\mathcal{D}_1$ features negative corrections to $\Delta \mathbb{T}_{VLQ}$. Thus, in terms of the oblique corrections between both sectors, $\mathcal{U}_1$ is capable of imposing more bounds on M_A, $M_{H^\pm}$ and $\cos(\beta - \alpha)$.

For doublets, the parameter space is larger and similar to $\mathcal{D}_1$ except for $\mathcal{D}_2$ where $\Delta \mathbb{S}$ contributes negative values. We should emphasize that, for cases where $\mathbb{S}_{VLQ}$ contributes negatively to cancel the positive effect of the $\mathbb{T}$ parameter, the allowed parameter spaces are effectively enlarged as seen in Fig. 6.7(c),(e) for $\mathcal{D}_X$ and $\mathcal{D}_Y$ models. In contrast, $\Delta \mathbb{S}$ is positive in $\mathcal{D}_2$ for $m_T \geq 645$ GeV. We also observe the behaviour from Eq. 6.53, where the $\mathcal{D}_2$ model does not contribute to (FCNC case) ZtT and ZbB channels, hence $\mathbb{S}$ is relatively larger than those in other doublets. Among all doublet models only $\mathcal{D}_X$ has a negative $\Delta \mathbb{T}_{VLQ}$ contribution. On the other hand, $\Delta \mathbb{T}_{VLQ}$ stays close to zero in $\mathcal{D}_Y$ model, making it more limited for rendering $\Delta \mathbb{T}_{2HDM}$ negative, compared to the $\mathcal{D}_2$ model, where the correction $\Delta \mathbb{T}_{VLQ} \geq 0.08$ yields $m_T > 1$ TeV.

Furthermore, at the TeV scale, the EWPO parameter space of the $\mathcal{D}_2$ model is in good

agreement with the vacuum stability requirements for $t-T$ mixing, while constraints in $\mathcal{D}_X$ and $b-B$ mixing in $\mathcal{D}_Y$ allow angles beyond the maximum allowed in the stability analysis.

The parameter space of the triplet $\mathcal{T}_X$ model in Fig. 6.8 is quite restricted, and $t-T$ and $b-B$ mixing allowed by the oblique parameters do no cross beyond the vacuum stability requirements. However, for the model $\mathcal{T}_Y$, constraints are more relaxed, though $\sin\theta_L^t > 0.2$ only exacerbate the constraints on vacuum stability. The relaxation of the mixing in the $\mathcal{T}_Y$ scenario compared to that in $\mathcal{T}_X$, can be described in terms of mixing relations Eq. 5.40. Since up and down type mixing angles are not independent for triplets, $s_L^t \simeq \frac{s_L^b}{\sqrt{2}}$[1], which enhances the Zbb coupling over the one in $\mathcal{T}_Y$, and thus leads to more severe corrections in $\mathbb{S}$ [227]. $\Delta\mathbb{T}_{VLQ}$ is always positive in $\mathcal{T}_Y$, while $\mathcal{T}_X$ has positive corrections to the $\mathbb{T}$ parameter for $m_T > 400$ GeV. As a consequence, the $\mathcal{T}_Y$ model is more relaxed as it compensates the negative corrections in 2HDM and it expands the parameter space through combined analysis of the oblique parameters.

6.7 Conclusions

We analyzed the stability of the electroweak vacuum resulting from the interplay between vector-like quarks and the extended bosonic sector of the Two Higgs Doublet Model by adopting various representations to scrutinize the potential effects of vector-like quarks on the Higgs sector. In particular, our work zooms in the effects of renormalization group flow that governs the energy scale and flavour dependent behaviour of interactions in the theory. Our investigation remains agnostic to specific parameter choices, while restricting the mixing of vector-like quarks to solely with the third generation SM quarks. The core of the analysis revolves around the delicate balance of the Higgs potential stability. It has been long assumed that the SM lies in a metastable state or there is an alternative mechanics behind the absolute stability of the vacuum. In fact, there is an effective approach to extend the Higgs sector of the SM with additional scalar bosons, as allowed by certain symmetries of the model. To this end, an auxiliary scalar doublet is introduced here to ameliorate the SM vacuum predicament. Using RGEs in 2HDM, we showed the additional degree of freedom in scalar sector enlarges the parameter space that might preserve the absolute stability of vacuum up to the Planck scale.

We then added all anomaly-free representations of vector-like quarks (two singlet, three doublet and two triplet representations). We showed that the inclusion of vector-like quarks, although analogous in their couplings to SM quarks, has complicated consequences. Although fermions contribute negatively to the couplings at RGE level, vector-like quarks effectively modify beta functions through the gauge and Yukawa portals. Even though the gauge portal effects are weaker than those of the Yukawa couplings, the corrections are multiplicative with respect to number of fermions in the family included. A natural and straightforward attempt could be add more vector-like quarks, considering their effect on gauge couplings modifications. However, there is a relationship between the number of vector-like quarks and their masses that imposes an upper bound on each, for which the vacuum can be stabilized. If m_{VLQ} is too large and n_F is too small, then RG evolutions fall into the negative perturbativity region before lifting it up. On the other hand, if n_F is too large and m_{VLQ} too small, RG evolutions are too strong and abruptly diverge, thus predictability is lost due to a Landau pole around $\mu < M_{Pl}$. Considering

---

[1]This relation is valid for the triplet model $\mathcal{T}_X$.

the strong gauge portal alone, this imposes the upper bounds: $m_{VLQ} \leq 10^6$ TeV and $n_F = [2, 18]$. Additionally, the hypercharge portal vanishes either by increasing m_{VLQ}, thus leaving insufficient RG evolution for the parameter space restrictions to be operative, or by increasing n_F causing a sub-Planckian theory breakdown. Increasing the hypercharge limits n_F to small values and to a narrower interval. Thus, allowed hypercharge values are obtained for smallest number of flavours n_F, and there is a fine-tuned mutual relation between mass, flavour and hypercharge of vector-like quarks that is capable to generate absolute stability of the vacuum.

We imposed perturbative unitarity and stability constraints for $\lambda_i(\mu)$ and $y_i(\mu)$ in both Type-I+VLQ and Type-II+VLQ up to the Planck scale. All VLQ representations require $\tan \beta \in [6, 12]$ for the mass regime assumed from both sectors, with small fermionic mixing $\sin \theta_L < 0.2$. Although larger $\tan \beta$ values might satisfy the stability requirements, we observed that they lead to a heavy suppression of the quartic couplings in small perturbation regions due to coupled nature. Initial conditions on $\lambda_{1,2}$ in Type-II+VLQ are stronger due to the split of the Yukawa terms coupling to different scalar doublets. Generally, Type-II +VLQs models require larger scalar masses compared to Type-I model counterparts. Accordingly, for a given set of fixed parameters in both types, the vacuum stability conditions are safer in VLQ+Type-II. Compared to T vector-like quarks, constraints on the B-like fermion masses and mixing angles are much more relaxed. This is simply a consequence of the fact that the mixing between vector-like quarks and the SM quarks is described in terms of the inverse of mass splitting between two quarks. Due to excessive number of negative quartic Yukawa terms appearing at the RGE level, the constraints arising in bare 2HDM have to be enlarged from the considerations above. To this end, we checked both theoretically and experimentally allowed regions of 2HDM and VLQ models by preserving the validity of 2HDM up to the Planck scale.

We also scanned over EWPO and found the space for $t - T$ and $b - B$ mixings versus the mass of vector-like quarks which includes stability regions, especially in the near decoupling limit. Furthermore, since the scalar and fermion parts of the oblique parameters are calculated separately and then combined, we found that the upper bound on the heavier CP-even scalar extends while preserving the vacuum stability conditions, especially when combined with triplet VLQs. For this reason, we assumed mass values of the heavier neutral scalar beyond the limits of 2HDM oblique parameters. However, the extension of the upper limit of M_H as $\cos(\beta - \alpha)$ approaches the alignment limit, also confirms the stability requirement on scalar masses near TeV scale.

Although mixing between CP-even states $\cos(\beta - \alpha) \neq 0$ is allowed by the oblique parameters, the stability requires at least near-alignment limit as $\cos(\beta - \alpha)$ remains close to zero. In fact, we observed that RGE running of λ_1 and λ_2 deteriorate and the condition for the potential to be bounded from below cannot be satisfied as $\cos(\beta - \alpha)$ strays away from the alignment limit. Accordingly, the lower limit on CP-even mixing angle from the stability and EWPO requirements also match the experimental Higgs bounds.

For the VLQ part of the oblique parameters, the allowed parameter space for $t - T$ and $b - B$ mixing is largest for cases where $\Delta \mathbb{S}$ contributes negatively and we have shown that, for all vector-like multiplets, the EWPO constraints lead to the alignment limit occurring naturally as $m_{VLQ} > 1$ TeV. In turn, constraints at higher TeV range from the oblique parameters become more consistent with the stability requirements. Thus the constraints to oblique parameters from vector-like quarks, combined with $\Delta \mathbb{S}$ and $\Delta \mathbb{S}$ from the 2HDM

are VLQ representation-dependent as well as differing for Type-I and Type-II 2HDM and can be used to distinguish among different scenarios. In a specific representation and model-type, these corrections may indicate an allowed deviation from the required cancellations, and this would impose further restrictions on the extra scalar and its mixing with the SM Higgs boson.

Chapter 7

Vector-like Leptons in the SM

7.1 Introduction

While the discovery of the Higgs boson with mass 125.66 ± 0.30 GeV and analysis of its properties [122, 228] completes the search for the particle content of the Standard Model (SM), confirming Higgs mechanism to be responsible for electroweak symmetry breaking, it also raises questions about naturalness. In particular, there are hints that the SM is incomplete, or perhaps just an effective theory at large scales, where the model becomes unstable. The metastability of the SM vacuum is driven by the behavior of the couplings in the model at high energy scales. In general, the SM couplings run slowly but at $\mu \sim 10^{10}$ GeV the Higgs quartic coupling λ flips sign, as evidenced by a downward spike, which indicates the onset of vacuum instability. Extending the validity of the SM to M_{Planck}, a second, deeper minimum develops, located near the Planck scale, such that the electroweak vacuum is metastable, i.e., implying that the theoretical transition lifetime of the electroweak vacuum to the deeper minimum is finite with lifetime $\sim 10^{300}$ years [62, 70, 229–233]. The issue is that the Higgs quartic coupling is renormalized not only by itself (λ increasing as the energy scale increases), but also by the Higgs (Yukawa) coupling to the top quark [234], which tends to drive it to smaller, even negative values at high scales μ.

Vacuum stability can be achieved through beyond the Standard Model (BSM) effects, as long as these enhance the Higgs quartic coupling sufficiently strongly. This is achieved by introducing new particles, which can couple to the gauge or Higgs fields. While coupling to gauge fields modify the SM beta functions and generally result in small changes, couplings to the Higgs can affect the running of the SM couplings more significantly.

Perhaps the simplest remedy to the stability problem is to augment the SM by an extra (singlet, as it is simplest) scalar boson which interacts solely with the SM Higgs boson [235–239]. The addition of a boson provides a positive boost to the coupling parameter, counteracting the effect of the top quark and contributing towards repairing the Higgs vacuum stability. In this scenario, the scalar couplings increase with energy scale, compensating for the SM Higgs coupling. Therefore, the addition of an extra scalar boson to the SM rescues the theory from vacuum instability, as long as its mixing with the SM Higgs boson is non-zero [1]. It has been shown that such a singlet scalar, if light, can also serve as dark matter (DM) candidate, obeying all constraints from relic abundance and direct detection [240]. The study of the scalar singlet DM has been extended, with additional portal couplings of the scalar added on top of the usual Higgs portal interaction.

Such possibility is to include DM portal couplings with new vector like leptons [241–247] and/or quarks [248–252].

Vector-like leptons (VLLs) are color-singlet fermions and vector-like quarks (VLQs) are color-triplet fermions, i.e., fermions with left- and right-handed components transforming the same way under the electroweak gauge symmetry group. Such new states arise in a wide variety of BSM scenarios, including, but not limited to, supersymmetric models [83,253–257] models with extra spatial dimensions [258,259] and grand unified theories. Expansions of the SM with one or more vector-like fermion families may provide a dark matter candidate [260–266], and account for the mass hierarchy between the different generations of particles in the SM via their mixings with the SM fermions [267–271].

Vector-like particles have been considered before in the context of stabilizing the vacuum of the SM in [85, 86], in the context of baryogenesis [87], to account for the anomalous magnetic moment of the muon and discrepancies in the W boson mass [88, 227, 272], and to help explain the observed excess at 750 GeV [89, 90]. Analyses of vacuum stability have served as guides for beyond the SM model building [55, 218, 273].

In a previous work [2] we analyzed the stability of the SM with additional vector-like quarks. We included all the possible non-anomalous representations, and analyzed a complete interplay of all possible vector-like quark representations. We investigated the restrictions on the masses and mixing angles for the all anomaly-free representations of vector-like quarks, as well as the additional boson field which is needed to be added for vacuum stabilization, including effects and restrictions induced by the vector-like fermions on the electroweak precision observables (EWPOs), $\mathbb{S}$ and $\mathbb{T}$. Previous works have also performed complementary analyses [274], some combining vacuum stability constraints with the possibility of allowing the new scalar to be the dark matter candidate [240, 275].

Here we complement our previous work here by performing an analysis of the stability of the SM with vector-like leptons. The study of the vacuum stability is different here as vector-like leptons do not have QCD couplings. Additionally, unlike the vector-like quarks, the leptons can still be light, the limit from LEP allowing vector-like charged fermions with masses above 100 GeV [96, 276, 277]. There have been previous studies of the vacuum stability of the SM in the presence of vector-like fermions [78, 240, 278]. Our analysis differs from previous ones in that we once again examine the effects of *all* possible non-anomalous vector-like lepton representations. Moreover, we shall show that stability of the SM with vector-like leptons does not require the additional scalar boson mixed with the Higgs bosons, and this result is consistent with parameter space restrictions on the electroweak precision observables, $\mathbb{S}, \mathbb{T}$ and $\mathbb{U}$.

Our work is organized as follows. In Sec. 7.2, we introduce six different vector-like lepton representations and describe their connections to the SM leptons through relevant Lagrangian. In Sec. 7.4 we present the vector-like lepton contributions to the electroweak precision observables and discuss the regions of parameter space that are consistent with the spectrum that ensures stability. Sec. 7.5 is dedicated to the examination of the running of the SM couplings and renormalization group equation (RGE) solutions in the presence of vector-like leptons along with allowed parameter space that satisfy the vacuum stability constraints.Further, we add two loop corrections to RGEs to check how the next-to-next-to-leading order accuracy affects the model couplings up to the Planck scale. Furthermore, we draw our conclusions in Sec. 7.6 and leave the complete set of RGEs up to two-loops and VLL modified EW couplings to the Appendix C and the Appendix E.2 respectively.

7.2 Setup for Vector-like Lepton Model

Here we explore an extension of the SM, incorporation only vector-like leptons. The selection of leptonic mixing via Yukawa interactions with the Higgs field constrains us to a finite set of anomaly-free and renormalizable $SU(2)$ gauge representations and hypercharge assignments for the new fermionic states. We give the list of the VLL representations under $SU(2)_L \times U(1)_Y$ symmetry in Table 7.1.

Table 7.1: Representations of Vector-Like Leptons, under gauge symmetry $SU(2)_L \times U(1)_Y$.

Name	$\mathcal{S}_1$	$\mathcal{S}_2$	$\mathcal{D}_1$	$\mathcal{D}_2$	$\mathcal{T}_1$	$\mathcal{T}_2$
Type	Singlet	Singlet	Doublet	Doublet	Triplet	Triplet
	L^0	L^-	$\begin{pmatrix} L^0 \\ L^- \end{pmatrix}$	$\begin{pmatrix} L^- \\ L^{--} \end{pmatrix}$	$\begin{pmatrix} L^+ \\ L^0 \\ L^- \end{pmatrix}$	$\begin{pmatrix} L^0 \\ L^- \\ L^{--} \end{pmatrix}$
SU(2)$_L$	1	1	2	2	3	3
Y	0	-1	-1/2	-3/2	0	-1

The renormalizable Lagrangian for these model, including the Yukawa interactions and Dirac mass terms of the weak multiplets contains the SM part, and additional interactions corresponding to the different interactions in Table 7.1:

$$
\begin{aligned}
\mathcal{L}_{SM} &= -y_\nu \bar{l}_L \Phi^c \nu_R - y_\tau \bar{l}_L \Phi \tau_R, \\
\mathcal{L}_{\mathcal{S}_1,\mathcal{S}_2} &= -y_{L^0} \bar{l}_L \Phi^c S_{1_R} - y_{L^-} \bar{l}_L \Phi S_{2_R} - y_M(\bar{S}_{1_L} \Phi S_{1_R} + \bar{S}_{2_L} \Phi S_{2_R}) \\
&\quad - M_{L^0} \bar{S}_{1_L} S_{1_R} - M_{L^-} \bar{S}_{2_L} S_{2_R}, \\
\mathcal{L}_{\mathcal{D}_1,\mathcal{D}_2} &= -y_{L^-} \bar{D}_{1_L} \Phi \tau_R - y_{L^0} \bar{D}_{1_L} \Phi^c \nu_R - y_{L^-} \bar{D}_{2_L} \Phi^c \tau_R - y_M(\bar{D}_{1_L} \Phi D_{1_R} + y_{L^-} \bar{D}_{2_L} \Phi^c D_{2_R}) \\
&\quad - M_{D_1} \bar{D}_{1_L} D_{1_R} - M_{D_2} \bar{D}_{2_L} D_{2_R}, \\
\mathcal{L}_{\mathcal{T}_1,\mathcal{T}_2} &= -y_{\mathcal{T}_1} \bar{l}_L \tau^a \Phi^c \mathcal{T}_{1_R}^a - y_{\mathcal{T}_2} \bar{l}_L \tau^a \Phi \mathcal{T}_{2_R}^a - y_M(\bar{\mathcal{T}}_{1_L} \tau^a \Phi^c \mathcal{T}_{1_R}^a + y_{L^-} \bar{\mathcal{T}}_{2_L} \tau^a \Phi \mathcal{T}_{2_R}^a) \\
&\quad - M_{L^+} \bar{\mathcal{T}}_{1_L} \mathcal{T}_{1_R} - M_{L^{--}} \bar{\mathcal{T}}_{2_L} \mathcal{T}_{2_R},
\end{aligned}
\tag{7.1}
$$

where the triplet models can equivalently be written as irreducible $SU(2)$ representations

$$
\tau^a \mathcal{T}_{1_R}^a = \begin{pmatrix} \frac{L^0}{\sqrt{2}} & L^+ \\ L^- & -\frac{L^0}{\sqrt{2}} \end{pmatrix}_R, \qquad
\tau^a \mathcal{T}_{2_R} = \begin{pmatrix} \frac{L^-}{\sqrt{2}} & L^0 \\ L^{--} & -\frac{L^-}{\sqrt{2}} \end{pmatrix}_R.
\tag{7.2}
$$

Here, $\Phi^c = i\sigma^2 \Phi^\star$, y_τ, y_ν, y_{L^0}, y_{L^-} and $y_{\mathcal{T}_{1,2}}$ are the Yukawa couplings of the Higgs field Φ to vector-like leptons and SM leptons[1], while y_M is the Yukawa coupling of the Higgs scalar field to vector-like leptons only.

---

[1]Although the SM does not inherently include a right-handed neutrino (ν_R), our analysis considers such state as added to the SM. This right-handed neutrino is required to preserve mixing between the VLL and the SM leptons through the Yukawa interactions present in our study. Although this state is included only in the SM and $\mathcal{D}_1$ part of Lagrangian in Eq. 7.1, its contribution appears in mass matrices throughout all six representations whenever the neutral sector is considered.

We assume that only the third generation SM leptons mix with VLLs in order to avoid unwanted complications from flavour-changing neutral current (FCNC) and lepton flavour violating (LFV) decays. If the VLLs mix with leptons of all generations, such mixing induces flavor transitions between the SM generations, which would lead to dangerous LFV processes. These are tightly constrained by experimental data, especially from processes like $\mu \to e\gamma$ decay [279] and $\mu \to e$ conversion [280], which are highly sensitive to new flavor-changing interactions. By restricting the VLL mixing to only the third-generation leptons, the model avoids these stringent flavor constraints, as the third-generation leptons are less sensitive to flavor-changing processes [281]. This is additionally motivated by the analysis of EWPOs and of renormalization group equations. Large mass splitting between the members of weak eigenstates in Eq. 7.3 can lead to adverse effects on initial conditions for the Yukawa couplings in the low mass regime of the first and the second generation SM leptons. Similarly, the EWPOs are sensitively dependent on logarithmic mass splitting between the SM and the vector-like leptons [282] as $\Delta\mathbb{T} \sim \frac{M_W^2}{\alpha_e} \ln(\frac{m_l^2}{M_{\mathrm{VLL}}^2})$, inducing large discrepancies to the global fit of the oblique $\mathbb{T}$-parameter [96] if the SM leptons of the first two generations couple to VLL.

The weak eigenstate lepton fields mix, for both chiralities in the neutral and charged sectors, and are respectively given as

$$\mathcal{N}_{L,R} = \begin{pmatrix} \nu \\ L^0 \end{pmatrix}_{L,R}, \qquad \mathcal{L}_{L,R} = \begin{pmatrix} \tau \\ L^- \end{pmatrix}_{L,R}. \tag{7.3}$$

The mass eigenstate fields are denoted as (n_1, n_2) and (l_1, l_2) and they correspond to bi-unitary transformation of weak eigenstates,

$$
\begin{aligned}
\mathbf{N}_{L,R} &= \begin{pmatrix} n_1 \\ n_2 \end{pmatrix}_{L,R} = V_{L,R}^0 \begin{pmatrix} \nu \\ L^0 \end{pmatrix}_{L,R} \\
\mathbf{L}_{L,R} &= \begin{pmatrix} l_1 \\ l_2 \end{pmatrix}_{L,R} = V_{L,R}^l \begin{pmatrix} \tau \\ L^- \end{pmatrix}_{L,R},
\end{aligned}
\tag{7.4}
$$

where the mixing matrices in neutral (0) and charged sector (l) follow as

$$V_{L,R}^0 = \begin{pmatrix} \cos\theta^u & -\sin\theta^u \\ \sin\theta^u & \cos\theta^u \end{pmatrix}_{L,R}, \qquad V_{L,R}^l = \begin{pmatrix} \cos\theta^d & -\sin\theta^d \\ \sin\theta^d & \cos\theta^d \end{pmatrix}_{L,R}. \tag{7.5}$$

By using these rotation operators we construct the diagonal mass matrices

$$M_{diag}^u = V_L^0 M^u (V_R^0)^\dagger = \begin{pmatrix} m_{n_1} & 0 \\ 0 & m_{n_2} \end{pmatrix} \quad , \quad M_{diag}^d = V_L^l M^d (V_R^l)^\dagger = \begin{pmatrix} m_{l_1} & 0 \\ 0 & m_{l_2} \end{pmatrix}. \tag{7.6}$$

Utilizing the gauge eigenstate fields, the mass matrices for both the neutral and charged sectors are obtained following spontaneous symmetry breaking

$$
\begin{aligned}
-\mathcal{L}_{Yuk}^u &= \begin{pmatrix} \nu_L & L_L^0 \end{pmatrix} \begin{pmatrix} y_\nu \frac{v}{\sqrt{2}} & y_{L^0} \frac{v}{\sqrt{2}} \\ y_{L^0} \frac{v}{\sqrt{2}} & y_M \frac{v}{\sqrt{2}} + M_{L^0} \end{pmatrix} \begin{pmatrix} \nu_R \\ L_R^0 \end{pmatrix}, \\
-\mathcal{L}_{Yuk}^d &= \begin{pmatrix} \tau_L & L_L^- \end{pmatrix} \begin{pmatrix} y_\tau \frac{v}{\sqrt{2}} & y_{L^-} \frac{v}{\sqrt{2}} \\ y_{L^-} \frac{v}{\sqrt{2}} & y_M \frac{v}{\sqrt{2}} + M_{L^-} \end{pmatrix} \begin{pmatrix} \tau_R \\ L_R^- \end{pmatrix}.
\end{aligned}
\tag{7.7}
$$

The Dirac mass term introduces another free parameter into VLL models and it appears as an uncoupled degree of parametric freedom in RGE level, so to this end, we absorb $M_{L^0,-}$ in Eq. 7.7 into y_M for all VLL representations. This is equivalent to assuming that the mass of the vector-like fermion are purely generated from the spontanous symmetry breaking, such that $m_{\text{Dirac}} = 0$.

7.3 Restrictions on Vector-like Lepton Masses

The CMS Collaboration has carried out three direct searches targeting extensions of the SM with VLLs in pp collisions at $\sqrt{s} = 13$ TeV collision data set. In the first of these searches, multilepton final states with electrons and muons were probed using a data set collected during 2016-2017, yielding the first direct constraints on doublet models with vector-like tau leptons in the mass range of 120–790 GeV [283]. A second search, targeting both doublet and singlet vector-like tau lepton models and conducted with the larger full Run-2 data set, included additional multilepton final states, including hadronically decaying tau leptons, and superseded the first result [284]. Lastly, a third search performed by the CMS Collaboration probed non-minimal SM extensions involving VLLs and other BSM states in the context of the 4321 model in all-hadronic final states involving multiple jets and hadronically decaying tau leptons [285]. Searches for vector-like leptons have also been performed at ATLAS, most recently for third-generation leptons in [286]. A description of the expectation at all colliders is summarized in [287], while for an up-to-date review of searches for vector-like fermions at LHC see [288].

In what follows, in order to allow exploration of the largest parameter space and to remove any model-dependency, we will impose the weakest constraints, as restricted by Particle Data, requiring masses above 100 GeV [96, 276, 277].

7.4 Corrections from the Oblique Parameters

In addition to the constraints defined in the previous subsections, electroweak precision observables (EWPOs) are essential tools for probing the SM and constraining possible extensions. These observables arise from precise measurements of electroweak processes, such as the properties of the W and Z bosons, and provide stringent tests for any new physics scenarios. The addition of new particles, particularly scalars and leptons, impacts these observables through loop corrections to gauge boson masses, leading to potential signals of new physics. A significant aspect of these constraints is encapsulated in the oblique parameters, also known as the Peskin-Takeuchi parameters, namely $\mathbb{S}$, $\mathbb{T}$, and $\mathbb{U}$ [97]. The latest fits for the oblique parameters give $\mathbb{S} = -0.04 \pm 0.10$ and $\mathbb{T} = 0.01 \pm 0.12$ at 90% CL [96]. These parameters quantify the effects of new physics on the vacuum polarization corrections to the gauge bosons. They provide a model-independent way to parameterize deviations from the SM predictions, thus offering a systematic approach to compare different theoretical models.

Since our work does not incorporate additional fields in the scalar sector, the corrections to the oblique parameters from Z_2 symmetric fields are the same as in the SM. The largest contribution from the fermionic sector to the $\mathbb{T}$ and $\mathbb{S}$ parameters in the SM comes from

the t and b quarks

$$\mathbb{T}_f^{SM} = \frac{3m_t^2}{4\pi e^2 v^2} \qquad , \qquad \mathbb{S}_f^{SM} = \frac{1}{2\pi}\left(1 - \frac{1}{3}\ln(\frac{m_t^2}{m_b^2})\right). \tag{7.8}$$

Previous analyses reproducing the oblique corrections for some vector-like representations have appeared in [119, 289]. In what follows, we investigate the contributions to these parameters by the additional vector-like states in our scenarios.

7.4.1 VLL contributions to the $\mathbb{S}$ and $\mathbb{T}$ parameters

In scenarios with additional fermions, such as VLLs, the oblique parameters require special consideration. These fermions can alter the gauge boson self-energies, leading to unique patterns in the oblique corrections. VLLs might transform under certain symmetries, such as Z_2, and may not interact with the SM Higgs boson, allowing their contributions to the oblique parameters to be isolated and studied separately. In VLL extensions, the physical states L and N contribute to the transverse component of the vacuum polarization for the gauge bosons in the SM through Feynman loop diagrams. To estimate their contributions to $\mathbb{S}$ and $\mathbb{T}$, one needs to compute the one loop diagrams that contribute to the electroweak gauge boson vacuum polarization amplitudes, as shown in Fig. 7.1. Adopting the general
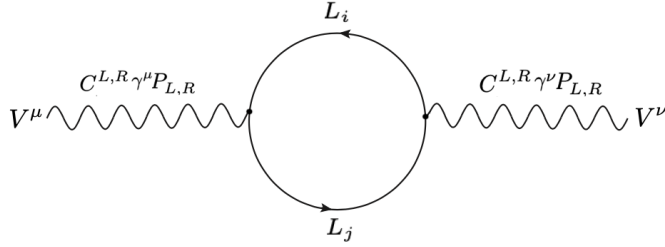
Figure 7.1: Vector-like lepton contribution to vacuum polarization amplitude of the SM gauge bosons. Here L_i and L_j are the mass eigenstates.

expression for the $\mathbb{T}$ and $\mathbb{S}$ parameter contributions from additional fermions [290]

$$\begin{aligned}
\mathbb{T}_{VLL} &= \frac{1}{\alpha_e}\left[\frac{\Pi_{WW}^{VLL}(0)}{M_W^2} - \frac{\Pi_{ZZ}^{VLL}(0)}{M_Z^2}\right], \\
\mathbb{S}_{VLL} &= \frac{4s_W^2 c_W^2}{\alpha_e M_Z^2}\left[\Pi_{ZZ}^{VLL}(M_Z^2) - \Pi_{ZZ}^{VLL}(0) - \Pi_{\gamma\gamma}^{VLL}(M_Z^2) - \frac{c_W^2 - s_W^2}{c_W s_W}\Pi_{\gamma Z}^{VLL}(M_Z^2)\right],
\end{aligned} \tag{7.9}$$

we initially calculate their gauge couplings with the vector bosons. The VLL mass matrices are given in Eq. 7.4, and the components of the diagonalizing matrices in Eq. 7.5. The couplings to W-boson and Z-boson are been modified by the VLLs through their mixing

with SM leptons in the relevant Lagrangian

$$
\begin{aligned}
\mathcal{L}_W &= \frac{g}{\sqrt{2}} \bar{L}_i \gamma^\mu (C^L_{L_i L_j} P_L + C^R_{L_i L_j} P_R) L_j W^+_\mu + h.c. \,, \\
\mathcal{L}_Z &= \frac{g}{2c_W} \bar{L}_i \gamma^\mu (Y_Z N^L_{L_i L_j} P_L + Y_Z N^R_{L_i L_j} P_R) L_j Z_\mu \,,
\end{aligned} \tag{7.10}
$$

where $L_{i,j}$ are any type of leptons in our electroweak Lagrangian and $Y_Z = T^3 - \mathbb{Q}_i s^2_W$. The condition $|\mathbb{Q}_i - \mathbb{Q}_j| = 1$ holds for all forms of $W - L_i - L_j$ interactions.

We further define VLL modified electroweak couplings to Z and W bosons in terms of the weak hypercharge operator and mixing identities

$$
\Omega^{L,R}_{W L_i L_j} = \frac{g}{\sqrt{2}} C^{L,R}_{L_i L_j} \qquad , \qquad \Omega^{L,R}_{Z L_i L_j} = \frac{g}{2c_W}(T^3 - \mathbb{Q}s^2_W) N^{L,R}_{L_i L_j} \,, \tag{7.11}
$$

yields the final form of modified electroweak interactions [1]

$$
\begin{aligned}
\mathcal{L}_W &\supset \gamma^\mu (\Omega^L_{W L_i L_j} \mathbb{L} + \Omega^R_{W L_i L_j} \mathbb{R}) W^+_\mu \,, \\
\mathcal{L}_Z &\supset \gamma^\mu (\Omega^L_{Z L_i L_j} \mathbb{L} + \Omega^R_{Z L_i L_j} \mathbb{R}) Z_\mu \,.
\end{aligned} \tag{7.12}
$$

The relevant electroweak couplings $\Omega^{L,R}_{V L_i L_j}$ are unique to each VLL representation and are given in the Appendix E.2. In fact, the expressions for the oblique parameters in Eq. 6.52 - 6.54 have been derived for vector-like fermions, and therefore they also apply to VLLs with the replacements $Q_{i,j} \to L_{i,j}$ and $N_c = 1$. Nonetheless, the number of possible neutral EW currents is relatively smaller than in the VLQ scenario. Subtracting the SM values in Eq. 7.8 from Eq. 7.13-7.18, we scan the oblique parameters with respect to neutral and charged vector-like leptons.

Singlet $\mathcal{S}_1$ (L^0), $Y = 0$

$$
\begin{aligned}
\Delta \mathbb{T} &= \frac{1}{16\pi c^2_W s^2_W M^2_Z} \left(m^2_\tau (c^u_L)^2 + m^2_{L^0} (s^u_L)^2 - \frac{m^2_{L^0} (s^u_L)^2 (c^u_L)^2}{2} \right) , \\
\Delta \mathbb{S} &= \frac{1}{36\pi} \left[(s^u_L)^2 (c^u_L)^2 \left(-5 - 3\ln(\frac{m_{\tau^2}}{m^2_{L^0}}) \right) - 2(s^u_L)^2 \left(\ln(\frac{m_{\tau^2}}{m^2_{L^0}}) - 3 \right) + 6(c^u_L)^2 \right] .
\end{aligned} \tag{7.13}
$$

---

[1]For neutral leptons, operator Y_Z generates a term proportional to $(-\frac{1}{2}\bar{L}_0 \gamma^\mu L^0)Z_\mu$, where the coefficients of these neutral currents are absorbed in $\Omega^{L,R}_{Z L_i L_j}$ throughout all VLL representations.

Singlet $\mathcal{S}_2$ (L^-), $Y = -1$

$$\Delta\mathbb{T} = \frac{1}{16\pi c_W^2 s_W^2 M_Z^2}\left(m_\tau^2(c_L^d)^2 + m_{L^-}^2(s_L^d)^2 - \frac{m_{L^-}^2(s_L^d)^2(c_L^d)^2}{2}\right),$$

$$\begin{aligned}
\Delta\mathbb{S} = \ &\frac{1}{36\pi}\left[-\frac{18m_{L^-}^2(s_L^d)^2}{m_Z^2} + 6\right.\\
&+\ \frac{(c_L^d)^2(s_L^d)^2}{(m_{L^-}^2 - m_\tau^2)^3}\left[(m_{L^-}^2 - m_\tau^2)\left(22m_{L^-}^2 m_\tau^2 - 5(m_{L^-}^4 + m_\tau^4)\right)\right.\\
&+\ \left.\left. -3\left(m_{L^-}^6 + m_\tau^6 - 3m_{L^-}^2 m_\tau^2(m_{L^-}^2 + m_\tau^2)\right)\ln(\frac{m_\tau^2}{m_{L^-}^2})\right]\right].
\end{aligned} \tag{7.14}$$

In Fig. 7.2, we illustrate the dependence of the oblique parameters on the mass of VLLs for two specific mixing angles. For a near-decoupling limit, $\sin\theta = 0.05$, neither of the oblique parameters imposes a constraint on VLL masses. However, increasing the mixing value to $\sin\theta \to 0.1$, the $\mathbb{S}$ parameter starts to disfavor $m_{L^0} > 520$ GeV in the neutral singlet model $\mathcal{S}_1$, whereas the entire spectrum of m_{L^-} is allowed by the $\mathbb{S}$ parameter in the $\mathcal{S}_2$ model. This is well-motivated, as the $\mathbb{S}$ parameter is influenced by the hypercharge of the new leptons, fundamentally measuring the difference in the running of the electroweak gauge couplings. In contrast, the $\mathbb{T}$ parameter is more restrictive for both singlet VLLs at larger mixing scales. While $m_{L^0} > 540$ GeV falls outside 2σ region for the $\mathbb{T}$ parameter, the upper bound for charged VLL extends to $m_{L^-} \sim 590$ GeV. The $\mathbb{T}$ parameter is more sensitive to weak isospin breaking and to the mass splitting between components of weak isospin multiplets. Due to the large mass splitting between members of neutral mass eigenstates as compared to charged mass eigenstates of $\mathcal{S}_2$, the $\mathbb{T}$ parameter imposes more constraint on $\mathcal{S}_1$. As expected, having the least number of possible electroweak couplings, singlet VLLs recover the SM limit for $\mathbb{T} \to 0$ as $\sin\theta \to 0$ because most terms in the $\mathbb{T}$ parameter are modified by weak isospin breaking.
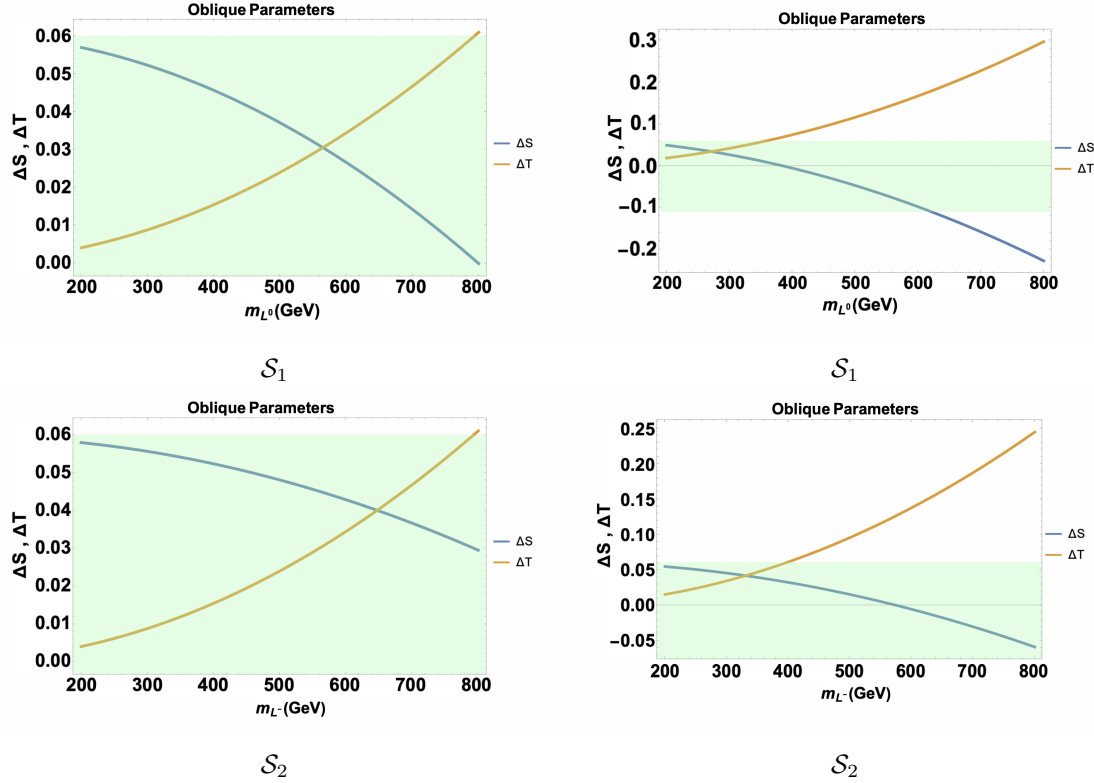
Figure 7.2: New physics contributions to the oblique parameters: $\mathbb{T}$ (orange) and $\mathbb{S}$ (blue) from singlet vector-like lepton representations for different VLL-SM lepton mixing $\sin\theta_L = 0.05$ (left) and $\sin\theta_L = 0.1$ (right). The green shaded region is the allowed space from the $\mathbb{S}$ and the $\mathbb{T}$ parameters in 2σ level.

Doublet $\mathcal{D}_1$ (L^0, L^-), $Y = -1/2$

$$\Delta\mathbb{T} = \frac{1}{8\pi c_W^2 s_W^2 M_Z^2}\left(4m_\tau^2 - \frac{2\left(m_{L^-}^2 + m_{L^0}^2\right)M_Z^2(s_L^u)^2}{3m_{L^-}m_{L^0}}\right.$$

$$+4\left(m_L^2 - m_\tau^2\right)(s_L^u)^2 + \frac{4\left(m_{L^0}^2 - m_\tau^4 + 2m_{L^0}^2 m_\tau^2 \ln\left(\frac{m_\tau^2}{m_{L^0}^2}\right)\right)}{\left(m_{L^0}^2 - m_\tau^2\right)}$$

$$+4(s_L^u)^2\left(m_{L^-}^2 - m_\tau^2 - \frac{2m_{L^-}^2 m_{L^0}^2 \ln\left(\frac{m_{L^-}^2}{m_{L^0}^2}\right)}{m_{L^-}^2 - m_{L^0}^2} - \frac{2m_{L^0}^2 m_\tau^2 \ln\left(\frac{m_\tau^2}{m_{L^0}^2}\right)}{m_{L^0}^2 - m_\tau^2}\right)$$

$$\left.-\frac{8(c_L^u)^2 m_{L^0}m_\tau\left(2\left(m_{L^0}^2 - m_\tau^2\right) + \left(m_{L^0}^2 + m_\tau^2\right)\ln\left(\frac{m_\tau^2}{m_{L^0}^2}\right)\right)}{m_{L^0}^2 - m_\tau^2}\right),$$

$$\Delta\mathbb{S} = \frac{1}{9\pi}\left(-3(c_L^u)^2\frac{m_{L^0}^2 + m_\tau^2}{m_{L^0}m_\tau} - 3(s_L^u)^2\frac{m_{L^0}^2 + m_{L^-}^2}{m_{L^0}m_{L^-}} - 4(s_L^u)^2\ln\left(\frac{m_{L^-}^2}{m_\tau^2}\right)\right.$$

$$\left.- 2\ln\left(\frac{m_\tau^2}{m_{L^0}^2}\right)\right).$$

$$(7.15)$$

Doublet $\mathcal{D}_2$ (L^-, L^{--}), $Y = -3/2$

$$
\begin{aligned}
\Delta\mathbb{T} \;=\;& \frac{1}{16\pi c_W^2 s_W^2 M_Z^2}\Bigg((c_R^d)^2 m_{\tau^2} + (s_R^d)^2 (m_{L^-}^2 + 2m_{L^{--}}^2) \\
&+ \frac{(2s_R^d)^2 \left(m_{L^-}^4 - m_{L^{--}}^4 - 2m_{L^{--}}^2 m_{L^-}^2 \ln\left(\frac{m_{L^-}^2}{m_{L^{--}}^2}\right)\right)}{(m_{L^-}^2 - m_{L^{--}}^2)} + \\
&+ \frac{4 m_{L^-} m_{L^{--}} (s_R^d)^2 \left(2m_{L^{--}}^2 - 2m_{L^-}^2 + (m_{L^-}^2 + m_{L^{--}}^2) \ln\left(\frac{m_{L^-}^2}{m_{L^{--}}^2}\right)\right)}{(m_{L^-}^2 - m_{L^{--}}^2)} + \\
&+ \frac{1}{2}(c_R^d)^2 (s_R^d)^2 \left(-5m_{L^-}^2 + \frac{8m_{L^-} m_\tau \left(2(m_{L^-}^2 - m_\tau^2) + (m_{L^-}^2 + m_\tau^2)\ln\left(\frac{m_\tau^2}{m_{L^-}^2}\right)\right)}{(m_{L^-}^2 - m_\tau^2)} \right) \\
&- \frac{4m_{L^{--}} m_\tau (s_R^d)^2 \left(2(m_{L^{--}}^2 - m_\tau^2) + (m_{L^{--}}^2 + m_\tau^2)\ln\left(\frac{m_\tau^2}{m_{L^{--}}^2}\right)\right)}{(m_{L^{--}}^2 - m_\tau^2)} \Bigg), \\
\Delta\mathbb{S} \;=\;& -\frac{1}{36\pi}\Bigg(\frac{6(c_R^d)^2 (m_{L^-}^2 + m_{L^{--}}^2)}{m_{L^-} m_{L^{--}}} + \frac{6(s_R^d)^2 (m_{L^{--}}^2 + m_\tau^2)}{m_{L^{--}} m_\tau} \\
&+ 4(s_R^d)^2 \left(-3 + \ln\left(\frac{m_\tau^2}{m_{L^-}^2}\right)\right) + 4(c_R^d)^2 \left(-3 + \ln\left(\frac{m_{L^-}^2}{m_{L^{--}}^2}\right)\right) \\
&- \frac{6(c_R^d)^2 (s_R^d)^2 \left(m_{L^-}^8 - 8m_{L^-}^6 m_\tau^2 + 8m_{L^-}^2 m_\tau^6 - m_\tau^8 - 12m_{L^-}^4 m_\tau^4 \ln\left(\frac{m_\tau^2}{m_{L^-}^2}\right)\right)}{m_{L^-} m_\tau \left(m_{L^-}^2 - m_\tau^2\right)^3} \\
&+ \frac{5(c_R^d)^2 (s_R^d)^2}{\left(m_{L^-}^2 - m_\tau^2\right)^3} \Big[\left(5m_{L^-}^6 + 27(m_{L^-}^2 m_\tau^4 - m_{L^-}^4 m_\tau^2) - 5m_\tau^6 \right) \\
&+ 3\left(m_{L^-}^6 - 3m_{L^-}^4 m_\tau^2 - 3m_{L^-}^2 m_\tau^4 + m_\tau^6 \right) \ln\left(\frac{m_\tau^2}{m_{L^-}^2}\right) \Big] \Bigg).
\end{aligned}
\tag{7.16}
$$

As shown in Fig. 7.3, the parameter space of $\mathcal{D}_2$ receives almost no constraint in the vicinity of the decoupling limit. The entire spectrum of m_{L^-} scanned is allowed by both oblique parameters in the 2σ region for $\sin\theta = 0.05$. However, the $\mathbb{S}$ parameter excludes $m_{L^0} > 730$ GeV in $\mathcal{D}_1$ model. The distinction between doublet models from the $\mathbb{S}$ parameter is sharper than that for singlet models. With six different weak hypercharge choices, the $\mathbb{S}$ parameter constraints are significant, due to the extended number of lepton-modified gauge boson propagators. Increasing the lepton mixing to $\sin\theta = 0.1$, the $\mathbb{T}$ parameter becomes restrictive for both doublet models. The mass of neutral VLL in $\mathcal{D}_1$ falls off the global fit of the oblique parameters for $m_{L^0} > 760$ GeV, whereas the charged VLL mass of $\mathcal{D}_2$ model must be $m_{L^-} < 670$ GeV to remain in 2σ region for the $\mathbb{T}$ parameter. In contrast, the $\mathbb{S}$ parameter imposes a minimum bound on $\mathcal{D}_2$ of $m_{L^-} > 400$ GeV.
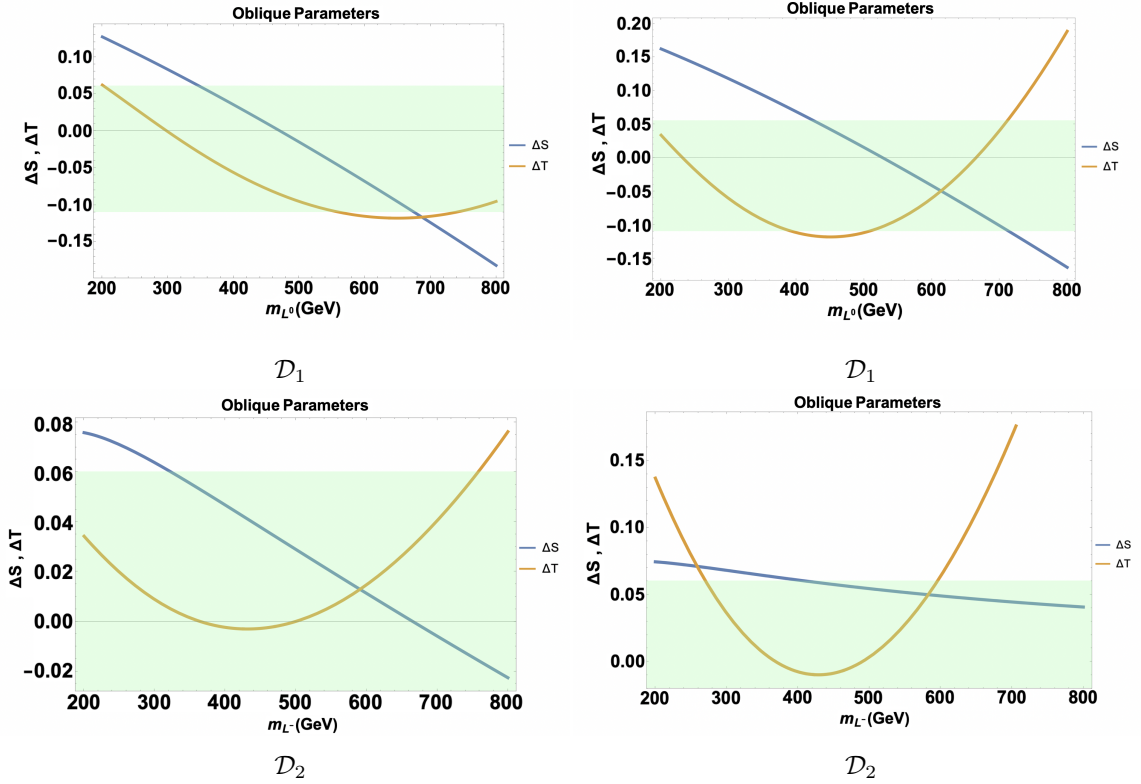
Figure 7.3: New physics contributions to the oblique parameters: $\mathbb{T}$ (orange) and $\mathbb{S}$ (blue) from doublet vector-like lepton representations for different VLL-SM lepton mixing $\sin\theta_L = 0.05$ (left) and $\sin\theta_L = 0.1$ (right).The green shaded region is the allowed space from the $\mathbb{S}$ and the $\mathbb{T}$ parameters in 2σ level.

Triplet $\mathcal{T}_1$ (L^+, L^0, L^-), $Y = 0$

$$
\begin{aligned}
\Delta\mathbb{T} \;=\;& \frac{1}{32\pi c_W^2 s_W^2 M_Z^2}\Big(2(c_L^u)^4 m_\tau^2 + 8(s_L^u)^2 m_{L^+}^2 + 4(s_L^u)^4\left(\sqrt{2}m_{L^0}^2 + \sqrt{2}m_{L^-}^2 + 2m_\tau^2\right) \\
&+\; (c_L^u)^2\Big(8m_{L^+}^2 - 32 m_{L^0}m_{L^+} + (s_L^u)^2(5-4\sqrt{2})m_{L^-}^2 - 16\sqrt{2}(s_L^u)^2 m_{L^0}m_{L^-} \\
&+\; (s_L^u)^2 4\sqrt{2}m_\tau^2 + m_{L^0}^2\left(8 + (9-4\sqrt{2})(s_L^u)^2\right)\Big) \\
&+\; \frac{8\sqrt{2}(s_L^u)^2\big[(c_L^u)^2 m_{L^0}m_{L^-}(m_{L^0}^2 + m_{L^-}^2) - (s_L^u)^2 m_{L^0}^2 m_{L^-}^2\big]\ln\left(\frac{m_{L^0}^2}{m_{L^-}^2}\right)}{m_{L^0}^2 - m_{L^-}^2} \\
&+\; \frac{16(c_L^u)^2\big[-m_{L^0}m_{L^+}^3 + m_{L^0}^2\left(m_{L^+}^2 - m_{L^0}m_{L^+}\right)\big]\ln\left(\frac{m_{L^+}^2}{m_{L^0}^2}\right)}{m_{L^0}^2 - m_{L^+}^2}\Big), \\[6pt]
\Delta\mathbb{S} \;=\;& -\frac{1}{36\pi}\Bigg(\frac{12(c_L^u)^2\left(m_{L^0}^2 + m_{L^+}^2\right)}{m_{L^0}m_{L^+}} - \frac{6(-2+\sqrt{2})(c_L^u)^2(s_L^u)^2\left(m_{L^0}^2 + m_\tau^2\right)}{m_{L^0}m_\tau} \\
&+\; \frac{6\left(2(c_L^u)^4 + \sqrt{2}(c_L^u)^2(s_L^u)^2\right)\left(m_{L^0}^2 + m_{L^-}^2\right)}{m_{L^0}m_{L^-}} + 8(s_L^u)^2\left(-3 + \ln\left(\frac{m_{L^+}^2}{m_{L^0}^2}\right)\right) \\
&+\; \left(8(c_L^u)^4 + 4\sqrt{2}(c_L^u)^2(s_L^u)^2 + 2(s_L^u)^4\right)\left(-3 + \ln\left(\frac{m_{L^0}^2}{m_{L^-}^2}\right)\right) \\
&+\; \frac{(c_L^u)^2(s_L^u)^2\left[5m_{L^0}^6 + 3m_{L^0}^6\ln\left(\frac{m_\tau^2}{m_{L^0}^2}\right)\right]}{m_{L^0}^6} \\
&-\; 2(c_L^u)^2(s_L^u)^2(-5+2\sqrt{2})\left(-3 + \ln\left(\frac{m_\tau^2}{m_{L^0}^2}\right)\right) \\
&-\; \frac{6(c_L^u)^2(s_L^u)^2\left(m_{L^-}^8 - 8m_{L^-}^6 m_\tau^2 - 8m_{L^-}^2 m_\tau^6 - m_\tau^8 - 12m_{L^-}^4 m_\tau^4\ln\left(\frac{m_\tau^2}{m_{L^-}^2}\right)\right)}{m_{L^-}m_\tau\left(m_{L^-}^2 - m_\tau^2\right)^3} \\
&+\; \frac{5(c_L^u)^2(s_L^u)^2}{\left(m_{L^-}^2 - m_\tau^2\right)^3}\big[5m_{L^-}^6 - 27m_{L^-}^4 m_\tau^2 + 27m_{L^-}^2 m_\tau^4 - 5m_\tau^6 \\
&+\; 3\left(m_{L^-}^6 - 3m_{L^-}^4 m_\tau^2 - 3m_{L^-}^2 m_\tau^4 + m_\tau^6\right)\ln\left(\frac{m_\tau^2}{m_{L^-}^2}\right)\big]\Bigg).
\end{aligned}
$$

$$(7.17)$$

Triplet $\mathcal{T}_2$ (L^0, L^-, L^{--}), $Y = -1$

$$
\begin{aligned}
\Delta\mathbb{T} &= \frac{1}{32\pi c_W^2 s_W^2 M_Z^2}\Bigg(\frac{8\sqrt{2}(s_L^u)^2\big[(c_L^u)^2(m_{L^0}^2 + m_{L^-}^2)m_{L^0}m_{L^-} - (s_L^u)^2 m_{L^0}^2 m_{L^-}^2\big]\ln\left(\frac{m_{L^0}^2}{m_{L^-}^2}\right)}{m_{L^0}^2 - m_{L^-}^2}\\
&+ \frac{1}{-m_{L^{--}}^2 + m_{L^-}^2}\Big[- ((m_{L^{--}}^2 - m_{L^-}^2)(2(c_L^u)^4 m_\tau^2 + (c_L^u)^2(s_L^u)^2[(5 - 4\sqrt{2})m_{L^0}^2\\
&+ (9 - 4\sqrt{2})m_{L^-}^2 + 4\sqrt{2}(-4m_{L^0}m_{L^-} + m_\tau^2)]\\
&+ 4(s_L^u)^2[4m_{L^{--}}^2 - 8m_{L^-}m_{L^{--}} + \sqrt{2}m_{L^0}^2(s_L^u)^2 + 2m_\tau^2(s_L^u)^2\\
&+ m_{L^-}^2(2 + \sqrt{2}(s_L^u)^2)]]))\\
&+ 16(s_L^u)^2[m_{L^-}^3 m_{L^{--}} + m_{L^{--}}^2(-m_{L^-}^2 + m_{L^-}m_{L^{--}})]\ln\left(\frac{m_{L^-}^2}{m_{L^{--}}^2}\right)\Big]\Bigg),
\end{aligned}
$$

$$
\begin{aligned}
\Delta\mathbb{S} &= -\frac{1}{36\pi}\Bigg(\frac{12(c_L^u)^2\,(m_{L^-}^2 + m_{L^{--}}^2)}{m_{L^-}m_{L^{--}}} - \frac{6(-2 + \sqrt{2})(c_L^u)^2(s_L^u)^2\,(m_{L^0}^2 + m_\tau^2)}{m_{L^0}m_\tau}\\
&+ \frac{6(2(c_L^u)^4 + \sqrt{2}(c_L^u)^2(s_L^u)^2)\,(m_{L^0}^2 + m_{L^-}^2)}{m_{L^0}m_{L^-}} + 8(c_L^u)^2\left(-3 + \ln\left(\frac{m_{L^-}^2}{m_{L^{--}}^2}\right)\right)\\
&+ (8(c_L^u)^4 + 4\sqrt{2}(c_L^u)^2(s_L^u)^2 + 2(s_L^u)^4)\left(-3 + \ln\left(\frac{m_{L^0}^2}{m_{L^-}^2}\right)\right)\\
&+ \frac{(c_L^u)^2(s_L^u)^2\left[25m_{L^0}^6 + 15m_{L^0}^6\ln\left(\frac{m_\tau^2}{m_{L^0}^2}\right)\right]}{m_{L^0}^6} + \frac{12(s_L^u)^2\,(m_{L^{--}}^2 + m_\tau^2)}{m_{L^{--}}m_\tau}\\
&- 2(c_L^u)^2(s_L^u)^2(-5 + 2\sqrt{2})\left(-3 + \ln\left(\frac{m_\tau^2}{m_{L^0}^2}\right)\right) + 8(s_L^u)^2\left(-3 + \ln\left(\frac{m_\tau^2}{m_{L^{--}}^2}\right)\right)\\
&+ \frac{(c_L^u)^2(s_L^u)^2}{\left(m_{L^-}^2 - m_\tau^2\right)^3}[5m_{L^-}^6 - 27m_{L^-}^4 m_\tau^2 + 27m_{L^-}^2 m_\tau^4 - 5m_\tau^6\\
&+ 3\left(m_{L^-}^6 - 3m_{L^-}^4 m_\tau^2 - 3m_{L^-}^2 m_\tau^4 + m_\tau^6\right)\ln\left(\frac{m_\tau^2}{m_{L^-}^2}\right)]\Bigg).
\end{aligned}
\tag{7.18}
$$

Finally, by comparing triplet VLL models at $\sin\theta = 0.05$, the allowed space of $\mathcal{T}_1$ is independent of the $\mathbb{S}$ and $\mathbb{T}$ parameters throughout the entire spectrum, as shown in Fig 7.4. While the $\mathbb{T}$ parameter shows almost VLL mass-independent behavior for $\mathcal{T}_2$ model, the $\mathbb{S}$ parameter excludes $m_{L^-} = [250, 510]$ GeV from constraints at the 3σ level. $\mathcal{T}_1$ has a similar $\mathbb{S}$ characteristic for larger mixing $\sin\theta = 0.1$, thus m_{L^-} is not limited. However, the upper bound from the $\mathbb{T}$ parameter occurs around $m_{L^-} \sim 650$ GeV. The constraints are more stringent on $\mathcal{T}_2$ representation as leptonic mixing increases due to its direct dependence on mass splitting between mass eigenstates. The upper bound from the $\mathbb{T}$ parameter occurs for $m_{L^-} \sim 590$ GeV.

As expected, a smaller mixing regime generates more relaxed constraints from the oblique parameters. We note that none of the representations is limited by the $\mathbb{T}$ parameter at $\sin\theta = 0.05$, though this freedom is limited as the mixing gets larger. Thus, the oblique parameter $\mathbb{T}$ becomes more restrictive as m_{VLL} gets larger. Furthermore, given different
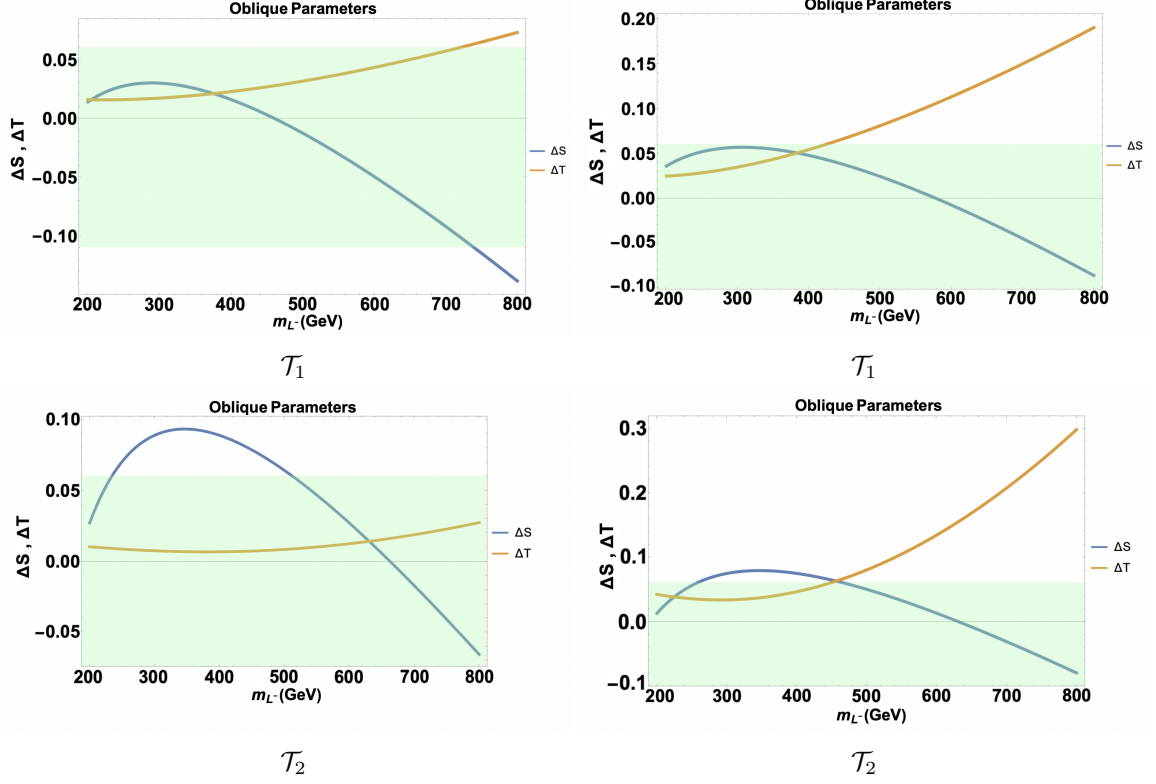
Figure 7.4: New physics contributions to the oblique parameters: $\mathbb{T}$ (orange) and $\mathbb{S}$ (blue) from triplet vector-like lepton representations for different VLL-SM lepton mixing $\sin\theta_L = 0.05$ (left) and $\sin\theta_L = 0.1$ (right). The green shaded region is the allowed space from the $\mathbb{S}$ and the $\mathbb{T}$ parameters in 2σ level.

weak hypercharge choices, the $\mathbb{S}$ parameter also shows varying constraints but may not be as constraining as the $\mathbb{T}$ parameter unless the hypercharge choices lead to significant changes in the gauge boson propagators.

7.5 RGE Allowed Parameter Space of Vector-like Leptons

Theories with additional fermions customarily enhance the instability of the Higgs self-coupling, driving it faster toward negative values at higher energy scales. This fundamentally signals the occurrence of an unbounded potential from below, thereby undermining vacuum stability. Such an outcome is already evident in the SM due to the top quark, which drives the Higgs quartic coupling negative around $\mu = 10^{10}$ GeV at one loop [56]. While supplementary scalar bosons can uphold the positivity of the Higgs self-coupling against the diminishing influences of the renormalization flow at higher energy scales, the introduction of vector-like fermions (VLFs) offers an intriguing alternative. These VLFs, through various gauge portals, have the potential to stabilize the electroweak vacuum. Therefore, the effects of VLFs have been studied in numerous extensions involving extensive scalar models. However, models with additional scalars are already promising when mixed with the Higgs fields, opening up a large parameter space due to considerable effects at the RGE level. The question remains, could one achieve vacuum stability *without* additional scalar(s)?

In this context, the inclusion of vector-like leptons (VLLs) exerts a strong influence on electroweak vacuum stability, predominantly through their effects on the Higgs quartic coupling via the weak hypercharge and isospin portals. In fact, additional charged fermions alone do not destabilize the Higgs potential. Their gauge interactions stabilize it, while their Yukawa couplings to the SM Higgs introduce new instabilities. Unlike the impact of vector-like quarks, VLLs engage differently with the gauge fields, leading to distinctive contributions to the RGEs of the Yukawa couplings $\Delta g_{1,2}$, due to the absence of the largest Δg_3 correction. Scenarios that allow more than one generation VLL that do not exhibit such couplings exist, and could be viable to stabilize the Higgs potential. The incorporation of VLLs introduces novel Yukawa interactions that generally serve to lower the Higgs quartic coupling. However, the gauge couplings g_1 and g_2, which are positively influenced by VLLs, are pivotal in counteracting this effect [210]. Furthermore, if VLL Yukawa couplings contribute sufficiently to balance the Higgs quartic coupling, compensating quartic effects $|\lambda_H y_L^2| > |y_L^4|$ along with gauge corrections, this can generate a viable parameter space that keeps $\lambda_H > 0$ for $\mu \leq M_{\text{Planck}}$, preventing its descent into negativity at elevated scales [86]. The intricate interplay between the Yukawa portal and the gauge couplings induced by the VLLs induces a non-trivial impact on the RGE flow, potentially unveiling regions of parameter space wherein the electroweak vacuum retains stability. This delicate equilibrium among the diverse contributions is paramount in determining the overall stability of the electroweak vacuum in the presence of VLLs. Allowed by the experimental constraints, masses $m \sim \mathcal{O}$ (TeV) survive from stability constraints for VLQ [1, 291]. However, we assume lighter scales $< \mathcal{O}$ (TeV) for VLL masses to obtain viable solutions that survive from the RGE flow. Hence, the examination of VLLs within the SM framework underscores a promising pathway for addressing vacuum stability without necessitating an extension of the scalar sector. To this end, we summarize our methodology as:

- We impose the minimum mass bounds on the neutral and charged sectors of VLLs and run RGEs over various models in Appendix C to generate the running of the Higgs and Yukawa couplings without encountering any Landau pole.

- We also provide the allowed space for SM-VLL mixing versus m_{VLL} by randomly generating $n_{VLL} + 1$ parameter points as solutions to RGEs while enforcing stability

and perturbative unitarity conditions on the couplings up to the Planck scale $\mu = M_{\text{Planck}}$.

- The initial conditions for the couplings appearing in the VLL representations are set at the energy scale $\mu_0 = m_t$.

- Additionally, new physics corrections are also manifested through gauge boson loops in self-energy diagrams, namely the oblique parameters $\mathbb{S}$ and $\mathbb{T}$ from VLLs. We check the region of electroweak observables (EWPO) and discuss the scale favoring our findings from the RGE analyses.

We now proceed to analyze the representations in Table 7.1.

7.5.1 Singlet VLL: $\mathcal{S}_1$ and $\mathcal{S}_2$

Singlet VLL extensions $\mathcal{S}_1$ and $\mathcal{S}_2$ of the SM generate the safest scenario for the Higgs quartic coupling among all the representations studied herein. Fixing the masses of neutral and charged vector fermions throughout our work to compare each model clearly showed that λ is more prone to stay away from the vacuum instability scale in singlet VLL models, as seen in Fig. 7.5. The $\mathcal{S}_2$ model generates a relatively larger parameter space up to $m_{L^-} \sim 150$ GeV, as seen in Fig. 7.6, surviving all theoretical constraints. The distinction between $\mathcal{S}_1$ and $\mathcal{S}_2$ is fully attributed to weak hypercharge difference, where $U(1)_Y$ gauge portal g_1 receives no correction from the L^0 field alone, hence it narrows the allowed space. This can also be shown in the RG running of y_M that defines the Higgs coupling to only VLLs. It strays dangerously close to the non-perturbative region in $\mathcal{S}_1$ model, for which the RGE controlling the y_M coupling is completely dictated by the Yukawa terms in Eq. C.1. The upward shift of the neutral Yukawa coupling in $\mathcal{S}_1$ compared to the charged Yukawa in $\mathcal{S}_2$ occurs due the fact that the mass splitting between neutrino and L^0 is larger than that between the τ and L^-, thus generating a larger initial condition. Having the least number of free parameters used for RGE solutions, the $\mathcal{S}_1$ and $\mathcal{S}_2$ models are highly dependent on the reciprocal relation between the mass of the field and its mixing with the SM lepton. Although lighter mass scales are excluded by the experimental data [96], we found that $m_{L^0,-} \gtrsim 110$ GeV; otherwise, the perturbativity of the Higgs coupling breaks down. Additionally, Fig. 7.6 shows that the mixing between VLLs and SM leptons remains non-zero, serving as the most important condition for stabilizing the electroweak vacuum in the presence of new fields. The absence of the color charge is prominent in Fig. 7.5, producing a unique feature of VLL Yukawa couplings that differ significantly from those of vector-like quarks [2]. Furthermore, we checked that, except for highly exotic weak hypercharge choices $Y > |3/2|$ [292], VLL Yukawa couplings tend to increase over energy scales, as the remain insensitive to the largest gauge portal correction g_3[1]. In this graph, we indicate the region shaded in pink which is disallowed by constraints coming from the electroweak precision observables as in Sec. 7.4.1.

---

[1]The relative strength of τ Yukawa is too small and the running coupling appears almost flat compared to other couplings in the model.
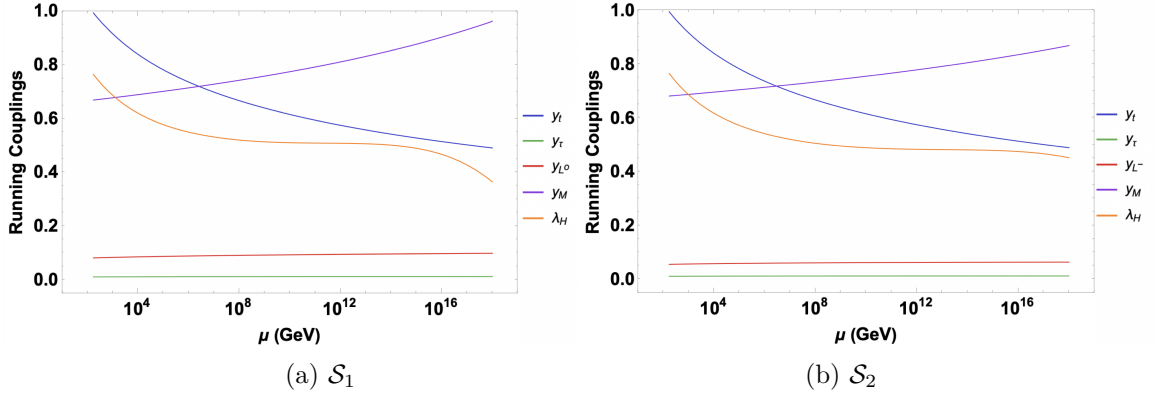
Figure 7.5: The RGE running of the Yukawa and the Higgs coupling for models with singlet vector-like lepton representations. We show singlet vector-like representation, $\mathcal{S}_1$ (a), and $\mathcal{S}_2$ (b). For singlet models, we have set $m_{L^0} = 120$ GeV, $m_{L^-} = 125$ GeV $\mu_0 = m_t$, and $\sin\theta_L = 0.1$.
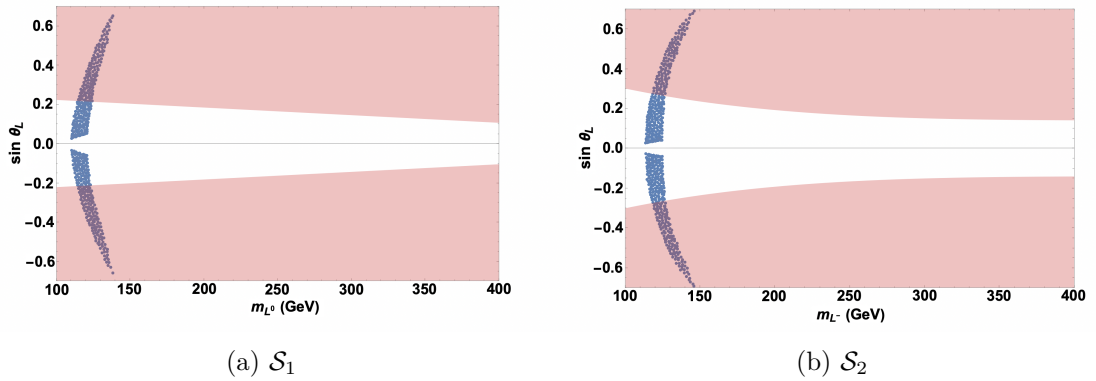
Figure 7.6: The allowed parameter space extracted from theoretical constraints for the mass of vector-like leptons and its dependence on mixing angle to the third generation SM leptons for singlet vector-like lepton representations. We show singlet $\mathcal{S}_1$ vector-like model (a), and singlet vector-like $\mathcal{S}_2$ model (b). The region shaded in pink is disallowed by constraints coming from the electroweak precision observables as in Sec. 7.4.1.

7.5.2 Doublet VLL: $\mathcal{D}_1$ and $\mathcal{D}_2$

In contrast to singlet models, RGE solutions of doublet models $\mathcal{D}_1$ and $\mathcal{D}_2$ exhibit a more sensitive behaviour with respect to the Higgs coupling, especially in the presence of non-SM-like charges. The uncoupled nature of doubly charged VLLs drastically adjusts the starting value of the running coupling $y_{L^{--}}$ as illustrated in Fig. 7.7. Consequently, this adjustment affects the Higgs RGE more significantly than for fields that mix with SM leptons across all multiplets. However, this phenomenon also imposes a soft upper bound on the mass of exotic leptons, constrained by perturbativity to $m_{L^{--}} < m_t$. As mentioned earlier, larger hypercharge values for VLLs can cause Yukawa couplings to decrease with increasing energy, similar to quark couplings in renormalization theory. As shown in the right panel of Fig. 7.7, y_L begins to decrease around $\mu \gtrsim 10^{13}$ GeV as might be expected from the effect of the largest hypercharge-carrying field $\mathcal{D}_2$. The vacuum stability condition requires smaller mixing angles to counterbalance initial conditions due to the mass increment; however, the Yukawa coupling y_M increases as the VLL-SM mixing scale approaches the decoupling region. Therefore, representations that exclude both neutral and charged VLLs simultaneously are more sensitive to the value of y_M due to the indirect effects of uncoupled leptons via RGEs. This sensitivity results in distinct parameter spaces for $\mathcal{S}_1$, $\mathcal{S}_2$ and $\mathcal{D}_2$ compared to other models. On the other hand, the model $\mathcal{D}_1$, including both L^0 and L^-, provides more space as both up and down sector mixings vary between extreme ends while maintaining λ in the vacuum stability regime. The extension of the RGE parameter space is also related to the additional number of positive quadratic and negative quartic Yukawa terms. The limits on doublet models are more relaxed compared to singlet VLLs with m_{L^-} upper bound reaching approximately 170 GeV for $\mathcal{D}_2$, and the mass of the charged lepton rising up to ~ 260 GeV in the $\mathcal{D}_1$ model, allowed by mixing angle $\sin\theta < 0.05$. In fact, we verified numerically that a scale $m_{VLL} > 260$ GeV breaks the perturbativity of Yukawa couplings before the Higgs quartic coupling becomes negative. Thus Fig. 7.8 shows that the upper bound on the mass of charged VLLs for $\mathcal{D}_2$ model corresponds to a critical value where λ starts to run to negative values before Yukawa couplings become non-perturbative. Finally, non-SM-like multiplets can generate heavier mass values that meet theoretical requirements; however, the Higgs constraints from VLLs limit the mixing domain, which is in particular constrained by the Higgs diphoton decay rate [293]. As before, in this graph, we indicate the region shaded in pink which is disallowed by constraints coming from the electroweak precision observables as in Sec. 7.4.1.
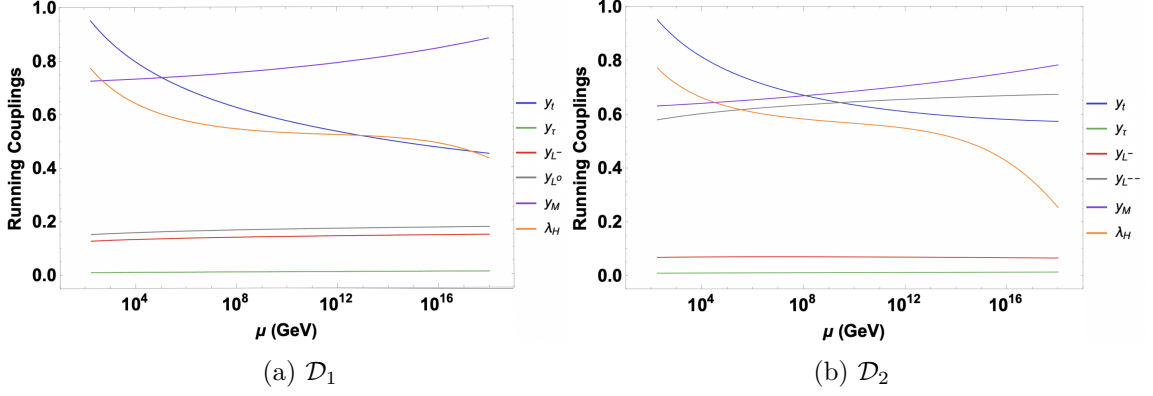
Figure 7.7: The RGE running of the Yukawa and the Higgs coupling for models with doublet vector-like leptons. We show doublet vector-like representation, $\mathcal{D}_1$ (a), and $\mathcal{D}_2$ (b). For doublet models, we have set $m_{L^0} = 150$ GeV, $m_{L^-} = 130$ GeV, $m_{L^{--}} = 160$ GeV, $\mu_0 = m_t$, and $\sin\theta_L = 0.1$.
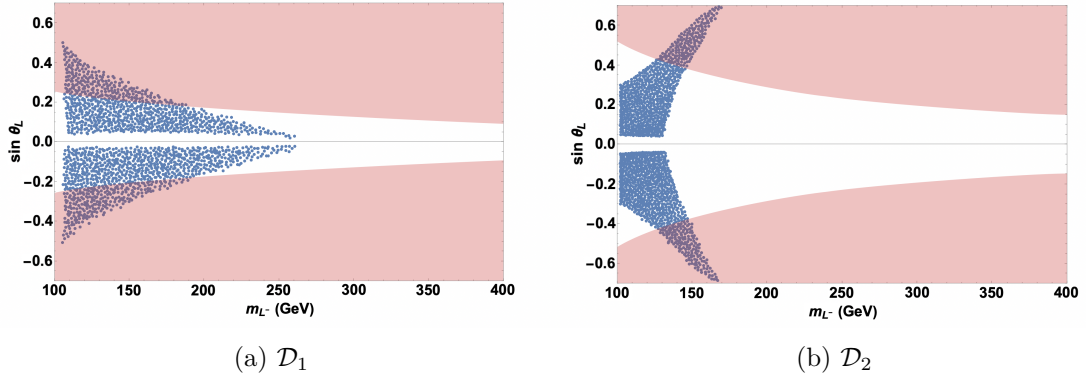
Figure 7.8: The allowed parameter space extracted from theoretical constraints for the mass of vector-like leptons and its dependence on mixing angle to the third generation SM leptons for doublet vector-like representations. We show doublet $\mathcal{D}_1$ vector-like model (a), and doublet vector-like $\mathcal{D}_2$ model (b). The region shaded in pink is disallowed by constraints coming from the electroweak precision observables as in Sec. 7.4.1.

7.5.3 Triplet VLL: $\mathcal{T}_1$ and $\mathcal{T}_2$

The case of triplets vector-like representations is affected by both the exotic L^+, L^{--}, and SM-like vector partners. In Fig. 7.10 the mixing is allowed to be either small or large in the low mass region, whereas larger masses generally require smaller mixing for both triplet models. The mass spectrum reaches up to 270 GeV, though the theoretical minimum would be allowed to be lower in our work, but is excluded by experimental constraints. Similar to singlet models, the distinction between parameter spaces arises from weak hypercharge. Nevertheless, RGE constraints on the triplet model $\mathcal{T}_1$ model are less relaxed due to the absence of g_1 correction, which imposes a smaller mixing regime compared to the $\mathcal{T}_2$ model. The minimum value of the mixing angle required to ensure vacuum stability is slightly larger than for all other representations. This feature is analytically motivated by the fact that triplets rely simultaneously on both neutral and charged Yukawa RGEs, thus requiring

a relatively larger minimum mixing across the entire mass spectrum. Moreover, λ in Fig. 7.9 approaches to zero in $\mathcal{T}_1$ while y_M is the largest correction among the models, directly correlating the allowed space to the inverse relationship between VLL mass and mixing angle shown in Fig. 7.10. Finally, we can conclude that VLL triplets are more promising for stabilizing the vacuum, as they scan over a larger spectrum while satisfying both stability and perturbative unitarity constraints. As for the case of singlets and doublets, we shade in pink the region which is disallowed by constraints coming from the electroweak precision observables as in Sec. 7.4.1.

(a) $\mathcal{T}_1$ (b) $\mathcal{T}_2$
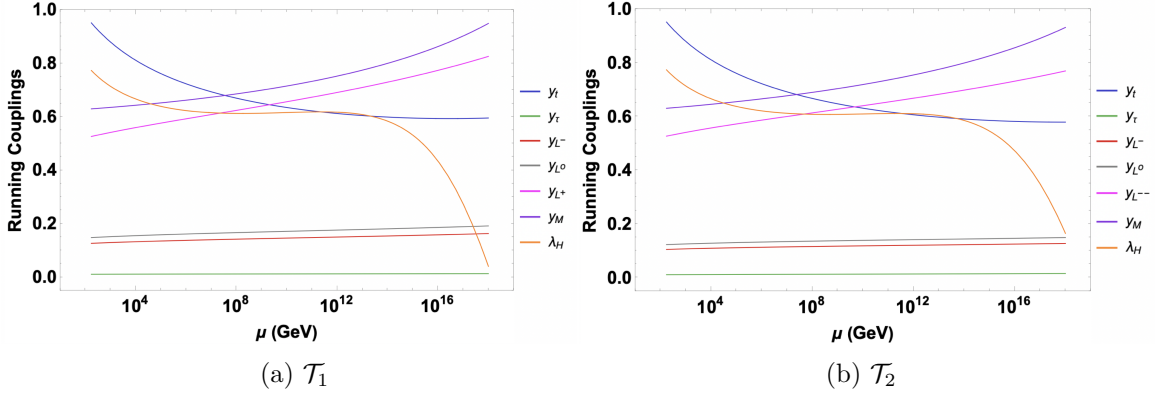
Figure 7.9: The RGE running of the Yukawa and the Higgs coupling for models with triplet vector-like leptons. We show triplet vector-like representation, $\mathcal{T}_1$ (a), and $\mathcal{T}_2$ (b). For triplet models, we have set $m_{L^0} = 150$ GeV, $m_{L^-} = 200$ GeV, $m_{L^+} = 170$ GeV, $m_{L^{--}} = 170$ GeV, $\mu_0 = m_t$, and $\sin\theta_L = 0.1$.


(a) $\mathcal{T}_1$ (b) $\mathcal{T}_2$
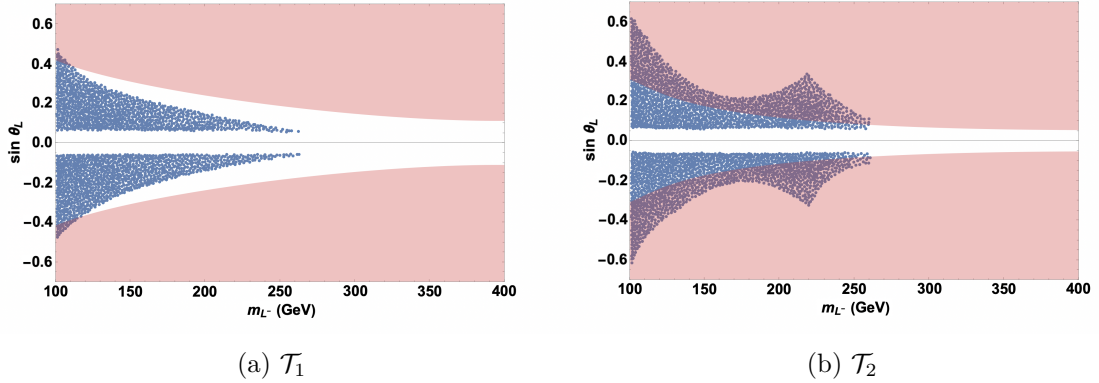
Figure 7.10: The allowed parameter space extracted from theoretical constraints for the mass of vector-like leptons and its dependence on mixing angle to the third generation SM leptons for triplet vector-like representations. We show triplet $\mathcal{T}_1$ vector-like model (a) and triplet vector-like $\mathcal{T}_2$ model (b). The region shaded in pink is disallowed by constraints coming from the electroweak precision observables as in Sec. 7.4.1.

### 7.5.4 Effects of Two Loop Corrections to the RGE

Here we analyse the effect of using the RGEs to two loop accuracy, and whether the next-to-next-to-leading order (NNLO) couplings evolve in such a way as to extend the VLL parameter space. The transition from one loop to two loop RGEs introduces nuanced changes to the running of all couplings, due to higher-order interactions and mixed terms that appear in two loop corrections. Effectively this allows all terms in the RGE to be influenced by the presence of different sectors, generating fully coupled equations. At the one loop level gauge couplings generally increase with energy due to contributions from additional fermions which enhances the gauge portal for vacuum stability concerns. When moving to two loop corrections, gauge couplings receive additional positive contributions from themselves, further enhancing their growth. However the Yukawa couplings mitigate the gauge coupling runnings to order $-g_i^4 y_F^2$. While the interplay between couplings becomes more complex at the two loop level, making deterministic interpretation difficult, it is expected that the gauge portal weakens as the multiplets include more fermions.

Even in the absence of VLL, the top Yukawa becomes smaller due to $-y_t^2 g_3^4$ correction. Additionally all VLLs contribute negatively to the overall running of the top Yukawa as seen in Figs. 7.11-7.13. Hence, the overall decline of the top Yukawa coupling directly affects the Higgs quartic coupling. For the two loop analysis, we found that all the VLL Yukawa couplings except y_M have a basically insignificant effect on RGEs from any type of cross term $y_i^2 y_j^4$, due to their relatively small initial values. Thus we only emphasize the effects of the terms that affect the two loop level and also strengthen the Higgs quartic coupling up to the Planck scale.

For singlet models, the $SU(2)_W$ portal from VLLs does not contribute to the top Yukawa coupling, so the only gauge portal correction from two loop is $g_1^4 y_{L^-}^2$, hence the overall difference of the top Yukawa running between two singlet models is almost insignificant, as seen in Fig. 7.11. We increased the masses of singlet VLL to $m_{L^0} = 150$ GeV and $m_{L^-} = 160$ GeV for $\mathcal{S}_1$ and $\mathcal{S}_2$ models as the greatest effect to $\lambda_{\text{RGE}}^{(2)}$ comes from $y_M^2 y_L^2 \lambda$, and it is additive for the number of VLLs in each representation. This is also seen from the two loop behaviour of y_M throughout all the VLL multiplets. In the next leading order, the Yukawa couplings do not decrease, an effect expected for y_{L^-} in $\mathcal{D}_2$ model because negative effects are fully associated with gauge couplings g_1 and g_2. On the other hand, the coupling of Yukawa terms is negative at two loop order, thus forcing y_M to decrease with respect to the energy scale. However, this feature is not manifested for the singlet models, as the dominance of one loop effects do not allow y_M to run downwards because the self coupling effects of this Yukawa term become larger with respect to the number of VLLs in a model. In an agreement with the one loop RGE results, $\mathcal{S}_2$ model allows larger VLL masses compared to $\mathcal{S}_1$ model, while the Higgs quartic coupling is safer away from instability region, mainly due to the effect of λg_1^4. Although the results from two loop RGE extended the parameter space for VLL masses, we found that λ changes direction around $\mu \sim 10^{14}$ GeV when $m_{VLL} > 170$ GeV and eventually hits the instability region.

The top Yukawa coupling becomes even smaller in the $\mathcal{D}_1$ model, leading to a greater boost for the parameter space surviving the stability constraint by ameliorating the effect on the Higgs quartic coupling. This is mainly due to the fact that $y_t^2 g_1^4$ effect is nine times stronger for $\mathcal{D}_2$ model. Thus, the relatively stronger top Yukawa coupling running in $\mathcal{D}_2$ exerts more pressure on λ up to the Planck scale. The most striking feature of two loop corrections for the Yukawa couplings is present in the models with non-SM like charges. The quartic and hexic Yukawa terms couple negatively in two loop and the coefficients

(a) $\mathcal{S}_1$ (b) $\mathcal{S}_2$
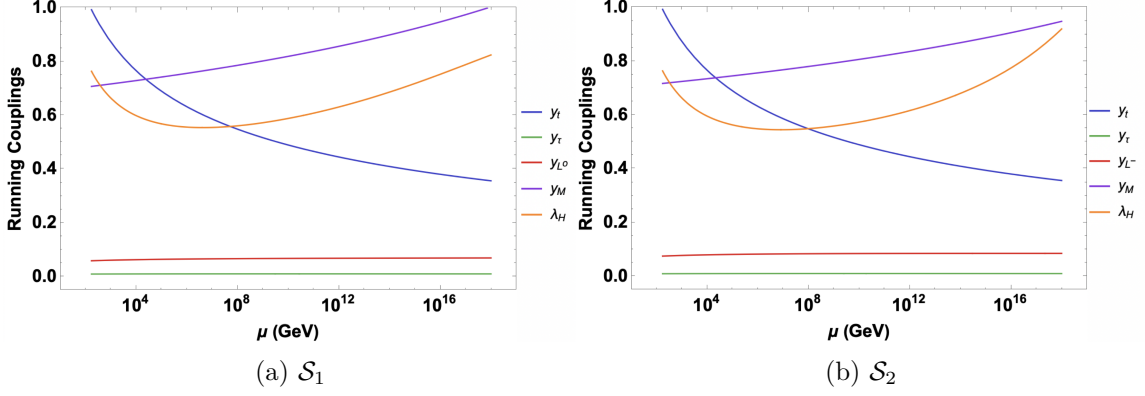
Figure 7.11: The two loop RGE running of the Yukawa and the Higgs coupling for models with singlet vector-like leptons. We show singlet vector-like representation, (a) $\mathcal{S}_1$, and (b) $\mathcal{S}_2$. For singlet models, we have set $m_{L^0} = 150$ GeV, $m_{L^-} = 160$ GeV $\mu_0 = m_t$, and $\sin\theta_L = 0.1$.

rapidly multiply in RGE level due to large number of VLL members. As the VLLs with exotic charges do not couple to SM leptons, their effect on the initial values to y_{L^+} and $y_{L^{--}}$ is more effective in y_M on both quadratic and quartic scale. Combined with the one loop $-Y^2 g_1^2$ effect, y_M runs downward throughout the entire spectrum in $\mathcal{D}_2$ as seen from Fig. 7.12. The consequence of this is to indirectly decrease the effect of $y_M^2 y_L^2 \lambda$ on $\lambda^{(2)}$, which can be counted as an additional reason why $\mathcal{D}_1$ allows larger parameter space to survive the vacuum stability condition. The two loop corrections to all doublet VLL RGEs extend the upper bound to $m_{VLL} \leq 290$ GeV. However, higher VLL masses either break the perturbativity of the Yukawa couplings, or destabilize the vacuum, depending on the leptonic mixing scale.

(a) $\mathcal{D}_1$ (b) $\mathcal{D}_2$
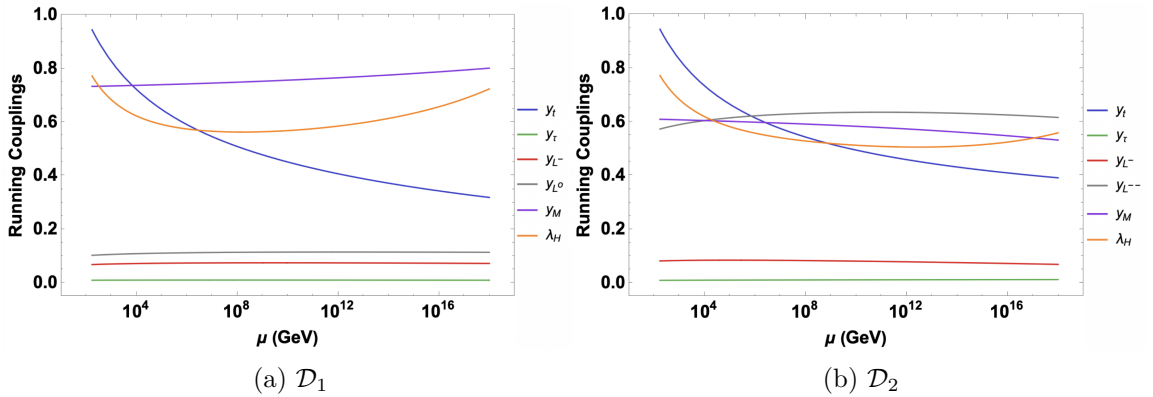
Figure 7.12: The two loop RGE running of the Yukawa and the Higgs coupling for models with doublet vector-like leptons. We show doublet vector-like representation, (a) $\mathcal{D}_1$, and (b) $\mathcal{D}_2$. For doublet models, we have set $m_{L^0} = 200$ GeV, $m_{L^-} = 220$ GeV, $m_{L^{--}} = 170$ GeV, $\mu_0 = m_t$, and $\sin\theta_L = 0.1$.

Finally, in triplet models, the absence of hypercharge terms in the $\mathcal{T}_1$ model uniquely determines the difference in the parameter space and in the running of couplings, whereas the Yukawa effects at the two loop level are similar, due to the particle content. The

intricate interplay between coupled terms at the two loop RGE level results in the largest mass bounds for triplets. However, with fixed VLL inputs, the Higgs quartic coupling runs to its smallest values in triplet models as shown in Fig. 7.13. The two loop corrections open up more space, up to $m_{L^0} < 290$ GeV and $m_{L^-} < 310$ GeV compared to the one loop results in Fig. 7.10. Thus the inclusion of two loop renormalization group equations in the analysis has proven to improve the predictive accuracy of the model's coupling evolution. As demonstrated, the two loop RGE study not only refines the running of the couplings but also extends the available parameter space by up to 20% for all six $SU(2)$ representations. This extension is primarily due to the introduction of more complex couplings inherent in the two loop structure, which effectively capture higher-order effects missing in the one loop approximation.

(a) $\mathcal{T}_1$ (b) $\mathcal{T}_2$
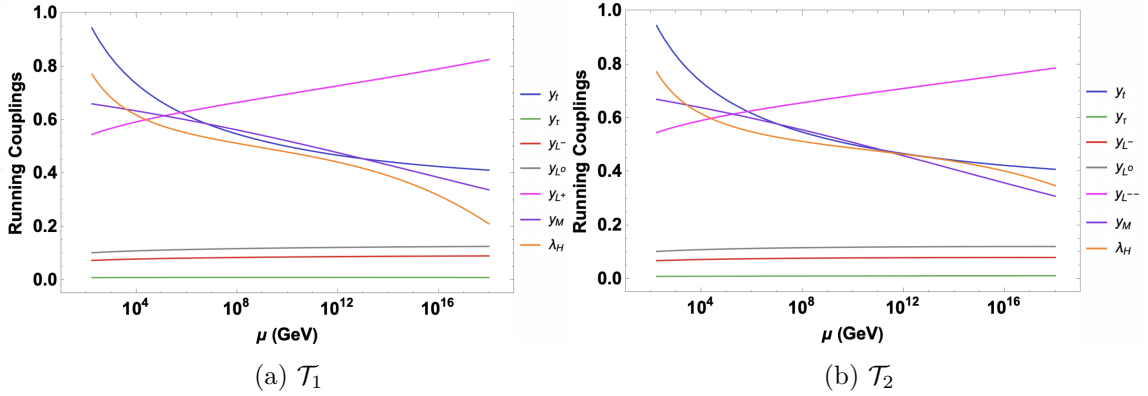
Figure 7.13: The two loop RGE running of the Yukawa and the Higgs coupling for models with triplet vector-like leptons. We show triplet vector-like representation, (a) $\mathcal{T}_1$, and (b) $\mathcal{T}_2$. For triplet models, we have set $m_{L^0} = 200$ GeV, $m_{L^-} = 220$ GeV, $m_{L^+} = 170$ GeV, $m_{L^{--}} = 170$ GeV, $\mu_0 = m_t$, and $\sin\theta_L = 0.1$.

7.6 Conclusions

We have studied SM extensions with six different vector-like lepton representations. Our main focus has been to study the effects of new vector-like lepton fields on electroweak vacuum stability, while also satisfying perturbative unitarity conditions for all the couplings appearing in various representations. We concentrated on the answering the question of whether, unlike the case where vector-like quarks are introduced, and stability requires introduction of an additional scalar field, one can achieve stability with VLL only, and without introducing any additional fields. If this is possible, this would be a novel feature of the SM with VLLs.

Our analysis shows that, while VLLs can stabilize the Higgs quartic coupling up to the Planck scale under certain conditions, significant constraints on Yukawa couplings and VLL masses exist. Specifically, with a particular choice of Yukawa couplings to the SM Higgs field, and given that λy_M^2 surpasses the large quartic terms at the RGE level, vector-like leptons have an allowed but limited parameter space that prevents the Higgs quartic coupling from diverging up to the Planck scale. The absence of the colour charge and the large number of VLLs lead to unconventional behaviour, causing Yukawa couplings to increase with the energy scale if the hypercharge is not sufficiently large. If the scale of new physics is very high and the number of flavours n_F is too small, the RG evolutions enter the non-perturbative region prematurely before rising again. Hence we assumed here VLLs masses of $\ll \mathcal{O}(\text{TeV})$ scale. Allowing all lepton generations from the SM to mix with VLLs could strengthen the gauge portal $\beta_{\Delta g_i}$. However, third-generation leptons are less constrained by flavour physics experiments compared to the first and second generations, where flavour-changing neutral currents (FCNCs) and lepton flavour violation (LFV) processes tightly constrain any mixings for the lighter generations. In addition, even if allowed, these mixings will be negligibly small due to the smallness of the first and second generation lepton masses.

The allowed strength of mixing between the SM and VLLs, according to RGE solutions, is determined by the presence of both neutral and charged VLL partners simultaneously, specifically the coexistence of mass splitting initial conditions. We found that large mixing is required if a model excludes both L^0 and L^-. Consequently, the relative weight on $\lambda(\mu)$ with respect to the largest Yukawa y_M becomes smaller, while its initial condition starts at a lower value. Even though singlet VLLs have a similar RGE structure, the difference in hypercharge eventually leads to a wider parameter space allowed for the charged sector m_{L^-}. Our findings from RGE analysis are consistent with the data, considering the minimum bound $m_{VLL} \gtrsim 110$ GeV. Doublet and triplet VLL models open up more allowed parameter space, as expected from additional terms at the RGE level, reaching around $m_{VLL} \sim 270$ GeV, while the leptonic mixing has a minimum bound $\sin \theta \gtrsim 0.05$. We further extended the RGE analysis to two loop corrections to check the amount of improvement to the running couplings in all models. The interplay between the number of higher order interactions generated an extra space for VLL masses, enlarging the maximum bound up to 20%, now reaching 310 GeV for charged VLL. The running of the Yukawa term y_M that connects left- and right-handed part of a VLL played a major role in the two loop evolution, along with the gauge couplings g_1, g_2 with the latter two becoming coupled at two loop level. Since new leptonic fields with exotic charges do not couple to the SM leptons through the Higgs, the upper bounds on their masses depend on perturbative unitarity conditions. Therefore, we assume $m_{L^+, --} < m_t$ in order to keep RG evolutions manageable. Although our renormalization analysis uses only two sets of free parameters, m_{VLL} and $\sin \theta_{L,R}^{u,d}$,

further studies can modify unconventional initial conditions for exotic $VLL_{L,R}$ fields in order to extend the allowed space from RGE solutions.

We also scanned the oblique parameters, ensuring that mixing constraints from the Higgs channel are considered. Generally, the $\mathbb{T}$ does not constrain VLL masses at $\sin\theta = 0.05$; however, the $\mathbb{T}$ parameter becomes restrictive with larger mixing $\sin\theta = 0.1$, rendering $m_{VLL} > 600$ GeV into the 3σ region. Moreover, the overall constraint from the $\mathbb{S}$ parameter relies more on hypercharge effects than on the mixing variance within the same multiplet, showing less severe differences as $\sin\theta$ increases. Limits from EWPO at a fixed mixing scale are more relaxed compared to vacuum stability bounds. Additionally, the parameter space obtained from RGE solutions does not exclude our results from the oblique parameters at $\sin\theta \leq 0.1$ as there is always a solution in $m_{VLL} = [100, 300]$ GeV throughout RGE level. Nevertheless, the oblique parameters rapidly deviate from the global fit for large mixings due to their direct dependence on mass splitting within multiplets.

Future investigations may build on this study by incorporating analyses of non-perturbative effects and higher-order corrections and by examining more intricate VLL representations. Furthermore, exploring the implications of varied initial conditions and potential new physics beyond VLLs could yield additional insights. This study enhances our understanding of the influence of novel fermion fields on electroweak vacuum stability and offers valuable guidance for the search for new particles and interactions in forthcoming experimental endeavours.

Finally, we note that adding a scalar singlet field undoubtedly increases the allowed mass range for VLL masses that satisfy RGE constraints (stability and perturbative unitarity) because the extra parameters from scalar sector allow to extend the range of VLL parameters. This approach was explored before, and, in our opinion, does not have much different or newer features than the model with vector-like quarks and an extra scalar, because apart from overall factors in RGE level, all that is different in Yukawa RGE sector are g_3 corrections terms, and these do not do not appear in scalar RGE terms.

Chapter 8

Conclusion

In this thesis, we embarked on a comprehensive exploration of the impact of vector-like quarks and vector-like leptons on the stability of the electroweak vacuum. The Standard Model, while successful in explaining a vast range of phenomena, leaves us with lingering questions, notably regarding the stability of its electroweak vacuum under sub-Planckian scales. To address these questions, we introduced extensions to the SM in the form of vector-like fermions—particles whose chiral structure and coupling structures differ from those of the SM fermions, yet still preserve the SM gauge invariance, the renormalizability and self-consistency of the theory.

Our investigation was driven by a dual motivation: to evaluate how these additional fermions might influence the stability of the electroweak vacuum, controlled by the renormalization group equation (RGE) structure, and to probe whether their inclusion could satisfy the electroweak precision observables. To this end, we imposed the recent bounds on the extended sector. In particular, we examined the behavior of the scalar potential for different scenarios where the 125 GeV Higgs field mixes with additional scalars.

In general, vector-like fermions (VLFs) offer two independent remedies to the vacuum stability condition for various scalar potentials, regardless of whether scalar mixing is present. On one hand, gauge portals of new fermions offer direct modifications to the RG running of the SM interactions without changing the Higgs quartic beta function itself and delaying the occurrence of Landau poles for gauge couplings. On the other hand, Yukawa portals offer mixing between the SM and the new fermions, which also bring coupled effect to Yukawa flavors in RG level. Additionally, the existence of the Yukawa portal, which includes both gauge portal effects and stability conditions, is largely insensitive to possible choices for connecting the Yukawa portal to the third-generation leptons, as mixed terms in the beta functions containing both SM and BSM Yukawa are numerically small with very little impact on the running of the parameters.

In the Higgs Singlet Model (HSM) with vector-like quarks (VLQs), we focused on the interplay between the Higgs potential stability and the introduction of additional scalar fields that could mitigate the destabilizing effects of vector-like fermions. The key observation was that these fermions, while not directly altering the Higgs couplings at the loop level, effectively contribute to the RGE running by modifying the Higgs self-couplings. Our results demonstrated that the introduction of a singlet scalar with TeV-scale VEVs

could stabilize the vacuum, provided that there is non-zero mixing between the SM Higgs and the additional scalar. The parameter space for the singlet scalar mass was constrained, with the most viable scenarios requiring the scalar mass to be at the O(TeV) scale and the VEV to be between 1 and 4 TeV. For vector-like quarks, the vacuum stability was found to be most restrictive when the scalar VEV was at or below 1 TeV, and the masses of the additional fermions were constrained to the TeV range. The allowed parameter space was found to be highly sensitive to the mass of the vector-like quarks and their mixing with the Standard Model top quark. Specifically, models with top-like vector-like quarks imposed stricter limits on the scalar VEV, and for smaller VEVs (around 1 TeV), many configurations were ruled out. This illustrates the delicate balance required between the mass of vector-like quarks, the singlet scalar and the mixing with the SM Higgs, with the stability condition being most restrictive in scenarios involving the (X,T) doublet model.

In the Two Higgs Doublet Model (2HDM) with VLQs, we explored the effects of an additional scalar doublet on vacuum stability. Our analysis showed that the enlarged scalar sector of the 2HDM could extend the region of vacuum stability up to the Planck scale, depending on the mass and mixing of the vector-like quarks. The most significant contributions to vacuum instability stemmed from the interplay between the Yukawa terms and the gauge couplings. While the gauge couplings had a relatively weaker effect on the RGE evolution compared to the Yukawa interactions, they still contributed in a multiplicative manner, making the overall effect of vector-like fermions highly sensitive to their number and mass. We found that if the number of vector-like quarks was too large or their masses too small, the RG evolution of the Higgs self-coupling would enter a non-perturbative regime before returning to the perturbative domain. This scenario would be highly unpredictable due to the formation of a Landau pole. Conversely, if the number of flavors was too small and the masses of the VLQs too large, the vacuum stability would be compromised. For example, the masses of VLQs were constrained to be less than 10^6 TeV to avoid destabilizing the vacuum. In terms of mixing, we showed that large mixing angles ($\sin\theta_{L,R} > 0.1$) led to violations of perturbative unitarity, while smaller mixing angles ($\sin\theta_{L,R} < 0.2$) were more consistent with vacuum stability. We also identified specific regions of the parameter space where the triplet VLQ representations would lead to an improved vacuum stability. In these models, the stability was found to improve with increasing scalar angle $\tan\beta$ value, which suggested that higher-scale physics could play a crucial role in mitigating the vacuum instability. Additionally, we determined that Type-II 2HDM models, which involve splitting the Yukawa terms between the two Higgs doublets, generally required larger scalar masses than Type-I models to satisfy the stability conditions up to the Planck scale.

In the case of SM extensions with vector-like leptons (VLLs), we focused on the novel question of whether vacuum stability could be achieved *without* introducing additional scalar fields. This scenario is particularly interesting, as vector-like leptons, unlike vector-like quarks, do not couple via strong interactions. Our analysis revealed that VLLs, while not as powerful as vector-like quarks in modifying the Higgs quartic coupling, could still stabilize the vacuum under certain conditions. However, these models had strict constraints on the Yukawa couplings and VLL masses. We observed that for a given VLL mass, the allowed mixing angle ($\sin\theta_{L,R}^{u,d}$) between the SM leptons and the VLLs must be small, with a lower bound of approximately 0.05 for the mixing angle. Larger mixing angles led to significant deviations in the electroweak precision observables (EWPO), particularly the $\mathbb{T}$

parameter, which placed a strict upper bound on the VLL mass when $\sin\theta$ approaches 0.1. The mass of the VLLs was constrained to lie between 110–310 GeV, with the most relaxed bounds coming from doublet and triplet VLL representations.

Our analysis also showed that the presence of exotic charges in vector-like leptons did not affect the SM leptons directly through the Higgs coupling, but their masses and mixing angles were tightly constrained by perturbative unitarity conditions. The RGE analysis of the Yukawa terms revealed that a fine balance between the masses and mixing angles of the VLLs was essential to prevent the theory from entering a non-perturbative regime. For singlet VLLs, this constraint led to a minimum mass bound of 110 GeV, while doublet and triplet VLLs allowed for a slightly larger range of masses, extending up to 270 GeV. The inclusion of higher-loop corrections further refined these bounds, enlarging the allowed parameter space by about 20%. The two-loop corrections played a significant role in improving the predictability of the model, especially in terms of Yukawa and gauge coupling evolution. The presence of higher-order interactions in the RGE equations allowed for a broader range of VLL masses that satisfied both the stability and perturbative unitarity requirements.

In conclusion, we have demonstrated that while vector-like fermions can indeed influence the stability of the electroweak vacuum, their effects vary significantly depending on their representation and the specific extension to the Standard Model. The introduction of vector-like quarks in the Higgs Singlet and Two Higgs Doublet Models suggests that additional scalars, such as singlet or doublet fields, are crucial for maintaining vacuum stability, especially when the vacuum expectation values are in the TeV range. On the other hand, the study of vector-like leptons revealed that it is possible to stabilize the vacuum without the need for extra scalars, although with tighter constraints on the fermion masses and Yukawa couplings. These results provide valuable insights into the viability of new physics models and the constraints on future experimental searches for vector-like fermions.

As a next step in the exploration of vacuum stability, future research could focus on refining the RGE analysis by including novel initial conditions (e.g. mixing relations) to model couplings, more precise two-loop corrections, exploring additional fermion representations, and extending the study to non-perturbative effects and higher-order corrections. Such studies will be crucial for further extending the potential implications of vector-like fermions in the context of vacuum stability and the search for new particles beyond the Standard Model. Additionally, there are different ways in which the gauge or Yukawa portal mechanisms can be exploited for various purposes. The gauge portal, in particular, lends itself naturally to the search for new GUTs or SM extensions with various Higgs representations. In fact, mild modifications to the RG running of couplings can be used to systematically search for vacuum stability, in combination with gauge coupling unification at or below the Planck scale. Furthermore, having control over the gauge, Yukawa, and Higgs couplings, along with their beta functions at the Planck scale, could prove valuable for identifying extensions of the SM that successfully connect with quantized gravity and address cosmological problems. To study the cosmological implications of the Standard Model (SM) in the presence of gravity, the SM Lagrangian must be coupled to a gravitational background. This introduces modifications to the effective potential and the running of couplings, especially at high energy scales, and can impact the vacuum stability. The scalar potential receives corrections that reflect the coupling of the Higgs (or other scalar

fields) to gravity. These corrections are typically small at low energies but become more significant at high scales, such as near the Planck scale, where spacetime curvature can introduce additional terms to the potential, potentially altering the vacuum structure and stability. Quantum gravity corrections, such as those from graviton loops or modifications to the metric, also contribute to the effective potential, with these effects being suppressed at low energies but potentially significant at higher scales. Gravity has the most direct impact on scalar couplings, particularly in the Higgs sector, where it modifies the effective potential by introducing curvature-dependent terms. In cosmological backgrounds (e.g., an expanding universe), these gravitational effects can lead to new contributions to the scalar beta functions, influencing the running of scalar self-couplings and other scalar parameters. While gravity generally has a smaller effect on Yukawa and gauge couplings at low energies, at high energies or in curved spacetimes, gravity can introduce corrections to their beta functions, affecting the running of these couplings. Overall, gravitational effects could modify vacuum stability and the running of scalar, Yukawa, and gauge couplings. These effects could become increasingly important at high energy scales or in regions of strong curvature, such as near the Planck scale.

Appendix A

RGEs for Higgs Singlet Model + Vector-like Quarks

We give below the renormalization group equations for the models studied in the text.

A.1 Singlet $\mathcal{U}_1$ (T), $Y = 2/3$

The relevant RGE for the Yukawa couplings are

$$
\begin{aligned}
\frac{dy_t^2}{d\ln\mu^2} &= \frac{y_t^2}{16\pi^2}\left(\frac{9y_t^2}{2} + \frac{9y_T^2}{2} - \frac{17g_1^2}{20} - \frac{9g_2^2}{4} - 8g_3^2\right), \\
\frac{dy_T^2}{d\ln\mu^2} &= \frac{y_T^2}{16\pi^2}\left(\frac{9y_t^2}{2} + \frac{9y_T^2}{2} + \frac{y_M^2}{4} - \frac{17g_1^2}{20} - \frac{9g_2^2}{4} - 8g_3^2\right), \\
\frac{dy_M^2}{d\ln\mu^2} &= \frac{y_M^2}{16\pi^2}\left(y_T^2 + \frac{9y_M^2}{2} - \frac{8g_1^2}{5} - 8g_3^2\right).
\end{aligned}
\tag{A.1}
$$

The Higgs sector RGEs, describing the interactions between the two bosons are:

$$
\begin{aligned}
\frac{d\lambda_H}{d\ln\mu^2} &= \frac{1}{16\pi^2}\left[\lambda_H\left(12\lambda_H + 6y_t^2 + 6y_T^2 - \frac{9g_1^2}{10} - \frac{9g_2^2}{2}\right) + \frac{\lambda_{SH}^2}{4} - 3y_t^4 - 3y_T^4 - 6y_t^2 y_T^2 \right. \\
&\quad + \left. \frac{27g_1^4}{100} + \frac{9g_2^4}{16} + \frac{9g_1^2 g_2^2}{40}\right], \\
\frac{d\lambda_S}{d\ln\mu^2} &= \frac{1}{16\pi^2}\left(9\lambda_S^2 + \lambda_{SH}^2 + 12y_M^2\lambda_S - 12y_M^4\right), \\
\frac{d\lambda_{SH}}{d\ln\mu^2} &= \frac{1}{16\pi^2}\left[\lambda_{SH}\left(2\lambda_{SH} + 6\lambda_H + 3\lambda_S + 3y_t^2 + 3y_T^2 + 6y_M^2 - \frac{9g_1^2}{20} - \frac{9g_2^2}{4}\right) \right. \\
&\quad - \left. 12y_T^2 y_M^2\right].
\end{aligned}
\tag{A.2}
$$

A.2 Singlet $\mathcal{D}_1$ (B), $Y = -1/3$

The relevant RGE for the Yukawa couplings are

$$\frac{dy_t^2}{d\ln\mu^2} = \frac{y_t^2}{16\pi^2}\left(\frac{9y_t^2}{2} + \frac{3y_B^2}{2} - \frac{17g_1^2}{20} - \frac{9g_2^2}{4} - 8g_3^2\right),$$

$$\frac{dy_B^2}{d\ln\mu^2} = \frac{y_B^2}{16\pi^2}\left(\frac{3y_t^2}{2} + \frac{9y_B^2}{2} + \frac{y_M^2}{4} - \frac{g_1^2}{4} - \frac{9g_2^2}{4} - 8g_3^2\right),$$

$$\frac{dy_M^2}{d\ln\mu^2} = \frac{y_M^2}{16\pi^2}\left(y_B^2 + \frac{9y_M^2}{2} - \frac{2g_1^2}{5} - 8g_3^2\right). \tag{A.3}$$

The Higgs sector RGEs, describing the interactions between the two bosons are:

$$\frac{d\lambda_H}{d\ln\mu^2} = \frac{1}{16\pi^2}\left[\lambda_H\left(12\lambda_H + 6y_t^2 + 6y_B^2 - \frac{9g_1^2}{10} - \frac{9g_2^2}{2}\right) + \frac{\lambda_{SH}^2}{4} - 3y_t^4 - 3y_B^4\right.$$

$$\left. + \frac{27g_1^4}{100} + \frac{9g_2^4}{16} + \frac{9g_1^2 g_2^2}{40}\right],$$

$$\frac{d\lambda_S}{d\ln\mu^2} = \frac{1}{16\pi^2}\left(9\lambda_S^2 + \lambda_{SH}^2 + 12y_M^2\lambda_S - 12y_M^4\right),$$

$$\frac{d\lambda_{SH}}{d\ln\mu^2} = \frac{1}{16\pi^2}\left[\lambda_{SH}\left(2\lambda_{SH} + 6\lambda_H + 3\lambda_S + 3y_t^2 + 3y_B^2 + 6y_M^2 - \frac{9g_1^2}{20} - \frac{9g_2^2}{4}\right)\right.$$

$$\left. - 12y_B^2 y_M^2\right]. \tag{A.4}$$

Finally the coupling constants gain additional terms due to the new fermion, for both models $\mathcal{U}_1$, $\mathcal{D}_1$ with singlet fermions as follows:

$$\frac{dg_1^2}{d\ln\mu^2} = \frac{g_1^4}{16\pi^2}\left(\frac{41}{10} + \frac{4}{15}\right),$$

$$\frac{dg_2^2}{d\ln\mu^2} = \frac{g_2^4}{16\pi^2}\left(-\frac{19}{6}\right),$$

$$\frac{dg_3^2}{d\ln\mu^2} = \frac{g_3^4}{16\pi^2}\left(-7 + \frac{2}{3}\right). \tag{A.5}$$

A.3 Doublet $\mathcal{D}_2$ (T, B), $Y = 1/6$

The relevant RGE for the Yukawa couplings are

$$\frac{dy_t^2}{d\ln\mu^2} = \frac{y_t^2}{16\pi^2}\left(\frac{9y_t^2}{2} + \frac{9y_T^2}{2} + \frac{3y_B^2}{2} + \frac{y_M^2}{2} - \frac{17g_1^2}{20} - \frac{9g_2^2}{4} - 8g_3^2\right),$$

$$\frac{dy_T^2}{d\ln\mu^2} = \frac{y_T^2}{16\pi^2}\left(\frac{9y_t^2}{2} + \frac{9y_T^2}{2} + \frac{3y_B^2}{2} + \frac{y_M^2}{2} - \frac{17g_1^2}{20} - \frac{9g_2^2}{4} - 8g_3^2\right),$$

$$\frac{dy_B^2}{d\ln\mu^2} = \frac{y_B^2}{16\pi^2}\left(\frac{9y_t^2}{2} + \frac{3y_T^2}{2} + \frac{9y_B^2}{2} + \frac{y_M^2}{2} - \frac{17g_1^2}{20} - \frac{9g_2^2}{4} - 8g_3^2\right),$$

$$\frac{dy_M^2}{d\ln\mu^2} = \frac{y_M^2}{16\pi^2}\left(y_T^2 + y_B^2 + \frac{11y_M^2}{2} - \frac{g_1^2}{40} - \frac{9g_2^2}{2} - 8g_3^2\right). \tag{A.6}$$

The Higgs sector RGEs, describing the interactions between the two bosons are:

$$
\begin{aligned}
\frac{d\lambda_H}{d\ln\mu^2} &= \frac{1}{16\pi^2}\left[\lambda_H\left(12\lambda_H + 6y_t^2 + 6y_T^2 + 6y_B^2 - \frac{9g_1^2}{10} - \frac{9g_2^2}{2}\right) + \frac{\lambda_{SH}^2}{4}\right. \\
&\quad - \left. 3y_t^4 - 3y_T^4 - 3y_B^2 - 6y_t^2y_T^2 - 2y_B^2y_T^2 + \frac{27g_1^4}{400} + \frac{9g_2^4}{16} + \frac{9g_1^2g_2^2}{40}\right], \\
\frac{d\lambda_S}{d\ln\mu^2} &= \frac{1}{16\pi^2}\left(9\lambda_S^2 + \lambda_{SH}^2 + 12y_M^2\lambda_S - 12y_M^4\right), \\
\frac{d\lambda_{SH}}{d\ln\mu^2} &= \frac{1}{16\pi^2}\left[\lambda_{SH}\left(2\lambda_{SH} + 6\lambda_H + 3\lambda_S + 3y_t^2 + 3y_T^2 + 3y_B^2 + 6y_M^2 - \frac{9g_1^2}{20} - \frac{9g_2^2}{4}\right)\right. \\
&\quad - \left. 12y_T^2y_M^2 - 12y_B^2y_M^2\right],
\end{aligned}
\tag{A.7}
$$

and the coupling constants gain additional terms due to the new fermion as follows:

$$
\begin{aligned}
\frac{dg_1^2}{d\ln\mu^2} &= \frac{g_1^4}{16\pi^2}\left(\frac{41}{10} + \frac{2}{15}\right), \\
\frac{dg_2^2}{d\ln\mu^2} &= \frac{g_2^4}{16\pi^2}\left(-\frac{19}{6} + \frac{13}{6}\right), \\
\frac{dg_3^2}{d\ln\mu^2} &= \frac{g_3^4}{16\pi^2}\left(-7 + \frac{4}{3}\right).
\end{aligned}
\tag{A.8}
$$

A.4 Non SM-like Doublet $\mathcal{D}_X$ (X, T), $Y = 7/6$

The relevant RGE for the Yukawa couplings are

$$
\begin{aligned}
\frac{dy_t^2}{d\ln\mu^2} &= \frac{y_t^2}{16\pi^2}\left(\frac{9y_t^2}{2} + \frac{9y_T^2}{2} + \frac{9y_X^2}{2} + \frac{y_M^2}{2} - \frac{17g_1^2}{20} - \frac{9g_2^2}{4} - 8g_3^2\right), \\
\frac{dy_T^2}{d\ln\mu^2} &= \frac{y_T^2}{16\pi^2}\left(\frac{9y_t^2}{2} + \frac{9y_X^2}{2} + \frac{9y_T^2}{2} + \frac{y_M^2}{2} - \frac{17g_1^2}{20} - \frac{9g_2^2}{4} - 8g_3^2\right), \\
\frac{dy_X^2}{d\ln\mu^2} &= \frac{y_X^2}{16\pi^2}\left(\frac{9y_t^2}{2} + \frac{9y_X^2}{2} + \frac{9y_T^2}{2} + \frac{y_M^2}{2} - \frac{17g_1^2}{20} - \frac{9g_2^2}{4} - 8g_3^2\right), \\
\frac{dy_M^2}{d\ln\mu^2} &= \frac{y_M^2}{16\pi^2}\left(y_T^2 + y_X^2 + \frac{11y_M^2}{2} - \frac{49g_1^2}{40} - \frac{9g_2^2}{2} - 8g_3^2\right).
\end{aligned}
\tag{A.9}
$$

The Higgs sector RGEs, describing the interactions between the two bosons are:

$$
\begin{aligned}
\frac{d\lambda_H}{d\ln\mu^2} &= \frac{1}{16\pi^2}\left[\lambda_H\left(12\lambda_H + 6y_t^2 + 6y_T^2 + 6y_X^2 - \frac{9g_1^2}{10} - \frac{9g_2^2}{2}\right) + \frac{\lambda_{SH}^2}{4}\right. \\
&\quad - \left. 3y_t^4 - 3y_T^4 - 3y_X^2 - 6y_t^2y_T^2 - 12y_X^2y_T^2 + \frac{27g_1^4}{400} + \frac{9g_2^4}{16} + \frac{9g_1^2g_2^2}{40}\right], \\
\frac{d\lambda_S}{d\ln\mu^2} &= \frac{1}{16\pi^2}\left(9\lambda_S^2 + \lambda_{SH}^2 + 12y_M^2\lambda_S - 12y_M^4\right), \\
\frac{d\lambda_{SH}}{d\ln\mu^2} &= \frac{1}{16\pi^2}\left[\lambda_{SH}\left(2\lambda_{SH} + 6\lambda_H + 3\lambda_S + 3y_t^2 + 3y_T^2 + 3y_X^2 + 3y_M^2 - \frac{9g_1^2}{20} - \frac{9g_2^2}{4}\right)\right. \\
&\quad - \left. 6y_T^2y_M^2 - 6y_X^2y_M^2\right],
\end{aligned}
\tag{A.10}
$$

and the coupling constants gain additional terms due to the new fermion as follows:

$$
\begin{aligned}
\frac{dg_1^2}{d\ln\mu^2} &= \frac{g_1^4}{16\pi^2}\left(\frac{41}{10}+\frac{98}{15}\right), \\
\frac{dg_2^2}{d\ln\mu^2} &= \frac{g_2^4}{16\pi^2}\left(-\frac{19}{6}+\frac{13}{6}\right), \\
\frac{dg_3^2}{d\ln\mu^2} &= \frac{g_3^4}{16\pi^2}\left(-7+\frac{4}{3}\right).
\end{aligned}
\tag{A.11}
$$

A.5   Non SM-like Doublet $\mathcal{D}_Y\ (B,Y),\ Y=-5/6$

The relevant RGE for the Yukawa couplings are

$$
\begin{aligned}
\frac{dy_t^2}{d\ln\mu^2} &= \frac{y_t^2}{16\pi^2}\left(\frac{9y_t^2}{2}+\frac{3y_B^2}{2}+\frac{9y_Y^2}{2}+\frac{y_M^2}{2}-\frac{17g_1^2}{20}-\frac{9g_2^2}{4}-8g_3^2\right), \\
\frac{dy_B^2}{d\ln\mu^2} &= \frac{y_T^2}{16\pi^2}\left(\frac{3y_t^2}{2}+\frac{9y_B^2}{2}+\frac{9y_Y^2}{2}+\frac{y_M^2}{2}-\frac{17g_1^2}{20}-\frac{9g_2^2}{4}-8g_3^2\right), \\
\frac{dy_Y^2}{d\ln\mu^2} &= \frac{y_Y^2}{16\pi^2}\left(\frac{9y_t^2}{2}+\frac{9y_Y^2}{2}+\frac{9y_B^2}{2}+\frac{y_M^2}{2}-2g_1^2-\frac{9g_2^2}{4}-8g_3^2\right), \\
\frac{dy_M^2}{d\ln\mu^2} &= \frac{y_M^2}{16\pi^2}\left(y_B^2+y_Y^2+\frac{9y_M^2}{2}-\frac{8g_1^2}{5}-8g_2^2\right).
\end{aligned}
\tag{A.12}
$$

The Higgs sector RGEs, describing the interactions between the two bosons are:

$$
\begin{aligned}
\frac{d\lambda_H}{d\ln\mu^2} &= \frac{1}{16\pi^2}\left[\lambda_H\left(12\lambda_H+6y_t^2+6y_B^2+6y_Y^2-\frac{9g_1^2}{10}-\frac{9g_2^2}{2}\right)+\frac{\lambda_{SH}^2}{4}\right. \\
&\quad\left. -\ 3y_t^4-3y_B^4-3y_Y^2+\frac{27g_1^4}{400}+\frac{9g_2^4}{16}+\frac{9g_1^2g_2^2}{40}\right], \\
\frac{d\lambda_S}{d\ln\mu^2} &= \frac{1}{16\pi^2}\left(9\lambda_S^2+\lambda_{SH}^2+12y_M^2\lambda_S-12y_M^4\right), \\
\frac{d\lambda_{SH}}{d\ln\mu^2} &= \frac{1}{16\pi^2}\left[\lambda_{SH}\left(2\lambda_{SH}+6\lambda_H+3\lambda_S+3y_t^2+3y_B^2+3y_Y^2+6y_M^2-\frac{9g_1^2}{20}-\frac{9g_2^2}{4}\right)\right. \\
&\quad\left. -\ 12y_B^2y_M^2-12y_Y^2y_M^2\right],
\end{aligned}
\tag{A.13}
$$

and the coupling constants gain additional terms due to the new fermion as follows:

$$
\begin{aligned}
\frac{dg_1^2}{d\ln\mu^2} &= \frac{g_1^4}{16\pi^2}\left(\frac{41}{10}+\frac{10}{3}\right), \\
\frac{dg_2^2}{d\ln\mu^2} &= \frac{g_2^4}{16\pi^2}\left(-\frac{19}{6}+\frac{13}{6}\right), \\
\frac{dg_3^2}{d\ln\mu^2} &= \frac{g_3^4}{16\pi^2}\left(-7+\frac{4}{3}\right).
\end{aligned}
\tag{A.14}
$$

A.6   Triplet $\mathcal{T}_X$ (X, T, B), $Y = 2/3$

The relevant RGE for the Yukawa couplings are

$$
\begin{aligned}
\frac{dy_t^2}{d\ln\mu^2} &= \frac{y_t^2}{16\pi^2}\left(\frac{9y_t^2}{2} + \frac{9y_T^2}{2} + \frac{9y_X^2}{2} + \frac{3y_B^2}{2} + \frac{y_M^2}{4} - \frac{17g_1^2}{20} - \frac{9g_2^2}{4} - 8g_3^2\right), \\
\frac{dy_T^2}{d\ln\mu^2} &= \frac{y_T^2}{16\pi^2}\left(\frac{9y_t^2}{2} + \frac{9y_X^2}{2} + \frac{9y_T^2}{2} + \frac{3y_B^2}{2} + \frac{y_M^2}{4} - \frac{17g_1^2}{20} - \frac{9g_2^2}{4} - 8g_3^2\right), \\
\frac{dy_X^2}{d\ln\mu^2} &= \frac{y_T^2}{16\pi^2}\left(\frac{9y_t^2}{2} + \frac{9y_X^2}{2} + \frac{9y_T^2}{2} + \frac{3y_B^2}{2} + \frac{y_M^2}{4} - \frac{41g_1^2}{20} - \frac{9g_2^2}{4} - 8g_3^2\right), \\
\frac{dy_B^2}{d\ln\mu^2} &= \frac{y_B^2}{16\pi^2}\left(\frac{3y_t^2}{2} + \frac{9y_B^2}{2} + \frac{9y_X^2}{2} + \frac{9y_T^2}{2} + \frac{y_M^2}{4} - \frac{17g_1^2}{20} - \frac{9g_2^2}{4} - 8g_3^2\right), \\
\frac{dy_M^2}{d\ln\mu^2} &= \frac{y_M^2}{16\pi^2}\left(y_T^2 + y_X^2 + y_B^2 + \frac{27y_M^2}{2} - \frac{8g_1^2}{5} - \frac{9g_2^2}{4} - 8g_3^2\right).
\end{aligned}
\tag{A.15}
$$

The Higgs sector RGEs, describing the interactions between the two bosons are:

$$
\begin{aligned}
\frac{d\lambda_H}{d\ln\mu^2} &= \frac{1}{16\pi^2}\left[\lambda_H\left(12\lambda_H + 6y_t^2 + 6y_T^2 + 6y_X^2 - \frac{9g_1^2}{5} - 9g_2^2\right) + \frac{\lambda_{SH}^2}{4}\right. \\
&\quad \left. - 3y_t^4 - 3y_T^4 - 3y_X^2 - 6y_t^2y_T^2 + \frac{27g_1^4}{200} + \frac{9g_2^4}{8} + \frac{18g_1^2g_2^2}{40}\right], \\
\frac{d\lambda_S}{d\ln\mu^2} &= \frac{1}{16\pi^2}\left(9\lambda_S^2 + \lambda_{SH}^2 + 12y_M^2\lambda_S - 12y_M^4\right), \\
\frac{d\lambda_{SH}}{d\ln\mu^2} &= \frac{1}{16\pi^2}\left[\lambda_{SH}\left(2\lambda_{SH} + 6\lambda_H + 3\lambda_S + 6y_t^2 + 6y_T^2 + 6y_X^2 + 6y_M^2 - \frac{9g_1^2}{10} - \frac{9g_2^2}{2}\right)\right. \\
&\quad \left. - 6y_T^2y_M^2 - 6y_B^2y_M^2 - 6y_X^2y_M^2\right],
\end{aligned}
\tag{A.16}
$$

and the coupling constants gain additional terms due to the new fermion as follows:

$$
\begin{aligned}
\frac{dg_1^2}{d\ln\mu^2} &= \frac{g_1^4}{16\pi^2}\left(\frac{41}{10} + \frac{4}{5}\right), \\
\frac{dg_2^2}{d\ln\mu^2} &= \frac{g_2^4}{16\pi^2}\left(-\frac{19}{6} + 8\right), \\
\frac{dg_3^2}{d\ln\mu^2} &= \frac{g_3^4}{16\pi^2}\left(-7 + 2\right).
\end{aligned}
\tag{A.17}
$$

A.7 Triplet $\mathcal{T}_Y$ (T, B, Y), $Y = -1/3$

The relevant RGE for the Yukawa couplings are

$$
\begin{aligned}
\frac{dy_t^2}{d\ln\mu^2} &= \frac{y_t^2}{16\pi^2}\left(\frac{3y_B^2}{2} + \frac{9y_t^2}{2} + \frac{9y_T^2}{2} + \frac{9y_Y^2}{2} + \frac{y_M^2}{2} - \frac{17g_1^2}{20} - \frac{9g_2^2}{4} - 8g_3^2\right), \\
\frac{dy_T^2}{d\ln\mu^2} &= \frac{y_T^2}{16\pi^2}\left(\frac{3y_B^2}{2} + \frac{9y_t^2}{2} + \frac{9y_Y^2}{2} + \frac{9y_T^2}{2} + \frac{y_M^2}{2} - \frac{17g_1^2}{20} - \frac{9g_2^2}{4} - 8g_3^2\right), \\
\frac{dy_B^2}{d\ln\mu^2} &= \frac{y_B^2}{16\pi^2}\left(\frac{3y_t^2}{2} + \frac{3y_T^2}{2} + \frac{9y_B^2}{2} + \frac{9y_Y^2}{2} + \frac{y_M^2}{4} - \frac{17g_1^2}{20} - \frac{9g_2^2}{4} - 8g_3^2\right), \\
\frac{dy_Y^2}{d\ln\mu^2} &= \frac{y_Y^2}{16\pi^2}\left(\frac{3y_t^2}{2} + \frac{9y_B^2}{2} + \frac{9y_Y^2}{2} + \frac{9y_T^2}{2} + \frac{y_M^2}{2} - \frac{17g_1^2}{20} - \frac{9g_2^2}{4} - 8g_3^2\right), \\
\frac{dy_M^2}{d\ln\mu^2} &= \frac{y_M^2}{16\pi^2}\left(y_T^2 + y_B^2 + y_Y^2 + \frac{15y_M^2}{2} - \frac{2g_1^2}{5} - 8g_3^2\right).
\end{aligned}
\tag{A.18}
$$

The Higgs sector RGEs, describing the interactions between the two bosons are:

$$
\begin{aligned}
\frac{d\lambda_H}{d\ln\mu^2} &= \frac{1}{16\pi^2}\left[\lambda_H\left(12\lambda_H + 6y_t^2 + 6y_B^2 + 6y_T^2 + 6y_Y^2 - \frac{9g_1^2}{5} - \frac{9g_2^2}{2}\right) + \frac{\lambda_{SH}^2}{4}\right. \\
&\quad \left. -\; 6y_t^4 - 6y_T^4 - 6y_Y^4 - 3y_B^2 - 6y_t^2y_T^2 + \frac{27g_1^4}{200} + \frac{9g_2^4}{8} + \frac{18g_1^2g_2^2}{40}\right], \\
\frac{d\lambda_S}{d\ln\mu^2} &= \frac{1}{16\pi^2}\left(9\lambda_S^2 + \lambda_{SH}^2 + 12y_M^2\lambda_S - 12y_M^4\right), \\
\frac{d\lambda_{SH}}{d\ln\mu^2} &= \frac{1}{16\pi^2}\left[\lambda_{SH}\left(2\lambda_{SH} + 6\lambda_H + 3\lambda_S + 6y_t^2 + 6y_T^2 + 6y_B^2 + 6y_Y^2 + 6y_M^2\right.\right. \\
&\quad \left.\left. -\; \frac{9g_1^2}{10} - \frac{9g_2^2}{2}\right) - 6y_T^2y_M^2 - 6y_Y^2y_M^2 - 6y_B^2y_M^2\right].
\end{aligned}
\tag{A.19}
$$

and the coupling constants gain additional terms due to the new fermion as follows:

$$
\begin{aligned}
\frac{dg_1^2}{d\ln\mu^2} &= \frac{g_1^4}{16\pi^2}\left(\frac{41}{10} + \frac{16}{5}\right), \\
\frac{dg_2^2}{d\ln\mu^2} &= \frac{g_2^4}{16\pi^2}\left(-\frac{19}{6} + 8\right), \\
\frac{dg_3^2}{d\ln\mu^2} &= \frac{g_3^4}{16\pi^2}\left(-7 + 2\right).
\end{aligned}
\tag{A.20}
$$

Appendix B

RGEs for Two Higgs Doublet Model + Vector-like Quarks

In the appendices below, for completeness, we give the renormalization group equations with respect to Type-I and Type-II models studied in the text.

B.1 RGEs for 2HDM + VLQ - Type I

B.1.1 Singlet $\mathcal{U}_1$ (T), $Y = 2/3$

The relevant RGE for the Yukawa couplings are

$$
\begin{aligned}
\frac{dy_t^2}{d\ln\mu^2} &= \frac{y_t^2}{16\pi^2}\left(\frac{9y_t^2}{2} + \frac{9y_T^2}{2} - \frac{17g_1^2}{12} - \frac{9g_2^2}{4} - 8g_3^2\right), \\
\frac{dy_T^2}{d\ln\mu^2} &= \frac{y_T^2}{16\pi^2}\left(\frac{9y_t^2}{2} + \frac{9y_T^2}{2} + \frac{3y_M^2}{2} - \frac{17g_1^2}{12} - \frac{9g_2^2}{4} - 8g_3^2\right), \\
\frac{dy_M^2}{d\ln\mu^2} &= \frac{y_M^2}{16\pi^2}\left(y_T^2 + \frac{9y_M^2}{2} - \frac{41g_1^2}{20} - 8g_3^2\right).
\end{aligned}
\tag{B.1}
$$

The Higgs sector RGEs, describing the interactions between the two bosons are

$$
\begin{aligned}
\frac{d\lambda_1}{d\ln\mu^2} &= \frac{1}{16\pi^2}\left[-4\lambda_1\left(\frac{3g_1^2}{4}+\frac{9g_2^2}{4}\right)+12\lambda_1^2+4\lambda_3^2+4\lambda_3\lambda_4+2\lambda_4^2+2\lambda_5^2\right.\\
&\quad+\left.\frac{3g_1^4}{4}+\frac{9g_2^4}{4}+\frac{3g_1^2g_2^2}{2}\right],\\
\frac{d\lambda_2}{d\ln\mu^2} &= \frac{1}{16\pi^2}\left[4\lambda_2\left(6y_t^2+6y_T^2-\frac{3g_1^2}{4}-\frac{9g_2^2}{4}\right)+12\lambda_2^2+4\lambda_3^2+4\lambda_3\lambda_4+2\lambda_4^2+2\lambda_5^2\right.\\
&\quad+\left.\frac{3g_1^4}{16}+\frac{9g_2^4}{4}+\frac{3g_1^2g_2^2}{2}-12y_t^4-24y_T^4-24y_t^2y_T^2\right],\\
\frac{d\lambda_3}{d\ln\mu^2} &= \frac{1}{16\pi^2}\left[2\lambda_3\left(6y_t^2+6y_T^2+12y_M^2-\frac{3g_1^2}{2}-\frac{9g_2^2}{2}\right)+4\lambda_3^2+2\lambda_4^2+2\lambda_5^2\right.\\
&\quad+\left.(\lambda_1+\lambda_2)(6\lambda_3+2\lambda_4)+\frac{3g_1^4}{4}+\frac{9g_2^4}{4}-\frac{3g_1^2g_2^2}{2}\right],\\
\frac{d\lambda_4}{d\ln\mu^2} &= \frac{1}{16\pi^2}\left[2\lambda_4\left(6y_t^2+6y_T^2+12y_M^2-\frac{3g_1^2}{2}-\frac{9g_2^2}{2}\right)+3g_1^2g_2^2\right.\\
&\quad+\left.4\lambda_4^2+8\lambda_5^2+8\lambda_3\lambda_4+2\lambda_4(\lambda_1+\lambda_2)\right],\\
\frac{d\lambda_5}{d\ln\mu^2} &= \frac{1}{16\pi^2}\left[2\lambda_5\left(6y_t^2+6y_T^2+12y_M^2-\frac{3g_1^2}{2}-\frac{9g_2^2}{2}\right)\right.\\
&\quad+\left.2\lambda_5(\lambda_1+\lambda_2+4\lambda_3+6\lambda_4)\right].
\end{aligned}
\tag{B.2}
$$

B.1.2 Singlet $\mathcal{D}_1$ (B), $Y=-1/3$

The relevant RGE for the Yukawa couplings are

$$
\begin{aligned}
\frac{dy_t^2}{d\ln\mu^2} &= \frac{y_t^2}{16\pi^2}\left(\frac{9y_t^2}{2}+\frac{3y_B^2}{2}-\frac{17g_1^2}{12}-\frac{9g_2^2}{4}-8g_3^2\right),\\
\frac{dy_B^2}{d\ln\mu^2} &= \frac{y_B^2}{16\pi^2}\left(\frac{3y_t^2}{2}+\frac{9y_B^2}{2}+\frac{3y_M^2}{2}-\frac{5g_1^2}{12}-\frac{9g_2^2}{4}-8g_3^2\right),\\
\frac{dy_M^2}{d\ln\mu^2} &= \frac{y_M^2}{16\pi^2}\left(\frac{9y_M^2}{2}+y_B^2-\frac{17g_1^2}{20}-8g_3^2\right).
\end{aligned}
\tag{B.3}
$$

The Higgs sector RGEs, describing the interactions between the two bosons are

$$
\begin{aligned}
\frac{d\lambda_1}{d\ln\mu^2} &= \frac{1}{16\pi^2}\left[-4\lambda_1\left(\frac{3g_1^2}{4}+\frac{9g_2^2}{4}\right)+12\lambda_1^2+4\lambda_3^2+4\lambda_3\lambda_4+2\lambda_4^2+2\lambda_5^2\right.\\
&\quad\left.+\ \frac{3g_1^4}{4}+\frac{9g_2^4}{4}+\frac{3g_1^2g_2^2}{2}\right],
\end{aligned}
$$

$$
\begin{aligned}
\frac{d\lambda_2}{d\ln\mu^2} &= \frac{1}{16\pi^2}\left[4\lambda_2\left(6y_t^2+6y_B^2-\frac{3g_1^2}{4}-\frac{9g_2^2}{4}\right)+12\lambda_2^2+4\lambda_3^2+4\lambda_3\lambda_4+2\lambda_4^2+2\lambda_5^2\right.\\
&\quad\left.+\ \frac{3g_1^4}{16}+\frac{9g_2^4}{4}+\frac{3g_1^2g_2^2}{2}-12y_t^4-24y_B^4\right],
\end{aligned}
$$

$$
\begin{aligned}
\frac{d\lambda_3}{d\ln\mu^2} &= \frac{1}{16\pi^2}\left[2\lambda_3\left(6y_t^2+6y_B^2+12y_M^2-\frac{3g_1^2}{2}-\frac{9g_2^2}{2}\right)+4\lambda_3^2+2\lambda_4^2+2\lambda_5^2\right.\\
&\quad\left.+\ (\lambda_1+\lambda_2)(6\lambda_3+2\lambda_4)+\frac{3g_1^4}{4}+\frac{9g_2^4}{4}-\frac{3g_1^2g_2^2}{2}\right],
\end{aligned}
$$

$$
\begin{aligned}
\frac{d\lambda_4}{d\ln\mu^2} &= \frac{1}{16\pi^2}\left[2\lambda_4\left(6y_t^2+6y_B^2+12y_M^2-\frac{3g_1^2}{2}-\frac{9g_2^2}{2}\right)+3g_1^2g_2^2\right.\\
&\quad\left.+\ 4\lambda_4^2+8\lambda_5^2+8\lambda_3\lambda_4+2\lambda_4(\lambda_1+\lambda_2)\right],
\end{aligned}
$$

$$
\begin{aligned}
\frac{d\lambda_5}{d\ln\mu^2} &= \frac{1}{16\pi^2}\left[2\lambda_5\left(6y_t^2+6y_B^2+12y_M^2-\frac{3g_1^2}{2}-\frac{9g_2^2}{2}\right)\right.\\
&\quad\left.+\ 2\lambda_5(\lambda_1+\lambda_2+4\lambda_3+6\lambda_4)\right]. \tag{B.4}
\end{aligned}
$$

Finally the coupling constants gain additional terms due to the new fermion, for both models $\mathcal{U}_1$, $\mathcal{D}_1$ with singlet fermions as follows:

$$
\begin{aligned}
\frac{dg_1^2}{d\ln\mu^2} &= \frac{g_1^4}{16\pi^2}\left(7+\frac{4}{15}\right),\\
\frac{dg_2^2}{d\ln\mu^2} &= \frac{g_2^4}{16\pi^2}\left(-3\right),\\
\frac{dg_3^2}{d\ln\mu^2} &= \frac{g_3^4}{16\pi^2}\left(-7+\frac{2}{3}\right). \tag{B.5}
\end{aligned}
$$

B.1.3 Doublet $\mathcal{D}_2$ (T,B), $Y=1/6$

The relevant RGE for the Yukawa couplings are

$$
\begin{aligned}
\frac{dy_t^2}{d\ln\mu^2} &= \frac{y_t^2}{16\pi^2}\left(\frac{9y_t^2}{2}+\frac{9y_T^2}{2}+\frac{3y_B^2}{2}+3y_M^2-\frac{17g_1^2}{12}-\frac{9g_2^2}{4}-8g_3^2\right),\\
\frac{dy_T^2}{d\ln\mu^2} &= \frac{y_T^2}{16\pi^2}\left(\frac{9y_t^2}{2}+\frac{9y_T^2}{2}+\frac{3y_B^2}{2}+3y_M^2-\frac{17g_1^2}{12}-\frac{9g_2^2}{4}-8g_3^2\right),\\
\frac{dy_B^2}{d\ln\mu^2} &= \frac{y_B^2}{16\pi^2}\left(\frac{9y_t^2}{2}+\frac{3y_T^2}{2}+\frac{9y_B^2}{2}+3y_M^2-\frac{5g_1^2}{12}-\frac{9g_2^2}{4}-8g_3^2\right),\\
\frac{dy_M^2}{d\ln\mu^2} &= \frac{y_M^2}{16\pi^2}\left(y_T^2+y_B^2+\frac{11y_M^2}{2}-\frac{19g_1^2}{40}-\frac{9g_2^2}{2}-8g_3^2\right). \tag{B.6}
\end{aligned}
$$

The Higgs sector RGEs, describing the interactions between the two bosons are

$$
\begin{aligned}
\frac{d\lambda_1}{d\ln\mu^2} &= \frac{1}{16\pi^2}\left[-4\lambda_1\left(\frac{3g_1^2}{4}+\frac{9g_2^2}{4}\right)+12\lambda_1^2+4\lambda_3^2+4\lambda_3\lambda_4+2\lambda_4^2+2\lambda_5^2\right.\\
&+\left.\frac{3g_1^4}{4}+\frac{9g_2^4}{4}+\frac{3g_1^2g_2^2}{2}\right],\\
\frac{d\lambda_2}{d\ln\mu^2} &= \frac{1}{16\pi^2}\left[4\lambda_2\left(3y_t^2+6y_T^2+6y_B^2-\frac{3g_1^2}{4}-\frac{9g_2^2}{4}\right)+12\lambda_2^2+4\lambda_3^2+4\lambda_3\lambda_4+2\lambda_4^2\right.\\
&+\left.2\lambda_5^2+\frac{3g_1^4}{4}+\frac{9g_2^4}{4}+\frac{3g_1^2g_2^2}{2}-12y_t^4-24y_T^4-24y_B^4-24y_t^2y_T^2-24y_T^2y_B^2\right],\\
\frac{d\lambda_3}{d\ln\mu^2} &= \frac{1}{16\pi^2}\left[2\lambda_3\left(3y_t^2+6y_T^2+6y_B^2+12y_M^2-\frac{3g_1^2}{2}-\frac{9g_2^2}{2}\right)+4\lambda_3^2+2\lambda_4^2+2\lambda_5^2\right.\\
&+\left.(\lambda_1+\lambda_2)(6\lambda_3+2\lambda_4)+\frac{3g_1^4}{4}+\frac{9g_2^4}{4}-\frac{3g_1^2g_2^2}{2}\right],\\
\frac{d\lambda_4}{d\ln\mu^2} &= \frac{1}{16\pi^2}\left[2\lambda_4\left(3y_t^2+6y_T^2+6y_B^2+12y_M^2-\frac{3g_1^2}{2}-\frac{9g_2^2}{2}\right)+3g_1^2g_2^2\right.\\
&+\left.4\lambda_4^2+8\lambda_5^2+8\lambda_3\lambda_4+2\lambda_4(\lambda_1+\lambda_2)\right],\\
\frac{d\lambda_5}{d\ln\mu^2} &= \frac{1}{16\pi^2}\left[2\lambda_5\left(3y_t^2+6y_T^2+6y_B^2+12y_M^2-\frac{3g_1^2}{2}-\frac{9g_2^2}{2}\right)\right.\\
&+\left.2\lambda_5(\lambda_1+\lambda_2+4\lambda_3+6\lambda_4)\right]. \tag{B.7}
\end{aligned}
$$

B.1.4 Non SM-like Doublet $\mathcal{D}_X$ (X,T), $Y=7/6$

The relevant RGE for the Yukawa couplings are

$$
\begin{aligned}
\frac{dy_t^2}{d\ln\mu^2} &= \frac{y_t^2}{16\pi^2}\left(\frac{9y_t^2}{2}+\frac{3y_T^2}{2}+\frac{9y_X^2}{2}+3y_M^2-\frac{17g_1^2}{12}-\frac{9g_2^2}{4}-8g_3^2\right),\\
\frac{dy_T^2}{d\ln\mu^2} &= \frac{y_T^2}{16\pi^2}\left(\frac{9y_t^2}{2}+\frac{3y_X^2}{2}+\frac{9y_T^2}{2}+3y_M^2-\frac{5g_1^2}{12}-\frac{9g_2^2}{4}-8g_3^2\right),\\
\frac{dy_X^2}{d\ln\mu^2} &= \frac{y_X^2}{16\pi^2}\left(\frac{9y_t^2}{2}+\frac{9y_X^2}{2}+\frac{3y_T^2}{2}+3y_M^2-\frac{17g_1^2}{12}-\frac{9g_2^2}{4}-8g_3^2\right),\\
\frac{dy_M^2}{d\ln\mu^2} &= \frac{y_M^2}{16\pi^2}\left(y_T^2+y_X^2+\frac{11y_M^2}{2}-\frac{67g_1^2}{40}-\frac{9g_2^2}{2}-8g_3^2\right). \tag{B.8}
\end{aligned}
$$

The Higgs sector RGEs, describing the interactions between the two bosons are

$$
\begin{aligned}
\frac{d\lambda_1}{d\ln\mu^2} &= \frac{1}{16\pi^2}\left[-4\lambda_1\left(\frac{3g_1^2}{4}+\frac{9g_2^2}{4}\right)+12\lambda_1^2+4\lambda_3^2+4\lambda_3\lambda_4+2\lambda_4^2+2\lambda_5^2\right.\\
&\quad\left.+\;\frac{3g_1^4}{4}+\frac{9g_2^4}{4}+\frac{3g_1^2 g_2^2}{2}\right],\\[2mm]
\frac{d\lambda_2}{d\ln\mu^2} &= \frac{1}{16\pi^2}\left[4\lambda_2\left(3y_t^2+6y_T^2+6y_X^2-\frac{3g_1^2}{4}-\frac{9g_2^2}{4}\right)+12\lambda_2^2+4\lambda_3^2+4\lambda_3\lambda_4+2\lambda_4^2\right.\\
&\quad\left.+\;2\lambda_5^2+\frac{3g_1^4}{4}+\frac{9g_2^4}{4}+\frac{3g_1^2 g_2^2}{2}-12y_t^4-24y_X^4-24y_T^4-24y_t^2 y_T^2-24y_X^2 y_T^2\right],\\[2mm]
\frac{d\lambda_3}{d\ln\mu^2} &= \frac{1}{16\pi^2}\left[2\lambda_3\left(3y_t^2+6y_T^2+6y_X^2+12y_M^2-\frac{3g_1^2}{2}-\frac{9g_2^2}{10}\right)+4\lambda_3^2+2\lambda_4^2+2\lambda_5^2\right.\\
&\quad\left.+\;(\lambda_1+\lambda_2)(6\lambda_3+2\lambda_4)+\frac{3g_1^4}{4}+\frac{9g_2^4}{4}-\frac{3g_1^2 g_2^2}{2}\right],\\[2mm]
\frac{d\lambda_4}{d\ln\mu^2} &= \frac{1}{16\pi^2}\left[2\lambda_4\left(3y_t^2+6y_T^2+6y_X^2+12y_M^2-\frac{3g_1^2}{2}-\frac{9g_2^2}{10}\right)+3g_1^2 g_2^2\right.\\
&\quad\left.+\;4\lambda_4^2+8\lambda_5^2+8\lambda_3\lambda_4+2\lambda_4(\lambda_1+\lambda_2)\right],\\[2mm]
\frac{d\lambda_5}{d\ln\mu^2} &= \frac{1}{16\pi^2}\left[2\lambda_5\left(3y_t^2+6y_T^2+6y_X^2+12y_M^2-\frac{3g_1^2}{2}-\frac{9g_2^2}{10}\right)\right.\\
&\quad\left.+\;2\lambda_5(\lambda_1+\lambda_2+4\lambda_3+6\lambda_4)\right]. \quad\quad\text{(B.9)}
\end{aligned}
$$

B.1.5 Non SM-like Doublet $\mathcal{D}_Y$ (B,Y), $Y=-5/6$

The relevant RGE for the Yukawa couplings are

$$
\begin{aligned}
\frac{dy_t^2}{d\ln\mu^2} &= \frac{y_t^2}{16\pi^2}\left(\frac{9y_t^2}{2}+\frac{9y_B^2}{2}+\frac{3y_Y^2}{2}+3y_M^2-\frac{17g_1^2}{12}-\frac{9g_2^2}{4}-8g_3^2\right),\\
\frac{dy_B^2}{d\ln\mu^2} &= \frac{y_T^2}{16\pi^2}\left(\frac{9y_t^2}{2}+\frac{9y_B^2}{2}+\frac{3y_Y^2}{2}+3y_M^2-\frac{17g_1^2}{12}-\frac{9g_2^2}{4}-8g_3^2\right),\\
\frac{dy_Y^2}{d\ln\mu^2} &= \frac{y_Y^2}{16\pi^2}\left(\frac{3y_t^2}{2}+\frac{9y_Y^2}{2}+\frac{3y_B^2}{2}+3y_M^2-\frac{5g_1^2}{12}-\frac{9g_2^2}{4}-8g_3^2\right),\\
\frac{dy_M^2}{d\ln\mu^2} &= \frac{y_M^2}{16\pi^2}\left(y_Y^2+y_B^2+\frac{11y_M^2}{2}-\frac{43g_1^2}{40}-\frac{9g_2^2}{2}-8g_3^2\right). \quad\quad\text{(B.10)}
\end{aligned}
$$

The Higgs sector RGEs, describing the interactions between the two bosons are:

$$
\begin{aligned}
\frac{d\lambda_1}{d\ln\mu^2} &= \frac{1}{16\pi^2}\left[-4\lambda_1\left(\frac{3g_1^2}{4}+\frac{9g_2^2}{4}\right)+12\lambda_1^2+4\lambda_3^2+4\lambda_3\lambda_4+2\lambda_4^2+2\lambda_5^2\right.\\
&\quad+\left.\frac{3g_1^4}{4}+\frac{9g_2^4}{4}+\frac{3g_1^2g_2^2}{2}\right],\\
\frac{d\lambda_2}{d\ln\mu^2} &= \frac{1}{16\pi^2}\left[4\lambda_2\left(3y_t^2+6y_B^2+6y_Y^2-\frac{3g_1^2}{4}-\frac{9g_2^2}{4}\right)+12\lambda_2^2+4\lambda_3^2+4\lambda_3\lambda_4+2\lambda_4^2\right.\\
&\quad+\left.2\lambda_5^2+\frac{3g_1^4}{4}+\frac{9g_2^4}{4}+\frac{3g_1^2g_2^2}{2}-12y_t^4-24y_B^4-24y_Y^4-24y_B^2y_Y^2\right],\\
\frac{d\lambda_3}{d\ln\mu^2} &= \frac{1}{16\pi^2}\left[2\lambda_3\left(3y_t^2+6y_B^2+6y_Y^2+12y_M^2-\frac{3g_1^2}{2}-\frac{9g_2^2}{2}\right)+4\lambda_3^2+2\lambda_4^2+2\lambda_5^2\right.\\
&\quad+\left.(\lambda_1+\lambda_2)(6\lambda_3+2\lambda_4)+\frac{3g_1^4}{4}+\frac{9g_2^4}{4}-\frac{3g_1^2g_2^2}{2}\right],\\
\frac{d\lambda_4}{d\ln\mu^2} &= \frac{1}{16\pi^2}\left[2\lambda_4\left(3y_t^2+6y_Y^2+6y_B^2+12y_M^2-\frac{3g_1^2}{2}-\frac{9g_2^2}{2}\right)+3g_1^2g_2^2\right.\\
&\quad+\left.4\lambda_4^2+8\lambda_5^2+8\lambda_3\lambda_4+2\lambda_4(\lambda_1+\lambda_2)\right],\\
\frac{d\lambda_5}{d\ln\mu^2} &= \frac{1}{16\pi^2}\left[2\lambda_5\left(3y_t^2+6y_Y^2+6y_B^2+12y_M^2-\frac{3g_1^2}{2}-\frac{9g_2^2}{10}\right)\right.\\
&\quad+\left.2\lambda_5(\lambda_1+\lambda_2+4\lambda_3+6\lambda_4)\right].
\end{aligned}
\tag{B.11}
$$

The coupling constants gain additional terms due to the new fermion in all doublet models as follows

$$
\begin{aligned}
\frac{dg_1^2}{d\ln\mu^2} &= \frac{g_1^4}{16\pi^2}\left(7+\frac{6}{5}\right),\\
\frac{dg_2^2}{d\ln\mu^2} &= \frac{g_2^4}{16\pi^2}\left(-3+2\right),\\
\frac{dg_3^2}{d\ln\mu^2} &= \frac{g_3^4}{16\pi^2}\left(-7+\frac{4}{3}\right).
\end{aligned}
\tag{B.12}
$$

B.1.6 Triplet $\mathcal{T}_X$ (X, T, B), $Y = 2/3$

The relevant RGE for the Yukawa couplings are

$$\frac{dy_t^2}{d\ln\mu^2} = \frac{y_t^2}{16\pi^2}\left(\frac{9y_t^2}{2} + \frac{9y_X^2}{2} + \frac{9y_T^2}{2} + \frac{3y_B^2}{2} + \frac{3y_M^2}{2} - \frac{17g_1^2}{12} - \frac{9g_2^2}{4} - 8g_3^2\right),$$

$$\frac{dy_T^2}{d\ln\mu^2} = \frac{y_T^2}{16\pi^2}\left(\frac{9y_t^2}{2} + \frac{9y_X^2}{2} + \frac{9y_T^2}{2} + \frac{3y_B^2}{2} + \frac{3y_M^2}{2} - \frac{17g_1^2}{12} - \frac{9g_2^2}{4} - 8g_3^2\right),$$

$$\frac{dy_X^2}{d\ln\mu^2} = \frac{y_T^2}{16\pi^2}\left(\frac{9y_t^2}{2} + \frac{9y_X^2}{2} + \frac{9y_T^2}{2} + \frac{3y_B^2}{2} + \frac{3y_M^2}{2} - \frac{41g_1^2}{20} - \frac{9g_2^2}{4} - 8g_3^2\right),$$

$$\frac{dy_B^2}{d\ln\mu^2} = \frac{y_B^2}{16\pi^2}\left(\frac{3y_t^2}{2} + \frac{3y_X^2}{2} + \frac{9y_T^2}{2} + \frac{9y_B^2}{2} + \frac{3y_M^2}{2} - \frac{5g_1^2}{12} - \frac{9g_2^2}{4} - 8g_3^2\right),$$

$$\frac{dy_M^2}{d\ln\mu^2} = \frac{y_M^2}{16\pi^2}\left(y_X^2 + y_T^2 + y_B^2 + \frac{15y_M^2}{2} - \frac{41g_1^2}{20} - \frac{9g_2^2}{4} - 8g_3^2\right). \tag{B.13}$$

The Higgs sector RGEs, describing the interactions between the two bosons are

$$\frac{d\lambda_1}{d\ln\mu^2} = \frac{1}{16\pi^2}\left[-4\lambda_1\left(\frac{3g_1^2}{4} + \frac{9g_2^2}{4}\right) + 12\lambda_1^2 + 4\lambda_3^2 + 4\lambda_3\lambda_4 + 2\lambda_4^2 + 2\lambda_5^2\right.$$
$$+ \left.\frac{3g_1^4}{4} + \frac{9g_2^4}{4} + \frac{3g_1^2 g_2^2}{2}\right],$$

$$\frac{d\lambda_2}{d\ln\mu^2} = \frac{1}{16\pi^2}\left[4\lambda_2\left(3y_t^2 + 6y_X^2 + 6y_T^2 + 6y_B^2 - \frac{3g_1^2}{2} - \frac{9g_2^2}{2}\right)\right.$$
$$+ 12\lambda_2^2 + 4\lambda_3^2 + 4\lambda_3\lambda_4 + 2\lambda_4^2 + 2\lambda_5^2 + \frac{3g_1^4}{2} + \frac{9g_2^2}{2} + 3g_1^2 g_2^2$$
$$- \left.12y_t^4 - 24y_X^4 - 24y_T^4 - 24y_B^4 - 24y_t^2 y_T^2 - 24y_T^2 y_B^2 - 24y_X^2 y_T^2\right],$$

$$\frac{d\lambda_3}{d\ln\mu^2} = \frac{1}{16\pi^2}\left[2\lambda_3\left(3y_t^2 + 6y_T^2 + 6y_X^2 + 6y_B^2 + 12y_M^2 - 3g_1^2 - 9g_2^2\right) + 4\lambda_3^2 + 2\lambda_4^2 + 2\lambda_5^2\right.$$
$$+ \left.(\lambda_1 + \lambda_2)(6\lambda_3 + 2\lambda_4) + \frac{3g_1^4}{2} + \frac{9g_2^4}{2} - 3g_1^2 g_2^2\right],$$

$$\frac{d\lambda_4}{d\ln\mu^2} = \frac{1}{16\pi^2}\left[2\lambda_4\left(3y_t^2 + 6y_X^2 + 6y_T^2 + 6y_B^2 + 12y_M^2 - 3g_1^2 - 9g_2^2\right) + 6g_1^2 g_2^2\right.$$
$$+ \left.4\lambda_4^2 + 8\lambda_5^2 + 8\lambda_3\lambda_4 + 2\lambda_4(\lambda_1 + \lambda_2)\right],$$

$$\frac{d\lambda_5}{d\ln\mu^2} = \frac{1}{16\pi^2}\left[2\lambda_5\left(3y_t^2 + 6y_T^2 + 6y_X^2 + 6y_B^2 + 12y_M^2 - 3g_1^2 - 9g_2^2\right)\right.$$
$$+ \left.2\lambda_5(\lambda_1 + \lambda_2 + 4\lambda_3 + 6\lambda_4)\right]. \tag{B.14}$$

B.1.7 Triplet $\mathcal{T}_Y$ (T, B, Y), $Y = -1/3$

The relevant RGE for the Yukawa couplings are

$$
\frac{dy_t^2}{d\ln\mu^2} = \frac{y_t^2}{16\pi^2}\left(\frac{9y_t^2}{2} + \frac{9y_T^2}{2} + \frac{3y_B^2}{2} + \frac{3y_Y^2}{2} + 3y_M^2 - \frac{17g_1^2}{12} - \frac{9g_2^2}{4} - 8g_3^2\right),
$$

$$
\frac{dy_T^2}{d\ln\mu^2} = \frac{y_T^2}{16\pi^2}\left(\frac{9y_t^2}{2} + \frac{9y_T^2}{2} + \frac{3y_B^2}{2} + \frac{3y_Y^2}{2} + 3y_M^2 - \frac{17g_1^2}{12} - \frac{9g_2^2}{4} - 8g_3^2\right),
$$

$$
\frac{dy_B^2}{d\ln\mu^2} = \frac{y_B^2}{16\pi^2}\left(\frac{3y_t^2}{2} + \frac{3y_T^2}{2} + \frac{9y_B^2}{2} + \frac{9y_Y^2}{2} + \frac{3y_M^2}{2} - \frac{5g_1^2}{12} - \frac{9g_2^2}{4} - 8g_3^2\right),
$$

$$
\frac{dy_Y^2}{d\ln\mu^2} = \frac{y_Y^2}{16\pi^2}\left(\frac{9y_Y^2}{2} + \frac{9y_B^2}{2} + \frac{3y_t^2}{2} + \frac{3y_T^2}{2} + 3y_M^2 - \frac{17g_1^2}{20} - \frac{9g_2^2}{4} - 8g_3^2\right),
$$

$$
\frac{dy_M^2}{d\ln\mu^2} = \frac{y_M^2}{16\pi^2}\left(y_T^2 + y_B^2 + y_Y^2 + \frac{15y_M^2}{2} - \frac{17g_1^2}{20} - \frac{9g_2^2}{4} - 8g_3^2\right). \tag{B.15}
$$

The Higgs sector RGEs, describing the interactions between the two bosons are

$$
\frac{d\lambda_1}{d\ln\mu^2} = \frac{1}{16\pi^2}\left[-4\lambda_1\left(\frac{3g_1^2}{4} + \frac{9g_2^2}{4}\right) + 12\lambda_1^2 + 4\lambda_3^2 + 4\lambda_3\lambda_4 + 2\lambda_4^2 + 2\lambda_5^2\right.
$$
$$
+ \left.\frac{3g_1^4}{4} + \frac{9g_2^4}{4} + \frac{3g_1^2g_2^2}{2}\right],
$$

$$
\frac{d\lambda_2}{d\ln\mu^2} = \frac{1}{16\pi^2}\left[4\lambda_2\left(3y_t^2 + 6y_T^2 + 6y_B^2 + 6y_Y^2 - \frac{3g_1^2}{2} - \frac{9g_2^2}{2}\right)\right.
$$
$$
+ 12\lambda_2^2 + 4\lambda_3^2 + 4\lambda_3\lambda_4 + 2\lambda_4^2 + 2\lambda_5^2 + \frac{3g_1^4}{2} + \frac{9g_2^4}{2} + 3g_1^2g_2^2
$$
$$
- \left.12y_t^4 - 24y_T^4 - 24y_B^4 - 24y_Y^4 - 24y_t^2y_T^2 - 24y_T^2y_B^2 - 24y_B^2y_Y^2\right],
$$

$$
\frac{d\lambda_3}{d\ln\mu^2} = \frac{1}{16\pi^2}\left[2\lambda_3\left(3y_t^2 + 6y_T^2 + 6y_B^2 + 6y_Y^2 + 12y_M^2 - 3g_1^2 - 9g_2^2\right) + 4\lambda_3^2 + 2\lambda_4^2 + 2\lambda_5^2\right.
$$
$$
+ \left.(\lambda_1 + \lambda_2)(6\lambda_3 + 2\lambda_4) + \frac{3g_1^4}{2} + \frac{9g_2^2}{4} - 3g_1^2g_2^2\right],
$$

$$
\frac{d\lambda_4}{d\ln\mu^2} = \frac{1}{16\pi^2}\left[2\lambda_4\left(3y_t^2 + 6y_T^2 + 6y_B^2 + 6y_Y^2 + 12y_M^2 - 3g_1^2 - 9g_2^2\right) + 6g_1^2g_2^2\right.
$$
$$
+ \left.4\lambda_4^2 + 8\lambda_5^2 + 8\lambda_3\lambda_4 + 2\lambda_4(\lambda_1 + \lambda_2)\right],
$$

$$
\frac{d\lambda_5}{d\ln\mu^2} = \frac{1}{16\pi^2}\left[2\lambda_5\left(3y_t^2 + 6y_T^2 + 6y_B^2 + 6y_Y^2 + 12y_M^2 - 3g_1^2 - 9g_2^2\right)\right.
$$
$$
+ \left.2\lambda_5(\lambda_1 + \lambda_2 + 4\lambda_3 + 6\lambda_4)\right]. \tag{B.16}
$$

The coupling constants gain additional terms due to the new fermions in both triplet models as follows

$$
\frac{dg_1^2}{d\ln\mu^2} = \frac{g_1^4}{16\pi^2}\left(7 + \frac{4}{5}\right),
$$

$$
\frac{dg_2^2}{d\ln\mu^2} = \frac{g_2^4}{16\pi^2}\left(-3 + 4\right),
$$

$$
\frac{dg_3^2}{d\ln\mu^2} = \frac{g_3^4}{16\pi^2}\left(-7 + 2\right). \tag{B.17}
$$

B.2 RGEs for 2HDM + VLQ - Type II

B.2.1 Singlet $\mathcal{U}_1$ (T), $Y = 2/3$

The relevant RGE for the Yukawa couplings are

$$\frac{dy_t^2}{d\ln\mu^2} = \frac{y_t^2}{16\pi^2}\left(\frac{9y_t^2}{2} + \frac{9y_T^2}{2} - \frac{17g_1^2}{12} - \frac{9g_2^2}{4} - 8g_3^2\right),$$

$$\frac{dy_T^2}{d\ln\mu^2} = \frac{y_T^2}{16\pi^2}\left(\frac{9y_t^2}{2} + \frac{9y_T^2}{2} + \frac{3y_M^2}{2} - \frac{17g_1^2}{12} - \frac{9g_2^2}{4} - 8g_3^2\right),$$

$$\frac{dy_M^2}{d\ln\mu^2} = \frac{y_M^2}{16\pi^2}\left(y_T^2 + \frac{9y_M^2}{2} - \frac{41g_1^2}{20} - 8g_3^2\right). \tag{B.18}$$

The Higgs sector RGEs, describing the interactions between the two bosons are

$$\frac{d\lambda_1}{d\ln\mu^2} = \frac{1}{16\pi^2}\left[-4\lambda_1\left(\frac{3g_1^2}{4} + \frac{9g_2^2}{4}\right) + 12\lambda_1^2 + 4\lambda_3^2 + 4\lambda_3\lambda_4 + 2\lambda_4^2 + 2\lambda_5^2\right.$$
$$+ \left.\frac{3g_1^4}{16} + \frac{9g_2^4}{4} + \frac{3g_1^2g_2^2}{2}\right],$$

$$\frac{d\lambda_2}{d\ln\mu^2} = \frac{1}{16\pi^2}\left[4\lambda_2\left(3y_t^2 + 6y_T^2 - \frac{3g_1^2}{4} - \frac{9g_2^2}{4}\right) + 12\lambda_2^2 + 4\lambda_3^2 + 4\lambda_3\lambda_4 + 2\lambda_4^2 + 2\lambda_5^2\right.$$
$$+ \left.\frac{3g_1^4}{16} + \frac{9g_2^4}{4} + \frac{3g_1^2g_2^2}{2} - 12y_t^4 - 24y_T^4 - 24y_M^4 - 24y_t^2y_T^2\right],$$

$$\frac{d\lambda_3}{d\ln\mu^2} = \frac{1}{16\pi^2}\left[2\lambda_3\left(3y_t^2 + 6y_T^2 + 6y_M^2 - \frac{3g_1^2}{2} - \frac{9g_2^2}{2}\right) + 4\lambda_3^2 + 2\lambda_4^2 + 2\lambda_5^2\right.$$
$$+ \left.(\lambda_1 + \lambda_2)(6\lambda_3 + 2\lambda_4) + \frac{3g_1^4}{4} + \frac{9g_2^4}{4} - \frac{3g_1^2g_2^2}{2} - 24y_T^2y_M^2\right],$$

$$\frac{d\lambda_4}{d\ln\mu^2} = \frac{1}{16\pi^2}\left[2\lambda_4\left(3y_t^2 + 6y_T^2 + 6y_M^2 - \frac{3g_1^2}{2} - \frac{9g_2^2}{2}\right) + 3g_1^2g_2^2\right.$$
$$+ \left.4\lambda_4^2 + 8\lambda_5^2 + 8\lambda_3\lambda_4 + 2\lambda_4(\lambda_1 + \lambda_2) + 24y_T^2y_M^2\right],$$

$$\frac{d\lambda_5}{d\ln\mu^2} = \frac{1}{16\pi^2}\left[2\lambda_5\left(3y_t^2 + 6y_T^2 + 6y_M^2 - \frac{3g_1^2}{2} - \frac{9g_2^2}{2}\right)\right.$$
$$+ \left.2\lambda_5(\lambda_1 + \lambda_2 + 4\lambda_3 + 6\lambda_4)\right]. \tag{B.19}$$

B.2.2 Singlet $\mathcal{D}_1$ (B), $Y = -1/3$

The relevant RGE for the Yukawa couplings are

$$\frac{dy_t^2}{d\ln\mu^2} = \frac{y_t^2}{16\pi^2}\left(\frac{9y_t^2}{2} + \frac{y_B^2}{2} - \frac{17g_1^2}{12} - \frac{9g_2^2}{4} - 8g_3^2\right),$$

$$\frac{dy_B^2}{d\ln\mu^2} = \frac{y_B^2}{16\pi^2}\left(\frac{y_t^2}{2} + \frac{9y_B^2}{2} + \frac{3y_M^2}{2} - \frac{5g_1^2}{12} - \frac{9g_2^2}{4} - 8g_3^2\right),$$

$$\frac{dy_M^2}{d\ln\mu^2} = \frac{y_M^2}{16\pi^2}\left(\frac{9y_M^2}{2} + y_B^2 - \frac{17g_1^2}{20} - 8g_3^2\right). \tag{B.20}$$

The Higgs sector RGEs, describing the interactions between the two bosons are

$$
\begin{aligned}
\frac{d\lambda_1}{d\ln\mu^2} &= \frac{1}{16\pi^2}\left[-4\lambda_1\left(\frac{3g_1^2}{4}+\frac{9g_2^2}{4}-6y_B^2\right)+12\lambda_1^2+4\lambda_3^2+4\lambda_3\lambda_4+2\lambda_4^2+2\lambda_5^2\right.\\
&\quad + \left.\frac{3g_1^4}{16}+\frac{9g_2^4}{4}+\frac{3g_1^2g_2^2}{2}-24y_B^4-24y_M^4\right],\\
\frac{d\lambda_2}{d\ln\mu^2} &= \frac{1}{16\pi^2}\left[4\lambda_2\left(3y_t^2-\frac{3g_1^2}{4}-\frac{9g_2^2}{4}\right)+12\lambda_2^2+4\lambda_3^2+4\lambda_3\lambda_4+2\lambda_4^2+2\lambda_5^2\right.\\
&\quad + \left.\frac{3g_1^4}{16}+\frac{9g_2^4}{4}+\frac{3g_1^2g_2^2}{2}-12y_t^4\right],\\
\frac{d\lambda_3}{d\ln\mu^2} &= \frac{1}{16\pi^2}\left[2\lambda_3\left(3y_t^2+6y_B^2+6y_M^2-\frac{3g_1^2}{2}-\frac{9g_2^2}{2}\right)+4\lambda_3^2+2\lambda_4^2+2\lambda_5^2\right.\\
&\quad + \left.(\lambda_1+\lambda_2)(6\lambda_3+2\lambda_4)+\frac{3g_1^4}{4}+\frac{9g_2^4}{4}-\frac{3g_1^2g_2^2}{2}-24y_B^2y_M^2\right],\\
\frac{d\lambda_4}{d\ln\mu^2} &= \frac{1}{16\pi^2}\left[2\lambda_4\left(3y_t^2+6y_B^2+6y_M^2-\frac{3g_1^2}{2}-\frac{9g_2^2}{2}\right)+3g_1^2g_2^2\right.\\
&\quad + \left.4\lambda_4^2+8\lambda_5^2+8\lambda_3\lambda_4+2\lambda_4(\lambda_1+\lambda_2)+24y_B^2y_M^2\right],\\
\frac{d\lambda_5}{d\ln\mu^2} &= \frac{1}{16\pi^2}\left[2\lambda_5\left(3y_t^2+6y_B^2+6y_M^2-\frac{3g_1^2}{2}-\frac{9g_2^2}{2}\right)\right.\\
&\quad + \left.2\lambda_5(\lambda_1+\lambda_2+4\lambda_3+6\lambda_4)\right].
\end{aligned}
\tag{B.21}
$$

Finally the coupling constants gain additional terms due to the new fermion, for both models $\mathcal{U}_1$, $\mathcal{D}_1$ with singlet fermions as follows

$$
\begin{aligned}
\frac{dg_1^2}{d\ln\mu^2} &= \frac{g_1^4}{16\pi^2}\left(7+\frac{4}{15}\right),\\
\frac{dg_2^2}{d\ln\mu^2} &= \frac{g_2^4}{16\pi^2}(-3),\\
\frac{dg_3^2}{d\ln\mu^2} &= \frac{g_3^4}{16\pi^2}\left(-7+\frac{2}{3}\right).
\end{aligned}
\tag{B.22}
$$

B.2.3 Doublet $\mathcal{D}_2$ (T,B), $Y=1/6$

The relevant RGE for the Yukawa couplings are

$$
\begin{aligned}
\frac{dy_t^2}{d\ln\mu^2} &= \frac{y_t^2}{16\pi^2}\left(\frac{9y_t^2}{2}+\frac{9y_T^2}{2}+\frac{y_B^2}{2}+3y_M^2-\frac{17g_1^2}{12}-\frac{9g_2^2}{4}-8g_3^2\right),\\
\frac{dy_T^2}{d\ln\mu^2} &= \frac{y_T^2}{16\pi^2}\left(\frac{9y_t^2}{2}+\frac{9y_T^2}{2}+\frac{y_B^2}{2}+3y_M^2-\frac{17g_1^2}{12}-\frac{9g_2^2}{4}-8g_3^2\right),\\
\frac{dy_B^2}{d\ln\mu^2} &= \frac{y_B^2}{16\pi^2}\left(\frac{3y_t^2}{2}+\frac{y_T^2}{2}+\frac{9y_B^2}{2}+3y_M^2-\frac{5g_1^2}{12}-\frac{9g_2^2}{4}-8g_3^2\right),\\
\frac{dy_M^2}{d\ln\mu^2} &= \frac{y_M^2}{16\pi^2}\left(y_T^2+y_B^2+\frac{11y_M^2}{2}-\frac{19g_1^2}{40}-\frac{9g_2^2}{2}-8g_3^2\right).
\end{aligned}
\tag{B.23}
$$

152

The Higgs sector RGEs, describing the interactions between the two bosons are

$$
\begin{aligned}
\frac{d\lambda_1}{d\ln\mu^2} &= \frac{1}{16\pi^2}\left[4\lambda_1\left(6y_B^2 - \frac{3g_1^2}{4} - \frac{9g_2^2}{4}\right) + 12\lambda_1^2 + 4\lambda_3^2 + 4\lambda_3\lambda_4 + 2\lambda_4^2 + 2\lambda_5^2 \right.\\
&\quad + \left.\frac{3g_1^4}{4} + \frac{9g_2^4}{4} + \frac{3g_1^2 g_2^2}{2} - 24y_B^4 - 24y_B^2 y_M^2\right],
\end{aligned}
$$

$$
\begin{aligned}
\frac{d\lambda_2}{d\ln\mu^2} &= \frac{1}{16\pi^2}\left[4\lambda_2\left(3y_t^2 + 6y_T^2 - \frac{3g_1^2}{4} - \frac{9g_2^2}{4}\right) + 12\lambda_2^2 + 4\lambda_3^2 + 4\lambda_3\lambda_4 + 2\lambda_4^2 + 2\lambda_5^2 \right.\\
&\quad + \left.\frac{3g_1^4}{4} + \frac{9g_2^4}{4} + \frac{3g_1^2 g_2^2}{2} - 12y_t^4 - 24y_T^4 - 24y_t^2 y_T^2 - 24y_T^2 y_M^2\right],
\end{aligned}
$$

$$
\begin{aligned}
\frac{d\lambda_3}{d\ln\mu^2} &= \frac{1}{16\pi^2}\left[2\lambda_3\left(3y_t^2 + 6y_T^2 + 6y_B^2 + 6y_M^2 - \frac{3g_1^2}{2} - \frac{9g_2^2}{2}\right) + 4\lambda_3^2 + 2\lambda_4^2 + 2\lambda_5^2 \right.\\
&\quad + \left.(\lambda_1 + \lambda_2)(6\lambda_3 + 2\lambda_4) + \frac{3g_1^4}{4} + \frac{9g_2^4}{4} - \frac{3g_1^2 g_2^2}{2} - 24y_T^2 y_M^2 - 24y_B^2 y_M^2\right],
\end{aligned}
$$

$$
\begin{aligned}
\frac{d\lambda_4}{d\ln\mu^2} &= \frac{1}{16\pi^2}\left[2\lambda_4\left(3y_t^2 + 6y_T^2 + 6y_B^2 + 6y_M^2 - \frac{3g_1^2}{2} - \frac{9g_2^2}{2}\right) + 3g_1^2 g_2^2 \right.\\
&\quad + \left.4\lambda_4^2 + 8\lambda_5^2 + 8\lambda_3\lambda_4 + 2\lambda_4(\lambda_1 + \lambda_2) + 24y_T^2 y_M^2 + 24y_B^2 y_M^2\right],
\end{aligned}
$$

$$
\begin{aligned}
\frac{d\lambda_5}{d\ln\mu^2} &= \frac{1}{16\pi^2}\left[2\lambda_5\left(3y_t^2 + 6y_T^2 + 6y_B^2 + 12y_M^2 - \frac{3g_1^2}{2} - \frac{9g_2^2}{2}\right)\right.\\
&\quad + \left.2\lambda_5(\lambda_1 + \lambda_2 + 4\lambda_3 + 6\lambda_4)\right].
\end{aligned} \tag{B.24}
$$

B.2.4 Non SM-like Doublet $\mathcal{D}_X$ (X,T), $Y = 7/6$

The relevant RGE for the Yukawa couplings are

$$
\begin{aligned}
\frac{dy_t^2}{d\ln\mu^2} &= \frac{y_t^2}{16\pi^2}\left(\frac{9y_t^2}{2} + \frac{y_T^2}{2} + \frac{9y_X^2}{2} + 3y_M^2 - \frac{17g_1^2}{12} - \frac{9g_2^2}{4} - 8g_3^2\right),\\
\frac{dy_T^2}{d\ln\mu^2} &= \frac{y_T^2}{16\pi^2}\left(\frac{3y_t^2}{2} + \frac{y_X^2}{2} + \frac{9y_T^2}{2} + 3y_M^2 - \frac{5g_1^2}{12} - \frac{9g_2^2}{4} - 8g_3^2\right),\\
\frac{dy_X^2}{d\ln\mu^2} &= \frac{y_X^2}{16\pi^2}\left(\frac{9y_t^2}{2} + \frac{9y_X^2}{2} + \frac{y_T^2}{2} + 3y_M^2 - \frac{17g_1^2}{12} - \frac{9g_2^2}{4} - 8g_3^2\right),\\
\frac{dy_M^2}{d\ln\mu^2} &= \frac{y_M^2}{16\pi^2}\left(y_T^2 + y_X^2 + \frac{11y_M^2}{2} - \frac{67g_1^2}{40} - \frac{9g_2^2}{2} - 8g_3^2\right).
\end{aligned} \tag{B.25}
$$

The Higgs sector RGEs, describing the interactions between the two bosons are

$$
\begin{aligned}
\frac{d\lambda_1}{d\ln\mu^2} &= \frac{1}{16\pi^2}\left[4\lambda_1\left(6y_T^2 - \frac{3g_1^2}{4} - \frac{9g_2^2}{2}\right) + 12\lambda_1^2 + 4\lambda_3^2 + 4\lambda_3\lambda_4 + 2\lambda_4^2 + 2\lambda_5^2\right.\\
&\quad + \left.\frac{3g_1^4}{4} + \frac{9g_2^4}{4} + \frac{3g_1^2 g_2^2}{2} - 24y_T^4 - 24y_T^2 y_M^2\right],\\[4pt]
\frac{d\lambda_2}{d\ln\mu^2} &= \frac{1}{16\pi^2}\left[4\lambda_2\left(3y_t^2 + 6y_X^2 - \frac{3g_1^2}{4} - \frac{9g_2^2}{4}\right) + 12\lambda_2^2 + 4\lambda_3^2 + 4\lambda_3\lambda_4 + 2\lambda_4^2 + 2\lambda_5^2\right.\\
&\quad + \left.\frac{3g_1^4}{4} + \frac{9g_2^4}{4} + \frac{3g_1^2 g_2^2}{2} - 12y_t^4 - 24y_X^4 - 24y_X^2 y_M^2\right],\\[4pt]
\frac{d\lambda_3}{d\ln\mu^2} &= \frac{1}{16\pi^2}\left[2\lambda_3\left(3y_t^2 + 6y_T^2 + 6y_X^2 + 6y_M^2 - \frac{3g_1^2}{2} - \frac{9g_2^2}{10}\right) + 4\lambda_3^2 + 2\lambda_4^2 + 2\lambda_5^2\right.\\
&\quad + \left.(\lambda_1 + \lambda_2)(6\lambda_3 + 2\lambda_4) + \frac{3g_1^4}{4} + \frac{9g_2^4}{4} - \frac{3g_1^2 g_2^2}{2} - 24y_X^2 y_M^2 - 24y_T^2 y_M^2\right],\\[4pt]
\frac{d\lambda_4}{d\ln\mu^2} &= \frac{1}{16\pi^2}\left[2\lambda_4\left(3y_t^2 + 6y_T^2 + 6y_X^2 + 6y_M^2 - \frac{3g_1^2}{2} - \frac{9g_2^2}{10}\right) + 3g_1^2 g_2^2\right.\\
&\quad + \left.4\lambda_4^2 + 8\lambda_5^2 + 8\lambda_3\lambda_4 + 2\lambda_4(\lambda_1 + \lambda_2) + 24y_X^2 y_M^2 + 24y_T^2 y_M^2\right],\\[4pt]
\frac{d\lambda_5}{d\ln\mu^2} &= \frac{1}{16\pi^2}\left[2\lambda_5\left(3y_t^2 + 6y_T^2 + 6y_X^2 + 6y_M^2 - \frac{3g_1^2}{2} - \frac{9g_2^2}{10}\right)\right.\\
&\quad + \left.2\lambda_5(\lambda_1 + \lambda_2 + 4\lambda_3 + 6\lambda_4)\right]. \tag{B.26}
\end{aligned}
$$

B.2.5 Non SM-like quark doublet $\mathcal{D}_Y$ (B, Y), $Y = -5/6$

The relevant RGE for the Yukawa couplings are

$$
\begin{aligned}
\frac{dy_t^2}{d\ln\mu^2} &= \frac{y_t^2}{16\pi^2}\left(\frac{9y_t^2}{2} + \frac{3y_B^2}{2} + \frac{y_Y^2}{2} + 3y_M^2 - \frac{17g_1^2}{12} - \frac{9g_2^2}{4} - 8g_3^2\right),\\[4pt]
\frac{dy_B^2}{d\ln\mu^2} &= \frac{y_T^2}{16\pi^2}\left(\frac{3y_t^2}{2} + \frac{9y_B^2}{2} + \frac{y_Y^2}{2} + 3y_M^2 - \frac{17g_1^2}{12} - \frac{9g_2^2}{4} - 8g_3^2\right),\\[4pt]
\frac{dy_Y^2}{d\ln\mu^2} &= \frac{y_Y^2}{16\pi^2}\left(\frac{3y_t^2}{2} + \frac{9y_Y^2}{2} + \frac{y_B^2}{2} + 3y_M^2 - \frac{5g_1^2}{12} - \frac{9g_2^2}{4} - 8g_3^2\right),\\[4pt]
\frac{dy_M^2}{d\ln\mu^2} &= \frac{y_M^2}{16\pi^2}\left(y_Y^2 + y_B^2 + \frac{11y_M^2}{2} - \frac{43g_1^2}{40} - \frac{9g_2^2}{2} - 8g_3^2\right). \tag{B.27}
\end{aligned}
$$

The Higgs sector RGEs, describing the interactions between the two bosons are

$$
\begin{aligned}
\frac{d\lambda_1}{d\ln\mu^2} &= \frac{1}{16\pi^2}\left[4\lambda_1\left(6y_Y^2 - \frac{3g_1^2}{4} - \frac{9g_2^2}{4}\right) + 12\lambda_1^2 + 4\lambda_3^2 + 4\lambda_3\lambda_4 + 2\lambda_4^2 + 2\lambda_5^2\right.\\
&\quad + \left.\frac{3g_1^4}{4} + \frac{9g_2^4}{4} + \frac{3g_1^2g_2^2}{2} - 24y_Y^4 - 24y_Y^2 y_M^2\right],\\[2mm]
\frac{d\lambda_2}{d\ln\mu^2} &= \frac{1}{16\pi^2}\left[4\lambda_2\left(3y_t^2 + 6y_B^2 - \frac{3g_1^2}{4} - \frac{9g_2^2}{4}\right) + 12\lambda_2^2 + 4\lambda_3^2 + 4\lambda_3\lambda_4 + 2\lambda_4^2 + 2\lambda_5^2\right.\\
&\quad + \left.\frac{3g_1^4}{4} + \frac{9g_2^4}{4} + \frac{3g_1^2g_2^2}{2} - 12y_t^4 - 24y_B^4 - 24y_B^2 y_M^2\right],\\[2mm]
\frac{d\lambda_3}{d\ln\mu^2} &= \frac{1}{16\pi^2}\left[2\lambda_3\left(3y_t^2 + 6y_B^2 + 6y_Y^2 + 6y_M^2 - \frac{3g_1^2}{2} - \frac{9g_2^2}{2}\right) + 4\lambda_3^2 + 2\lambda_4^2 + 2\lambda_5^2\right.\\
&\quad + \left.(\lambda_1 + \lambda_2)(6\lambda_3 + 2\lambda_4) + \frac{3g_1^4}{4} + \frac{9g_2^4}{4} - \frac{3g_1^2g_2^2}{2} - 24y_B^2 y_M^2 - 24y_Y^2 y_M^2\right],\\[2mm]
\frac{d\lambda_4}{d\ln\mu^2} &= \frac{1}{16\pi^2}\left[2\lambda_4\left(3y_t^2 + 6y_Y^2 + 6y_B^2 + 6y_M^2 - \frac{3g_1^2}{2} - \frac{9g_2^2}{2}\right) + 3g_1^2g_2^2\right.\\
&\quad + \left.4\lambda_4^2 + 8\lambda_5^2 + 8\lambda_3\lambda_4 + 2\lambda_4(\lambda_1 + \lambda_2) + 24y_B^2 y_M^2 + 24y_Y^2 y_M^2\right],\\[2mm]
\frac{d\lambda_5}{d\ln\mu^2} &= \frac{1}{16\pi^2}\left[2\lambda_5\left(3y_t^2 + 6y_Y^2 + 6y_B^2 + 6y_M^2 - \frac{3g_1^2}{2} - \frac{9g_2^2}{2}\right)\right.\\
&\quad + \left.2\lambda_5(\lambda_1 + \lambda_2 + 4\lambda_3 + 6\lambda_4)\right]. \tag{B.28}
\end{aligned}
$$

The coupling constants gain additional terms due to the new fermion in all doublet models as follows:

$$
\begin{aligned}
\frac{dg_1^2}{d\ln\mu^2} &= \frac{g_1^4}{16\pi^2}\left(7 + \frac{6}{5}\right),\\
\frac{dg_2^2}{d\ln\mu^2} &= \frac{g_2^4}{16\pi^2}\left(-3 + 2\right),\\
\frac{dg_3^2}{d\ln\mu^2} &= \frac{g_3^4}{16\pi^2}\left(-7 + \frac{4}{3}\right). \tag{B.29}
\end{aligned}
$$

B.2.6 Triplet $\mathcal{T}_X$ (X, T, B), $Y = 2/3$

The relevant RGE for the Yukawa couplings are

$$
\frac{dy_t^2}{d\ln\mu^2} = \frac{y_t^2}{16\pi^2}\left(\frac{9y_t^2}{2} + \frac{9y_X^2}{2} + \frac{9y_T^2}{2} + \frac{y_B^2}{2} + \frac{3y_M^2}{2} - \frac{17g_1^2}{12} - \frac{9g_2^2}{4} - 8g_3^2\right),
$$

$$
\frac{dy_T^2}{d\ln\mu^2} = \frac{y_T^2}{16\pi^2}\left(\frac{9y_t^2}{2} + \frac{9y_X^2}{2} + \frac{9y_T^2}{2} + \frac{y_B^2}{2} + \frac{3y_M^2}{2} - \frac{17g_1^2}{12} - \frac{9g_2^2}{4} - 8g_3^2\right),
$$

$$
\frac{dy_X^2}{d\ln\mu^2} = \frac{y_T^2}{16\pi^2}\left(\frac{9y_t^2}{2} + \frac{9y_X^2}{2} + \frac{9y_T^2}{2} + \frac{y_B^2}{2} + \frac{3y_M^2}{2} - \frac{41g_1^2}{20} - \frac{9g_2^2}{4} - 8g_3^2\right),
$$

$$
\frac{dy_B^2}{d\ln\mu^2} = \frac{y_B^2}{16\pi^2}\left(\frac{3y_t^2}{2} + \frac{y_X^2}{2} + \frac{3y_T^2}{2} + \frac{9y_B^2}{2} + \frac{3y_M^2}{2} - \frac{5g_1^2}{12} - \frac{9g_2^2}{4} - 8g_3^2\right),
$$

$$
\frac{dy_M^2}{d\ln\mu^2} = \frac{y_M^2}{16\pi^2}\left(y_X^2 + y_T^2 + y_B^2 + \frac{15y_M^2}{2} - \frac{41g_1^2}{20} - \frac{9g_2^2}{4} - 8g_3^2\right). \tag{B.30}
$$

The Higgs sector RGEs, describing the interactions between the two bosons are

$$
\frac{d\lambda_1}{d\ln\mu^2} = \frac{1}{16\pi^2}\left[4\lambda_1\left(6y_B^2 + 6y_T^2 - \frac{3g_1^2}{2} - \frac{9g_2^2}{2}\right) + 12\lambda_1^2 + 4\lambda_3^2 + 4\lambda_3\lambda_4 + 2\lambda_4^2 + 2\lambda_5^2 \right.
$$
$$
\left. + \frac{3g_1^4}{2} + \frac{9g_2^4}{2} + 3g_1^2g_2^2 - 24y_B^4 - 24y_T^4 - 24y_B^2y_M^2 - 24y_T^2y_M^2\right],
$$

$$
\frac{d\lambda_2}{d\ln\mu^2} = \frac{1}{16\pi^2}\left[4\lambda_2\left(3y_t^2 + 6y_X^2 + 6y_T^2 - \frac{3g_1^2}{2} - \frac{9g_2^2}{2}\right) + 12\lambda_2^2 + 4\lambda_3^2 + 4\lambda_3\lambda_4 + 2\lambda_4^2 + 2\lambda_5^2 \right.
$$
$$
\left. + \frac{3g_1^4}{2} + \frac{9g_2^2}{2} + 3g_1^2g_2^2 - 12y_t^4 - 24y_X^4 - 24y_T^4 - 24y_t^2y_T^2 - 24y_X^2y_M^2 - 24y_T^2y_M^2\right],
$$

$$
\frac{d\lambda_3}{d\ln\mu^2} = \frac{1}{16\pi^2}\left[2\lambda_3\left(3y_t^2 + 6y_T^2 + 6y_X^2 + 6y_B^2 + 6y_M^2 - 3g_1^2 - 9g_2^2\right) + 4\lambda_3^2 + 2\lambda_4^2 + 2\lambda_5^2 \right.
$$
$$
\left. + (\lambda_1 + \lambda_2)(6\lambda_3 + 2\lambda_4) + \frac{3g_1^4}{2} + \frac{9g_2^4}{2} - 3g_1^2g_2^2 - 24y_X^2y_M^2 - 24y_T^2y_M^2 - 24y_B^2y_M^2\right],
$$

$$
\frac{d\lambda_4}{d\ln\mu^2} = \frac{1}{16\pi^2}\left[2\lambda_4\left(3y_t^2 + 6y_X^2 + 6y_T^2 + 6y_B^2 + 6y_M^2 - 3g_1^2 - 9g_2^2\right) + 6g_1^2g_2^2 \right.
$$
$$
\left. + 4\lambda_4^2 + 8\lambda_5^2 + 8\lambda_3\lambda_4 + 2\lambda_4(\lambda_1 + \lambda_2) + 24y_X^2y_M^2 + 24y_T^2y_M^2 + 24y_B^2y_M^2\right],
$$

$$
\frac{d\lambda_5}{d\ln\mu^2} = \frac{1}{16\pi^2}\left[2\lambda_5\left(3y_t^2 + 6y_T^2 + 6y_X^2 + 6y_B^2 + 6y_M^2 - 3g_1^2 - 9g_2^2\right) \right.
$$
$$
\left. + 2\lambda_5(\lambda_1 + \lambda_2 + 4\lambda_3 + 6\lambda_4)\right]. \tag{B.31}
$$

B.2.7 Triplet $\mathcal{T}_Y$ (T, B, Y), $Y = -1/3$

The relevant RGE for the Yukawa couplings are

$$
\frac{dy_t^2}{d\ln\mu^2} = \frac{y_t^2}{16\pi^2}\left(\frac{9y_t^2}{2} + \frac{9y_T^2}{2} + \frac{3y_B^2}{2} + \frac{y_Y^2}{2} + 3y_M^2 - \frac{17g_1^2}{12} - \frac{9g_2^2}{4} - 8g_3^2\right),
$$

$$
\frac{dy_T^2}{d\ln\mu^2} = \frac{y_T^2}{16\pi^2}\left(\frac{9y_t^2}{2} + \frac{9y_T^2}{2} + \frac{9y_B^2}{2} + \frac{y_Y^2}{2} + 3y_M^2 - \frac{17g_1^2}{12} - \frac{9g_2^2}{4} - 8g_3^2\right),
$$

$$
\frac{dy_B^2}{d\ln\mu^2} = \frac{y_B^2}{16\pi^2}\left(\frac{3y_t^2}{2} + \frac{y_T^2}{2} + \frac{9y_B^2}{2} + \frac{9y_Y^2}{2} + \frac{3y_M^2}{2} - \frac{5g_1^2}{12} - \frac{9g_2^2}{4} - 8g_3^2\right),
$$

$$
\frac{dy_Y^2}{d\ln\mu^2} = \frac{y_Y^2}{16\pi^2}\left(\frac{9y_Y^2}{2} + \frac{9y_B^2}{2} + \frac{3y_t^2}{2} + \frac{y_T^2}{2} + 3y_M^2 - \frac{17g_1^2}{20} - \frac{9g_2^2}{4} - 8g_3^2\right),
$$

$$
\frac{dy_M^2}{d\ln\mu^2} = \frac{y_M^2}{16\pi^2}\left(y_T^2 + y_B^2 + y_Y^2 + \frac{15y_M^2}{2} - \frac{17g_1^2}{20} - \frac{9g_2^2}{4} - 8g_3^2\right). \tag{B.32}
$$

The Higgs sector RGEs, describing the interactions between the two bosons are

$$
\frac{d\lambda_1}{d\ln\mu^2} = \frac{1}{16\pi^2}\left[4\lambda_1\left(6y_B^2 + 6y_Y^2 - \frac{3g_1^2}{2} - \frac{9g_2^2}{2}\right) + 12\lambda_1^2 + 4\lambda_3^2 + 4\lambda_3\lambda_4 + 2\lambda_4^2 + 2\lambda_5^2\right.
$$
$$
\left. + \frac{3g_1^4}{2} + \frac{9g_2^4}{2} + 3g_1^2 g_2^2 - 24y_B^4 - 24y_Y^4 - 24y_B^2 y_M^2 - 24y_Y^2 y_M^2\right],
$$

$$
\frac{d\lambda_2}{d\ln\mu^2} = \frac{1}{16\pi^2}\left[4\lambda_2\left(3y_t^2 + 6y_T^2 + 6y_B^2 - \frac{3g_1^2}{2} - \frac{9g_2^2}{2}\right) + 12\lambda_2^2 + 4\lambda_3^2 + 4\lambda_3\lambda_4 + 2\lambda_4^2 + 2\lambda_5^2\right.
$$
$$
\left. + \frac{3g_1^4}{2} + \frac{9g_2^4}{2} + 3g_1^2 g_2^2 - 12y_t^4 - 24y_T^4 - 24y_B^4 - 24y_t^2 y_T^2 - 24y_T^2 y_M^2 - 24y_B^2 y_M^2\right],
$$

$$
\frac{d\lambda_3}{d\ln\mu^2} = \frac{1}{16\pi^2}\left[2\lambda_3\left(3y_t^2 + 6y_T^2 + 6y_B^2 + 6y_Y^2 + 6y_M^2 - 3g_1^2 - 9g_2^2\right) + 4\lambda_3^2 + 2\lambda_4^2 + 2\lambda_5^2\right.
$$
$$
\left. + (\lambda_1 + \lambda_2)(6\lambda_3 + 2\lambda_4) + \frac{3g_1^4}{2} + \frac{9g_2^2}{2} - 3g_1^2 g_2^2 - 24y_T^2 y_M^2 - 24y_B^2 y_M^2 - 24y_Y^2 y_M^2\right],
$$

$$
\frac{d\lambda_4}{d\ln\mu^2} = \frac{1}{16\pi^2}\left[2\lambda_4\left(3y_t^2 + 6y_T^2 + 6y_B^2 + 6y_Y^2 + 6y_M^2 - 3g_1^2 - 9g_2^2\right) + 6g_1^2 g_2^2\right.
$$
$$
\left. + 4\lambda_4^2 + 8\lambda_5^2 + 8\lambda_3\lambda_4 + 2\lambda_4(\lambda_1 + \lambda_2) + 24y_T^2 y_M^2 + 24y_B^2 y_M^2 + 24y_Y^2 y_M^2\right],
$$

$$
\frac{d\lambda_5}{d\ln\mu^2} = \frac{1}{16\pi^2}\left[2\lambda_5\left(3y_t^2 + 6y_T^2 + 6y_B^2 + 6y_Y^2 + 6y_M^2 - 3g_1^2 - 9g_2^2\right)\right.
$$
$$
\left. + 2\lambda_5(\lambda_1 + \lambda_2 + 4\lambda_3 + 6\lambda_4)\right]. \tag{B.33}
$$

The coupling constants gain additional terms due to the new fermions in both triplet models as follows

$$
\frac{dg_1^2}{d\ln\mu^2} = \frac{g_1^4}{16\pi^2}\left(7 + \frac{4}{5}\right),
$$
$$
\frac{dg_2^2}{d\ln\mu^2} = \frac{g_2^4}{16\pi^2}\left(-3 + 4\right),
$$
$$
\frac{dg_3^2}{d\ln\mu^2} = \frac{g_3^4}{16\pi^2}\left(-7 + 2\right). \tag{B.34}
$$

Appendix C

2-Loop RGEs for VLLs

The results are based on [54, 220, 221, 294, 295], with our choice of convention for the group representation-dependent quantities as specified in Sec. 3.1.

C.1 Singlet $\mathcal{S}_1$ (L^0), $Y = 0$

The relevant RGE for the Yukawa couplings are

$$
\begin{aligned}
\frac{dy_t^2}{d\ln\mu^2} &= \frac{y_t^2}{16\pi^2}\left(\frac{9y_t^2}{2} + y_\tau^2 + 2y_{L^0}^2 - \frac{17g_1^2}{20} - \frac{9g_2^2}{4} - 8g_3^2\right) \\
&+ \frac{y_t^2}{(4\pi)^4}\left[y_t^2\left(-12y_t^2 - \frac{9}{4}y_\tau^2 + 36g_3^2 + \frac{225}{16}g_2^2 + \frac{393}{80}g_1^2 - \frac{27}{2}y_{L^0}^2 - 12\lambda\right)\right. \\
&+ y_\tau^2\left(-\frac{9}{4}y_\tau^2 - \frac{9}{2}y_{L^0}^2 + \frac{15}{8}g_1^2 + \frac{15}{8}g_2^2\right) + y_{L^0}^2\left(-\frac{27}{2}y_M^2 + \frac{15}{4}g_1^2 + \frac{45}{4}g_2^2\right) \\
&- \frac{27}{2}y_{L^0}^4 - \frac{27}{2}y_\tau^4 - 108g_3^4 - \frac{23}{4}g_2^4 + \frac{1187}{600}g_1^4 + 9g_3^2g_2^2 + \frac{19}{15}g_3^2g_1^2 - \frac{9}{20}g_1^2g_2^2 + 6\lambda^2\right], \\
\frac{dy_\tau^2}{d\ln\mu^2} &= \frac{y_\tau^2}{16\pi^2}\left(\frac{5y_\tau^2}{2} + 3y_t^2 + 2y_{L^0}^2 - \frac{9g_1^2}{4} - \frac{9g_2^2}{4}\right) \\
&+ \frac{y_\tau^2}{(4\pi)^4}\left[y_\tau^2\left(-3y_\tau^2 - \frac{9}{2}y_{L^0}^2 + \frac{537}{80}g_1^2 + \frac{165}{16}g_2^2 - 12\lambda\right)\right. \\
&+ y_t^2\left(-\frac{27}{4}y_t^2 - \frac{27}{4}y_\tau^2 - \frac{27}{4}y_{L^0}^2 + \frac{17}{8}g_1^2 + \frac{45}{8}g_2^2 + 20g_3^2\right) \\
&- \frac{23}{4}g_2^4 + \frac{1371}{200}g_1^4 + \frac{27}{20}g_1^2g_2^2 + 6\lambda^2\right].
\end{aligned}
$$

$$
\frac{dy_{L^0}^2}{d\ln\mu^2} = \frac{y_{L^0}^2}{16\pi^2}\left(3y_t^2 + \frac{5y_{L^0}^2}{2} + \frac{y_\tau^2}{2} + \frac{y_M^2}{4} - \frac{9g_1^2}{20} - \frac{9g_2^2}{4}\right)
$$

$$
+ \frac{y_{L^0}^2}{(4\pi)^4}\left[y_{L^0}^2\left(-\frac{27}{2}y_t^2 - \frac{9}{2}y_\tau^2 - \frac{456}{32}y_M^2 + \frac{123}{8}g_1^2 + \frac{225}{8}g_2^2 - 24\lambda\right)\right.
$$

$$
+ y_t^2\left(-\frac{27}{2}y_t^2 + \frac{85}{12}g_1^2 + \frac{45}{4}g_2^2 + 40g_3^2\right) - 24y_{L^0}^4 - \frac{27}{4}y_M^4
$$

$$
\left. + \frac{35}{12}g_1^4 - \frac{23}{2}g_2^4 + \frac{9}{2}g_1^2 g_2^2 + 12\lambda^2\right],
$$

$$
\frac{dy_M^2}{d\ln\mu^2} = \frac{y_M^2}{16\pi^2}\left(y_{L^0}^2 + \frac{5y_M^2}{2}\right)
$$

$$
+ \frac{y_M^2}{(4\pi)^4}\left[y_M^2\left(-\frac{37}{2}y_M^2 - \frac{9}{2}y_{L^0}^2\right) + y_{L^0}^2\left(-\frac{19}{2}y_{L^0}^2 - 9y_t^2 + \frac{17}{4}g_1^2 + \frac{51}{4}g_2^2\right)\right].
$$

$$\tag{C.1}$$

The Higgs sector RGE, describing the interactions between the scalar boson and all fermions

$$
\frac{d\lambda}{d\ln\mu^2} = \frac{1}{16\pi^2}\left[\lambda\left(-\frac{9g_1^2}{10} - \frac{9g_2^2}{2} + 6y_t^2 + 4y_{L^0}^2 + 4y_M^2 + 2y_\tau^2\right) + 12\lambda^2\right.
$$

$$
+ \frac{27g_1^4}{400} + \frac{9g_2^4}{16} + \frac{9g_1^2 g_2^2}{40} - 6y_t^4 - 4y_\tau^4 - 4y_{L^0}^4 - 4y_M^4 - 4y_M^2 y_{L^0}^2\right]
$$

$$
+ \beta_{\text{SM-2}}^\lambda + \frac{y_{L^0}^2}{(4\pi)^4}\left[-144\lambda^2 - 3\lambda y_{L^0}^2 - 27\lambda y_M^2 + 18y_M^2 y_{L^0}^2 + 30y_{L^0}^4\right.
$$

$$
\left. + \lambda\left(\frac{15}{2}g_1^2 + \frac{45}{2}g_2^2\right) - \frac{3}{4}g_1^4 - \frac{9}{4}g_2^4 - \frac{3}{2}g_1^2 g_2^2\right].
$$

$$\tag{C.2}$$

Finally the gauge terms gain additional coupled terms from fermions in 2-loop corrections

$$
\frac{dg_1^2}{d\ln\mu^2} = \frac{g_1^4}{16\pi^2}\left(\frac{41}{10}\right)
$$

$$
+ \frac{g_1^4}{(4\pi^4)}\left[\frac{199}{9}g_1^2 + 9g_2^2 + \frac{88}{3}g_3^2 - \frac{17}{3}y_t^2 - \frac{3}{2}y_\tau^2 - 3y_{L^0}^2\right],
$$

$$
\frac{dg_2^2}{d\ln\mu^2} = \frac{g_2^4}{16\pi^2}\left(-\frac{19}{6}\right)
$$

$$
+ \frac{g_2^4}{(4\pi^4)}\left[3g_1^2 + \frac{35}{3}g_2^2 + 24g_3^2 - 3y_t^2 - \frac{1}{2}y_\tau^2 - 3y_{L^0}^2\right],
$$

$$
\frac{dg_3^2}{d\ln\mu^2} = \frac{g_3^4}{16\pi^2}(-7)
$$

$$
+ \frac{g_3^4}{(4\pi^4)}\left[\frac{11}{3}g_1^2 + 9g_2^2 - 52g_3^2 - 4y_t^2\right].
$$

$$\tag{C.3}$$

C.2   Singlet $\mathcal{S}_2$ (L^-), $Y = -1$

The relevant RGE for the Yukawa couplings are

$$
\begin{aligned}
\frac{dy_t^2}{d\ln\mu^2} &= \frac{y_t^2}{16\pi^2}\left(\frac{9y_t^2}{2} + y_\tau^2 + 2y_{L^-}^2 - \frac{17g_1^2}{20} - \frac{9g_2^2}{4} - 8g_3^2\right) \\
&+ \frac{y_t^2}{(4\pi)^4}\left[y_t^2\left(-12y_t^2 - \frac{9}{4}y_\tau^2 + 36g_3^2 + \frac{225}{16}g_2^2 + \frac{393}{80}g_1^2 - \frac{27}{2}y_{L^-}^2 - 12\lambda\right)\right. \\
&+ y_\tau^2\left(-\frac{9}{4}y_\tau^2 - \frac{9}{2}y_{L^-}^2 + \frac{15}{8}g_1^2 + \frac{15}{8}g_2^2\right) + y_{L^-}^2\left(-\frac{27}{2}y_M^2 + \frac{75}{4}g_1^2 + \frac{45}{4}g_2^2\right) + \frac{58}{9}g_1^4 \\
&\left.- \frac{27}{2}y_{L^-}^4 - \frac{27}{2}y_\tau^4 - 108g_3^4 - \frac{23}{4}g_2^4 + \frac{1187}{600}g_1^4 + 9g_3^2g_2^2 + \frac{19}{15}g_3^2g_1^2 - \frac{9}{20}g_1^2g_2^2 + 6\lambda^2\right], \\
\frac{dy_\tau^2}{d\ln\mu^2} &= \frac{y_\tau^2}{16\pi^2}\left(\frac{5y_\tau^2}{2} + 3y_t^2 + 2y_{L^-}^2 - \frac{9g_1^2}{4} - \frac{9g_2^2}{4}\right) \\
&+ \frac{y_\tau^2}{(4\pi)^4}\left[y_\tau^2\left(-3y_\tau^2 - \frac{9}{2}y_{L^-}^2 + \frac{537}{80}g_1^2 + \frac{165}{16}g_2^2 - 12\lambda\right)\right. \\
&+ y_t^2\left(-\frac{27}{4}y_t^2 - \frac{27}{4}y_\tau^2 - \frac{27}{4}y_{L^-}^2 + \frac{17}{8}g_1^2 + \frac{45}{8}g_2^2 + 20g_3^2\right) + \frac{116}{3}g_1^4 \\
&\left.- \frac{23}{4}g_2^4 + \frac{1371}{200}g_1^4 + \frac{27}{20}g_1^2g_2^2 + 6\lambda^2\right], \\
\frac{dy_{L^-}^2}{d\ln\mu^2} &= \frac{y_{L^-}^2}{16\pi^2}\left(3y_t^2 + \frac{5y_{L^-}^2}{2} + \frac{y_\tau^2}{2} + \frac{y_M^2}{4} - \frac{9g_1^2}{4} - \frac{9g_2^2}{4}\right) \\
&+ \frac{y_{L^-}^2}{(4\pi)^4}\left[y_{L^-}^2\left(-\frac{27}{2}y_t^2 - \frac{9}{2}y_\tau^2 - \frac{456}{32}y_M^2 + \frac{279}{8}g_1^2 + \frac{225}{8}g_2^2 - 24\lambda\right)\right. \\
&+ y_t^2\left(-\frac{27}{2}y_t^2 + \frac{85}{12}g_1^2 + \frac{45}{4}g_2^2 + 40g_3^2\right) - 24y_{L^-}^4 - \frac{27}{4}y_M^4 + 6g_1^2y_M^2 \\
&\left.+ \frac{721}{12}g_1^4 - \frac{23}{2}g_2^4 + \frac{9}{2}g_1^2g_2^2 + 12\lambda^2\right], \\
\frac{dy_M^2}{d\ln\mu^2} &= \frac{y_M^2}{16\pi^2}\left(y_{L^-}^2 + \frac{5y_M^2}{2} - \frac{18}{5}g_1^2\right) \\
&+ \frac{y_M^2}{(4\pi)^4}\left[y_M^2\left(-\frac{37}{2}y_M^2 - \frac{9}{2}y_{L^-}^2 + 58g_1^2\right) + \frac{313}{3}g_1^4\right. \\
&\left.+ y_{L^-}^2\left(-\frac{19}{2}y_{L^-}^2 - 9y_t^2 + \frac{37}{4}g_1^2 + \frac{51}{4}g_2^2\right)\right]. \tag{C.4}
\end{aligned}
$$

The Higgs sector RGE, describing the interactions between the scalar boson and all fermions:

$$
\begin{aligned}
\frac{d\lambda}{d\ln\mu^2} =\ & \frac{1}{16\pi^2}\left[\lambda\left(-\frac{9g_1^2}{10}-\frac{9g_2^2}{2}+6y_t^2+4y_{L-}^2+4y_M^2+2y_\tau^2\right)+12\lambda^2\right.\\
& + \frac{27g_1^4}{400}+\frac{9g_2^4}{16}+\frac{9g_1^2g_2^2}{40}-6y_t^4-4y_\tau^4-4y_{L-}^4-4y_M^4-4y_\tau^2y_{L-}^2-4y_M^2y_{L-}^2\Bigg]\\
& + \beta_{\text{SM-2}}^\lambda+\frac{y_{L-}^2}{(4\pi)^4}\left[-144\lambda^2-3\lambda y_{L-}^2-27\lambda y_M^2+18y_M^2y_{L-}^2+30y_{L-}^4-12g_1^2y_{L-}^2\right.\\
& - \lambda\left(\frac{75}{2}g_1^2+\frac{45}{2}g_2^2\right)-\frac{75}{4}g_1^4-\frac{9}{4}g_2^4+\frac{33}{2}g_1^2g_2^2\Bigg]\\
& + \frac{1}{(4\pi)^4}\left[10\lambda g_1^4-4g_1^6-4g_1^4g_2^2\right].
\end{aligned}
\tag{C.5}
$$

Finally the gauge terms gain additional coupled terms from fermions in 2-loop corrections

$$
\begin{aligned}
\frac{dg_1^2}{d\ln\mu^2} =\ & \frac{g_1^4}{16\pi^2}\left(\frac{41}{10}+\frac{4}{5}\right)\\
& + \frac{g_1^4}{(4\pi^4)}\left[\frac{415}{9}g_1^2+9g_2^2+\frac{88}{3}g_3^2-\frac{17}{3}y_t^2-\frac{3}{2}y_\tau^2-15y_{L-}^2-36y_M^2\right],\\
\frac{dg_2^2}{d\ln\mu^2} =\ & \frac{g_2^4}{16\pi^2}\left(-\frac{19}{6}\right)\\
& + \frac{g_2^4}{(4\pi^4)}\left[3g_1^2+\frac{35}{3}g_2^2+24g_3^2-3y_t^2-\frac{1}{2}y_\tau^2-3y_{L-}^2\right],\\
\frac{dg_3^2}{d\ln\mu^2} =\ & \frac{g_3^4}{16\pi^2}\left(-7\right)\\
& + \frac{g_3^4}{(4\pi^4)}\left[\frac{11}{3}g_1^2+9g_2^2-52g_3^2-4y_t^2\right].
\end{aligned}
\tag{C.6}
$$

C.3 Doublet $\mathcal{D}_1$ (L^0, L^-), $Y = -1/2$

The relevant RGE for the Yukawa couplings are

$$
\begin{aligned}
\frac{dy_t^2}{d\ln\mu^2} &= \frac{y_t^2}{16\pi^2}\left(\frac{9y_t^2}{2} + y_\tau^2 + 2y_{L^-}^2 + 2y_{L^0}^2 - \frac{17g_1^2}{20} - \frac{9g_2^2}{4} - 8g_3^2\right) \\
&+ \frac{y_t^2}{(4\pi)^4}\left[y_t^2\left(-12y_t^2 - \frac{9}{4}y_\tau^2 + 36g_3^2 + \frac{225}{16}g_2^2 + \frac{393}{80}g_1^2 - \frac{27}{2}y_{L^0}^2 - \frac{27}{2}y_{L^-}^2 - 12\lambda\right)\right. \\
&+ y_\tau^2\left(-\frac{9}{4}y_\tau^2 - \frac{9}{2}y_{L^0}^2 - \frac{9}{2}y_{L^-}^2 + \frac{15}{8}g_1^2 + \frac{15}{8}g_2^2\right) \\
&+ (y_{L^-}^2 + y_{L^0}^2)\left(-\frac{27}{2}y_M^2 + \frac{75}{4}g_1^2 + \frac{45}{4}g_2^2\right) - \frac{27}{2}y_{L^0}^4 - \frac{27}{2}y_{L^-}^4 + \frac{29}{9}g_1^4 + 3g_2^4 \\
&- \left.\frac{27}{2}y_\tau^4 - 108g_3^4 - \frac{23}{4}g_2^4 + \frac{1187}{600}g_1^4 + 9g_3^2g_2^2 + \frac{19}{15}g_3^2g_1^2 - \frac{9}{20}g_1^2g_2^2 + 6\lambda^2\right], \\
\frac{dy_\tau^2}{d\ln\mu^2} &= \frac{y_\tau^2}{16\pi^2}\left(\frac{5y_\tau^2}{2} + \frac{5y_{L^-}^2}{2} + 3y_t^2 + \frac{y_{L^0}^2}{2} - \frac{9g_1^2}{4} - \frac{9g_2^2}{4}\right) \\
&+ \frac{y_\tau^2}{(4\pi)^4}\left[y_\tau^2\left(-3y_\tau^2 - \frac{9}{2}y_{L^0}^2 - \frac{9}{2}y_{L^-}^2 + \frac{537}{80}g_1^2 + \frac{165}{16}g_2^2 - 12\lambda\right)\right. \\
&+ y_t^2\left(-\frac{27}{4}y_t^2 - \frac{27}{4}y_\tau^2 - \frac{27}{4}y_{L^0}^2 - \frac{27}{4}y_{L^-}^2 + \frac{17}{8}g_1^2 + \frac{45}{8}g_2^2 + 20g_3^2\right) + \frac{58}{3}g_1^4 \\
&- \left.\frac{11}{4}g_2^4 + \frac{1371}{200}g_1^4 + \frac{27}{20}g_1^2g_2^2 + 6\lambda^2\right], \\
\frac{dy_{L^0}^2}{d\ln\mu^2} &= \frac{y_{L^0}^2}{16\pi^2}\left(3y_t^2 + \frac{5y_{L^0}^2}{2} + \frac{y_{L^-}^2}{2} + y_\tau^2 + \frac{y_M^2}{2} - \frac{9g_1^2}{4} - \frac{9g_2^2}{4}\right) \\
&+ \frac{y_{L^0}^2}{(4\pi)^4}\left[y_{L^0}^2\left(-\frac{27}{2}y_t^2 - \frac{9}{2}y_\tau^2 - 15y_M^2 + \frac{279}{8}g_1^2 + \frac{225}{8}g_2^2 - 24\lambda\right)\right. \\
&+ y_{L^-}^2\left(-\frac{27}{2}y_t^2 - \frac{9}{2}y_\tau^2 - 15y_M^2 + \frac{123}{8}g_1^2 + \frac{225}{8}g_2^2 - 24\lambda\right) \\
&+ y_t^2\left(-\frac{27}{2}y_t^2 + \frac{85}{12}g_1^2 + \frac{45}{4}g_2^2 + 40g_3^2\right) - 24y_{L^0}^4 - 2y_{L^-}^4 - \frac{45}{4}y_M^4 + 15g_1^2y_M^2 \\
&+ \left.9g_2^2y_M^2 + \frac{589}{12}g_1^4 - \frac{51}{6}g_2^4 + \frac{9}{2}g_1^2g_2^2 + 12\lambda^2\right], \\
\frac{dy_{L^-}^2}{d\ln\mu^2} &= \frac{y_{L^-}^2}{16\pi^2}\left(3y_t^2 + \frac{5y_{L^-}^2}{2} + \frac{y_{L^0}^2}{2} + y_\tau^2 + \frac{y_M^2}{2} - \frac{15g_1^2}{4} - \frac{9g_2^2}{4}\right) \\
&+ \frac{y_{L^-}^2}{(4\pi)^4}\left[y_{L^0}^2\left(-\frac{27}{2}y_t^2 - \frac{9}{2}y_\tau^2 - 15y_M^2 + \frac{123}{8}g_1^2 + \frac{225}{8}g_2^2 - 24\lambda\right)\right. \\
&+ y_{L^-}^2\left(-\frac{27}{2}y_t^2 - \frac{9}{2}y_\tau^2 - 15y_M^2 + \frac{279}{8}g_1^2 + \frac{225}{8}g_2^2 - 24\lambda\right) \\
&+ y_t^2\left(-\frac{27}{2}y_t^2 + \frac{85}{12}g_1^2 + \frac{45}{4}g_2^2 + 40g_3^2\right) - 2y_{L^0}^4 - 24y_{L^-}^4 - \frac{45}{4}y_M^4 + 15g_1^2y_M^2 \\
&+ \left.9g_2^2y_M^2 + \frac{589}{12}g_1^4 - \frac{51}{6}g_2^4 + \frac{9}{2}g_1^2g_2^2 + 12\lambda^2\right], \tag{C.7}
\end{aligned}
$$

$$\frac{dy_M^2}{d\ln\mu^2} = \frac{y_M^2}{16\pi^2}\left(y_{L^-}^2 + y_{L^0}^2 + \frac{7y_M^2}{2} - \frac{9}{10}g_1^2 - \frac{9}{2}g_2^2\right)$$

$$+ \frac{y_M^2}{(4\pi)^4}\left[y_M^2\left(-\frac{73}{2}y_M^2 - \frac{15}{4}y_{L^0}^2 - \frac{15}{4}y_{L^-}^2 + 17g_1^2 + 51g_2^2\right) - 5y_{L^0}^4 - 5y_{L^-}^4\right.$$

$$+ \left. (y_{L^0}^2 + y_{L^-}^2)\left(-\frac{9}{2}y_t^2 + \frac{55}{8}g_1^2 + \frac{33}{8}g_2^2\right) + \frac{707}{24}g_1^4 - \frac{421}{8}g_2^4 - \frac{9}{4}g_1^2g_2^2\right] \qquad (C.8)$$

The Higgs sector RGE, describing the interactions between the scalar boson and all fermions

$$\frac{d\lambda}{d\ln\mu^2} = \frac{1}{16\pi^2}\left[\lambda\left(-\frac{9g_1^2}{5} - 9g_2^2 + 6y_t^2 + 4y_{L^-}^2 + 4y_{L^0}^2 + 4y_M^2 + 2y_\tau^2\right) + 12\lambda^2\right.$$

$$+ \frac{27g_1^4}{200} + \frac{9g_2^4}{8} + \frac{9g_1^2g_2^2}{20} - 6y_t^4 - 4y_\tau^4 - 4y_{L^-}^4 - 4y_{L^0}^4 - 4y_M^4$$

$$- \left. 4y_\tau^2y_{L^-}^2 - 4y_M^2y_{L^-}^2 - 4y_M^2y_{L^0}^2\right]$$

$$+ \beta_{\text{SM-2}}^\lambda + \frac{(y_{L^0}^2 + y_{L^-}^2)}{(4\pi)^4}\left[-144\lambda^2 - 3\lambda(y_{L^0}^2 + y_{L^-}^2) - 27\lambda y_M^2 + 18y_M^2(y_{L^0}^2 + y_{L^-}^2)\right.$$

$$+ 30y_{L^0}^4 + 30y_{L^-}^4 - 12g_1^2(y_{L^0}^2 + y_{L^-}^2) - \frac{75}{4}g_1^4 - \frac{9}{4}g_2^4 + \frac{33}{2}g_1^2g_2^2$$

$$+ \left. \lambda\left(\frac{75}{2}g_1^2 + \frac{45}{2}g_2^2\right)\right]$$

$$+ \frac{1}{(4\pi)^4}\left[5\lambda g_1^4 + 15\lambda g_2^4 - 2g_1^6 - 2g_1^4g_2^2 - 2g_1^2g_2^4 - 6g_2^6\right]. \qquad (C.9)$$

The gauge couplings gain additional terms due to the new fermions from 2-loop corrections

$$\frac{dg_1^2}{d\ln\mu^2} = \frac{g_1^4}{16\pi^2}\left(\frac{41}{10} + \frac{18}{5}\right)$$

$$+ \frac{g_1^4}{(4\pi^4)}\left[\frac{226}{9}g_1^2 + 18g_2^2 + \frac{88}{3}g_3^2 - \frac{17}{3}y_t^2 - \frac{3}{2}y_\tau^2 - 15y_{L^0}^2 - 15y_{L^-}^2 - 18y_M^2\right],$$

$$\frac{dg_2^2}{d\ln\mu^2} = \frac{g_2^4}{16\pi^2}\left(-\frac{19}{6} + \frac{7}{3}\right)$$

$$+ \frac{g_2^4}{(4\pi^4)}\left[6g_1^2 + \frac{182}{3}g_2^2 + 24g_3^2 - 3y_t^2 - \frac{1}{2}y_\tau^2 - 3y_{L^0}^2 - 3y_{L^-}^2 - 18y_M^2\right],$$

$$\frac{dg_3^2}{d\ln\mu^2} = \frac{g_3^4}{16\pi^2}(-7)$$

$$+ \frac{g_3^4}{(4\pi^4)}\left[\frac{11}{3}g_1^2 + 9g_2^2 - 52g_3^2 - 4y_t^2\right]. \qquad (C.10)$$

C.4   Doublet $\mathcal{D}_2$ (L^-, L^{--}), $Y = -3/2$

The relevant RGE for the Yukawa couplings are

$$
\begin{aligned}
\frac{dy_t^2}{d\ln\mu^2} &= \frac{y_t^2}{16\pi^2}\left(\frac{9y_t^2}{2} + y_\tau^2 + 2y_{L^-}^2 + 2y_{L^{--}}^2 - \frac{17g_1^2}{20} - \frac{9g_2^2}{4} - 8g_3^2\right) \\
&+ \frac{y_t^2}{(4\pi)^4}\left[y_t^2\left(-12y_t^2 - \frac{9}{4}y_\tau^2 + 36g_3^2 + \frac{225}{16}g_2^2 + \frac{393}{80}g_1^2 - \frac{27}{2}y_{L^-}^2 - \frac{27}{2}y_{L^{--}}^2 - 12\lambda\right)\right. \\
&+ y_\tau^2\left(-\frac{9}{4}y_\tau^2 - \frac{9}{2}y_{L^-}^2 - \frac{9}{2}y_{L^{--}}^2 + \frac{15}{8}g_1^2 + \frac{15}{8}g_2^2\right) \\
&+ (y_{L^-}^2 + y_{L^{--}}^2)\left(-\frac{27}{2}y_M^2 + \frac{195}{4}g_1^2 + \frac{45}{4}g_2^2\right) - \frac{27}{2}y_{L^-}^4 - \frac{27}{2}y_{L^{--}}^4 + 29g_1^4 + 3g_2^4 \\
&\left. - \frac{27}{2}y_\tau^4 - 108g_3^4 - \frac{23}{4}g_2^4 + \frac{1187}{600}g_1^4 + 9g_3^2g_2^2 + \frac{19}{15}g_3^2g_1^2 - \frac{9}{20}g_1^2g_2^2 + 6\lambda^2\right], \\
\frac{dy_\tau^2}{d\ln\mu^2} &= \frac{y_\tau^2}{16\pi^2}\left(\frac{5y_\tau^2}{2} + \frac{5y_{L^{--}}^2}{2} + 3y_t^2 + \frac{y_{L^-}^2}{2} - \frac{9g_1^2}{4} - \frac{9g_2^2}{4}\right) \\
&+ \frac{y_\tau^2}{(4\pi)^4}\left[y_\tau^2\left(-3y_\tau^2 - \frac{9}{2}y_{L^-}^2 - \frac{9}{2}y_{L^{--}}^2 + \frac{537}{80}g_1^2 + \frac{165}{16}g_2^2 - 12\lambda\right)\right. \\
&+ y_t^2\left(-\frac{27}{4}y_t^2 - \frac{27}{4}y_\tau^2 - \frac{27}{4}y_{L^-}^2 - \frac{27}{4}y_{L^{--}}^2 + \frac{17}{8}g_1^2 + \frac{45}{8}g_2^2 + 20g_3^2\right) + 174g_1^4 \\
&\left. - \frac{11}{4}g_2^4 + \frac{1371}{200}g_1^4 + \frac{27}{20}g_1^2g_2^2 + 6\lambda^2\right], \\
\frac{dy_{L^-}^2}{d\ln\mu^2} &= \frac{y_{L^-}^2}{16\pi^2}\left(3y_t^2 + \frac{5y_{L^-}^2}{2} + \frac{y_{L^{--}}^2}{2} + y_\tau^2 + \frac{y_M^2}{2} - \frac{27g_1^2}{2} - \frac{9g_2^2}{4}\right) \\
&+ \frac{y_{L^-}^2}{(4\pi)^4}\left[y_{L^-}^2\left(-\frac{27}{2}y_t^2 - \frac{9}{2}y_\tau^2 - 15y_M^2 + \frac{831}{8}g_1^2 + \frac{225}{8}g_2^2 - 24\lambda\right)\right. \\
&+ y_{L^{--}}^2\left(-\frac{27}{2}y_t^2 - \frac{9}{2}y_\tau^2 - 15y_M^2 + \frac{279}{8}g_1^2 + \frac{225}{8}g_2^2 - 24\lambda\right) \\
&+ y_t^2\left(-\frac{27}{2}y_t^2 + \frac{85}{12}g_1^2 + \frac{45}{4}g_2^2 + 40g_3^2\right) - 2y_{L^{--}}^4 - 24y_{L^-}^4 - \frac{45}{4}y_M^4 + 27g_1^2y_M^2 \\
&\left. + 9g_2^2y_M^2 + \frac{4541}{12}g_1^4 - \frac{51}{6}g_2^4 + \frac{27}{2}g_1^2g_2^2 + 12\lambda^2\right], \\
\frac{dy_{L^{--}}^2}{d\ln\mu^2} &= \frac{y_{L^{--}}^2}{16\pi^2}\left(3y_t^2 + \frac{5y_{L^{--}}^2}{2} + \frac{y_{L^-}^2}{2} + y_\tau^2 + \frac{y_M^2}{2} - \frac{45g_1^2}{4} - \frac{9g_2^2}{4}\right) \\
&+ \frac{y_{L^{--}}^2}{(4\pi)^4}\left[y_{L^{--}}^2\left(-\frac{27}{2}y_t^2 - \frac{9}{2}y_\tau^2 - 15y_M^2 + \frac{831}{8}g_1^2 + \frac{225}{8}g_2^2 - 24\lambda\right)\right. \\
&+ y_{L^-}^2\left(-\frac{27}{2}y_t^2 - \frac{9}{2}y_\tau^2 - 15y_M^2 + \frac{279}{8}g_1^2 + \frac{225}{8}g_2^2 - 24\lambda\right) \\
&+ y_t^2\left(-\frac{27}{2}y_t^2 + \frac{85}{12}g_1^2 + \frac{45}{4}g_2^2 + 40g_3^2\right) - 24y_{L^{--}}^4 - 2y_{L^-}^4 - \frac{45}{4}y_M^4 + 27g_1^2y_M^2 \\
&\left. + 9g_2^2y_M^2 + \frac{4541}{12}g_1^4 - \frac{51}{6}g_2^4 + \frac{27}{2}g_1^2g_2^2 + 12\lambda^2\right], \quad\quad\quad\text{(C.11)}
\end{aligned}
$$

$$\frac{dy_M^2}{d\ln\mu^2} = \frac{y_M^2}{16\pi^2}\left(y_{L-}^2 + y_{L--}^2 + \frac{7y_M^2}{2} - \frac{27}{2}g_1^2 - \frac{9}{4}g_2^2\right)$$
$$+ \frac{y_M^2}{(4\pi)^4}\left[y_M^2\left(-\frac{73}{2}y_M^2 - \frac{15}{4}y_{L-}^2 - \frac{15}{4}y_{L--}^2 + 153g_1^2 + 51g_2^2\right) - 5y_{L-}^4 - 5y_{L--}^4\right.$$
$$+ \left.(y_{L-}^2 + y_{L--}^2)\left(-\frac{9}{2}y_t^2 + \frac{95}{8}g_1^2 + \frac{33}{8}g_2^2\right) + \frac{4263}{8}g_1^4 - \frac{421}{8}g_2^4 - \frac{81}{4}g_1^2g_2^2\right].$$

$$(\text{C.12})$$

The Higgs sector RGE, describing the interactions between the scalar boson and all fermions

$$\frac{d\lambda}{d\ln\mu^2} = \frac{1}{16\pi^2}\left[\lambda\left(-\frac{9g_1^2}{5} - 9g_2^2 + 6y_t^2 + 4y_{L-}^2 + 4y_{L--}^2 + 4y_M^2 + 2y_\tau^2\right) + 12\lambda^2\right.$$
$$+ \frac{27g_1^4}{200} + \frac{9g_2^4}{8} + \frac{9g_1^9 g_2^2}{20} - 6y_t^4 - 4y_\tau^4 - 4y_{L-}^4 - 4y_{L--}^4 - 4y_M^4$$
$$- \left.4y_\tau^2 y_{L-}^2 - 4y_M^2 y_{L-}^2 - 4y_M^2 y_{L--}^2\right]$$
$$+ \beta_{\text{SM-2}}^\lambda + \frac{(y_{L-}^2 + y_{L--}^2)}{(4\pi)^4}\left[-144\lambda^2 - 3\lambda(y_{L-}^2 + y_{L--}^2) + 18y_M^2(y_{L-}^2 + y_{L--}^2)\right.$$
$$- 27\lambda y_M^2 + 30y_{L-}^4 + 30y_{L--}^4 - 36g_1^2(y_{L-}^2 + y_{L--}^2) + \lambda\left(\frac{195}{2}g_1^2 + \frac{45}{2}g_2^2\right)$$
$$- \left.\frac{219}{4}g_1^4 - \frac{9}{4}g_2^4 - \frac{39}{2}g_1^2g_2^2\right]$$
$$+ \frac{1}{(4\pi)^4}\left[45\lambda g_1^4 + 15\lambda g_2^4 - 18g_1^6 - 18g_1^4 g_2^2 - 2g_1^2 g_2^4 - 6g_2^6\right].\qquad (\text{C.13})$$

The gauge couplings gain additional terms due to the new fermions from 2-loop corrections

$$\frac{dg_1^2}{d\ln\mu^2} = \frac{g_1^4}{16\pi^2}\left(\frac{41}{10} + \frac{27}{5}\right)$$
$$+ \frac{g_1^4}{(4\pi^4)}\left[\frac{2386}{9}g_1^2 + 90g_2^2 + \frac{88}{3}g_3^2 - \frac{17}{3}y_t^2 - \frac{3}{2}y_\tau^2 - 39y_{L-}^2 - 39y_{L--}^2 - 162y_M^2\right],$$
$$\frac{dg_2^2}{d\ln\mu^2} = \frac{g_2^4}{16\pi^2}\left(-\frac{19}{6} + \frac{7}{3}\right)$$
$$+ \frac{g_2^4}{(4\pi^4)}\left[30g_1^2 + \frac{182}{3}g_2^2 + 24g_3^2 - 3y_t^2 - \frac{1}{2}y_\tau^2 - 3y_{L-}^2 - 3y_{L--}^2 - 18y_M^2\right],$$
$$\frac{dg_3^2}{d\ln\mu^2} = \frac{g_3^4}{16\pi^2}(-7)$$
$$+ \frac{g_3^4}{(4\pi^4)}\left[\frac{11}{3}g_1^2 + 9g_2^2 - 52g_3^2 - 4y_t^2\right].\qquad (\text{C.14})$$

C.5 Triplet $\mathcal{T}_1$ (L^+, L^0, L^-), $Y = 0$

The relevant RGE for the Yukawa couplings are

$$
\begin{aligned}
\frac{dy_t^2}{d\ln\mu^2} &= \frac{y_t^2}{16\pi^2}\left(\frac{9y_t^2}{2} + y_\tau^2 + 2y_{L^+}^2 + 2y_{L^-}^2 + 2y_{L^0}^2 - \frac{17g_1^2}{20} - \frac{9g_2^2}{4} - 8g_3^2\right) \\
&+ \frac{y_t^2}{(4\pi)^4}\left[y_t^2\left(-12y_t^2 - \frac{9}{4}y_\tau^2 + 36g_3^2 + \frac{225}{16}g_2^2 + \frac{393}{80}g_1^2\right.\right. \\
&\quad\left. - 12\lambda - \frac{81}{8}y_{L^+}^2 - \frac{81}{8}y_{L^0}^2 - \frac{81}{8}y_{L^-}^2\right) \\
&+ y_\tau^2\left(-\frac{9}{4}y_\tau^2 - \frac{9}{2}y_{L^+}^2 - \frac{9}{2}y_{L^-}^2 - \frac{9}{2}y_{L^-}^2 + \frac{15}{8}g_1^2 + \frac{15}{8}g_2^2\right) \\
&+ (y_{L^+}^2 + y_{L^0}^2 + y_{L^-}^2)\left(-\frac{81}{8}y_M^2 + \frac{45}{16}g_1^2 + \frac{495}{16}g_2^2\right) \\
&- \frac{135}{32}y_{L^+}^4 - \frac{135}{32}y_{L^0}^4 - \frac{135}{32}y_{L^-}^4 + 12g_2^4 \\
&\left. - \frac{27}{2}y_\tau^4 - 108g_3^4 - \frac{23}{4}g_2^4 + \frac{1187}{600}g_1^4 + 9g_3^2g_2^2 + \frac{19}{15}g_3^2g_1^2 - \frac{9}{20}g_1^2g_2^2 + 6\lambda^2\right], \\[4pt]
\frac{dy_\tau^2}{d\ln\mu^2} &= \frac{y_\tau^2}{16\pi^2}\left(\frac{5y_\tau^2}{2} + \frac{5y_{L^0}^2}{2} + \frac{5y_{L^-}^2}{2} + 3y_t^2 + \frac{y_{L^+}^2}{2} - \frac{9g_1^2}{4} - \frac{9g_2^2}{4}\right) \\
&+ \frac{y_\tau^2}{(4\pi)^4}\left[y_\tau^2\left(-3y_\tau^2 - \frac{9}{2}y_{L^+}^2 - \frac{9}{2}y_{L^0}^2 - \frac{9}{2}y_{L^-}^2 + \frac{537}{80}g_1^2 + \frac{165}{16}g_2^2 - 12\lambda\right)\right. \\
&+ y_t^2\left(-\frac{27}{4}y_t^2 - \frac{27}{4}y_\tau^2 - \frac{27}{4}y_{L^+}^2 - \frac{27}{4}y_{L^0}^2 - \frac{27}{4}y_{L^-}^2 + \frac{17}{8}g_1^2 + \frac{45}{8}g_2^2 + 20g_3^2\right) \\
&\left. + \frac{25}{4}g_2^4 + \frac{1371}{200}g_1^4 + \frac{27}{20}g_1^2g_2^2 + 6\lambda^2\right], \\[4pt]
\frac{dy_{L^+}^2}{d\ln\mu^2} &= \frac{y_{L^+}^2}{16\pi^2}\left(3y_t^2 + \frac{5y_{L^+}^2}{2} + \frac{y_{L^0}^2}{2} + \frac{y_{L^-}^2}{2} + y_\tau^2 + \frac{y_M^2}{4} - \frac{9g_1^2}{20} - \frac{9g_2^2}{4}\right) \\
&+ \frac{y_{L^+}^2}{(4\pi)^4}\left[y_{L^+}^2\left(-\frac{45}{8}y_t^2 - \frac{9}{2}y_\tau^2 - \frac{342}{32}y_M^2 + \frac{205}{32}g_1^2 + \frac{1343}{32}g_2^2 - 10\lambda\right)\right. \\
&+ y_{L^0}^2\left(-\frac{45}{8}y_t^2 - \frac{9}{2}y_\tau^2 - \frac{342}{32}y_M^2 + \frac{123}{8}g_1^2 + \frac{1343}{32}g_2^2 - 10\lambda\right) \\
&+ y_{L^-}^2\left(-\frac{45}{8}y_t^2 - \frac{9}{2}y_\tau^2 - \frac{342}{32}y_M^2 + \frac{279}{8}g_1^2 + \frac{1343}{32}g_2^2 - 10\lambda\right) \\
&+ y_t^2\left(-\frac{27}{2}y_t^2 + \frac{85}{12}g_1^2 + \frac{45}{4}g_2^2 + 40g_3^2\right) - \frac{59}{8}y_{L^+}^4 - \frac{59}{96}y_{L^0}^4 - \frac{59}{96}y_{L^-}^4 - \frac{63}{4}y_M^4 \\
&\left. + 60g_2^2y_M^2 + \frac{35}{12}g_1^4 + \frac{5}{6}g_2^4 + \frac{3}{2}g_1^2g_2^2 + 12\lambda^2\right], \tag{C.15}
\end{aligned}
$$

$$
\begin{aligned}
\frac{dy^2_{L^0}}{d\ln\mu^2} &= \frac{y^2_{L^0}}{16\pi^2}\left(3y_t^2 + \frac{5y^2_{L^0}}{2} + \frac{y^2_{L^+}}{2} + \frac{y^2_{L^-}}{2} + y_\tau^2 + \frac{y_M^2}{4} - \frac{9g_1^2}{20} - \frac{9g_2^2}{4}\right) \\
&+ \frac{y^2_{L^0}}{(4\pi)^4}\left[y^2_{L^+}\left(-\frac{45}{8}y_t^2 - \frac{9}{2}y_\tau^2 - \frac{342}{32}y_M^2 + \frac{123}{3}g_1^2 + \frac{1343}{32}g_2^2 - 10\lambda\right)\right. \\
&+ y^2_{L^0}\left(-\frac{45}{8}y_t^2 - \frac{9}{2}y_\tau^2 - \frac{342}{32}y_M^2 + \frac{205}{32}g_1^2 + \frac{1343}{32}g_2^2 - 10\lambda\right) \\
&+ y^2_{L^-}\left(-\frac{45}{8}y_t^2 - \frac{9}{2}y_\tau^2 - \frac{342}{32}y_M^2 + \frac{279}{8}g_1^2 + \frac{1343}{32}g_2^2 - 10\lambda\right) \\
&+ y_t^2\left(-\frac{27}{2}y_t^2 + \frac{85}{12}g_1^2 + \frac{45}{4}g_2^2 + 40g_3^2\right) - \frac{59}{96}y^4_{L^+} - \frac{59}{8}y^4_{L^0} - \frac{59}{96}y^4_{L^-} - \frac{63}{4}y^4_M \\
&+ \left.60g_2^2 y_M^2 + \frac{35}{12}g_1^4 + \frac{5}{6}g_2^4 + \frac{3}{2}g_1^2 g_2^2 + 12\lambda^2\right], \\
\frac{dy^2_{L^-}}{d\ln\mu^2} &= \frac{y^2_{L^-}}{16\pi^2}\left(3y_t^2 + \frac{5y^2_{L^-}}{2} + \frac{y^2_{L^0}}{2} + \frac{y^2_{L^+}}{2} + y_\tau^2 + \frac{y_M^2}{4} - \frac{9g_1^2}{20} - \frac{9g_2^2}{4}\right) \\
&+ \frac{y^2_{L^-}}{(4\pi)^4}\left[y^2_{L^+}\left(-\frac{45}{8}y_t^2 - \frac{9}{2}y_\tau^2 - \frac{342}{32}y_M^2 + \frac{123}{8}g_1^2 + \frac{1343}{32}g_2^2 - 10\lambda\right)\right. \\
&+ y^2_{L^0}\left(-\frac{45}{8}y_t^2 - \frac{9}{2}y_\tau^2 - \frac{342}{32}y_M^2 + \frac{279}{8}g_1^2 + \frac{1343}{32}g_2^2 - 10\lambda\right) \\
&+ y^2_{L^-}\left(-\frac{45}{8}y_t^2 - \frac{9}{2}y_\tau^2 - \frac{342}{32}y_M^2 + \frac{205}{32}g_1^2 + \frac{1343}{32}g_2^2 - 10\lambda\right) \\
&+ y_t^2\left(-\frac{27}{2}y_t^2 + \frac{85}{12}g_1^2 + \frac{45}{4}g_2^2 + 40g_3^2\right) - \frac{59}{96}y^4_{L^+} - \frac{59}{96}y^4_{L^0} - \frac{59}{8}y^4_{L^-} - \frac{63}{4}y^4_M \\
&+ \left.60g_2^2 y_M^2 + \frac{35}{12}g_1^4 + \frac{5}{6}g_2^4 + \frac{3}{2}g_1^2 g_2^2 + 12\lambda^2\right], \\
\frac{dy^2_M}{d\ln\mu^2} &= \frac{y^2_M}{16\pi^2}\left(y^2_{L^+} + y^2_{L^-} + y^2_{L^0} + \frac{9y_M^2}{2} - 12g_2^2\right) \\
&+ \frac{y^2_M}{(4\pi)^4}\left[y^2_M\left(-\frac{109}{2}y_M^2 - \frac{21}{8}y^2_{L^+} - \frac{21}{8}y^2_{L^0} - \frac{21}{8}y^2_{L^-} + 156g_2^2\right)\right. \\
&- \frac{57}{32}y^4_{L^+} - \frac{57}{32}y^4_{L^0} - \frac{57}{32}y^4_{L^-} \\
&+ \left.(y^2_{L^+} + y^2_{L^0} + y^2_{L^-})\left(-\frac{9}{4}y_t^2 + \frac{17}{4}g_1^2 - \frac{101}{16}g_2^2\right) - \frac{106}{3}g_2^4\right]
\end{aligned}
\tag{C.16}
$$

The Higgs sector RGE, describing the interactions between the scalar boson and all fermions

$$
\begin{aligned}
\frac{d\lambda}{d\ln\mu^2} &= \frac{1}{16\pi^2}\left[\lambda\left(-\frac{9g_1^2}{10}-\frac{9g_2^2}{2}+6y_t^2+4y_{L^-}^2+4y_{L^+}^2+4y_{L^0}^2+4y_M^2+2y_\tau^2\right)+12\lambda^2\right.\\
&\quad + \frac{27g_1^4}{400}+\frac{9g_2^4}{16}+\frac{9g_1^2g_2^2}{20}-6y_t^4-4y_\tau^4-4y_{L^+}^4-4y_{L^-}^4-4y_{L^0}^4-4y_M^4\\
&\quad \left. - 4y_\tau^2 y_{L^-}^2-4y_M^2 y_{L^+}^2-4y_M^2 y_{L^-}^2-4y_M^2 y_{L^0}^2\right]\\
&\quad + \beta_{\text{SM-2}}^\lambda + \frac{(y_{L^+}^2+y_{L^0}^2+y_{L^-}^2)}{(4\pi)^4}\left[-108\lambda^2-\frac{15}{16}\lambda(y_{L^+}^2+y_{L^0}^2+y_{L^-}^2)-\frac{81}{12}\lambda y_M^2\right.\\
&\quad + \frac{45}{8}y_M^2(y_{L^+}^2+y_{L^0}^2+y_{L^-}^2)+\frac{141}{32}y_{L^+}^4+\frac{141}{32}y_{L^0}^4+\frac{141}{32}y_{L^-}^4+\lambda\left(\frac{45}{8}g_1^2+\frac{495}{8}g_2^2\right)\\
&\quad \left. - \frac{15}{2}g_2^2(y_{L^+}^2+y_{L^0}^2+y_{L^-}^2)-\frac{9}{16}g_1^4+\frac{21}{16}g_2^4-\frac{57}{8}g_1^2g_2^2\right]\\
&\quad + \frac{1}{(4\pi)^4}\left[60\lambda g_2^4-8g_1^2g_2^4-24g_2^6\right]. \quad\quad\quad\quad\quad\quad\quad\quad\quad\quad\text{(C.17)}
\end{aligned}
$$

The gauge couplings gain additional terms due to the new fermions from 2-loop corrections

$$
\begin{aligned}
\frac{dg_1^2}{d\ln\mu^2} &= \frac{g_1^4}{16\pi^2}\left(\frac{41}{10}\right)\\
&\quad + \frac{g_1^4}{(4\pi^4)}\left[\frac{199}{9}g_1^2+9g_2^2+\frac{88}{3}g_3^2-\frac{17}{3}y_t^2-\frac{3}{2}y_\tau^2-\frac{9}{4}y_{L^+}^2-\frac{9}{4}y_{L^0}^2-\frac{9}{4}y_{L^-}^2\right],\\
\frac{dg_2^2}{d\ln\mu^2} &= \frac{g_2^4}{16\pi^2}\left(-\frac{19}{6}+\frac{16}{3}\right)\\
&\quad + \frac{g_2^4}{(4\pi^4)}\left[3g_1^2+\frac{803}{3}g_2^2+24g_3^2-3y_t^2-\frac{1}{2}y_\tau^2-\frac{33}{4}y_{L^+}^2-\frac{33}{4}y_{L^0}^2-\frac{33}{4}y_{L^-}^2-72y_M^2\right],\\
\frac{dg_3^2}{d\ln\mu^2} &= \frac{g_3^4}{16\pi^2}(-7)\\
&\quad + \frac{g_3^4}{(4\pi^4)}\left[\frac{11}{3}g_1^2+9g_2^2-52g_3^2-4y_t^2\right]. \quad\quad\quad\quad\quad\quad\quad\quad\quad\text{(C.18)}
\end{aligned}
$$

C.6 Triplet $\mathcal{T}_2$ (L^0, L^-, L^{--}), $Y = -1$

$$
\begin{aligned}
\frac{dy_t^2}{d\ln\mu^2} &= \frac{y_t^2}{16\pi^2}\left(\frac{9y_t^2}{2} + y_\tau^2 + 2y_{L^{--}}^2 + 2y_{L^-}^2 + 2y_{L^0}^2 - \frac{17g_1^2}{20} - \frac{9g_2^2}{4} - 8g_3^2\right) \\
&+ \frac{y_t^2}{(4\pi)^4}\left[y_t^2\left(-12y_t^2 - \frac{9}{4}y_\tau^2 + 36g_3^2 + \frac{225}{16}g_2^2 + \frac{393}{80}g_1^2 - 12\lambda\right.\right. \\
&- \frac{81}{8}y_{L^0}^2 - \frac{81}{8}y_{L^-}^2 - \frac{81}{8}y_{L^{--}}^2\bigg) \\
&+ y_\tau^2\left(-\frac{9}{4}y_\tau^2 - \frac{9}{2}y_{L^0}^2 - \frac{9}{2}y_{L^-}^2 - \frac{9}{2}y_{L^{--}}^2 + \frac{15}{8}g_1^2 + \frac{15}{8}g_2^2\right) \\
&+ (y_{L^0}^2 + y_{L^-}^2 + y_{L^{--}}^2)\left(-\frac{81}{8}y_M^2 + \frac{225}{16}g_1^2 + \frac{495}{16}g_2^2\right) \\
&- \frac{135}{32}y_{L^0}^4 - \frac{135}{32}y_{L^-}^4 - \frac{135}{32}y_{L^{--}}^4 + \frac{58}{3}g_1^4 + 12g_2^4 \\
&- \frac{27}{2}y_\tau^4 - 108g_3^4 - \frac{23}{4}g_2^4 + \frac{1187}{600}g_1^4 + 9g_3^2g_2^2 + \frac{19}{15}g_3^2g_1^2 - \frac{9}{20}g_1^2g_2^2 + 6\lambda^2\bigg], \\
\frac{dy_\tau^2}{d\ln\mu^2} &= \frac{y_\tau^2}{16\pi^2}\left(\frac{5y_\tau^2}{2} + \frac{5y_{L^-}^2}{2} + \frac{5y_{L^{--}}^2}{2} + 3y_t^2 + \frac{y_{L^0}^2}{2} - \frac{9g_1^2}{4} - \frac{9g_2^2}{4}\right) \\
&+ \frac{y_\tau^2}{(4\pi)^4}\left[y_\tau^2\left(-3y_\tau^2 - \frac{9}{2}y_{L^0}^2 - \frac{9}{2}y_{L^-}^2 - \frac{9}{2}y_{L^{--}}^2 + \frac{537}{80}g_1^2 + \frac{165}{16}g_2^2 - 12\lambda\right)\right. \\
&+ y_t^2\left(-\frac{27}{4}y_t^2 - \frac{27}{4}y_\tau^2 - \frac{27}{4}y_{L^0}^2 - \frac{27}{4}y_{L^-}^2 - \frac{27}{4}y_{L^{--}}^2 + \frac{17}{8}g_1^2 + \frac{45}{8}g_2^2 + 20g_3^2\right) \\
&+ 29g_1^4 + \frac{25}{4}g_2^4 + \frac{1371}{200}g_1^4 + \frac{27}{20}g_1^2g_2^2 + 6\lambda^2\bigg], \\
\frac{dy_{L^0}^2}{d\ln\mu^2} &= \frac{y_{L^0}^2}{16\pi^2}\left(3y_t^2 + \frac{5y_{L^0}^2}{2} + \frac{y_{L^-}^2}{2} + \frac{y_{L^{--}}^2}{2} + y_\tau^2 + \frac{y_M^2}{4} - \frac{9g_1^2}{4} - \frac{9g_2^2}{4}\right) \\
&+ \frac{y_{L^0}^2}{(4\pi)^4}\left[y_{L^0}^2\left(-\frac{45}{8}y_t^2 - \frac{9}{2}y_\tau^2 - \frac{342}{32}y_M^2 + \frac{785}{32}g_1^2 + \frac{1343}{32}g_2^2 - 10\lambda\right)\right. \\
&+ y_{L^-}^2\left(-\frac{45}{8}y_t^2 - \frac{9}{2}y_\tau^2 - \frac{342}{32}y_M^2 + \frac{279}{32}g_1^2 + \frac{1343}{32}g_2^2 - 10\lambda\right) \\
&+ y_{L^{--}}^2\left(-\frac{45}{8}y_t^2 - \frac{9}{2}y_\tau^2 - \frac{342}{32}y_M^2 + \frac{785}{32}g_1^2 + \frac{1343}{32}g_2^2 - 10\lambda\right) \\
&+ y_t^2\left(-\frac{27}{2}y_t^2 + \frac{85}{12}g_1^2 + \frac{45}{4}g_2^2 + 40g_3^2\right) - \frac{59}{8}y_{L^0}^4 - \frac{59}{96}y_{L^-}^4 - \frac{59}{96}y_{L^{--}}^4 - \frac{63}{4}y_M^4 \\
&+ 6g_1^2y_M^2 + 60g_2^2y_M^2 + \frac{1249}{12}g_1^4 + \frac{5}{6}g_2^4 - \frac{3}{2}g_1^2g_2^2 + 12\lambda^2\bigg], \quad\quad (C.19)
\end{aligned}
$$

$$\frac{dy_{L^-}^2}{d\ln\mu^2} = \frac{y_{L^-}^2}{16\pi^2}\left(3y_t^2 + \frac{5y_{L^-}^2}{2} + \frac{y_{L^0}^2}{2} + \frac{y_{L^{--}}^2}{2} + y_\tau^2 + \frac{y_M^2}{4} - \frac{9g_1^2}{4} - \frac{9g_2^2}{4}\right)$$

$$+ \frac{y_{L^0}^2}{(4\pi)^4}\left[y_{L^0}^2\left(-\frac{45}{8}y_t^2 - \frac{9}{2}y_\tau^2 - \frac{342}{32}y_M^2 + \frac{123}{8}g_1^2 + \frac{1343}{32}g_2^2 - 10\lambda\right)\right.$$

$$+ \; y_{L^-}^2\left(-\frac{45}{8}y_t^2 - \frac{9}{2}y_\tau^2 - \frac{342}{32}y_M^2 + \frac{785}{32}g_1^2 + \frac{1343}{32}g_2^2 - 10\lambda\right)$$

$$+ \; y_{L^{--}}^2\left(-\frac{45}{8}y_t^2 - \frac{9}{2}y_\tau^2 - \frac{342}{32}y_M^2 + \frac{785}{32}g_1^2 + \frac{1343}{32}g_2^2 - 10\lambda\right)$$

$$+ \; y_t^2\left(-\frac{27}{2}y_t^2 + \frac{85}{12}g_1^2 + \frac{45}{4}g_2^2 + 40g_3^2\right) - \frac{59}{96}y_{L^0}^4 - \frac{59}{8}y_{L^-}^4 - \frac{59}{96}y_{L^{--}}^4 - \frac{63}{4}y_M^4$$

$$+ \; 6g_1^2 y_M^2 + 60g_2^2 y_M^2 + \frac{1249}{12}g_1^4 + \frac{5}{6}g_2^4 - \frac{3}{2}g_1^2 g_2^2 + 12\lambda^2\bigg],$$

$$\frac{dy_{L^{--}}^2}{d\ln\mu^2} = \frac{y_{L^{--}}^2}{16\pi^2}\left(3y_t^2 + \frac{5y_{L^{--}}^2}{2} + \frac{y_{L^0}^2}{2} + \frac{y_{L^-}^2}{2} + y_\tau^2 + \frac{y_M^2}{4} - \frac{9g_1^2}{4} - \frac{9g_2^2}{4}\right)$$

$$+ \frac{y_{L^0}^2}{(4\pi)^4}\left[y_{L^0}^2\left(-\frac{45}{8}y_t^2 - \frac{9}{2}y_\tau^2 - \frac{342}{32}y_M^2 + \frac{279}{8}g_1^2 + \frac{1343}{32}g_2^2 - 10\lambda\right)\right.$$

$$+ \; y_{L^-}^2\left(-\frac{45}{8}y_t^2 - \frac{9}{2}y_\tau^2 - \frac{342}{32}y_M^2 + \frac{279}{8}g_1^2 + \frac{1343}{32}g_2^2 - 10\lambda\right)$$

$$+ \; y_{L^{--}}^2\left(-\frac{45}{8}y_t^2 - \frac{9}{2}y_\tau^2 - \frac{342}{32}y_M^2 + \frac{785}{32}g_1^2 + \frac{1343}{32}g_2^2 - 10\lambda\right)$$

$$+ \; y_t^2\left(-\frac{27}{2}y_t^2 + \frac{85}{12}g_1^2 + \frac{45}{4}g_2^2 + 40g_3^2\right) - \frac{59}{96}y_{L^0}^4 - \frac{59}{96}y_{L^-}^4 - \frac{59}{8}y_{L^{--}}^4 - \frac{63}{4}y_M^4$$

$$+ \; 6g_1^2 y_M^2 + 60g_2^2 y_M^2 + \frac{1249}{12}g_1^4 + \frac{5}{6}g_2^4 - \frac{3}{2}g_1^2 g_2^2 + 12\lambda^2\bigg],$$

$$\frac{dy_M^2}{d\ln\mu^2} = \frac{y_M^2}{16\pi^2}\left(y_{L^0}^2 + y_{L^-}^2 + y_{L^{--}}^2 + \frac{9y_M^2}{2} - \frac{81}{20}g_1^2 - 12g_2^2\right)$$

$$+ \frac{y_M^2}{(4\pi)^4}\left[y_M^2\left(-\frac{109}{2}y_M^2 - \frac{21}{8}y_{L^0}^2 - \frac{21}{8}y_{L^-}^2 - \frac{21}{8}y_{L^{--}}^2 + 78g_1^2 + 156g_2^2\right)\right.$$

$$- \; \frac{57}{32}y_{L^0}^4 - \frac{57}{32}y_{L^-}^4 - \frac{57}{32}y_{L^{--}}^4 + (y_{L^0}^2 + y_{L^-}^2 + y_{L^{--}}^2)\left(-\frac{9}{4}y_t^2 + \frac{37}{4}g_1^2 - \frac{101}{16}g_2^2\right)$$

$$+ \; \frac{553}{3}g_1^4 - \frac{106}{3}g_2^4 - 24g_1^2 g_2^2\bigg]. \tag{C.20}$$

The Higgs sector RGE, describing the interactions between the scalar boson and all fermions:

$$
\begin{aligned}
\frac{d\lambda}{d\ln\mu^2} =\ & \frac{1}{16\pi^2}\left[\lambda\left(-\frac{9g_1^2}{5} - 9g_2^2 + 6y_t^2 + 4y_{L-}^2 + 4y_{L--}^2 + 4y_{L^0}^2 + 4y_M^2 + 2y_\tau^2\right) + 12\lambda^2\right. \\
& +\ \frac{27g_1^4}{400} + \frac{9g_2^4}{16} + \frac{9g_1^2 g_2^2}{20} - 6y_t^4 - 4y_\tau^4 - 4y_{L--}^4 - 4y_{L-}^4 - 4y_{L^0}^4 - 4y_M^4 \\
& -\ 4y_\tau^2 y_{L-}^2 - 4y_M^2 y_{L--}^2 - 4y_M^2 y_{L-}^2 - 4y_M^2 y_{L^0}^2 \Big] \\
& +\ \beta_{\text{SM-2}}^\lambda + \frac{(y_{L^0}^2 + y_{L-}^2 + y_{L--}^2)}{(4\pi)^4}\left[-108\lambda^2 - \frac{15}{16}\lambda(y_{L^0}^2 + y_{L-}^2 + y_{L--}^2) - \frac{81}{12}\lambda y_M^2\right. \\
& +\ \frac{45}{8}y_M^2(y_{L^0}^2 + y_{L-}^2 + y_{L--}^2) + \frac{141}{32}y_{L^0}^4 + \frac{141}{32}y_{L-}^4 + \frac{141}{32}y_{L--}^4 \\
& +\ +\lambda\left(\frac{225}{8}g_1^2 + \frac{495}{8}g_2^2\right) - \frac{15}{4}g_1^2(y_{L^0}^2 + y_{L-}^2 + y_{L--}^2) - \frac{15}{2}g_2^2(y_{L^0}^2 + y_{L-}^2 + y_{L--}^2) \\
& -\ \frac{225}{16}g_1^4 + \frac{21}{16}g_2^4 + \frac{51}{8}g_1^2 g_2^2 \Big] \\
& +\ \frac{1}{(4\pi)^4}\left[30\lambda g_1^4 + 60\lambda g_2^4 - 12g_1^6 - 12g_1^4 g_2^2 - 8g_1^2 g_2^4 - 24g_2^6\right].
\end{aligned}
\tag{C.21}
$$

The gauge couplings gain additional terms due to the new fermions from 2-loop corrections

$$
\begin{aligned}
\frac{dg_1^2}{d\ln\mu^2} =\ & \frac{g_1^4}{16\pi^2}\left(\frac{41}{10} + \frac{12}{5}\right) \\
& +\ \frac{g_1^4}{(4\pi^4)}\left[\frac{847}{9}g_1^2 + 105g_2^2 + \frac{88}{3}g_3^2 - \frac{17}{3}y_t^2 - \frac{3}{2}y_\tau^2 - \frac{45}{4}y_{L^0}^2 - \frac{45}{4}y_{L-}^2 - \frac{45}{4}y_{L--}^2 \right. \\
& \left. -108y_M^2\right], \\
\frac{dg_2^2}{d\ln\mu^2} =\ & \frac{g_2^4}{16\pi^2}\left(-\frac{19}{6} + \frac{16}{3}\right) \\
& +\ \frac{g_2^4}{(4\pi^4)}\left[51g_1^2 + \frac{803}{3}g_2^2 + 24g_3^2 - 3y_t^2 - \frac{1}{2}y_\tau^2 - \frac{33}{4}y_{L^0}^2 - \frac{33}{4}y_{L-}^2 - \frac{33}{4}y_{L--}^2 \right. \\
& \left. -72y_M^2\right], \\
\frac{dg_3^2}{d\ln\mu^2} =\ & \frac{g_3^4}{16\pi^2}\left(-7\right) \\
& +\ \frac{g_3^4}{(4\pi^4)}\left[\frac{11}{3}g_1^2 + 9g_2^2 - 52g_3^2 - 4y_t^2\right].
\end{aligned}
\tag{C.22}
$$

And the SM part of the 2-loop RGE for the Higgs quartic coupling in all VLL models read [296]

$$
\begin{aligned}
\frac{d\lambda_{\text{SM-2}}}{d\ln\mu^2} =\ & \frac{1}{(4\pi)^4} \left[\lambda^2 \left(-156\lambda - 72y_t^2 - 72y_b^2 - 24y_\tau^2 + 54g_2^2 + \frac{54}{5}g_1^2 \right) \right. \\
& + \lambda y_t^2 \left(-\frac{3}{2}y_t^2 - 21y_b^2 + 40g_3^2 + \frac{45}{4}g_2^2 + \frac{17}{4}g_1^2 \right) + \lambda y_\tau^2 \left(-\frac{1}{2}y_\tau^2 + \frac{15}{4}g_2^2 + \frac{15}{4}g_1^2 \right) \\
& + \lambda y_b^2 \left(-\frac{3}{2}y_b^2 + 40g_3^2 + \frac{45}{4}g_2^2 + \frac{5}{4}g_1^2 \right) + \lambda \left(-\frac{73}{16}g_2^4 + \frac{1887}{400}g_1^4 + \frac{117}{40}g_1^2 g_2^2 \right) \\
& + y_t^4 \left(15y_t^2 - 3y_b^2 - 16g_3^2 - \frac{4}{5}g_1^2 \right) + y_t^2 \left(-\frac{9}{8}g_2^4 - \frac{171}{200}g_1^4 + \frac{63}{20}g_1^2 g_2^2 \right) \\
& + y_b^4 \left(-3y_t^2 + 15y_b^2 - 16g_3^2 + \frac{2}{5}g_1^2 \right) + y_b^2 \left(-\frac{9}{8}g_2^4 + \frac{9}{40}g_1^4 + \frac{27}{20}g_1^2 g_2^2 \right) \\
& + y_\tau^4 \left(5y_\tau^2 - \frac{6}{5}g_2^2 \right) + y_\tau^2 \left(-\frac{3}{8}g_2^4 - \frac{9}{8}g_1^4 + \frac{33}{20}g_1^2 g_2^2 \right) \\
& \left. + \frac{305}{32}g_2^6 - \frac{3411}{4000}g_1^6 - \frac{289}{160}g_1^2 g_2^4 - \frac{1677}{800}g_1^4 g_2^2 \right].
\end{aligned}
$$

(C.23)

Appendix D

Passarino-Veltman Integrals

Although a more detailed discussion about Passarino-Veltman (PV) reduction appears elsewhere [297], we give a generic one-loop tensor integral as the following

$$T_\rho^{\nu_i} = \frac{(2\pi\mu)^{4-D}}{i\pi^2} \int d^D p \frac{p^{\nu_i} \cdots p^{\nu_n}}{\mathbb{D}_1 \cdots \mathbb{D}_\rho} \tag{D.1}$$

where the propagators are described by

$$\begin{aligned}
\mathbb{D}_1 &= p^2 - m_1^2 + i\epsilon, \\
\mathbb{D}_2 &= (p+q_1)^2 - m_2^2 + i\epsilon, \\
\mathbb{D}_3 &= (p+q_1+q_2)^2 - m_3^2 + i\epsilon, \tag{D.2}
\end{aligned}$$

After factoring out the $i/(16\pi^2)$, scalar, vector and tensor functions are defined from the generic one-loop tensor integral Eq. D.1:

$$\begin{aligned}
A(m_1) &= \mu^{4-D} \int \frac{d^D p}{(2\pi)^D \mathbb{D}_1}, \\
[B_0, B^\mu, B^{\mu\nu}](q_1^2, m_1^2, m_2^2) &= \mu^{4-D} \int \frac{d^D p}{(2\pi)^D} \frac{[1, p^\mu, p^\mu p^\nu]}{\mathbb{D}_1 \mathbb{D}_2}, \\
[C_0, C^\mu, C^{\mu\nu}](q_1^2, q_2^2, (q_1+q_2)^2, m_1^2, m_2^2, m_3^2) &= \mu^{4-D} \int \frac{d^D p}{(2\pi)^D} \frac{[1, p^\mu, p^\mu p^\nu]}{\mathbb{D}_1 \mathbb{D}_2 \mathbb{D}_3} \tag{D.3}
\end{aligned}$$

Scalar and tensor integrals are not independent. In fact, tensor forms can be decomposed in terms of scalar functions:

$$\begin{aligned}
B^\mu &= q_1^\mu B_1, & C^\mu &= q_1^\mu C_1 + q_2^\mu C_2, \\
B^{\mu\nu} &= q_1^\mu q_1^\nu B_{11} + g^{\mu\nu} B_{00}, & C^{\mu\nu} &= \sum_{i=1}^2 q_i^\mu q_j^\nu C_{ij} + g^{\mu\nu} C_{00} \\
& & C^{\mu\nu\delta} &= \sum_{i,j,k=1}^2 q_i^\mu q_j^\nu q_k^\delta C_{ijk} + \sum_{i=1}^2 (q_i^\mu g^{\nu\delta} + q_i^\nu g^{\delta\mu} + q_i^\delta g^{\mu\nu}) C_{00i}
\end{aligned}$$
$$\tag{D.4}$$

Scalar integrals or vacuum integrals play a main role for all intents and purposes throughout this work. Furthermore, there are only four type of independent scalar(vacuum) integrals.

The rest of the vacuum integrals carried out throughout this work are combination of the following definitions:

$$
\begin{aligned}
A_0(m_1^2) &= \frac{(2\pi\mu)^\epsilon}{i\pi^2} \int d^D p \frac{1}{p^2 - m_1^2}, \\
B_0(q_1^2, m_1^2, m_2^2) &= \frac{(2\pi\mu)^\epsilon}{i\pi^2} \int d^D p \frac{1}{[p^2 - m_1^2]} \frac{1}{[(p+q_1)^2 - m_2^2]}, \\
C_0(q_i^2, q_{ij}^2, m_i^2) &= \frac{(2\pi\mu)^\epsilon}{i\pi^2} \int d^D p \frac{1}{[p^2 - m_1^2]} \frac{1}{[(p+q_1)^2 - m_2^2]} \frac{1}{[(p+q_{12})^2 - m_3^2]}, \\
D_0(q_i^2, q_{ij}^2, m_i^2) &= \frac{(2\pi\mu)^\epsilon}{i\pi^2} \int d^D p \frac{1}{[p^2 - m_1^2]} \frac{1}{[(p+q_1)^2 - m_2^2]} \frac{1}{[(p+q_{12})^2 - m_3^2]} \\
&\quad \times \frac{1}{[(p+q_{123})^2 - m_4^2]}
\end{aligned}
$$

(D.5)

where $\epsilon = 4 - D$. Explicit analytical expressions of widely used PV functions are defined as

$$
\begin{aligned}
A_0(m^2) &= m^2 \left(1 - \ln \frac{m^2}{\mu^2}\right), \\
B_0(0, m_1^2, m_2^2) &= \frac{A_0(m_1^2) - A_0(m_2^2)}{m_1^2 - m_2^2}, \\
B_0(0, m_1^2, m_1^2) &= \frac{A_0(m_1^2)}{m_1^2} - 1, \\
B_0(m_1^2, 0, m_1^2) &= \frac{A_0(m_1^2)}{m_1^2} + 1, \\
B_1(0, m_1^2, m_2^2) &= \frac{2y^2 \ln y_2 - 4y_2 \ln y_2 - y_2^2 + 4y_2 - 3}{4(y_2 - 1)^2} + \frac{1}{2} \ln \frac{m_1^2}{\mu^2}, \\
B_{00}(m_1^2, m_2^2, m_3^2) &= \frac{(m_1^2 - m_2^2)(m_1^2 - m_3^2)(m_2^2 - m_3^2) B_0(m_1^2, m_2^2, m_3^2)}{4(1-D)m_1^2} \\
&\quad + \frac{A_0(m_2^2)(m_1^2 + m_2^2 - m_3^2)}{4(1-D)m_1^2} - \frac{A_0(m_3^2)(m_1^2 - m_2^2 + m_3^2)}{4(1-D)m_1^2}, \\
B_{00}(0, m_2^2, m_3^2) &= -\frac{A_0(m_3^2)}{2(1-D)} - \frac{m_2^2 B_0(0, m_2^2, m_3^2)}{1-D} - \frac{(m_2^2 - m_3^2) B_1(0, m_2^2, m_3^2)}{2(1-D)}, \\
B_{00}(0, m^2, m^2) &= -\frac{A_0(m^2)}{2(1-D)} - \frac{m^2 B_0(0, m^2, m^2)}{1-D}, \\
B_{00}(m_1^2, m_2^2, m_2^2) &= \frac{(m_1^2 - 4m_2^2) B_0(m_1^2, m_2^2, m_2^2)}{4(1-D)} - \frac{A_0(m_2^2)}{2(1-D)}, \\
C_0(m_1^2, m_2^2, m_3^2) &= \frac{1}{m_1^2} \frac{y_2 \ln y_2 - y_3 \ln y_3 - y_2 y_3 \ln y_2 + y_2 y_3 \ln y_3}{(y_2 - 1)(y_3 - 1)(y_2 - y_3)}, \\
C_0(m_1^2, m_2^2, m_2^2) &= \frac{1}{m_1^2} \frac{\ln y_2 - y_2 + 1}{(y_2 - 1)^2}, \\
C_0(m^2, m^2, m^2) &= -\frac{1}{2m^2},
\end{aligned}
$$

(D.6)

and the mass ratio parameter

$$
y_i = \frac{m_i^2}{m_1^2}.
$$

It is useful to isolate the divergent part of the Passarino-Veltman integrals:

$$
\begin{aligned}
\mathrm{Div}\left[A_0(m^2)\right] &= \Delta_\epsilon\, m^2, \\
\mathrm{Div}\left[B_0(p_{21}^2, m_1^2, m_2^2)\right] &= \Delta_\epsilon, \\
\mathrm{Div}\left[B_1(p_{21}^2, m_1^2, m_2^2)\right] &= -\frac{1}{2}\Delta_\epsilon, \\
\mathrm{Div}\left[B_{00}(p_{21}^2, m_1^2, m_2^2)\right] &= \frac{1}{12}\Delta_\epsilon\left(3m_1^2 + 3m_2^2 - p_{21}^2\right), \\
\mathrm{Div}\left[B_{11}(p_{21}^2, m_1^2, m_2^2)\right] &= \frac{1}{3}\Delta_\epsilon, \\
\mathrm{Div}\left[B_{00}(m_1^2, m_2^2, m_3^2)\right] &= \frac{1}{4}\Delta_\epsilon,
\end{aligned}
\tag{D.7}
$$

where the divergent term in MS scheme is given by

$$
\Delta_\epsilon = \frac{2}{\epsilon} - \gamma_E + \ln 4\pi\,.
\tag{D.8}
$$

Finally, the complementary relations to the definitions above can be summarized with the following four scalar functions:

$$
\begin{aligned}
B_2(p^2, m_1^2, m_2^2) &= B_{21}(p^2, m_1^2, m_2^2), \\
B_3(p^2, m_1^2, m_2^2) &= -B_1(p^2, m_1^2, m_2^2) - B_{21}(p^2, m_1^2, m_2^2), \\
B_4(p^2, m_1^2, m_2^2) &= -m_1^2 B_1(p^2, m_2^2, m_1^2) - m_2^2 B_1(p^2, m_1^2, m_2^2), \\
B_5(p^2, m_1^2, m_2^2) &= A_0(m_1^2) + A_0(m_2^2) - 4B_{22}(p^2, m_1^2, m_2^2).
\end{aligned}
\tag{D.9}
$$

Appendix E

Electroweak couplings of vector-like fermions and the SM fermions

Couplings of the SM gauge bosons to fermions are uniquely modified with new mass eigenstates of vector-like fermions in terms of mass splitting expressions. We give the complete list of electroweak couplings used in calculation of Peskin-Takeuchi parameters.

E.1 EW corrections from VLQs

E.1.1 Singlet $\mathcal{U}_1$ (T), $Y = 2/3$

$$
\Omega_{Wtb}^L = \frac{ec_L^t}{\sqrt{2}s_W} \qquad\qquad \Omega_{Ztt}^L = \frac{e}{2s_W c_W}(c_L^{t2} - \frac{4}{3}s_W^2)
$$

$$
\Omega_{Wtb}^R = 0 \qquad\qquad \Omega_{Ztt}^R = -\frac{2es_W}{3c_W}
$$

$$
\Omega_{WTb}^L = \frac{es_L^t}{\sqrt{2}s_W} \qquad\qquad \Omega_{ZTT}^L = \frac{e}{2s_W c_W}(s_L^{t2} - \frac{4}{3}s_W^2)
$$

$$
\Omega_{WTb}^R = 0 \qquad\qquad \Omega_{ZTT}^R = -\frac{2es_W}{3c_W}
$$

$$
\Omega_{Zbb}^L = \frac{e}{2s_W c_W}(\frac{2}{3}s_W^2 - 1)
$$

$$
\Omega_{Zbb}^R = \frac{es_W}{3c_W}
$$

$$
\Omega_{ZtT}^L = \frac{es_L^t c_L^t}{2s_W c_W}
$$

$$
\Omega_{ZtT}^R = 0 \qquad\qquad\qquad\qquad (\text{E.1})
$$

E.1.2 Singlet $\mathcal{D}_1$ (B), $Y = -1/3$

$$\Omega_{Wtb}^L = \frac{ec_L^b}{\sqrt{2}s_W} \qquad\qquad \Omega_{Ztt}^L = \frac{e}{2s_Wc_W}(1 - \frac{4}{3}s_W^2)$$

$$\Omega_{Wtb}^R = 0 \qquad\qquad \Omega_{Ztt}^R = -\frac{2es_W}{3c_W}$$

$$\Omega_{WtB}^L = \frac{es_L^b}{\sqrt{2}s_W} \qquad\qquad \Omega_{Zbb}^L = \frac{e}{2s_Wc_W}(\frac{2}{3}s_W^2 - c_L^{b2})$$

$$\Omega_{WtB}^R = 0 \qquad\qquad \Omega_{Zbb}^R = \frac{es_W}{3c_W}$$

$$\Omega_{ZBB}^L = \frac{e}{2s_Wc_W}(\frac{2}{3}s_W^2 - s_L^{b2})$$

$$\Omega_{ZBB}^R = \frac{es_W}{3c_W}$$

$$\Omega_{ZbB}^L = -\frac{es_L^bc_L^b}{2s_Wc_W}$$

$$\Omega_{ZbB}^R = 0 \qquad\qquad\qquad (E.2)$$

E.1.3 Doublet $\mathcal{D}_2$ (T, B), $Y = 1/6$

$$\Omega_{Wtb}^L = \frac{e}{\sqrt{2}s_W}(s_L^ts_L^b + c_L^tc_L^b) \qquad\qquad \Omega_{Ztt}^L = \frac{e}{2s_Wc_W}(1 - \frac{4}{3}s_W^2)$$

$$\Omega_{Wtb}^R = \frac{es_R^ts_R^b}{\sqrt{2}s_W} \qquad\qquad \Omega_{Ztt}^R = \frac{e}{2s_Wc_W}(s_R^{t2} - \frac{4}{3}s_W^2)$$

$$\Omega_{WTb}^L = \frac{e}{\sqrt{2}s_W}(s_L^tc_L^b - s_L^bc_L^t) \qquad\qquad \Omega_{Zbb}^L = \frac{e}{2s_Wc_W}(\frac{2}{3}s_W^2 - 1)$$

$$\Omega_{WTb}^R = -\frac{es_R^bc_R^t}{\sqrt{2}s_W} \qquad\qquad \Omega_{Zbb}^R = \frac{e}{2s_Wc_W}(\frac{2}{3}s_W^2 - s_R^{b2})$$

$$\Omega_{WtB}^L = \frac{e}{\sqrt{2}s_W}(s_L^bc_L^t - s_L^tc_L^b) \qquad\qquad \Omega_{ZtT}^L = 0$$

$$\Omega_{WtB}^R = -\frac{es_R^tc_R^b}{\sqrt{2}s_W} \qquad\qquad \Omega_{ZtT}^R = -\frac{es_R^tc_R^t}{2s_Wc_W}$$

$$\Omega_{WTB}^L = \frac{e}{\sqrt{2}s_W}(s_L^ts_L^b + c_L^tc_L^b) \qquad\qquad \Omega_{ZbB}^L = 0$$

$$\Omega_{WTB}^R = \frac{ec_R^tc_R^b}{\sqrt{2}s_W} \qquad\qquad \Omega_{ZbB}^R = \frac{es_R^bc_R^b}{2s_Wc_W}$$

$$\Omega_{ZTT}^L = \frac{e}{2s_Wc_W}(1 - \frac{4}{3}s_W^2)$$

$$\Omega_{ZTT}^R = \frac{e}{2s_Wc_W}(c_R^{t2} - \frac{4}{3}s_W^2)$$

$$\Omega_{ZBB}^L = \frac{e}{2s_Wc_W}(\frac{2}{3}s_W^2 - 1)$$

$$\Omega_{ZBB}^R = \frac{e}{2s_Wc_W}(\frac{2}{3}s_W^2 - c_R^{b2}) \qquad (E.3)$$

E.1.4 Doublet $\mathcal{D}_X$ (X, T), $Y = 7/6$

$$\Omega_{Wtb}^L = \frac{ec_L^t}{\sqrt{2}s_W}$$

$$\Omega_{Wtb}^R = 0$$

$$\Omega_{WTb}^L = \frac{es_L^t}{\sqrt{2}s_W}$$

$$\Omega_{WTb}^R = 0$$

$$\Omega_{WtX}^L = -\frac{es_L^t}{\sqrt{2}s_W}$$

$$\Omega_{WtX}^R = -\frac{es_R^t}{\sqrt{2}s_W}$$

$$\Omega_{WTX}^L = \frac{ec_L^t}{\sqrt{2}s_W}$$

$$\Omega_{WTX}^R = \frac{ec_R^t}{\sqrt{2}s_W}$$

$$\Omega_{Ztt}^L = \frac{e}{2s_Wc_W}(1 - \frac{4}{3}s_W^2 - 2s_L^{t2})$$

$$\Omega_{Ztt}^R = -\frac{e}{2s_Wc_W}(\frac{4}{3}s_W^2 + s_R^{t2})$$

$$\Omega_{Zbb}^L = \frac{e}{2s_Wc_W}(\frac{2}{3}s_W^2 - 1)$$

$$\Omega_{Zbb}^R = \frac{es_W}{3c_W}$$

$$\Omega_{ZtT}^L = \frac{es_L^tc_L^t}{s_Wc_W}$$

$$\Omega_{ZtT}^R = \frac{es_R^tc_R^t}{2s_Wc_W}$$

$$\Omega_{ZTT}^L = \frac{e}{2s_Wc_W}(1 - \frac{4}{3}s_W^2 - c_L^{t2})$$

$$\Omega_{ZTT}^R = -\frac{e}{2s_Wc_W}(c_R^{t2} + \frac{4}{3}s_W^2)$$

$$\Omega_{ZXX}^L = \frac{e}{2s_Wc_W}(1 - \frac{10}{3}s_W^2)$$

$$\Omega_{ZXX}^R = \frac{e}{2s_Wc_W}(1 - \frac{10}{3}s_W^2) \tag{E.4}$$

E.1.5 Doublet $\mathcal{D}_Y$ (B, Y), $Y = -5/6$

$$\Omega_{Wtb}^L = \frac{ec_L^b}{\sqrt{2}s_W}$$

$$\Omega_{Wtb}^R = 0$$

$$\Omega_{WBt}^L = \frac{es_L^b}{\sqrt{2}s_W}$$

$$\Omega_{WBt}^R = 0$$

$$\Omega_{WbY}^L = -\frac{es_L^b}{\sqrt{2}s_W}$$

$$\Omega_{WbY}^R = -\frac{es_R^b}{\sqrt{2}s_W}$$

$$\Omega_{WBY}^L = \frac{ec_L^b}{\sqrt{2}s_W}$$

$$\Omega_{WBY}^R = \frac{ec_R^b}{\sqrt{2}s_W}$$

$$\Omega_{Ztt}^L = \frac{e}{2s_Wc_W}(1 - \frac{4}{3}s_W^2)$$

$$\Omega_{Ztt}^R = -\frac{2es_W}{3c_W}$$

$$\Omega_{Zbb}^L = \frac{e}{2s_Wc_W}(\frac{2}{3}s_W^2 + 2s_L^{b2} - 1)$$

$$\Omega_{Zbb}^R = \frac{e}{2s_Wc_W}(s_R^{b2} + \frac{2}{3}s_W^2)$$

$$\Omega_{ZbB}^L = -\frac{es_L^bc_L^b}{s_Wc_W}$$

$$\Omega_{ZbB}^R = -\frac{es_R^bc_R^b}{2s_Wc_W}$$

$$\Omega_{ZBB}^L = \frac{e}{2s_Wc_W}(\frac{2}{3}s_W^2 + 2c_L^{b2} - 1)$$

$$\Omega_{ZBB}^R = \frac{e}{2s_Wc_W}(c_R^{b2} + \frac{2}{3}s_W^2)$$

$$\Omega_{ZYY}^L = -\frac{e}{2s_Wc_W}(1 - \frac{8}{3}s_W^2)$$

$$\Omega_{ZYY}^R = -\frac{e}{2s_Wc_W}(1 - \frac{8}{3}s_W^2) \tag{E.5}$$

178

E.1.6 Triplet $\mathcal{T}_X$ (X, T, B), $Y = 2/3$

$$\Omega^L_{Wtb} = \frac{e}{\sqrt{2}s_W}(\sqrt{2}s^t_L s^b_L + c^t_L c^b_L) \qquad \Omega^L_{Ztt} = \frac{e}{2s_W c_W}(c^{t2}_L - \frac{4}{3}s^2_W)$$

$$\Omega^R_{Wtb} = \frac{es^t_R s^b_R}{s_W} \qquad \Omega^R_{Ztt} = -\frac{2es_W}{3c_W}$$

$$\Omega^L_{WTb} = \frac{e}{\sqrt{2}s_W}(s^t_L c^b_L - \sqrt{2}s^b_L c^t_L) \qquad \Omega^L_{Zbb} = \frac{e}{2s_W c_W}(\frac{2}{3}s^2_W - s^{b2}_L - 1)$$

$$\Omega^R_{WTb} = -\frac{es^b_R c^t_R}{s_W} \qquad \Omega^R_{Zbb} = \frac{e}{2s_W c_W}(\frac{2}{3}s^2_W - 2s^{b2}_R)$$

$$\Omega^L_{WtB} = \frac{e}{\sqrt{2}s_W}(s^b_L c^t_L - \sqrt{2}s^t_L c^b_L) \qquad \Omega^L_{ZtT} = \frac{es^t_L c^t_L}{2s_W c_W}$$

$$\Omega^R_{WtB} = -\frac{es^t_R c^b_R}{s_W} \qquad \Omega^R_{ZtT} = 0$$

$$\Omega^L_{WtX} = -\frac{es^t_L}{s_W} \qquad \Omega^L_{ZbB} = \frac{es^b_L c^b_L}{2s_W c_W}$$

$$\Omega^R_{WtX} = -\frac{es^t_R}{s_W} \qquad \Omega^R_{ZbB} = \frac{es^b_R c^b_R}{s_W c_W}$$

$$\Omega^L_{WTB} = \frac{e}{\sqrt{2}s_W}(s^t_L s^b_L + \sqrt{2}c^t_L c^b_L) \qquad \Omega^L_{ZTT} = \frac{e}{2s_W c_W}(s^{t2}_L - \frac{4}{3}s^2_W)$$

$$\Omega^R_{WTB} = \frac{ec^t_R c^b_R}{s_W} \qquad \Omega^R_{ZTT} = -\frac{2es_W}{3c_W}$$

$$\Omega^L_{WTX} = \frac{ec^t_L}{s_W} \qquad \Omega^L_{ZBB} = \frac{e}{2s_W c_W}(\frac{2}{3}s^2_W - c^{b2}_L - 1)$$

$$\Omega^R_{WTX} = \frac{ec^t_R}{s_W} \qquad \Omega^R_{ZBB} = \frac{e}{2s_W c_W}(\frac{2}{3}s^2_W - 2c^{b2}_R)$$

$$\Omega^L_{ZXX} = \frac{e}{2s_W c_W}(2 - \frac{10}{3}s^2_W)$$

$$\Omega^R_{ZXX} = \frac{e}{2s_W c_W}(2 - \frac{10}{3}s^2_W) \qquad \text{(E.6)}$$

E.1.7   Triplet $\mathcal{T}_Y$ (T, B, Y), $Y = -1/3$

$$\Omega^L_{Wtb} = \frac{e}{\sqrt{2}s_W}(\sqrt{2}s^t_L s^b_L + c^t_L c^b_L)$$

$$\Omega^R_{Wtb} = \frac{e s^t_R s^b_R}{s_W}$$

$$\Omega^L_{WTb} = \frac{e}{\sqrt{2}s_W}(s^t_L c^b_L - \sqrt{2}s^b_L c^t_L)$$

$$\Omega^R_{WTb} = -\frac{e s^b_R c^t_R}{s_W}$$

$$\Omega^L_{WtB} = \frac{e}{\sqrt{2}s_W}(s^b_L c^t_L - \sqrt{2}s^t_L c^b_L)$$

$$\Omega^R_{WtB} = -\frac{e s^t_R c^b_R}{s_W}$$

$$\Omega^L_{WbY} = -\frac{e s^b_L}{s_W}$$

$$\Omega^R_{WbY} = -\frac{e s^b_R}{s_W}$$

$$\Omega^L_{WTB} = \frac{e}{\sqrt{2}s_W}(s^t_L s^b_L + \sqrt{2}c^t_L c^b_L)$$

$$\Omega^R_{WTB} = \frac{e c^t_R c^b_R}{s_W}$$

$$\Omega^L_{WBY} = \frac{e c^b_L}{s_W}$$

$$\Omega^R_{WBY} = \frac{e c^b_R}{s_W}$$

$$\Omega^L_{Ztt} = \frac{e}{2s_W c_W}(-\frac{4}{3}s^2_W + s^{t2}_L + 1)$$

$$\Omega^R_{Ztt} = \frac{e}{2s_W c_W}(2s^{t2}_R - \frac{4}{3}s^2_W)$$

$$\Omega^L_{Zbb} = \frac{e}{2s_W c_W}(\frac{2}{3}s^2_W - c^{b2}_L)$$

$$\Omega^R_{Zbb} = \frac{e s_W}{3c_W}$$

$$\Omega^L_{ZtT} = -\frac{e s^t_L c^t_L}{2s_W c_W}$$

$$\Omega^R_{ZtT} = -\frac{e s^t_R c^t_R}{s_W c_W}$$

$$\Omega^L_{ZbB} = -\frac{e s^b_L c^b_L}{2s_W c_W}$$

$$\Omega^R_{ZbB} = 0$$

$$\Omega^L_{ZTT} = \frac{e}{2s_W c_W}(-\frac{4}{3}s^2_W + c^{t2}_L + 1)$$

$$\Omega^R_{ZTT} = \frac{e}{2s_W c_W}(2c^{t2}_R - \frac{4}{3}s^2_W)$$

$$\Omega^L_{ZBB} = \frac{e}{2s_W c_W}(\frac{2}{3}s^2_W - s^{b2}_L)$$

$$\Omega^R_{ZBB} = \frac{e s_W}{3c_W}$$

$$\Omega^L_{ZYY} = -\frac{e}{2s_W c_W}(2 - \frac{8}{3}s^2_W)$$

$$\Omega^R_{ZYY} = -\frac{e}{2s_W c_W}(2 - \frac{8}{3}s^2_W) \tag{E.7}$$

E.2 EW corrections from VLLs

E.2.1 Singlet $\mathcal{S}_1$ (L^0), $Y = 0$

$$\Omega^L_{W\nu\tau} = \frac{ec^u_L}{\sqrt{2}s_W} \qquad\qquad \Omega^L_{Z\nu\nu} = \frac{ec^{u^2}_L}{2s_Wc_W}$$

$$\Omega^R_{W\nu\tau} = 0 \qquad\qquad \Omega^R_{Z\nu\nu} = 0$$

$$\Omega^L_{W\tau L^0} = \frac{es^u_L}{\sqrt{2}s_W} \qquad\qquad \Omega^L_{Z\tau\tau} = \frac{e}{2s_Wc_W}(-1 + 2s^2_W)$$

$$\Omega^R_{W\tau L^0} = 0 \qquad\qquad \Omega^R_{Z\tau\tau} = \frac{es_W}{c_W}$$

$$\Omega^L_{Z\nu L^0} = \frac{es^u_L c^u_L}{2s_Wc_W}$$

$$\Omega^R_{Z\nu L^0} = 0$$

$$\Omega^L_{ZL^0 L^0} = \frac{es^{u^2}_L}{2s_Wc_W}$$

$$\Omega^R_{ZL^0 L^0} = 0 \qquad\qquad\qquad\qquad \text{(E.8)}$$

E.2.2 Singlet $\mathcal{S}_2$ (L^-), $Y = -1$

$$\Omega^L_{W\nu\tau} = \frac{ec^d_L}{\sqrt{2}s_W} \qquad\qquad \Omega^L_{Z\nu\nu} = \frac{e}{2s_Wc_W}$$

$$\Omega^R_{W\nu\tau} = 0 \qquad\qquad \Omega^R_{Z\nu\nu} = 0$$

$$\Omega^L_{W\nu L^-} = \frac{es^d_L}{\sqrt{2}s_W} \qquad\qquad \Omega^L_{Z\tau\tau} = \frac{e}{2s_Wc_W}(-c^{d^2}_L + 2s^2_W)$$

$$\Omega^R_{W\nu L^-} = 0 \qquad\qquad \Omega^R_{Z\tau\tau} = \frac{es_W}{c_W}$$

$$\Omega^L_{Z\tau L^-} = -\frac{es^d_L c^d_L}{2s_Wc_W}$$

$$\Omega^R_{Z\tau L^-} = 0$$

$$\Omega^L_{ZL^- L^-} = \frac{e}{2s_Wc_W}(-s^{d^2}_L + 2s^2_W)$$

$$\Omega^R_{ZL^- L^-} = \frac{es_W}{c_W} \qquad\qquad\qquad\qquad \text{(E.9)}$$

E.2.3 Doublet $\mathcal{D}_1$ (L^0, L^-), $Y = -1/2$

$$\Omega^L_{W\nu\tau} = \frac{e}{\sqrt{2}s_W}(c^u_L c^d_L + s^u_L s^d_L) \qquad \Omega^L_{Z\nu\nu} = \frac{e}{2s_W c_W}$$

$$\Omega^R_{W\nu\tau} = \frac{e s^u_R s^d_R}{\sqrt{2}s_W} \qquad \Omega^R_{Z\nu\nu} = \frac{e s^{u2}_R}{2s_W c_W}$$

$$\Omega^L_{W\tau L^0} = \frac{e}{\sqrt{2}s_W}(c^d_L s^u_L - c^u_L s^d_L) \qquad \Omega^L_{Z\tau\tau} = \frac{e}{2s_W c_W}(-1 + 2s^2_W)$$

$$\Omega^R_{W\tau L^0} = -\frac{e c^u_R s^d_R}{\sqrt{2}s_W} \qquad \Omega^R_{Z\tau\tau} = \frac{e}{2s_W c_W}(-s^{d2}_R + 2s^2_W)$$

$$\Omega^L_{W\nu L^-} = \frac{e}{\sqrt{2}s_W}(c^u_L s^d_L - c^d_L s^u_L) \qquad \Omega^L_{Z\nu L^0} = 0$$

$$\Omega^R_{W\nu L^-} = -\frac{e c^d_R s^u_R}{\sqrt{2}s_W} \qquad \Omega^R_{Z\nu L^0} = -\frac{e c^u_R s^u_R}{2s_W c_W}$$

$$\Omega^L_{W L^0 L^-} = \frac{e}{\sqrt{2}s_W}(c^u_L c^d_L + s^u_L s^d_L) \qquad \Omega^L_{Z\tau L^-} = 0$$

$$\Omega^R_{W L^0 L^-} = \frac{e c^u_R c^d_R}{\sqrt{2}s_W} \qquad \Omega^R_{Z\tau L^-} = \frac{e c^d_R s^d_R}{2s_W c_W}$$

$$\Omega^L_{Z L^0 L^0} = \frac{e}{2s_W c_W}$$

$$\Omega^R_{Z L^0 L^0} = \frac{e c^{u2}_R}{2s_W c_W}$$

$$\Omega^L_{Z L^- L^-} = \frac{e}{2s_W c_W}(-1 + 2s^2_W)$$

$$\Omega^R_{Z L^- L^-} = \frac{e}{2s_W c_W}(-c^{d2}_R + 2s^2_W) \qquad (\text{E.10})$$

E.2.4 Doublet $\mathcal{D}_2$ (L^-, L^{--}), $Y = -3/2$

$$\Omega^L_{W\nu\tau} = \frac{ec^d_L}{\sqrt{2}s_W} \qquad\qquad \Omega^L_{Z\nu\nu} = \frac{e}{2s_W c_W}$$

$$\Omega^R_{W\nu\tau} = 0 \qquad\qquad \Omega^R_{Z\nu\nu} = 0$$

$$\Omega^L_{W\nu L^-} = \frac{es^d_L}{\sqrt{2}s_W} \qquad\qquad \Omega^L_{Z\tau\tau} = \frac{e}{2s_W c_W}(2s_L^{d^2} + 2s_W^2 - 1)$$

$$\Omega^R_{W\nu L^-} = 0 \qquad\qquad \Omega^R_{Z\tau\tau} = \frac{e}{2s_W c_W}(s_R^{d^2} + 2s_W^2)$$

$$\Omega^L_{W\tau L^{--}} = -\frac{es^d_L}{\sqrt{2}s_W} \qquad\qquad \Omega^L_{Z\tau L^-} = -\frac{ec^d_L s^d_L}{s_W c_W}$$

$$\Omega^R_{W\tau L^{--}} = -\frac{es^d_R}{\sqrt{2}s_W} \qquad\qquad \Omega^R_{Z\tau L^-} = -\frac{ec^d_R s^d_R}{2s_W c_W}$$

$$\Omega^L_{WL^- L^{--}} = \frac{ec^d_L}{\sqrt{2}s_W} \qquad\qquad \Omega^L_{ZL^- L^-} = \frac{e}{2s_W c_W}(2c_L^{d^2} + 2s_W^2 - 1)$$

$$\Omega^R_{WL^- L^{--}} = \frac{ec^d_R}{\sqrt{2}s_W} \qquad\qquad \Omega^R_{ZL^- L^-} = \frac{e}{2s_W c_W}(c_R^{d^2} + 2s_W^2)$$

$$\Omega^L_{ZL^{--} L^{--}} = \frac{e}{2s_W c_W}(-1 + 4s_W^2)$$

$$\Omega^R_{ZL^{--} L^{--}} = \frac{e}{2s_W c_W}(-1 + 4s_W^2) \qquad\qquad \text{(E.11)}$$

E.2.5 Triplet $\mathcal{T}_1$ (L^+, L^0, L^-), $Y = 0$

$$\Omega^L_{W\nu\tau} = \frac{e}{\sqrt{2}s_W}(c_L^u c_L^d + \sqrt{2}s_L^u s_L^d) \qquad \Omega^L_{Z\nu\nu} = \frac{e c_L^{u^2}}{2s_W c_W}$$

$$\Omega^R_{W\nu\tau} = \frac{e s_R^u s_R^d}{s_W} \qquad \Omega^R_{Z\nu\nu} = 0$$

$$\Omega^L_{W\nu L^+} = -\frac{e s_L^u}{s_W} \qquad \Omega^L_{Z\tau\tau} = -\frac{e}{2s_W c_W}(s_L^{d^2} - 2s_W^2 + 1)$$

$$\Omega^R_{W\nu L^+} = -\frac{e s_R^u}{s_W} \qquad \Omega^R_{Z\tau\tau} = -\frac{e}{2s_W c_W}(2s_R^{d^2} - 2s_W^2)$$

$$\Omega^L_{W\nu L^-} = \frac{e}{\sqrt{2}s_W}(c_L^u s_L^d - \sqrt{2}c_L^d s_L^u) \qquad \Omega^L_{Z\nu L^0} = \frac{e c_L^u s_L^u}{2s_W c_W}$$

$$\Omega^R_{W\nu L^-} = -\frac{e c_R^d s_R^u}{s_W} \qquad \Omega^R_{Z\nu L^0} = 0$$

$$\Omega^L_{W\tau L^0} = \frac{e}{\sqrt{2}s_W}(c_L^d s_L^u - \sqrt{2}c_L^u s_L^d) \qquad \Omega^L_{Z\tau L^-} = \frac{e c_L^d s_L^d}{2s_W c_W}$$

$$\Omega^R_{W\tau L^0} = -\frac{e c_R^u s_R^d}{s_W} \qquad \Omega^R_{Z\tau L^-} = \frac{e c_R^d s_R^d}{s_W c_W}$$

$$\Omega^L_{WL^+ L^0} = \frac{e c_L^u}{s_W} \qquad \Omega^L_{ZL^+ L^+} = \frac{e}{s_W c_W}(1 - s_W^2)$$

$$\Omega^R_{WL^+ L^0} = \frac{e c_R^u}{s_W} \qquad \Omega^R_{ZL^+ L^+} = \frac{e}{s_W c_W}(1 - s_W^2)$$

$$\Omega^L_{WL^0 L^-} = \frac{e}{\sqrt{2}s_W}(s_L^u s_L^d + \sqrt{2}c_L^u c_L^d) \qquad \Omega^L_{ZL^0 L^0} = \frac{e s_L^{u^2}}{2s_W c_W}$$

$$\Omega^R_{WL^0 L^-} = \frac{e c_R^u c_R^d}{s_W} \qquad \Omega^R_{ZL^0 L^0} = 0$$

$$\Omega^L_{ZL^- L^-} = -\frac{e}{2s_W c_W}(c_L^{d^2} - 2s_W^2 + 1)$$

$$\Omega^R_{ZL^- L^-} = -\frac{e}{2s_W c_W}(2c_R^{d^2} - 2s_W^2) \qquad \text{(E.12)}$$

E.2.6 Triplet $\mathcal{T}_2$ (L^0, L^-, L^{--}), $Y = -1$

$$\Omega^L_{W\nu\tau} = \frac{e}{\sqrt{2}s_W}(c^u_L c^d_L + \sqrt{2}s^u_L s^d_L)$$

$$\Omega^R_{W\nu\tau} = \frac{es^u_R s^d_R}{s_W}$$

$$\Omega^L_{W\nu L^-} = \frac{e}{\sqrt{2}s_W}(c^u_L s^d_L - \sqrt{2}s^u_L c^d_L)$$

$$\Omega^R_{W\nu L^-} = -\frac{es^u_R c^d_R}{s_W}$$

$$\Omega^L_{W\tau L^0} = \frac{e}{\sqrt{2}s_W}(c^d_L s^u_L - \sqrt{2}c^u_L s^d_L)$$

$$\Omega^R_{W\tau L^0} = -\frac{es^d_R c^u_R}{s_W}$$

$$\Omega^L_{W\tau L^{--}} = -\frac{es^d_L}{s_W}$$

$$\Omega^R_{W\tau L^{--}} = -\frac{es^d_R}{s_W}$$

$$\Omega^L_{WL^0 L^-} = \frac{e}{\sqrt{2}s_W}(s^u_L s^d_L + \sqrt{2}c^u_L c^d_L)$$

$$\Omega^R_{WL^0 L^-} = \frac{ec^u_R c^d_R}{s_W}$$

$$\Omega^L_{WL^- L^{--}} = \frac{ec^d_L}{s_W}$$

$$\Omega^R_{WL^- L^{--}} = \frac{ec^d_R}{s_W}$$

$$\Omega^L_{Z\nu\nu} = \frac{e}{2s_W c_W}(1 + s^{u^2}_L)$$

$$\Omega^R_{Z\nu\nu} = \frac{es^{u^2}_R}{s_W c_W}$$

$$\Omega^L_{Z\tau\tau} = \frac{e}{2s_W c_W}(-c^{d^2}_L + 2s^2_W)$$

$$\Omega^R_{Z\tau\tau} = \frac{es_W}{c_W}$$

$$\Omega^L_{Z\nu L^0} = -\frac{es^u_L c^u_L}{2s_W c_W}$$

$$\Omega^R_{Z\nu L^0} = -\frac{es^u_R c^u_R}{s_W c_W}$$

$$\Omega^L_{Z\tau L^-} = -\frac{ec^d_L s^d_L}{2s_W c_W}$$

$$\Omega^R_{Z\tau L^-} = 0$$

$$\Omega^L_{ZL^0 L^0} = \frac{e}{2s_W c_W}(1 + c^{u^2}_L)$$

$$\Omega^R_{ZL^0 L^0} = \frac{ec^{u^2}_R}{s_W c_W}$$

$$\Omega^L_{ZL^- L^-} = \frac{e}{2s_W c_W}(-s^{d^2}_L + 2s^2_W)$$

$$\Omega^R_{ZL^- L^-} = \frac{es_W}{c_W}$$

$$\Omega^L_{ZL^- L^{--}} = \frac{e}{s_W c_W}(-1 + 2s^2_W)$$

$$\Omega^R_{ZL^- L^{--}} = \frac{e}{s_W c_W}(-1 + 2s^2_W) \qquad \text{(E.13)}$$

References

[1] A. Arsenault, K. Y. Cingiloglu, and M. Frank, "Vacuum stability in the Standard Model with vectorlike fermions," *Phys. Rev. D*, vol. 107, no. 3, p. 036018, 2023.

[2] K. Y. Cingiloglu and M. Frank, "Vacuum stability and electroweak precision in the two-Higgs-doublet model with vectorlike quarks," *Phys. Rev. D*, vol. 109, no. 3, p. 036016, 2024.

[3] K. Y. Cingiloglu and M. Frank, "Stability of the standard model vacuum with vectorlike leptons: A critical examination," *Phys. Rev. D*, vol. 111, p. 016025, Jan 2025.

[4] G. Aad *et al.*, "Observation of a new particle in the search for the Standard Model Higgs boson with the ATLAS detector at the LHC," *Phys. Lett. B*, vol. 716, pp. 1–29, 2012.

[5] S. Chatrchyan *et al.*, "Observation of a New Boson at a Mass of 125 GeV with the CMS Experiment at the LHC," *Phys. Lett. B*, vol. 716, pp. 30–61, 2012.

[6] S. P. Martin, "A Supersymmetry primer," *Adv. Ser. Direct. High Energy Phys.*, vol. 18, pp. 1–98, 1998.

[7] F. Gabbiani, E. Gabrielli, A. Masiero, and L. Silvestrini, "A complete analysis of fcnc and cp constraints in general susy extensions of the standard model," *Nuclear Physics B*, vol. 477, no. 2, pp. 321–352, 1996.

[8] J. J. van der Bij, "The Minimal non-minimal standard model," *Phys. Lett. B*, vol. 636, pp. 56–59, 2006.

[9] J. J. van der Bij and S. Dilcher, "A Higher dimensional explanation of the excess of Higgs-like events at CERN LEP," *Phys. Lett. B*, vol. 638, pp. 234–238, 2006.

[10] R. D. Peccei, "The Strong CP problem and axions," *Lect. Notes Phys.*, vol. 741, pp. 3–17, 2008.

[11] L. Abbott and P. Sikivie, "A cosmological bound on the invisible axion," *Physics Letters B*, vol. 120, no. 1, pp. 133–136, 1983.

[12] M. Asano and M. Kato, "New Covariant Gauges in String Field Theory," *Prog. Theor. Phys.*, vol. 117, pp. 569–587, 2007.

[13] Y. Baba, N. Ishibashi, and K. Murakami, "Light-Cone Gauge String Field Theory in Noncritical Dimensions," *JHEP*, vol. 12, p. 010, 2009.

[14] N. Berkovits, Y. Okawa, and B. Zwiebach, "WZW-like action for heterotic string field theory," *JHEP*, vol. 11, p. 038, 2004.

[15] L. Randall and R. Sundrum, "Large mass hierarchy from a small extra dimension," *Phys. Rev. Lett.*, vol. 83, pp. 3370–3373, Oct 1999.

[16] M. Shifman, "Large Extra Dimensions: Becoming acquainted with an alternative paradigm," *Int. J. Mod. Phys. A*, vol. 25, pp. 199–225, 2010.

[17] C. P. Burgess, "Introduction to Effective Field Theory," *Ann. Rev. Nucl. Part. Sci.*, vol. 57, pp. 329–362, 2007.

[18] S. Willenbrock and C. Zhang, "Effective Field Theory Beyond the Standard Model," *Ann. Rev. Nucl. Part. Sci.*, vol. 64, pp. 83–100, 2014.

[19] T. Kinoshita, "Mass singularities of Feynman amplitudes," *J. Math. Phys.*, vol. 3, pp. 650–677, 1962.

[20] T. D. Lee and M. Nauenberg, "Degenerate systems and mass singularities," *Phys. Rev.*, vol. 133, pp. B1549–B1562, Mar 1964.

[21] C. T. H. Davies, E. Follana, A. Gray, G. P. Lepage, Q. Mason, M. Nobes, J. Shigemitsu, H. D. Trottier, M. Wingate, C. Aubin, C. Bernard, T. Burch, C. DeTar, S. Gottlieb, E. B. Gregory, U. M. Heller, J. E. Hetrick, J. Osborn, R. Sugar, D. Toussaint, M. D. Pierro, A. El-Khadra, A. S. Kronfeld, P. B. Mackenzie, D. Menscher, and J. Simone, "High-precision lattice qcd confronts experiment," *Phys. Rev. Lett.*, vol. 92, p. 022001, Jan 2004.

[22] A. Bazavov *et al.*, "Nonperturbative QCD Simulations with 2+1 Flavors of Improved Staggered Quarks," *Rev. Mod. Phys.*, vol. 82, pp. 1349–1417, 2010.

[23] P. Petreczky, "Lattice QCD at non-zero temperature," *J. Phys. G*, vol. 39, p. 093002, 2012.

[24] G. Bellini, L. Ludhova, G. Ranucci, and F. L. Villante, "Neutrino oscillations," *Advances in High Energy Physics*, vol. 2014, p. 1–28, 2014.

[25] M. Flechl, "Higgs physics: Review of recent results and prospects from atlas and cms," *Journal of Physics: Conference Series*, vol. 631, p. 012028, July 2015.

[26] T. W. B. Kibble, "Symmetry breaking in non-abelian gauge theories," *Phys. Rev.*, vol. 155, pp. 1554–1561, Mar 1967.

[27] S. Weinberg, "General theory of broken local symmetries," *Phys. Rev. D*, vol. 7, pp. 1068–1082, Feb 1973.

[28] D. Ross and M. Veltman, "Neutral currents and the higgs mechanism," *Nuclear Physics B*, vol. 95, no. 1, pp. 135–147, 1975.

[29] M. Kobayashi and T. Maskawa, "CP Violation in the Renormalizable Theory of Weak Interaction," *Prog. Theor. Phys.*, vol. 49, pp. 652–657, 1973.

[30] N. Aghanim *et al.*, "Planck 2018 results. I. Overview and the cosmological legacy of Planck," *Astron. Astrophys.*, vol. 641, p. A1, 2020.

[31] N. Arkani-Hamed, D. P. Finkbeiner, T. R. Slatyer, and N. Weiner, "A theory of dark matter," *Phys. Rev. D*, vol. 79, p. 015014, Jan 2009.

[32] L. Hui, J. P. Ostriker, S. Tremaine, and E. Witten, "Ultralight scalars as cosmological dark matter," *Phys. Rev. D*, vol. 95, p. 043541, Feb 2017.

[33] S. L. Cheng, C. Q. Geng, and W.-T. Ni, "Axion-photon couplings in invisible axion models," *Phys. Rev. D*, vol. 52, pp. 3132–3135, Sep 1995.

[34] D. M. Lazarus, G. C. Smith, R. Cameron, A. C. Melissinos, G. Ruoso, Y. K. Semertzidis, and F. A. Nezrick, "Search for solar axions," *Phys. Rev. Lett.*, vol. 69, pp. 2333–2336, Oct 1992.

[35] A. D. Sakharov, "Violation of CP Invariance, C asymmetry, and baryon asymmetry of the universe," *Pisma Zh. Eksp. Teor. Fiz.*, vol. 5, pp. 32–35, 1967.

[36] R. D. Peccei and H. R. Quinn, "CP conservation in the presence of pseudoparticles," *Phys. Rev. Lett.*, vol. 38, pp. 1440–1443, Jun 1977.

[37] M. Gronau and J. Schechter, "Physical CP phase and maximal CP nonconservation," *Phys. Rev. Lett.*, vol. 54, pp. 385–388, Feb 1985.

[38] M. J. Savage, "Constraining flavour changing neutral currents with $b \to \mu^+\mu^-$," *Physics Letters B*, vol. 266, no. 1, pp. 135–141, 1991.

[39] M. Luke and M. J. Savage, "Flavour changing neutral currents, weak-scale scalars and rare top decays," *Physics Letters B*, vol. 307, no. 3, pp. 387–393, 1993.

[40] A. Jaramillo and L. A. Sánchez, "Flavor changing neutral currents, *cp* violation, and implications for some rare decays in a $su(4)_L \bigotimes u(1)_X$ extension of the standard model," *Phys. Rev. D*, vol. 84, p. 115001, Dec 2011.

[41] Q. R. Ahmad, R. C. Allen, T. C. Andersen, J. D. Anglin, G. Bühler, J. C. Barton, E. W. Beier, M. Bercovitch, J. Bigu, S. Biller, R. A. Black, I. Blevis, R. J. Boardman, J. Boger, E. Bonvin, M. G. Boulay, M. G. Bowler, T. J. Bowles, S. J. Brice, M. C. Browne, T. V. Bullard, T. H. Burritt, K. Cameron, J. Cameron, Y. D. Chan, M. Chen, H. H. Chen, X. Chen, M. C. Chon, B. T. Cleveland, E. T. H. Clifford, J. H. M. Cowan, D. F. Cowen, G. A. Cox, Y. Dai, X. Dai, F. Dalnoki-Veress, W. F. Davidson, P. J. Doe, G. Doucas, M. R. Dragowsky, C. A. Duba, F. A. Duncan, J. Dunmore, E. D. Earle, S. R. Elliott, H. C. Evans, G. T. Ewan, J. Farine, H. Fergani, A. P. Ferraris, R. J. Ford, M. M. Fowler, K. Frame, E. D. Frank, W. Frati, J. V. Germani, S. Gil, A. Goldschmidt, D. R. Grant, R. L. Hahn, A. L. Hallin, E. D. Hallman, A. Hamer, A. A. Hamian, R. U. Haq, C. K. Hargrove, P. J. Harvey, R. Hazama, R. Heaton, K. M. Heeger, W. J. Heintzelman, J. Heise, R. L. Helmer, J. D. Hepburn, H. Heron, J. Hewett, A. Hime, M. Howe, J. G. Hykawy, M. C. P. Isaac, P. Jagam, N. A. Jelley, C. Jillings, G. Jonkmans, J. Karn, P. T. Keener, K. Kirch, J. R. Klein, A. B. Knox, R. J. Komar, R. Kouzes, T. Kutter, C. C. M. Kyba, J. Law, I. T. Lawson, M. Lay, H. W. Lee, K. T. Lesko, J. R. Leslie, I. Levine, W. Locke, M. M. Lowry, S. Luoma, J. Lyon, S. Majerus, H. B. Mak, A. D. Marino, N. McCauley, A. B. McDonald, D. S. McDonald, K. McFarlane, G. McGregor, W. McLatchie, R. M. Drees, H. Mes, C. Mifflin, G. G. Miller, G. Milton, B. A. Moffat, M. Moorhead, C. W. Nally, M. S.

Neubauer, F. M. Newcomer, H. S. Ng, A. J. Noble, E. B. Norman, V. M. Novikov, M. O'Neill, C. E. Okada, R. W. Ollerhead, M. Omori, J. L. Orrell, S. M. Oser, A. W. P. Poon, T. J. Radcliffe, A. Roberge, B. C. Robertson, R. G. H. Robertson, J. K. Rowley, V. L. Rusu, E. Saettler, K. K. Schaffer, A. Schuelke, M. H. Schwendener, H. Seifert, M. Shatkay, J. J. Simpson, D. Sinclair, P. Skensved, A. R. Smith, M. W. E. Smith, N. Starinsky, T. D. Steiger, R. G. Stokstad, R. S. Storey, B. Sur, R. Tafirout, N. Tagg, N. W. Tanner, R. K. Taplin, M. Thorman, P. Thornewell, P. T. Trent, Y. I. Tserkovnyak, R. Van Berg, R. G. Van de Water, C. J. Virtue, C. E. Waltham, J.-X. Wang, D. L. Wark, N. West, J. B. Wilhelmy, J. F. Wilkerson, J. Wilson, P. Wittich, J. M. Wouters, and M. Yeh, "Measurement of the rate of $\nu_e + d \rightarrow p + p + e^-$ interactions produced by ^8b solar neutrinos at the sudbury neutrino observatory," *Phys. Rev. Lett.*, vol. 87, p. 071301, Jul 2001.

[42] S. Chakrabarty and A. Lahiri, "Geometrical contribution to neutrino mass matrix," *Eur. Phys. J. C*, vol. 79, no. 8, p. 697, 2019.

[43] S. Hessenberger and W. Hollik, "Two-loop corrections to the ρ parameter in Two-Higgs-Doublet Models," *Eur. Phys. J. C*, vol. 77, no. 3, p. 178, 2017.

[44] H. Georgi and A. Pais, "Calculability and naturalness in gauge theories," *Phys. Rev. D*, vol. 10, pp. 539–558, Jul 1974.

[45] J. L. F. Barbón and J. R. Espinosa, "On the naturalness of higgs inflation," *Phys. Rev. D*, vol. 79, p. 081302, Apr 2009.

[46] G. Dvali, "Black Holes and Large N Species Solution to the Hierarchy Problem," *Fortsch. Phys.*, vol. 58, pp. 528–536, 2010.

[47] X. Calmet, M. Graesser, and S. D. H. Hsu, "Minimum length from quantum mechanics and classical general relativity," *Phys. Rev. Lett.*, vol. 93, p. 211101, Nov 2004.

[48] X. Calmet, S. D. H. Hsu, and D. Reeb, "Quantum gravity at a tev and the renormalization of newton's constant," *Phys. Rev. D*, vol. 77, p. 125015, Jun 2008.

[49] G. Dvali, G. Gabadadze, M. Kolanović, and F. Nitti, "Scales of gravity," *Phys. Rev. D*, vol. 65, p. 024031, Dec 2001.

[50] S. Dawson and H. Georgi, "Generalized gauge hierarchies," *Phys. Rev. Lett.*, vol. 43, pp. 821–823, Sep 1979.

[51] G. Dvali and A. Vilenkin, "Cosmic attractors and gauge hierarchy," *Phys. Rev. D*, vol. 70, p. 063501, Sep 2004.

[52] E. Gildener, "Gauge-symmetry hierarchies," *Phys. Rev. D*, vol. 14, pp. 1667–1672, Sep 1976.

[53] C. G. Callan, "Broken scale invariance in scalar field theory," *Phys. Rev. D*, vol. 2, pp. 1541–1547, Oct 1970.

[54] M. E. Machacek and M. T. Vaughn, "Two-loop renormalization group equations in a general quantum field theory: (i). wave function renormalization," *Nuclear Physics B*, vol. 222, no. 1, pp. 83–103, 1983.

[55] A. D. Bond, G. Hiller, K. Kowalska, and D. F. Litim, "Directions for model building from asymptotic safety," *JHEP*, vol. 08, p. 004, 2017.

[56] D. Buttazzo, G. Degrassi, P. P. Giardino, G. F. Giudice, F. Sala, A. Salvio, and A. Strumia, "Investigating the near-criticality of the Higgs boson," *JHEP*, vol. 12, p. 089, 2013.

[57] S. Coleman and E. Weinberg, "Radiative corrections as the origin of spontaneous symmetry breaking," *Phys. Rev. D*, vol. 7, pp. 1888–1910, Mar 1973.

[58] G. C. Wick, "Properties of bethe-salpeter wave functions," *Phys. Rev.*, vol. 96, pp. 1124–1134, Nov 1954.

[59] S. R. Coleman, V. Glaser, and A. Martin, "Action Minima Among Solutions to a Class of Euclidean Scalar Field Equations," *Commun. Math. Phys.*, vol. 58, pp. 211–221, 1978.

[60] S. Coleman, "Fate of the false vacuum: Semiclassical theory," *Phys. Rev. D*, vol. 15, pp. 2929–2936, May 1977.

[61] C. G. Callan and S. Coleman, "Fate of the false vacuum. ii. first quantum corrections," *Phys. Rev. D*, vol. 16, pp. 1762–1768, Sep 1977.

[62] M. Sher, "Electroweak higgs potential and vacuum stability," *Physics Reports*, vol. 179, no. 5, pp. 273–418, 1989.

[63] P. B. Arnold, "Can the electroweak vacuum be unstable?," *Phys. Rev. D*, vol. 40, pp. 613–619, Jul 1989.

[64] P. Arnold and S. Vokos, "Instability of hot electroweak theory: Bounds on m_h and m_t," *Phys. Rev. D*, vol. 44, pp. 3620–3627, Dec 1991.

[65] S. Coleman and F. De Luccia, "Gravitational effects on and of vacuum decay," *Phys. Rev. D*, vol. 21, pp. 3305–3315, Jun 1980.

[66] S. Dawson and C. W. Murphy, "Standard model eft and extended scalar sectors," *Phys. Rev. D*, vol. 96, p. 015041, Jul 2017.

[67] S. Navas *et al.*, "Review of particle physics," *Phys. Rev. D*, vol. 110, no. 3, p. 030001, 2024.

[68] S. L. Glashow, "Partial-symmetries of weak interactions," *Nuclear Physics*, vol. 22, no. 4, pp. 579–588, 1961.

[69] A. H. Guth, "Inflationary universe: A possible solution to the horizon and flatness problems," *Phys. Rev. D*, vol. 23, pp. 347–356, Jan 1981.

[70] G. Degrassi, S. Di Vita, J. Elias-Miro, J. R. Espinosa, G. F. Giudice, G. Isidori, and A. Strumia, "Higgs mass and vacuum stability in the Standard Model at NNLO," *JHEP*, vol. 08, p. 098, 2012.

[71] F. Bezrukov, A. Magnin, M. Shaposhnikov, and S. Sibiryakov, "Higgs inflation: consistency and generalisations," *JHEP*, vol. 01, p. 016, 2011.

[72] F. Bezrukov, D. Gorbunov, and M. Shaposhnikov, "On initial conditions for the Hot Big Bang," *JCAP*, vol. 06, p. 029, 2009.

[73] A. De Simone, M. P. Hertzberg, and F. Wilczek, "Running Inflation in the Standard Model," *Phys. Lett. B*, vol. 678, pp. 1–8, 2009.

[74] C. P. Burgess, H. M. Lee, and M. Trott, "Comment on Higgs Inflation and Naturalness," *JHEP*, vol. 07, p. 007, 2010.

[75] M. Atkins and X. Calmet, "Remarks on Higgs Inflation," *Phys. Lett. B*, vol. 697, pp. 37–40, 2011.

[76] J. F. Gunion and H. E. Haber, "Cp-conserving two-higgs-doublet model: The approach to the decoupling limit," *Phys. Rev. D*, vol. 67, p. 075019, Apr 2003.

[77] J. A. Aguilar-Saavedra, "Effects of mixing with quark singlets," *Phys. Rev. D*, vol. 67, p. 035003, Feb 2003.

[78] S. A. R. Ellis, R. M. Godbole, S. Gopalakrishna, and J. D. Wells, "Survey of vector-like fermion extensions of the Standard Model and their phenomenological implications," *JHEP*, vol. 09, p. 130, 2014.

[79] S. Gopalakrishna, T. Mandal, S. Mitra, and G. Moreau, "LHC Signatures of Warped-space Vectorlike Quarks," *JHEP*, vol. 08, p. 079, 2014.

[80] R. Contino, L. Da Rold, and A. Pomarol, "Light custodians in natural composite higgs models," *Phys. Rev. D*, vol. 75, p. 055014, Mar 2007.

[81] C. Anastasiou, E. Furlan, and J. Santiago, "Realistic composite higgs models," *Phys. Rev. D*, vol. 79, p. 075003, Apr 2009.

[82] J. Hubisz and P. Meade, "Phenomenology of the littlest higgs model with t-parity," *Phys. Rev. D*, vol. 71, p. 035016, Feb 2005.

[83] S. P. Martin, "Extra vectorlike matter and the lightest higgs scalar boson mass in low-energy supersymmetry," *Phys. Rev. D*, vol. 81, p. 035004, Feb 2010.

[84] G. Couture, M. Frank, C. Hamzaoui, and M. Toharia, "Top and bottom partners, higgs boson on the brane, and the tth signal," *Phys. Rev. D*, vol. 95, p. 095038, May 2017.

[85] M.-L. Xiao and J.-H. Yu, "Stabilizing electroweak vacuum in a vectorlike fermion model," *Phys. Rev. D*, vol. 90, p. 014007, Jul 2014.

[86] G. Hiller, T. Höhne, D. F. Litim, and T. Steudtner, "Portals into higgs vacuum stability," *Phys. Rev. D*, vol. 106, p. 115004, Dec 2022.

[87] D. Egana-Ugrinovic, "The minimal fermionic model of electroweak baryogenesis," *JHEP*, vol. 12, p. 064, 2017.

[88] S.-P. He, "Leptoquark and vector-like quark extended model for simultaneous explanation of w boson mass and muon g–2 anomalies*," *Chinese Physics C*, vol. 47, p. 043102, apr 2023.

[89] M. Dhuria and G. Goswami, "Perturbativity, vacuum stability, and inflation in the light of 750 gev diphoton excess," *Phys. Rev. D*, vol. 94, p. 055009, Sep 2016.

[90] J. Zhang and S. Zhou, "Electroweak vacuum stability and diphoton excess at 750 gev*," *Chinese Physics C*, vol. 40, p. 081001, aug 2016.

[91] D. Carmi, A. Falkowski, E. Kuflik, and T. Volansky, "Interpreting LHC Higgs Results from Natural New Physics Perspective," *JHEP*, vol. 07, p. 136, 2012.

[92] P. Ghorbani, "Vacuum stability vs. positivity in real singlet scalar extension of the standard model," *Nuclear Physics B*, vol. 971, p. 115533, 2021.

[93] A. Ilnicka, T. Robens, and T. Stefaniak, "Constraining Extended Scalar Sectors at the LHC and beyond," *Mod. Phys. Lett. A*, vol. 33, no. 10n11, p. 1830007, 2018.

[94] O. Lebedev, "The higgs portal to cosmology," *Progress in Particle and Nuclear Physics*, vol. 120, p. 103881, 2021.

[95] D. López-Val and T. Robens, "Δr and the w-boson mass in the singlet extension of the standard model," *Phys. Rev. D*, vol. 90, p. 114018, Dec 2014.

[96] R. L. Workman *et al.*, "Review of Particle Physics," *PTEP*, vol. 2022, p. 083C01, 2022.

[97] M. E. Peskin and T. Takeuchi, "Estimation of oblique electroweak corrections," *Phys. Rev. D*, vol. 46, pp. 381–409, Jul 1992.

[98] M. Gorbahn, J. M. No, and V. Sanz, "Benchmarks for Higgs Effective Theory: Extended Higgs Sectors," *JHEP*, vol. 10, p. 036, 2015.

[99] S. Kanemura, M. Kikuchi, K. Mawatari, K. Sakurai, and K. Yagyu, "Full next-to-leading-order calculations of higgs boson decay rates in models with non-minimal scalar sectors," *Nuclear Physics B*, vol. 949, p. 114791, 2019.

[100] B. W. Lee, C. Quigg, and H. B. Thacker, "Weak interactions at very high energies: The role of the higgs-boson mass," *Phys. Rev. D*, vol. 16, pp. 1519–1531, Sep 1977.

[101] T. Robens and T. Stefaniak, "Status of the Higgs Singlet Extension of the Standard Model after LHC Run 1," *Eur. Phys. J. C*, vol. 75, p. 104, 2015.

[102] B. W. Lee, C. Quigg, and H. B. Thacker, "Strength of weak interactions at very high energies and the higgs boson mass," *Phys. Rev. Lett.*, vol. 38, pp. 883–885, Apr 1977.

[103] CERN, "Cern yellow reports: Monographs, vol 2 (2017): Handbook of lhc higgs cross sections: 4. deciphering the nature of the higgs sector," 2017.

[104] C. Sturm, B. Summ, and S. Uccirati, "Electroweak corrections to $g + g \to H_{l,h}$ and $H_{l,h} \to \gamma + \gamma$ in the Higgs-singlet extension of the Standard model," *JHEP*, vol. 11, p. 113, 2023.

[105] Y. Xiao, J. M. Yang, and Y. Zhang, "Dilution of dark matter relic density in singlet extension models," *JHEP*, vol. 02, p. 008, 2023.

[106] E. Fernández-Martínez, J. López-Pavón, J. M. No, T. Ota, and S. Rosauro-Alcaraz, "ν Electroweak baryogenesis: the scalar singlet strikes back," *Eur. Phys. J. C*, vol. 83, no. 8, p. 715, 2023.

[107] P. Athron, J. M. Cornell, F. Kahlhoefer, J. Mckay, P. Scott, and S. Wild, "Impact of vacuum stability, perturbativity and XENON1T on global fits of $\mathbb{Z}_2$ and $\mathbb{Z}_3$ scalar singlet dark matter," *Eur. Phys. J. C*, vol. 78, no. 10, p. 830, 2018.

[108] C. Balázs, Y. Xiao, J. M. Yang, and Y. Zhang, "New vacuum stability limit from cosmological history," *Nuclear Physics B*, vol. 1002, p. 116533, 2024.

[109] C. Ford, D. R. T. Jones, P. W. Stephenson, and M. B. Einhorn, "The Effective potential and the renormalization group," *Nucl. Phys. B*, vol. 395, pp. 17–34, 1993.

[110] S. Kanemura, M. Kikuchi, and K. Yagyu, "One-loop corrections to the higgs self-couplings in the singlet extension," *Nuclear Physics B*, vol. 917, pp. 154–177, 2017.

[111] R. Hempfling and B. A. Kniehl, "Relation between the fermion pole mass and ms⁻ yukawa coupling in the standard model," *Phys. Rev. D*, vol. 51, pp. 1386–1394, Feb 1995.

[112] A. Sirlin and R. Zucchini, "Dependence of the higgs coupling hms(m) on mh and the possible onset of new physics," *Nuclear Physics B*, vol. 266, no. 2, pp. 389–409, 1986.

[113] J. A. Aguilar-Saavedra, R. Benbrik, S. Heinemeyer, and M. Pérez-Victoria, "Handbook of vectorlike quarks: Mixing and single production," *Phys. Rev. D*, vol. 88, p. 094010, Nov 2013.

[114] C.-Y. Chen, S. Dawson, and E. Furlan, "Vectorlike fermions and higgs effective field theory revisited," *Phys. Rev. D*, vol. 96, p. 015006, Jul 2017.

[115] A. M. Sirunyan *et al.*, "Search for pair production of vector-like T and B quarks in single-lepton final states using boosted jet substructure in proton-proton collisions at $\sqrt{s} = 13$ TeV," *JHEP*, vol. 11, p. 085, 2017.

[116] N. Nikiforou, "Searches for new heavy quarks in ATLAS," in *53rd Rencontres de Moriond on Electroweak Interactions and Unified Theories*, pp. 161–166, 2018.

[117] M. Aaboud *et al.*, "Search for pair production of vector-like top quarks in events with one lepton, jets, and missing transverse momentum in $\sqrt{s} = 13$ TeV *pp* collisions with the ATLAS detector," *JHEP*, vol. 08, p. 052, 2017.

[118] S. Kanemura, M. Kikuchi, and K. Yagyu, "Radiative corrections to the higgs boson couplings in the model with an additional real singlet scalar field," *Nuclear Physics B*, vol. 907, pp. 286–322, 2016.

[119] L. Lavoura and J. a. P. Silva, "Oblique corrections from vectorlike singlet and doublet quarks," *Phys. Rev. D*, vol. 47, pp. 2046–2057, Mar 1993.

[120] S. Bahrami and M. Frank, "Vector quarks in the higgs triplet model," *Phys. Rev. D*, vol. 90, p. 035017, Aug 2014.

[121] G. Aad *et al.*, "Constraints on the Higgs boson self-coupling from single- and double-Higgs production with the ATLAS detector using pp collisions at s=13 TeV," *Phys. Lett. B*, vol. 843, p. 137745, 2023.

[122] A. Tumasyan *et al.*, "A portrait of the Higgs boson by the CMS experiment ten years after the discovery.," *Nature*, vol. 607, no. 7917, pp. 60–68, 2022.

[123] M. Cepeda *et al.*, "Report from Working Group 2: Higgs Physics at the HL-LHC and HE-LHC," *CERN Yellow Rep. Monogr.*, vol. 7, pp. 221–584, 2019.

[124] J. Alison *et al.*, "Higgs boson potential at colliders: Status and perspectives," *Rev. Phys.*, vol. 5, p. 100045, 2020.

[125] K. Agashe, R. Contino, and A. Pomarol, "The Minimal composite Higgs model," *Nucl. Phys. B*, vol. 719, pp. 165–187, 2005.

[126] G. Ferretti and D. Karateev, "Fermionic UV completions of Composite Higgs models," *JHEP*, vol. 03, p. 077, 2014.

[127] D. B. Kaplan, "Flavor at SSC energies: A New mechanism for dynamically generated fermion masses," *Nucl. Phys. B*, vol. 365, pp. 259–278, 1991.

[128] G. Ferretti, "UV Completions of Partial Compositeness: The Case for a SU(4) Gauge Group," *JHEP*, vol. 06, p. 142, 2014.

[129] S. Chang, J. Hisano, H. Nakano, N. Okada, and M. Yamaguchi, "Bulk standard model in the Randall-Sundrum background," *Phys. Rev. D*, vol. 62, p. 084025, 2000.

[130] T. Gherghetta and A. Pomarol, "Bulk fields and supersymmetry in a slice of AdS," *Nucl. Phys. B*, vol. 586, pp. 141–162, 2000.

[131] R. Contino, Y. Nomura, and A. Pomarol, "Higgs as a holographic pseudoGoldstone boson," *Nucl. Phys. B*, vol. 671, pp. 148–174, 2003.

[132] S. Gopalakrishna, T. Mandal, S. Mitra, and R. Tibrewala, "LHC Signatures of a Vector-like b'," *Phys. Rev. D*, vol. 84, p. 055001, 2011.

[133] G. Couture, M. Frank, C. Hamzaoui, and M. Toharia, "Top and bottom partners, Higgs boson on the brane, and the tth signal," *Phys. Rev. D*, vol. 95, no. 9, p. 095038, 2017.

[134] N. Arkani-Hamed, A. G. Cohen, E. Katz, A. E. Nelson, T. Gregoire, and J. G. Wacker, "The Minimal moose for a little Higgs," *JHEP*, vol. 08, p. 021, 2002.

[135] M. Perelstein, M. E. Peskin, and A. Pierce, "Top quarks and electroweak symmetry breaking in little Higgs models," *Phys. Rev. D*, vol. 69, p. 075002, 2004.

[136] M. Schmaltz, "Physics beyond the standard model (theory): Introducing the little Higgs," *Nucl. Phys. B Proc. Suppl.*, vol. 117, pp. 40–49, 2003.

[137] S. P. Martin, "Raising the Higgs Mass with Yukawa Couplings for Isotriplets in Vector-Like Extensions of Minimal Supersymmetry," *Phys. Rev. D*, vol. 82, p. 055019, 2010.

[138] S. P. Martin, "Extra vector-like matter and the lightest Higgs scalar boson mass in low-energy supersymmetry," *Phys. Rev. D*, vol. 81, p. 035004, 2010.

[139] K. S. Babu, I. Gogoladze, M. U. Rehman, and Q. Shafi, "Higgs Boson Mass, Sparticle Spectrum and Little Hierarchy Problem in Extended MSSM," *Phys. Rev. D*, vol. 78, p. 055017, 2008.

[140] J. Kang, P. Langacker, and B. D. Nelson, "Theory and Phenomenology of Exotic Isosinglet Quarks and Squarks," *Phys. Rev. D*, vol. 77, p. 035003, 2008.

[141] S. Aoki *et al.*, "FLAG Review 2019: Flavour Lattice Averaging Group (FLAG)," *Eur. Phys. J. C*, vol. 80, no. 2, p. 113, 2020.

[142] D. Bryman, V. Cirigliano, A. Crivellin, and G. Inguglia, "Testing Lepton Flavor Universality with Pion, Kaon, Tau, and Beta Decays," *Ann. Rev. Nucl. Part. Sci.*, vol. 72, pp. 69–91, 2022.

[143] G. C. Branco, J. T. Penedo, P. M. F. Pereira, M. N. Rebelo, and J. I. Silva-Marcos, "Addressing the CKM unitarity problem with a vector-like up quark," *JHEP*, vol. 07, p. 099, 2021.

[144] M. Kirk, "Cabibbo angle anomalies and a global fit to vector-like quarks," in *21st Conference on Flavor Physics and CP Violation*, 8 2023.

[145] F. Albergaria and G. C. Branco, "Unitarity Relations in the Presence of Vector-Like Quarks," *2307.13073*, 7 2023.

[146] A. E. Cárcamo Hernández, S. F. King, and H. Lee, "Z mediated flavor changing neutral currents with a fourth vectorlike family," *Phys. Rev. D*, vol. 105, no. 1, p. 015021, 2022.

[147] G. Altarelli and G. Isidori, "Lower limit on the Higgs mass in the standard model: An Update," *Phys. Lett. B*, vol. 337, pp. 141–144, 1994.

[148] G. C. Branco, P. M. Ferreira, L. Lavoura, M. N. Rebelo, M. Sher, and J. P. Silva, "Theory and phenomenology of two-Higgs-doublet models," *Phys. Rept.*, vol. 516, pp. 1–102, 2012.

[149] J. F. Gunion and H. E. Haber, "The CP conserving two Higgs doublet model: The Approach to the decoupling limit," *Phys. Rev. D*, vol. 67, p. 075019, 2003.

[150] B. Coleppa, F. Kling, and S. Su, "Constraining Type II 2HDM in Light of LHC Higgs Searches," *JHEP*, vol. 01, p. 161, 2014.

[151] W. Altmannshofer, S. Gori, and G. D. Kribs, "A Minimal Flavor Violating 2HDM at the LHC," *Phys. Rev. D*, vol. 86, p. 115009, 2012.

[152] I. P. Ivanov, "Minkowski space structure of the Higgs potential in 2HDM," *Phys. Rev. D*, vol. 75, p. 035001, 2007. [Erratum: Phys.Rev.D 76, 039902 (2007)].

[153] I. F. Ginzburg and I. P. Ivanov, "Tree-level unitarity constraints in the most general 2HDM," *Phys. Rev. D*, vol. 72, p. 115010, 2005.

[154] P. Basler, P. M. Ferreira, M. Mühlleitner, and R. Santos, "High scale impact in alignment and decoupling in two-Higgs doublet models," *Phys. Rev. D*, vol. 97, no. 9, p. 095024, 2018.

[155] E. Accomando, C. Byers, D. Englert, J. Hays, and S. Moretti, "Lhc data interpretation within the 2hdm type ii via a new analysis toolkit," *Phys. Rev. D*, vol. 105, p. 115004, Jun 2022.

[156] H. Song, W. Su, and M. Zhang, "Electroweak phase transition in 2HDM under Higgs, Z-pole, and W precision measurements," *JHEP*, vol. 10, p. 048, 2022.

[157] A. Cherchiglia, D. Stöckinger, and H. Stöckinger-Kim, "Muon g-2 in the 2HDM: maximum results and detailed phenomenology," *Phys. Rev. D*, vol. 98, p. 035001, 2018.

[158] H. E. Haber and O. Stål, "New LHC benchmarks for the $\mathcal{CP}$ -conserving two-Higgs-doublet model," *Eur. Phys. J. C*, vol. 75, no. 10, p. 491, 2015. [Erratum: Eur.Phys.J.C 76, 312 (2016)].

[159] P. S. Bhupal Dev and A. Pilaftsis, "Maximally Symmetric Two Higgs Doublet Model with Natural Standard Model Alignment," *JHEP*, vol. 12, p. 024, 2014. [Erratum: JHEP 11, 147 (2015)].

[160] J. Baglio, O. Eberhardt, U. Nierste, and M. Wiebusch, "Benchmarks for Higgs Pair Production and Heavy Higgs boson Searches in the Two-Higgs-Doublet Model of Type II," *Phys. Rev. D*, vol. 90, no. 1, p. 015008, 2014.

[161] O. Eberhardt, U. Nierste, and M. Wiebusch, "Status of the two-Higgs-doublet model of type II," *JHEP*, vol. 07, p. 118, 2013.

[162] A. Barroso, P. M. Ferreira, I. P. Ivanov, and R. Santos, "Metastability bounds on the two Higgs doublet model," *JHEP*, vol. 06, p. 045, 2013.

[163] D. Eriksson, J. Rathsman, and O. Stal, "2HDMC: Two-Higgs-Doublet Model Calculator Physics and Manual," *Comput. Phys. Commun.*, vol. 181, pp. 189–205, 2010.

[164] A. W. E. Kaffas, P. Osland, and O. M. Ogreid, "Constraining the two-higgs-doublet-model parameter space," *Phys. Rev. D*, vol. 76, p. 095001, Nov 2007.

[165] M. Maniatis, A. von Manteuffel, O. Nachtmann, and F. Nagel, "Stability and symmetry breaking in the general two-Higgs-doublet model," *Eur. Phys. J. C*, vol. 48, pp. 805–823, 2006.

[166] S. Davidson and H. E. Haber, "Basis-independent methods for the two-Higgs-doublet model," *Phys. Rev. D*, vol. 72, p. 035004, 2005. [Erratum: Phys.Rev.D 72, 099902 (2005)].

[167] J. E. Kim, "Light Pseudoscalars, Particle Physics and Cosmology," *Phys. Rept.*, vol. 150, pp. 1–177, 1987.

[168] R. D. Peccei and H. R. Quinn, "CP Conservation in the Presence of Instantons," *Phys. Rev. Lett.*, vol. 38, pp. 1440–1443, 1977.

[169] M. Trodden, "Electroweak baryogenesis: A Brief review," in *33rd Rencontres de Moriond: Electroweak Interactions and Unified Theories*, pp. 471–480, 1998.

[170] P. Ferreira, R. Santos, and A. Barroso, "Stability of the tree-level vacuum in two higgs doublet models against charge or cp spontaneous violation," *Physics Letters B*, vol. 603, p. 219–229, Dec. 2004.

[171] A. Barroso, P. Ferreira, and R. Santos, "Neutral minima in two-higgs doublet models," *Physics Letters B*, vol. 652, p. 181–193, Aug. 2007.

[172] P. M. Ferreira and B. SwieŻewska, "One-loop contributions to neutral minima in the inert doublet model," *Journal of High Energy Physics*, vol. 2016, p. 1–35, Apr. 2016.

[173] P. Ferreira, L. Morrison, and S. Profumo, "One-loop charge-breaking minima in the two-higgs doublet model," *Journal of High Energy Physics*, vol. 2020, Apr. 2020.

[174] I. P. Ivanov, "Minkowski space structure of the higgs potential in the two-higgs-doublet model. ii. minima, symmetries, and topology," *Physical Review D*, vol. 77, Jan. 2008.

[175] P. M. Ferreira, H. E. Haber, and E. Santos, "Preserving the validity of the two-higgs-doublet model up to the planck scale," *Phys. Rev. D*, vol. 92, p. 033003, Aug 2015.

[176] H. Bahl, M. Carena, N. M. Coyle, A. Ireland, and C. E. M. Wagner, "New tools for dissecting the general 2hdm," *Journal of High Energy Physics*, vol. 2023, Mar. 2023.

[177] S. Kanemura, T. Kubota, and E. Takasugi, "Lee-quigg-thacker bounds for higgs boson masses in a two-doublet model," *Physics Letters B*, vol. 313, p. 155–160, Aug. 1993.

[178] J. Horejsi and M. Kladiva, "Tree-unitarity bounds for THDM Higgs masses revisited," *Eur. Phys. J. C*, vol. 46, pp. 81–91, 2006.

[179] S. Kanemura, T. Kasai, and Y. Okada, "Mass bounds of the lightest cp-even higgs boson in the two-higgs-doublet model," 1999.

[180] S. Kanemura, M. Kikuchi, and K. Yagyu, "Radiative corrections to the yukawa coupling constants in two higgs doublet models," *Physics Letters B*, vol. 731, pp. 27–35, 2014.

[181] R. Dermíšek, E. Lunghi, and S. Shin, "Hunting for Vectorlike Quarks," *JHEP*, vol. 04, p. 019, 2019. [Erratum: JHEP 10, 058 (2020)].

[182] R. Dermisek, E. Lunghi, and S. Shin, "Cascade decays of heavy Higgs bosons through vectorlike quarks in two Higgs doublet models," *JHEP*, vol. 03, p. 029, 2020.

[183] R. Dermisek, E. Lunghi, N. McGinnis, and S. Shin, "Signals with six bottom quarks for charged and neutral Higgs bosons," *JHEP*, vol. 07, p. 241, 2020.

[184] R. Dermisek, E. Lunghi, N. Mcginnis, and S. Shin, "Tau-jet signatures of vectorlike quark decays to heavy charged and neutral Higgs bosons," *JHEP*, vol. 08, p. 159, 2021.

[185] R. Dermisek, J. Kawamura, E. Lunghi, N. McGinnis, and S. Shin, "Combined signatures of heavy Higgses and vectorlike fermions at the HL-LHC," in *Snowmass 2021*, 3 2022.

[186] J. A. Aguilar-Saavedra, "Mixing with vector-like quarks: constraints and expectations," *EPJ Web Conf.*, vol. 60, p. 16012, 2013.

[187] S. Fajfer, A. Greljo, J. F. Kamenik, and I. Mustac, "Light Higgs and Vector-like Quarks without Prejudice," *JHEP*, vol. 07, p. 155, 2013.

[188] J. a. M. Alves, G. C. Branco, A. L. Cherchiglia, C. C. Nishi, J. T. Penedo, P. M. F. Pereira, M. N. Rebelo, and J. I. Silva-Marcos, "Vector-like singlet quarks: A roadmap," *Phys. Rept.*, vol. 1057, pp. 1–69, 2024.

[189] G. Aad *et al.*, "Search for the production of single vector-like and excited quarks in the Wt final state in pp collisions at $\sqrt{s} = 8$ TeV with the ATLAS detector," *JHEP*, vol. 02, p. 110, 2016.

[190] G. Aad *et al.*, "Search for single production of vector-like quarks decaying into Wb in pp collisions at $\sqrt{s} = 8$ TeV with the ATLAS detector," *Eur. Phys. J. C*, vol. 76, no. 8, p. 442, 2016.

[191] G. Aad *et al.*, "Search for production of vector-like quark pairs and of four top quarks in the lepton-plus-jets final state in pp collisions at $\sqrt{s} = 8$ TeV with the ATLAS detector," *JHEP*, vol. 08, p. 105, 2015.

[192] G. Aad *et al.*, "Search for vector-like B quarks in events with one isolated lepton, missing transverse momentum and jets at $\sqrt{s} = 8$ TeV with the ATLAS detector," *Phys. Rev. D*, vol. 91, no. 11, p. 112011, 2015.

[193] A. M. Sirunyan *et al.*, "Search for single production of vector-like quarks decaying to a Z boson and a top or a bottom quark in proton-proton collisions at $\sqrt{s} = 13$ TeV," *JHEP*, vol. 05, p. 029, 2017.

[194] V. Khachatryan *et al.*, "Search for pair-produced vectorlike B quarks in proton-proton collisions at $\sqrt{s}$=8 TeV," *Phys. Rev. D*, vol. 93, no. 11, p. 112009, 2016.

[195] V. Khachatryan *et al.*, "Search for vector-like T quarks decaying to top quarks and Higgs bosons in the all-hadronic channel using jet substructure," *JHEP*, vol. 06, p. 080, 2015.

[196] S. Chatrchyan *et al.*, "Search for Top-Quark Partners with Charge 5/3 in the Same-Sign Dilepton Final State," *Phys. Rev. Lett.*, vol. 112, no. 17, p. 171801, 2014.

[197] S. Chatrchyan *et al.*, "Inclusive Search for a Vector-Like T Quark with Charge $\frac{2}{3}$ in pp Collisions at $\sqrt{s} = 8$ TeV," *Phys. Lett. B*, vol. 729, pp. 149–171, 2014.

[198] G. Aad *et al.*, "Search for singly produced vector-like top partners in multilepton final states with 139 fb^{-1} of pp collision data at $\sqrt{s} = 13$ TeV with the ATLAS detector," *2307.07584*, 7 2023.

[199] G. Aad *et al.*, "Search for pair-production of vector-like quarks in pp collision events at s=13 TeV with at least one leptonically decaying Z boson and a third-generation quark with the ATLAS detector," *Phys. Lett. B*, vol. 843, p. 138019, 2023.

[200] M. Aaboud *et al.*, "Search for pair production of up-type vector-like quarks and for four-top-quark events in final states with multiple b-jets with the ATLAS detector," *JHEP*, vol. 07, p. 089, 2018.

[201] G. Aad *et al.*, "Search for single production of vector-like T quarks decaying into Ht or Zt in pp collisions at $\sqrt{s} = 13$ TeV with the ATLAS detector," *JHEP*, vol. 08, p. 153, 2023.

[202] T. Aaltonen *et al.*, "High-precision measurement of the W boson mass with the CDF II detector," *Science*, vol. 376, no. 6589, pp. 170–176, 2022.

[203] Y. Shimizu and S. Takeshita, "W boson mass and grand unification via the type-II seesaw-like mechanism," *Nucl. Phys. B*, vol. 994, p. 116290, 2023.

[204] J. A. Aguilar-Saavedra, "Light Higgs boson discovery from fermion mixing," *JHEP*, vol. 12, p. 033, 2006.

[205] S. Dawson and E. Furlan, "A Higgs Conundrum with Vector Fermions," *Phys. Rev. D*, vol. 86, p. 015021, 2012.

[206] R. Benbrik, C.-H. Chen, and T. Nomura, "Higgs singlet boson as a diphoton resonance in a vectorlike quark model," *Phys. Rev. D*, vol. 93, no. 5, p. 055034, 2016.

[207] A. Arhrib, R. Benbrik, S. J. D. King, B. Manaut, S. Moretti, and C. S. Un, "Phenomenology of 2HDM with vectorlike quarks," *Phys. Rev. D*, vol. 97, p. 095015, 2018.

[208] R. Benbrik, M. Boukidi, and S. Moretti, "Probing charged higgs bosons in the two-higgs-doublet model type ii with vectorlike quarks," *Phys. Rev. D*, vol. 109, p. 055016, Mar 2024.

[209] B. Grinstein, C. W. Murphy, and P. Uttayarat, "One-loop corrections to the perturbative unitarity bounds in the cp-conserving two-higgs doublet model with a softly broken $\mathbb{Z}_2$ symmetry," *Journal of High Energy Physics*, vol. 2016, June 2016.

[210] Y. Tang, "Vacuum Stability in the Standard Model," *Mod. Phys. Lett. A*, vol. 28, p. 1330002, 2013.

[211] S. Gopalakrishna and A. Velusamy, "Higgs vacuum stability with vectorlike fermions," *Phys. Rev. D*, vol. 99, no. 11, p. 115020, 2019.

[212] A. Abdesselam *et al.*, "Measurement of the inclusive $B \to X_{s+d}\gamma$ branching fraction, photon energy spectrum and HQE parameters," in *38th International Conference on High Energy Physics*, 8 2016.

[213] M. Misiak and M. Steinhauser, "Weak radiative decays of the b meson and bounds on $m_{H^\pm}$ in the two-higgs-doublet model," *The European Physical Journal C*, vol. 77, Mar. 2017.

[214] G. Abbiendi *et al.*, "Search for Charged Higgs bosons: Combined Results Using LEP Data," *Eur. Phys. J. C*, vol. 73, p. 2463, 2013.

[215] S. K. Kang, J. Kim, S. Lee, and J. Song, "Disentangling the high- and low-cutoff scales via the trilinear Higgs couplings in the type-I two-Higgs-doublet model," *Phys. Rev. D*, vol. 107, no. 1, p. 015025, 2023.

[216] S. Lee, K. Cheung, J. Kim, C.-T. Lu, and J. Song, "Status of the two-higgs-doublet model in light of the cdf m_W measurement," *Phys. Rev. D*, vol. 106, p. 075013, Oct 2022.

[217] G. Aad *et al.*, "Search for single production of a vectorlike T quark decaying into a Higgs boson and top quark with fully hadronic final states using the ATLAS detector," *Phys. Rev. D*, vol. 105, no. 9, p. 092012, 2022.

[218] G. Hiller, T. Höhne, D. F. Litim, and T. Steudtner, "Vacuum Stability as a Guide for Model Bulding," in *57th Rencontres de Moriond on Electroweak Interactions and Unified Theories*, 5 2023.

[219] Y. Heo, D.-W. Jung, and J. S. Lee, "Impact of the CDF W-mass anomaly on two Higgs doublet model," *Phys. Lett. B*, vol. 833, p. 137274, 2022.

[220] M. E. Machacek and M. T. Vaughn, "Two Loop Renormalization Group Equations in a General Quantum Field Theory. 2. Yukawa Couplings," *Nucl. Phys. B*, vol. 236, pp. 221–232, 1984.

[221] M. E. Machacek and M. T. Vaughn, "Two Loop Renormalization Group Equations in a General Quantum Field Theory. 3. Scalar Quartic Couplings," *Nucl. Phys. B*, vol. 249, pp. 70–92, 1985.

[222] P. A. Zyla *et al.*, "Review of Particle Physics," *PTEP*, vol. 2020, no. 8, p. 083C01, 2020.

[223] T. Hahn, "Loop calculations with FeynArts, FormCalc, and LoopTools," *Acta Phys. Polon. B*, vol. 30, pp. 3469–3475, 1999.

[224] V. Shtabovenko, R. Mertig, and F. Orellana, "FeynCalc 9.3: New features and improvements," *Comput. Phys. Commun.*, vol. 256, p. 107478, 2020.

[225] G. Aad *et al.*, "Measurements of differential cross sections of Higgs boson production through gluon fusion in the $H \to WW^* \to e\nu\mu\nu$ final state at $\sqrt{s} = 13$ TeV with the ATLAS detector," *CERN-EP-2022-228*, 1 2023.

[226] S. Kanemura, M. Kikuchi, and K. Yagyu, "Fingerprinting the extended Higgs sector using one-loop corrected Higgs boson couplings and future precision measurements," *Nucl. Phys. B*, vol. 896, pp. 80–137, 2015.

[227] J. Cao, L. Meng, L. Shang, S. Wang, and B. Yang, "Interpreting the W-mass anomaly in vectorlike quark models," *Phys. Rev. D*, vol. 106, no. 5, p. 055042, 2022.

[228] G. Aad *et al.*, "A detailed map of Higgs boson interactions by the ATLAS experiment ten years after the discovery," *Nature*, vol. 607, no. 7917, pp. 52–59, 2022. [Erratum: Nature 612, E24 (2022)].

[229] M. Sher, "Precise vacuum stability bound in the standard model," *Phys. Lett. B*, vol. 317, pp. 159–163, 1993. [Addendum: Phys.Lett.B 331, 448–448 (1994)].

[230] J. Elias-Miro, J. R. Espinosa, G. F. Giudice, G. Isidori, A. Riotto, and A. Strumia, "Higgs mass implications on the stability of the electroweak vacuum," *Phys. Lett. B*, vol. 709, pp. 222–228, 2012.

[231] L. A. Anchordoqui, I. Antoniadis, H. Goldberg, X. Huang, D. Lust, T. R. Taylor, and B. Vlcek, "Vacuum Stability of Standard Model^{++}," *JHEP*, vol. 02, p. 074, 2013.

[232] O. Lebedev, "On Stability of the Electroweak Vacuum and the Higgs Portal," *Eur. Phys. J. C*, vol. 72, p. 2058, 2012.

[233] A. V. Bednyakov, B. A. Kniehl, A. F. Pikelner, and O. L. Veretin, "Stability of the Electroweak Vacuum: Gauge Independence and Advanced Precision," *Phys. Rev. Lett.*, vol. 115, no. 20, p. 201802, 2015.

[234] S. Alekhin, A. Djouadi, and S. Moch, "The top quark and higgs boson masses and the stability of the electroweak vacuum," *Physics Letters B*, vol. 716, p. 214–219, Sept. 2012.

[235] M. Gonderinger, H. Lim, and M. J. Ramsey-Musolf, "Complex Scalar Singlet Dark Matter: Vacuum Stability and Phenomenology," *Phys. Rev. D*, vol. 86, p. 043511, 2012.

[236] A. Falkowski, C. Gross, and O. Lebedev, "A second Higgs from the Higgs portal," *JHEP*, vol. 05, p. 057, 2015.

[237] N. Khan and S. Rakshit, "Study of electroweak vacuum metastability with a singlet scalar dark matter," *Phys. Rev. D*, vol. 90, no. 11, p. 113008, 2014.

[238] H. Han and S. Zheng, "New Constraints on Higgs-portal Scalar Dark Matter," *JHEP*, vol. 12, p. 044, 2015.

[239] I. Garg, S. Goswami, K. N. Vishnudath, and N. Khan, "Electroweak vacuum stability in presence of singlet scalar dark matter in TeV scale seesaw models," *Phys. Rev. D*, vol. 96, no. 5, p. 055020, 2017.

[240] D. Borah, R. Roshan, and A. Sil, "Sub-TeV singlet scalar dark matter and electroweak vacuum stability with vectorlike fermions," *Phys. Rev. D*, vol. 102, no. 7, p. 075034, 2020.

[241] T. Toma, "Internal Bremsstrahlung Signature of Real Scalar Dark Matter and Consistency with Thermal Relic Density," *Phys. Rev. Lett.*, vol. 111, p. 091301, 2013.

[242] F. Giacchino, L. Lopez-Honorez, and M. H. G. Tytgat, "Scalar Dark Matter Models with Significant Internal Bremsstrahlung," *JCAP*, vol. 10, p. 025, 2013.

[243] F. Giacchino, L. Lopez-Honorez, and M. H. G. Tytgat, "Bremsstrahlung and Gamma Ray Lines in 3 Scenarios of Dark Matter Annihilation," *JCAP*, vol. 08, p. 046, 2014.

[244] A. Ibarra, T. Toma, M. Totzauer, and S. Wild, "Sharp Gamma-ray Spectral Features from Scalar Dark Matter Annihilations," *Phys. Rev. D*, vol. 90, no. 4, p. 043526, 2014.

[245] B. Barman, S. Bhattacharya, P. Ghosh, S. Kadam, and N. Sahu, "Fermion Dark Matter with Scalar Triplet at Direct and Collider Searches," *Phys. Rev. D*, vol. 100, no. 1, p. 015027, 2019.

[246] B. Barman, D. Borah, P. Ghosh, and A. K. Saha, "Flavoured gauge extension of singlet-doublet fermionic dark matter: neutrino mass, high scale validity and collider signatures," *JHEP*, vol. 10, p. 275, 2019.

[247] B. Barman, A. Dutta Banik, and A. Paul, "Singlet-doublet fermionic dark matter and gravitational waves in a two-Higgs-doublet extension of the Standard Model," *Phys. Rev. D*, vol. 101, no. 5, p. 055028, 2020.

[248] F. Giacchino, A. Ibarra, L. Lopez Honorez, M. H. G. Tytgat, and S. Wild, "Signatures from Scalar Dark Matter with a Vector-like Quark Mediator," *JCAP*, vol. 02, p. 002, 2016.

[249] S. Baek, P. Ko, and P. Wu, "Top-philic Scalar Dark Matter with a Vector-like Fermionic Top Partner," *JHEP*, vol. 10, p. 117, 2016.

[250] S. Baek, P. Ko, and P. Wu, "Heavy quark-philic scalar dark matter with a vector-like fermion portal," *JCAP*, vol. 07, p. 008, 2018.

[251] S. Colucci, B. Fuks, F. Giacchino, L. Lopez Honorez, M. H. G. Tytgat, and J. Vandecasteele, "Top-philic Vector-Like Portal to Scalar Dark Matter," *Phys. Rev. D*, vol. 98, p. 035002, 2018.

[252] S. Biondini and S. Vogl, "Scalar dark matter coannihilating with a coloured fermion," *JHEP*, vol. 11, p. 147, 2019.

[253] S. Zheng, "Minimal Vectorlike Model in Supersymmetric Unification," *Eur. Phys. J. C*, vol. 80, no. 3, p. 273, 2020.

[254] P. W. Graham, A. Ismail, S. Rajendran, and P. Saraswat, "A Little Solution to the Little Hierarchy Problem: A Vector-like Generation," *Phys. Rev. D*, vol. 81, p. 055016, 2010.

[255] M. Endo, K. Hamaguchi, S. Iwamoto, and N. Yokozaki, "Higgs Mass and Muon Anomalous Magnetic Moment in Supersymmetric Models with Vector-Like Matters," *Phys. Rev. D*, vol. 84, p. 075017, 2011.

[256] J. Y. Araz, S. Banerjee, M. Frank, B. Fuks, and A. Goudelis, "Dark matter and collider signals in an MSSM extension with vector-like multiplets," *Phys. Rev. D*, vol. 98, no. 11, p. 115009, 2018.

[257] W.-Z. Feng and P. Nath, "Higgs diphoton rate and mass enhancement with vectorlike leptons and the scale of supersymmetry," *Phys. Rev. D*, vol. 87, p. 075018, Apr 2013.

[258] K. Kong, S. C. Park, and T. G. Rizzo, "A vector-like fourth generation with a discrete symmetry from Split-UED," *JHEP*, vol. 07, p. 059, 2010.

[259] G.-Y. Huang, K. Kong, and S. C. Park, "Bounds on the Fermion-Bulk Masses in Models with Universal Extra Dimensions," *JHEP*, vol. 06, p. 099, 2012.

[260] P. Schwaller, T. M. P. Tait, and R. Vega-Morales, "Dark Matter and Vectorlike Leptons from Gauged Lepton Number," *Phys. Rev. D*, vol. 88, no. 3, p. 035001, 2013.

[261] J. Halverson, N. Orlofsky, and A. Pierce, "Vectorlike Leptons as the Tip of the Dark Matter Iceberg," *Phys. Rev. D*, vol. 90, no. 1, p. 015002, 2014.

[262] S. Bahrami, M. Frank, D. K. Ghosh, N. Ghosh, and I. Saha, "Dark matter and collider studies in the left-right symmetric model with vectorlike leptons," *Phys. Rev. D*, vol. 95, no. 9, p. 095024, 2017.

[263] S. Bhattacharya, P. Ghosh, N. Sahoo, and N. Sahu, "Mini Review on Vector-Like Leptonic Dark Matter, Neutrino Mass, and Collider Signatures," *Front. in Phys.*, vol. 7, p. 80, 2019.

[264] A. Joglekar, P. Schwaller, and C. E. M. Wagner, "Dark Matter and Enhanced Higgs to Di-photon Rate from Vector-like Leptons," *JHEP*, vol. 12, p. 064, 2012.

[265] H. M. Lee, M. Park, and W.-I. Park, "Axion-mediated dark matter and Higgs diphoton signal," *JHEP*, vol. 12, p. 037, 2012.

[266] C. Arina, R. N. Mohapatra, and N. Sahu, "Co-genesis of matter and dark matter with vector-like fourth generation leptons," *Physics Letters B*, vol. 720, no. 1, pp. 130–136, 2013.

[267] K. Agashe, T. Okui, and R. Sundrum, "A Common Origin for Neutrino Anarchy and Charged Hierarchies," *Phys. Rev. Lett.*, vol. 102, p. 101801, 2009.

[268] M. Redi, "Leptons in Composite MFV," *JHEP*, vol. 09, p. 060, 2013.

[269] A. Falkowski, D. M. Straub, and A. Vicente, "Vector-like leptons: Higgs decays and collider phenomenology," *JHEP*, vol. 05, p. 092, 2014.

[270] M. Frank, C. Hamzaoui, N. Pourtolami, and M. Toharia, "Unified Flavor Symmetry from warped dimensions," *Phys. Lett. B*, vol. 742, pp. 178–182, 2015.

[271] J. Kearney, A. Pierce, and N. Weiner, "Vectorlike fermions and higgs couplings," *Phys. Rev. D*, vol. 86, p. 113005, Dec 2012.

[272] G. Hiller, C. Hormigos-Feliu, D. F. Litim, and T. Steudtner, "Anomalous magnetic moments from asymptotic safety," *Phys. Rev. D*, vol. 102, no. 7, p. 071901, 2020.

[273] E. Gabrielli, M. Heikinheimo, K. Kannike, A. Racioppi, M. Raidal, and C. Spethmann, "Towards Completing the Standard Model: Vacuum Stability, EWSB and Dark Matter," *Phys. Rev. D*, vol. 89, no. 1, p. 015017, 2014.

[274] G. Hiller, T. Höhne, D. F. Litim, and T. Steudtner, "Vacuum Stability in the Standard Model and Beyond," 1 2024.

[275] V. V. Khoze, C. McCabe, and G. Ro, "Higgs vacuum stability from the dark matter portal," *JHEP*, vol. 08, p. 026, 2014.

[276] P. Achard *et al.*, "Search for heavy neutral and charged leptons in e^+e^- annihilation at LEP," *Phys. Lett. B*, vol. 517, pp. 75–85, 2001.

[277] J. Abdallah *et al.*, "Searches for supersymmetric particles in e+ e- collisions up to 208-GeV and interpretation of the results within the MSSM," *Eur. Phys. J. C*, vol. 31, pp. 421–479, 2003.

[278] R. Mann, J. Meffe, F. Sannino, T. Steele, Z.-W. Wang, and C. Zhang, "Asymptotically Safe Standard Model via Vectorlike Fermions," *Phys. Rev. Lett.*, vol. 119, no. 26, p. 261802, 2017.

[279] M. Chiappini and on behalf of the MEG II collaboration, "Meg ii physics and detector performance," *Journal of Instrumentation*, vol. 18, p. C10020, oct 2023.

[280] G. Pezzullo, "The mu2e experiment at fermilab: a search for lepton flavor violation," *Nuclear and Particle Physics Proceedings*, vol. 285?286, p. 3?7, Apr. 2017.

[281] A. E. Blechman, A. A. Petrov, and G. K. Yeghiyan, "The flavor puzzle in multi-higgs models," *Journal of High Energy Physics*, vol. 2010, pp. 1–28, 2010.

[282] N. Bizot and M. Frigerio, "Fermionic extensions of the Standard Model in light of the Higgs couplings," *JHEP*, vol. 01, p. 036, 2016.

[283] A. M. Sirunyan *et al.*, "Search for vector-like leptons in multilepton final states in proton-proton collisions at $\sqrt{s} = 13$ TeV," *Phys. Rev. D*, vol. 100, no. 5, p. 052003, 2019.

[284] A. Tumasyan *et al.*, "Inclusive nonresonant multilepton probes of new phenomena at $\sqrt{s}$=13 TeV," *Phys. Rev. D*, vol. 105, no. 11, p. 112007, 2022.

[285] A. Tumasyan *et al.*, "Search for pair-produced vector-like leptons in final states with third-generation leptons and at least three b quark jets in proton-proton collisions at s=13TeV," *Phys. Lett. B*, vol. 846, p. 137713, 2023.

[286] G. Aad *et al.*, "Search for third-generation vector-like leptons in *pp* collisions at $\sqrt{s} = 13$ TeV with the ATLAS detector," *JHEP*, vol. 07, p. 118, 2023.

[287] S. Sultansoy, "Energy frontier lepton-hadron colliders, vector-like quarks and leptons, preons and so on," 1 2019.

[288] A. Hayrapetyan *et al.*, "Review of searches for vector-like quarks, vector-like leptons, and heavy neutral leptons in proton-proton collisions at $\sqrt{s} = 13$ TeV at the CMS experiment," 5 2024.

[289] G. Cynolter and E. Lendvai, "Electroweak Precision Constraints on Vector-like Fermions," *Eur. Phys. J. C*, vol. 58, pp. 463–469, 2008.

[290] S. K. Garg and C. S. Kim, "Vector like leptons with extended higgs sector," 2013.

[291] A. Adhikary, M. Olechowski, J. Rosiek, and M. Ryczkowski, "Theoretical constraints on models with vectorlike fermions," *Phys. Rev. D*, vol. 110, p. 075029, Oct 2024.

[292] W. Altmannshofer, M. Bauer, and M. Carena, "Exotic leptons: Higgs, flavor and collider phenomenology," *Journal of High Energy Physics*, vol. 2014, Jan. 2014.

[293] D. Barducci, L. Di Luzio, M. Nardecchia, and C. Toni, "Closing in on new chiral leptons at the lhc," *Journal of High Energy Physics*, vol. 2023, Dec. 2023.

[294] M. Luo, H. Wang, and Y. Xiao, "Two-loop renormalization group equations in general gauge field theories," *Phys. Rev. D*, vol. 67, p. 065019, Mar 2003.

[295] I. Schienbein, F. Staub, T. Steudtner, and K. Svirina, "Revisiting RGEs for general gauge theories," *Nucl. Phys. B*, vol. 939, pp. 1–48, 2019. [Erratum: Nucl.Phys.B 966, 115339 (2021)].

[296] K. G. Chetyrkin and M. F. Zoller, "Three-loop \beta-functions for top-Yukawa and the Higgs self-interaction in the Standard Model," *JHEP*, vol. 06, p. 033, 2012.

[297] K. Hagiwara, S. Matsumoto, D. Haidt, and C. S. Kim, "A Novel approach to confront electroweak data and theory," *Z. Phys. C*, vol. 64, pp. 559–620, 1994. [Erratum: Z.Phys.C 68, 352 (1995)].